An Abundance Survey of the Ap stars of the Southern Hemisphere

Martin Hall

A thesis submitted in partial fulfilment
of the requirements for the degree of
Doctor of Philosophy

Jeremiah Horrocks Institute for Maths, Physics and Astronomy
University of Central Lancashire

February 2020

Declaration

Type of Award: Doctor of Philosophy

School: Physical Sciences and Computing

I declare that while registered as a candidate for the research degree, I have not been a registered candidate or enrolled student for another award of the University or other academic or professional institution.

I declare that no material contained in the thesis has been used in any other submission for an academic award and is solely my own work.

No proof-reading service was used in the compilation of this thesis.

Martin Hall

February 2020

Abstract

The atmospheres of Chemically Peculiar A stars provide a fascinating area of research on many levels: their slow rotation, strong magnetic fields and lack of turbulent convection give rise to stratification of different ionic species of the same element through a process of radiative levitation. In particular, this phenomenon has already been seen in the abundance disequilibria of Iron, and rare earth elements such as Neodymium (Nd) and Praseodymium (Pr). The research work described in this thesis involves the development of a semi-automated set of routines coded in the programming language IDL to measure equivalent widths of selected Fe lines, and the application of these routines to perform an abundance survey of Fe I and Fe II species on the high-resolution spectra of approximately 350 Ap stars collected between 2007 and 2010 on the FEROS Echelle spectrograph housed at the 2.2–m telescope at European Southern Observatory at La Silla, Chile. The results show strong correlations with effective temperature as a consequence of atmospheric stratification. The approach is then extended to the ionic pairs of rare earth species Pr II / Pr III and Nd II / Nd III to investigate whether these abundance disequilibria in the rapidly oscillating Ap stars are a consequence of the relatively cool temperatures of those stars, or rather a signature of pulsation. We believe that the onset of this disequilibrium phenomenon observed in the cooler Ap stars is more likely to be a temperature effect, rather than a signature of pulsation.

Contents

List of Tables

List of Figures

To my late wife Alison

Acknowledgements

This thesis represents the culmination of an extremely enjoyable association with the JHI at UCLan. First and foremost, I would like to thank my supervisor Professor Don Kurtz for his constant support throughout this assignment. Studying for a PhD on a part-time basis is never an easy undertaking, and there have been some periods of personal difficulty, but Don has always been there throughout, to give advice and encouragement, and for that I am extremely grateful. I should also like to thank Vladimir Elkin for his support and advice on many aspects of abundance analysis; to Hans Bruntt for his insightful advice on using the VWA software, and to Christian Nitschelm for his assistance during my time at the ESO Observatory at La Silla, collecting some of the spectra for this work. I am indebted to my fellow student Kelly Hambleton for many conversations, scientific and otherwise, over a cake and cuppa on campus! I am grateful also to my good friend Lesley Roberts for her general encouragement and support. Finally, I would like to thank my family: my late wife Ali, James and Sarah, for being a rock of love and support throughout, and for allowing me the time and space to engage on this project. The award of an Arnoux Bursary by the University in support of this work is also gratefully acknowledged.

Chapter 1

Introduction

1.1 Introduction

In its broadest sense the term Chemically Peculiar may be given to any stellar object where the surface chemical composition may be deemed to be significantly different to that of the solar photosphere. There are many types, spanning a significant range of effective temperatures and evolutionary stages. These reflect a number of underlying processes resulting in such peculiarity, from stripped stellar cores (Wolf–Rayet stars), Barium stars, where accretion from a companion star has occurred, to the gravitational settling and radiative levitation of the Chemically Peculiar or CP stars.

Unlike stars in other regions of the Hertzsprung–Russell (HR) diagram, where atmospheric dynamics appear to be dominated by one particular effect, Main Sequence stars appear to have atmospheres that are characterised by a number of competing physical phenomena of comparable magnitude; magnetic effects, pulsation, convection, rotation, element diffusion. The Chemically Peculiar stars are Upper Main Sequence objects, and form a significant proportion of the stars in this region of the HR diagram; approximately 10–15% of the A–type main sequence stars may be classified in this way (Aller et al. 1982) – see Fig. 1.1. The term 'peculiar' was

first used by Antonia Maury at Harvard in 1897 to describe spectral features in the spectrum of α^2 CVn (Maury & Pickering 1897) as part of her work on the Henry Draper Memorial Survey. She remarked that the K line was unusually weak, and on the presence of a strong Si II doublet at 4128.5 and 4131.4 Å. Maury classified two further stars as belonging to the same group: θ Aur and 81 UMa, which are now known to be true Ap stars. Annie Cannon, a contemporary of Maury, was the first to work on the bright stars of the Southern hemisphere, discovering a number of peculiar A stars whose spectra contained lines of ionised silicon (as Maury had done) and ionised strontium (Cannon & Pickering 1901). Cannon also found stars with strong metallic and weak Ca lines, later classified as Am stars.

Spectroscopic work by Lockyer & Baxendall (1906) identified 'strange lines' and the work of Ludendorff (1907) showed such lines to vary in intensity. Later analysis by Belopolsky (1913) showed that the Eu line intensity at 4129 Å in the spectrum of α^2 CVn varied with a period of 5.5 days. He also measured the rotational velocities of the Eu lines, and he found that the radial velocities varied in quadrature with the changes in line intensity. By 1914, following work by Guthnick & Prager (1914) on measurements of the light curve of of α^2 CVn, it was established that α^2 CVn was a spectral and photometric variable, that the light curve and Eu line intensities varied synchronously, and that the spectral variations and radial velocity were in quadrature. During 1916–17 Carl Keiss from the University of Michigan studied the line identifications and wavelengths of a number of stars from the Henry Draper Catalogue. In particular, from his investigations of α^2 CVn he was able to identify the presence of yttrium and a number of rare earth elements, including lanthanum, gadolinium, terbium and dysprosium, and he confirmed the periodicity of radial velocity and intensity variations identified earlier by Belopolsky (Kiess 1917).

The early 1930s marked a significant increase in activity surrounding the investigation of Ap stars. In particular, Morgan made a number of discoveries, including

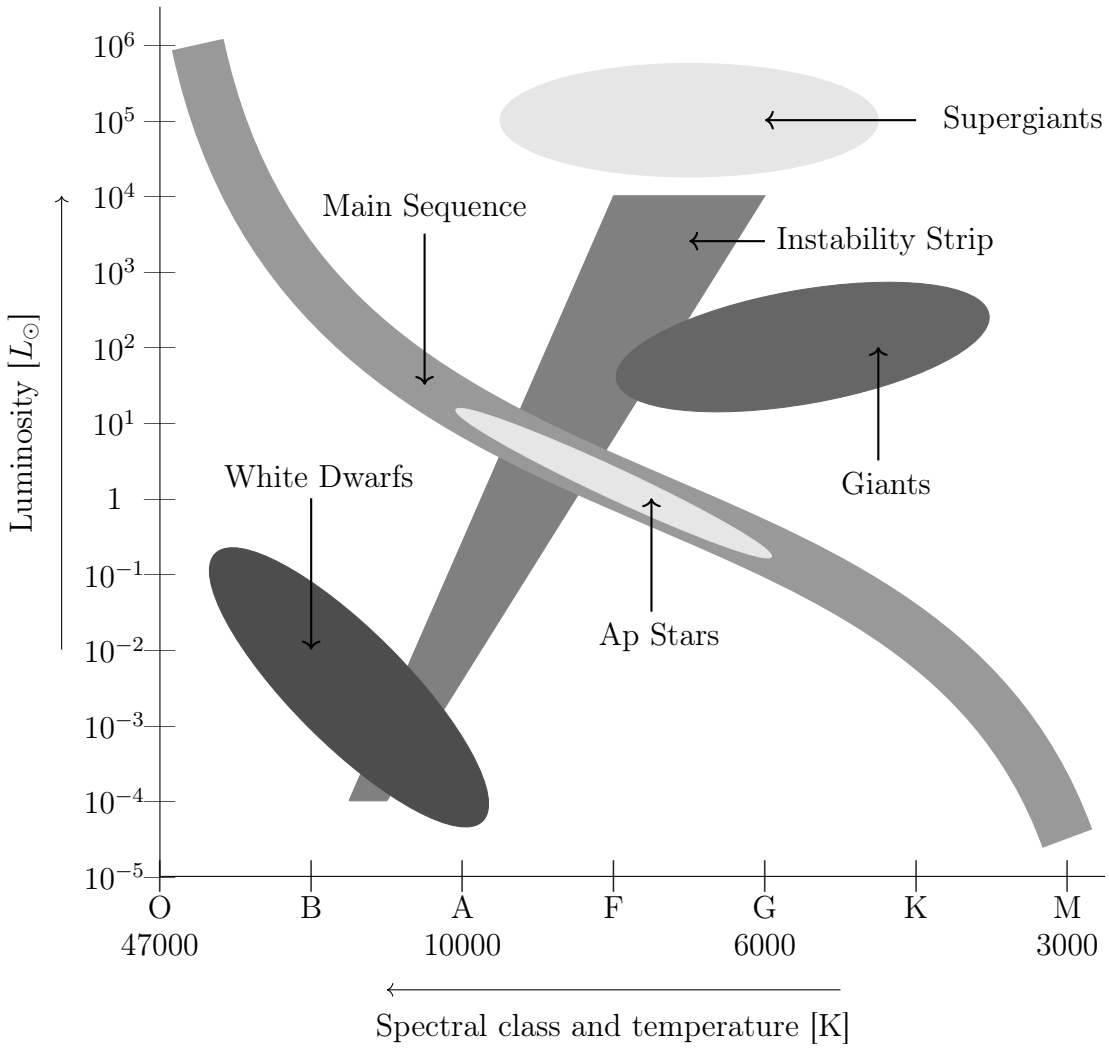

Figure 1.1: HR diagram showing the location of the Ap stars

a new class of peculiar manganese stars (Mn II) of spectral type B8–A0; fourteen were categorised in this way (Morgan 1931a). These differed from the α^2 CVn type of stars in being non-variable. He also found that the peculiar star HD 125248 had strong lines of chromium which varied in intensity in antiphase with Eu II (Morgan 1931b). Further studies by Morgan (1933) showed that these observations were typical of Ap stars.

A satisfactory explanation for the observations associated with Ap stars had to wait until the discovery of the presence of variable magnetic fields. Babcock looked for the presence of Zeeman splittings in the spectra of Ap stars, and his observations demonstrated the presence of such effects in 78 Vir (Babcock 1947c) and α^2 CVn (Babcock 1947a), and indeed the majority of sharp–lined Ap stars. Babcock also observed the aforementioned Cr–Eu star, HD 125248, and observed that the dipolar magnetic field strength varied between $+7\,000$ G and $-6\,200$ G, with the same periodicity as the line strengths (Babcock 1947b). The oblique rotator model was proposed by Babcock in 1949 to explain these observations; see Fig. 1.2, although he was not an enthusiastic proponent. The model proposed that Ap stars were slowly rotating stars with a permanent magnetic dipole, fixed in strength, inclined at an angle to the axis of rotation. Independently, Stibbs proposed the oblique rotator model, and demonstrated how it could account for the observed variations in photometric variability, spectral line intensity and magnetic field in HD 125248 (Stibbs 1950). The field is assumed to be 'frozen in' to the surface and co–rotates with it. The spectral line intensities are consistent with this model if the elements are concentrated in patches on the stellar surface. To reinforce the success of the model, in the same paper, Stibbs performed mathematical calculations representing differing angles subtended between the rotational and magnetic axes – see Fig. 1.3. The oblique rotator model has been the only one to explain the observations of the Ap stars over the years. A practical example of the theory is shown for variations

in equivalent width, brightness and mean longitudinal magnetic field component as a function of phase for the Ap star HD 119419 in Fig. 1.4 (Landstreet 2009).

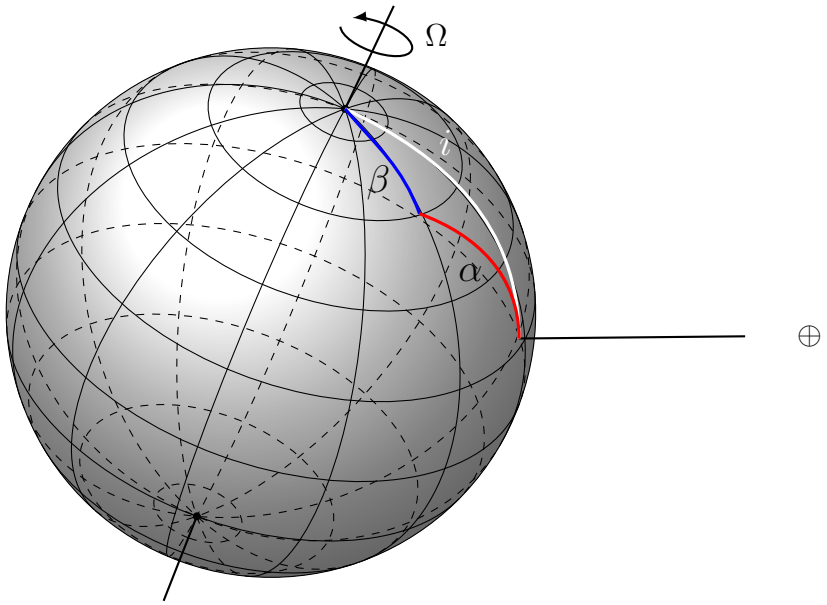

Figure 1.2: The Oblique Rotator model (Stibbs 1950). The Earth–based observer is denoted by the symbol ⊕. The angle subtended between the axis of rotation and the direction of the observer is given by i. The angle β denotes the angle between the rotational axis and the magnetic axis, while α denotes the angle between the magnetic axis and the observer. Ω denotes the speed of angular rotation.

The combination of slow rotation, and in many cases, the presence of a strong magnetic field, promote stability in the outer atmospheric layers, and an absence of turbulent convection. Such conditions allow radiative levitation processes to occur, whereby heavy elements in partially ionised states with large photon absorption cross–sections can absorb photons resulting in a proportion of the photons' momentum being converted to outward momentum of the absorbing species. This works in competition with gravitational settling of lighter atomic species, leading to a gradual concentration gradient dependent on optical depth. Michaud (1970) set out the mechanics of just such a diffusion theory, which has been successful in explaining

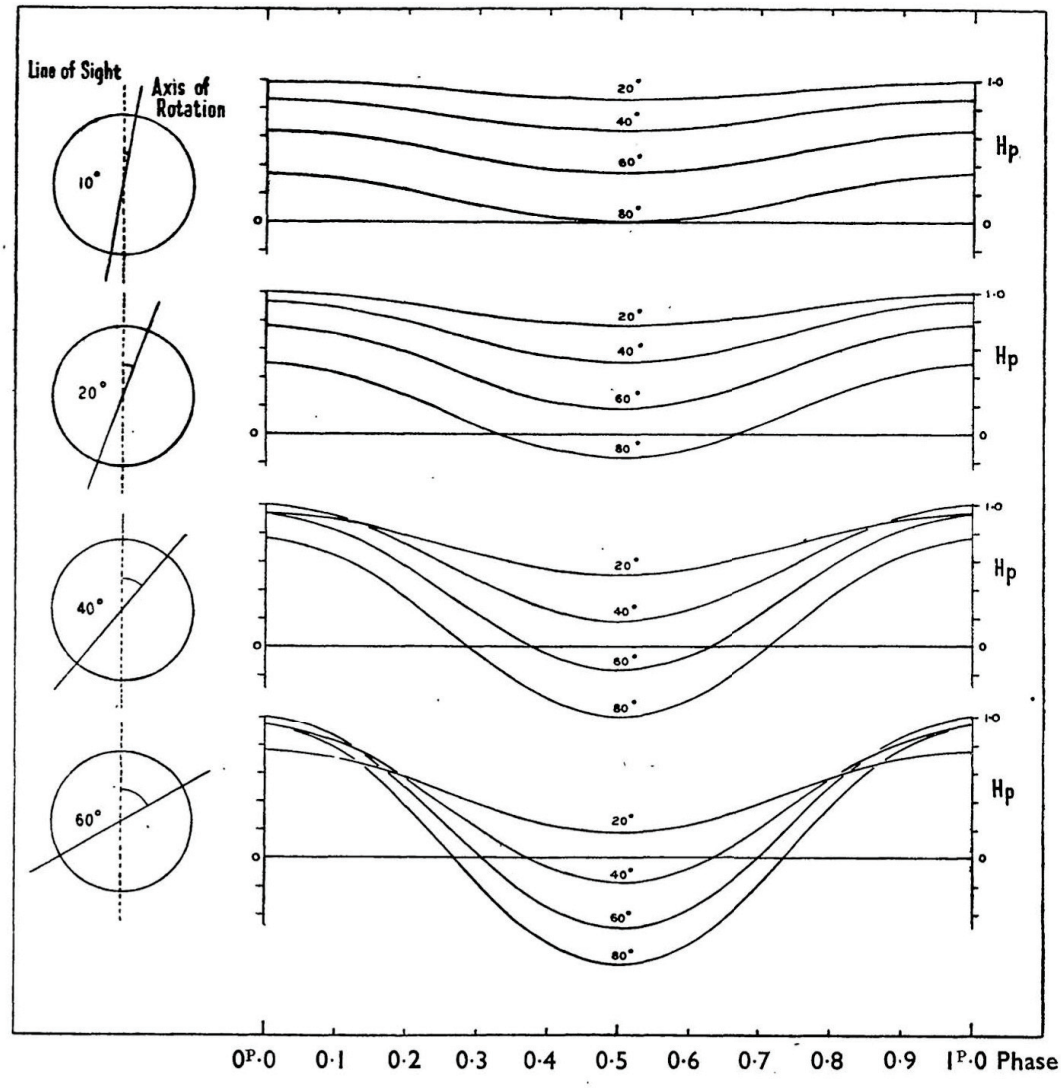

Figure 1.3: Apparent magnitude variations during the rotation of a star when viewed obliquely to the axis of rotation, the magnetic and rotational axes not being coincident. The four curves shown for each inclination to the line of sight are for colatitudes 20°, 40°, 60° and 80° of the magnetic pole (Stibbs 1950)

the observations of chemical peculiarities observed in the high-resolution spectra of several different groups of CP stars. The radiative acceleration of a given species i at a given depth can be approximated by the expression (Hui-Bon-Hoa et al. 2002):

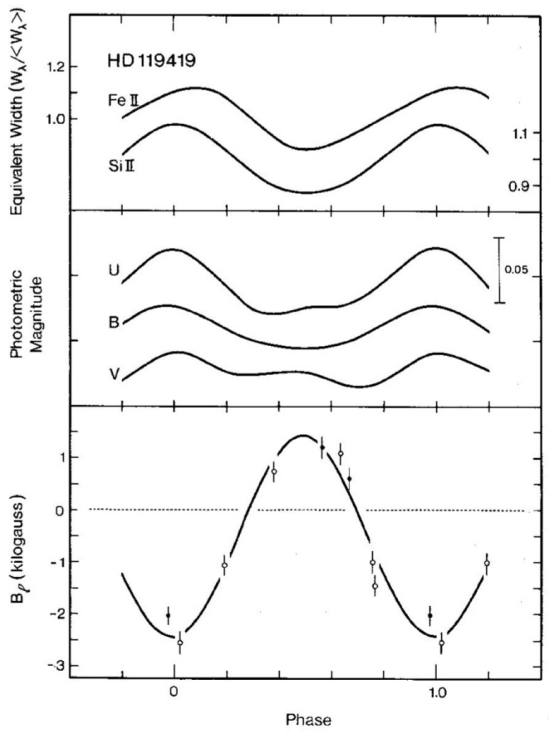

Figure 1.4: Variations observed in the magnetic Ap star HD 119419 as a function of phase. The top curve shows the variations of equivalent width of Fe and Si lines: the middle curve: the variation of brightness in the Johnson UBV bands: the bottom curve, the mean longitudinal magnetic field component $< B_z >$ (Landstreet 2009)

$$g^i_{rad} = \frac{4\pi}{c}\frac{1}{X_i}\int_0^\infty k^i_\nu H_\nu d\nu$$

where X_i is the mass fraction of species i, k^i_ν is its opacity (frequency–dependent) and H_ν is the Eddington Flux at the depth under consideration. The radiative acceleration of a species therefore depends on its opacity, and it is a feature of the absorption spectra of ionised rare earth elements that they tend to have a large number of absorption lines in the spectral region associated with the effective temperature of these stars. The basic premise is that in a stable atmosphere, these rare earth elements experience an acceleration upwards in the atmosphere and will be driven upwards and concentrated in the line-forming regions of the atmosphere. In

contrast, elements which have few atomic transitions in the spectral region of the stellar flux will tend to sink to the lower levels of the atmospheric envelope under the influence of gravitational settling. It is this separation of elemental ionic species that explains the relatively high abundance of rare earth elements in the spectra of Ap stars.

1.2 Spectral Classification of Chemically Peculiar Stars

Ever since their discovery well over a hundred years ago, the Chemically Peculiar stars of the Upper Main Sequence have been extensively discussed in the literature, since they exhibit a variety of interesting phenomena for investigation, including photometric variability, slow rotation, magnetic and spectral anomalies.

The Chemically Peculiar stars may be categorised into four groups (originally CP1–CP4) (Preston 1974). CP1 stars are Am type stars (m for metallic); CP2 stars are Ap (and Bp) stars (where the p denotes peculiar); CP3 stars are HgMn stars, characterised in their spectra by a large overabundance of Hg and Mn; finally the CP4 or He–weak stars exhibit a low He abundance at their surface. See Table 1.1.

The λ Bootis class are classified typically within the spectral range A0–F0. Their main feature within a typically weak metallic–line spectrum is a prominent absorption line of Mg II at 4481 Å. The intensity ratio of Mg / Fe at 4481 / 4383 Å in this class is significantly smaller than that of normal A–type stars (Gray 1988).

The Am–Fm or CP1 metal-line stars are classified in the spectral class A0–F4 and are categorised by the weakness of the Ca II K line, given the spectral class. The abundances of calcium and scandium are also low, by a factor of 0.5–1.0 dex. However, the other metal lines are typically much stronger than is usual for the

CHAPTER 1

Table 1.1: Classification of the Chemically Peculiar Stars of the Upper Main Sequence (Smith 1996)

Classical Name	Preston Classification	Criteria	Spectral Type	T_{eff} Range
Boo λ	–	weak Mg II and weak metals	A0–F0	9 600–7 500 K
Am–Fm	CP1	weak Ca II and/or Sc II; enhanced metals	A0–F4	9 600–6 800 K
Bp–Ap	CP2	enhanced Sr, Cr, Eu and/or Si	B6–F4	14 400–6 800 K
HgMn	CP3	enhanced Hg II and/or Mn II	B6–A0	14 400–9 600 K
He–weak	CP4	weak He I compared with colours	B2–B8	21 000–12 300 K

spectral class, with Fe abundance typically 1.0 dex higher. In all examples, a magnetic field is absent. Although the majority are believed to be members of relatively close binary systems, a significant proportion (perhaps $\sim 35\%$) are thought to be isolated stars (Henry & Fekel 2005; Carquillat & Prieur 2007). Examples include Sirius A, 63 Tau, δ Nor and τ uMa.

The Bp–Ap or CP2 class of stars, of which α^2 CVn is an example, are found in the spectral range F4–B6. They exhibit enhanced spectral lines for Si, Sr, Cr, Eu and other rare earths and have very strong magnetic fields; typically in the range 0.5–6 kG. The spectra of four typical Ap stars (Si II Bp star ϕ Dra, a SrEu star HD 224801, and two SrCrEu stars, HD 2453 and β CrB) are shown stacked from top to bottom, respectively, in Fig. 1.5 (Gray & Corbally 2009). For comparison, the spectra of four normal A-type stars are shown in Fig. 1.6 in order of increasing $T_{\rm eff}$ from top to bottom (Gray & Corbally 2009). The hydrogen Balmer absorption sequence from H_γ – H_9 is prominent in both cases.

The HgMn (CP3) class were first discovered in 1906 (Lockyer & Baxendall 1906). It was noticed that the spectra contained prominent absorption lines at 3944, 3984, 4136, 4206 and 4252 Å which could not be assigned at that time. It turned out that, with the exception of the line at 3984 Å, which was associated with Hg II, these lines were identified as ionised Mn II. The stars in this category are all classed as late B, with slow rotation, but unlike the Bp–Ap class, their magnetic fields are considerably weaker, with a flux density typically < 100 G, and do not exhibit spectral or photometric variability. Typical examples are α And and γ Crv.

The He–weak (CP4) stars were discovered in the 1960s, exhibiting weak He lines, together with sharp absorptions of P II, Ga II, and of noble gases. They are characterised with weak magnetic fields. α Scl is an example.

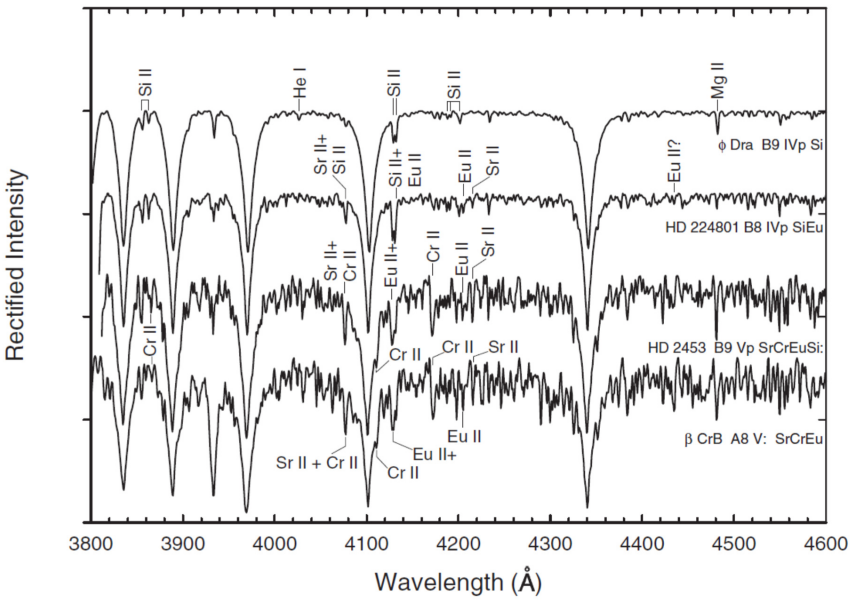

Figure 1.5: Stacked spectra of four typical Ap stars (Si II Bp star ϕ Dra, a SrEu star HD 224801, and two SrCrEu stars, HD 2453 and β CrB), indicating absorption lines due to enhanced abundances of Si, Cr, Eu and Sr (Gray & Corbally 2009)

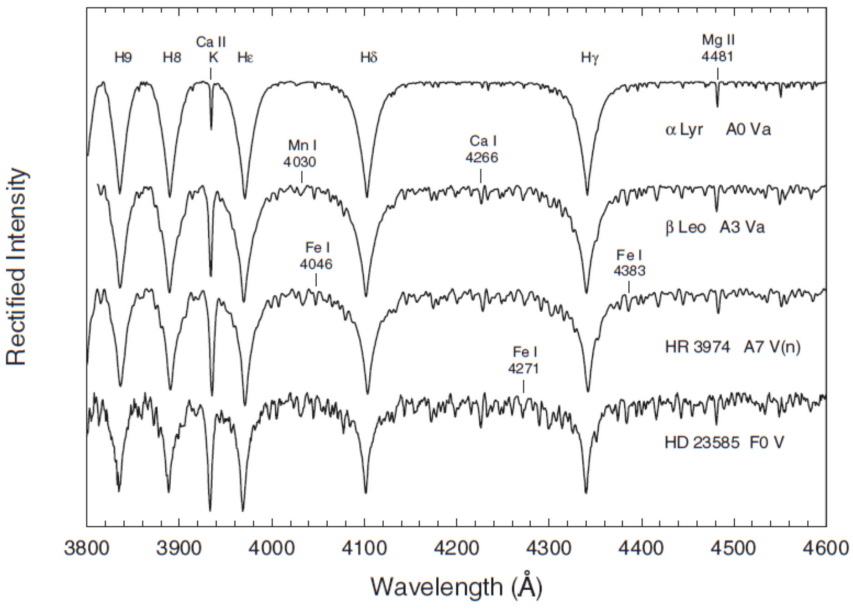

Figure 1.6: Stacked spectra of four typical A-type stars (α Lyr, β Leo, HR 3974, HD 23585) in order of increasing T_{eff} from top to bottom (Gray & Corbally 2009)

1.3 Abundance analysis

A great deal of information about the physical conditions in the atmospheres of stars may be obtained by investigating the photometry and spectroscopy of these systems. Information on the fundamental parameters of such stars, including the effective temperature $T_{\rm eff}$, surface gravity $\log g$, and chemical composition and degree of peculiarity may be ascertained by analysing the photometry. In addition, an investigation of the absorption lines may yield information on chemical composition, which in turn provides insight into the physical processes going on in the stellar atmosphere.

One classical approach to performing an abundance analysis of the A stars involves the following steps:

1. Derivation of the $T_{\rm eff}$, $\log g$ and metallicity of the star from an analysis of the stellar photometry.

2. Investigation of the stellar absorption spectrum; assignment of the absorption lines to known electronic transitions and measurement of the associated equivalent widths of the lines.

3. Combination of the fundamental parameters and measured equivalent widths of the identified lines, together with line data (oscillator strengths, damping constants, excitation potentials of the ground and upper states, degeneracy) as derived in the laboratory, together with an appropriate atmospheric model to derive a set of abundances for the element lines that have been measured.

This process is outlined schematically in Fig. 1.7 and described in the following subsections.

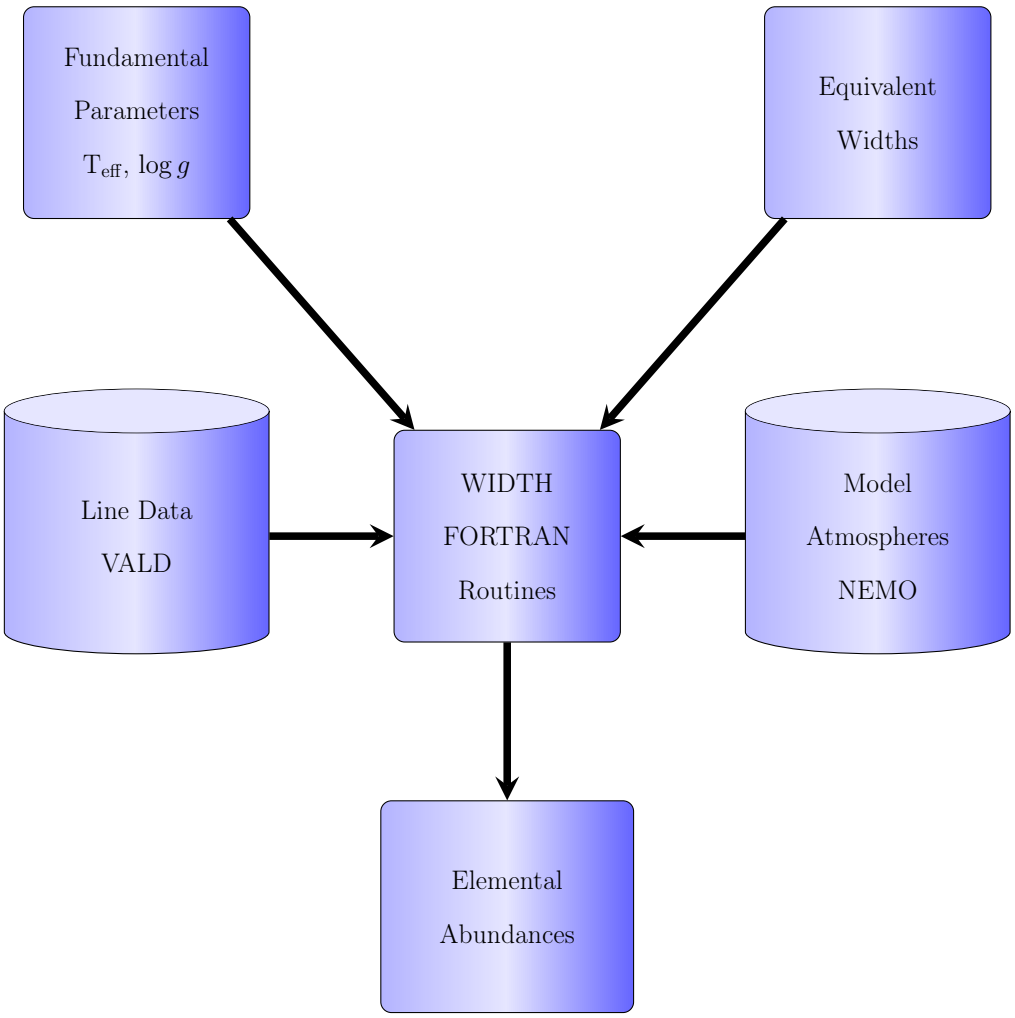

Figure 1.7: Flowchart showing derivation of abundances. Fundamental parameters for each of the target stars are derived from photometric data, and together with the measured equivalent width for each selected absorption line are input to the WIDTH program, which uses reference data, such as atomic line data (oscillator strengths, degeneracy, damping constants) and model atmospheres relevant to the selected fundamental conditions, to derive a set of abundances for the elements under consideration.

1.3.1 Photometry of Ap Stars and Determination of Fundamental Parameters

Astronomical photometry can be used to determine certain characteristics of stellar objects, such as T_{eff}, $\log g$ and metallicity. There are several photometric systems

in existence; the Strömgren $uvby\beta$ photometric system was developed by Strömgren (1956) and later extended (Crawford 1958). It is an intermediate band width system, with filters placed at specific points over the optical spectrum. The u (ultraviolet) filter is placed at 350 nm, between the regions of atmospheric cutoff and Balmer discontinuity. The v (violet) filter is centred at the absorption line of H_δ at a wavelength of 411 nm. It represents a region where line blanketing effects are particularly strong (blanketing is the combination of the decrease of energy in certain wavelengths due to the metal absorption lines, and the re-emission of this energy over the entire spectrum). The b filter (blue) is located at 467 nm, at a longer wavelength than the blanketing region, so tends to be less affected by blanketing. The y filter is centered at 547 nm. The transmission characteristics of the filters are shown in Fig. 1.8.

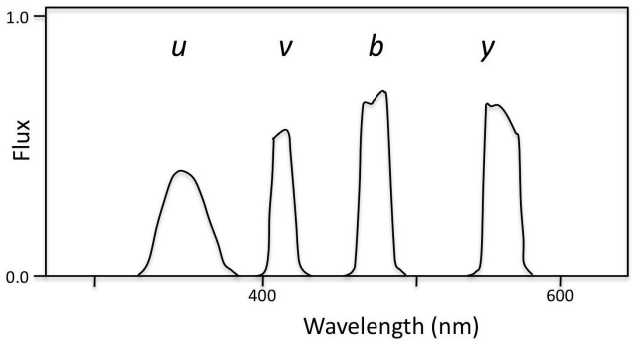

Figure 1.8: Filter throughput curves for Strömgren filters. Filter curves are from the database of filters used with the wide-field camera on the Isaac Newton Telescope (Árnadóttir et al. 2010).

Photometric measurements using these four filters are also combined with two filters of different bandwidth both centered on the H_β absorption line (hence the $uvby\beta$ system). From combinations of Strömgren filters, one can define four independent colour indices which provide information about physical parameters of the

stars:

$(b-y)$

$c_1 = (u-v)-(v-b)$

$m_1 = (v-b)-(b-y)$

$\beta \ = \beta_{\rm wide} - \beta_{\rm narrow}$

The $(b-y)$ index is relatively unaffected by blanketing and is a good indicator of the effective temperature of the star. The c_1 index measures the Balmer discontinuity and is sensitive to the surface gravity. In contrast, the m_1 index is a measure of line blanketing in the region of 410 nm and is sensitive to metallicity (it is sometimes referred to as a peculiarity indicator). Finally, the β index, which is intrinsically independent of the reddening, measures the strength of the H_β line. It has the characteristic that for late type stars it provides an estimation of the temperature and for early type stars it is a measure of the intrinsic brightness. The first three indices are all affected by reddening. This can be corrected by applying a standard extinction law (Golay 1974) to give corrected indices:

${c_1}' = c_1 - 0.20(b-y)$

${m_1}' = m_1 + 0.18(b-y)$

The photometric measurements used in determining the physical characteristics of the Ap stars in this survey were acquired using a modular photometer mounted on the 0.5-m Boller and Chivens Cassegrain telescope of the South African Astronomical Observatory (SAAO), collected between 1990 May and 1992 June (Martinez

Table 1.2: Table illustrating sample values for the corrected Strömgren indices used in the analysis of the Ap stars, taken from Martinez (1993)

Star	$(b-y)$	(m'_1)	(c'_1)	β
HD2202	0.246	0.123	0.454	2.693
HD2883	0.295	0.226	0.317	2.660
HD2957	−0.001	0.208	0.973	2.885

1993). Typical integration times of 25 s per filter for bright stars (apparent magnitude $V < 7.0$) and 60 s per filter for fainter stars ($V > 7.0$). A sample set of indices available from Martinez' thesis is shown in Table 1.2.

From the calculated values for the Strömgren indices, values for $T_{\rm eff}$, $\log g$ and metallicity are derived for each star in the survey using TEMPLOGG, a menu driven application written in the C–Shell script (Kupka & Bruntt 2001). The conversion is based mostly on the calibrations of Moon & Dworetsky (1985) and (Napiwotzki et al. 1993). Typical error estimates due to the calibration itself are of the order of 150 K to 250 K in $T_{\rm eff}$, 0.15 to 0.2 dex in $\log g$ and 0.1 dex in metallicity [M/H]. These values are then also used as a basis for selecting the model atmosphere appropriate to each target star.

1.3.2 Equivalent Width and Derivation of Abundances

In order to extract abundances from the recorded Ap spectra, the equivalent widths of each of the atomic species of interest need to be measured, and then converted into a value for an abundance using a combination of derived stellar parameters from the photometry ($T_{\rm eff}$, $\log g$) and an appropriate model atmosphere. The equivalent width W_λ of an atomic absorption line is defined as the width of a theoretical atomic

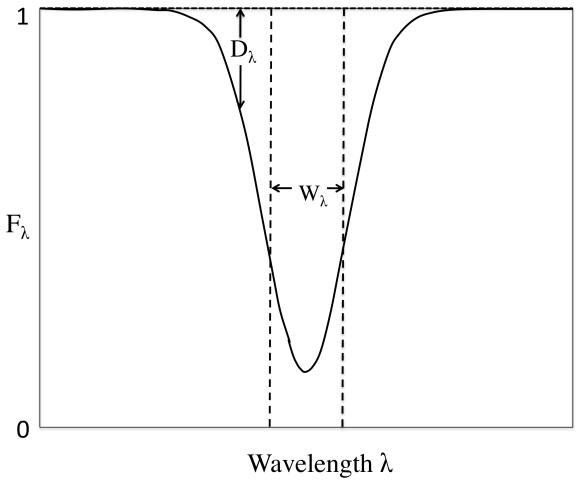

Figure 1.9: Definition of the equivalent width W_λ of an atomic line. The rectangular box which absorbs all photons within it has a width such that is absorbs the same flux as the atomic line with which it is associated.

line of rectangular shape that absorbs the same total radiative flux as the atomic line it is associated with. In other words, if the line depth (the depth of the flux within the line below the continuum level) is represented by D_λ, then the equivalent width is equal to the integration of this absorption line depth across the whole wavelength range of the line (see Fig. 1.9):

$$W_\lambda = \int D_\lambda d\lambda$$

The line strength increases with abundance, but it is not a simple relation; it is dependent on the relative interplay of factors affecting the absorption at different concentrations. For weak lines, the core of the line profile dominates, and the equivalent width is proportional to the abundance A, i.e. $W_\lambda \propto A$. As the central depth reaches a maximum, the line saturates, and then the processes forming the wings of the line begin to dominate; in this region the equivalent width, $W_\lambda \propto (\ln \mathrm{A})^{1/2}$. Finally, as the abundance increases still further, the absorption in the wings becomes dominant due to pressure broadening, and the equivalent width then varies as $\sqrt{A}$.

This relationship between abundance and equivalent width is known as the 'curve of growth' and is illustrated in Fig. 1.10. Is is for this reason that weaker lines tend to be selected for abundance analysis, where the dependency of equivalent width on abundance takes a simpler form.

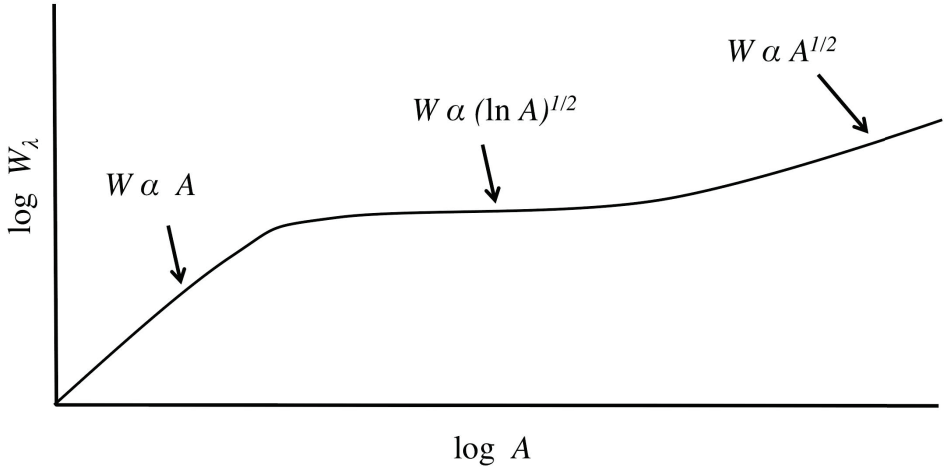

Figure 1.10: Graph showing the relationship between equivalent width W_λ and abundance A for an atomic absorption line, indicating three regions of dependence as the abundance of the species increases.

The WIDTH program used in this analysis to derive abundances from measured equivalent widths consists of a set of routines written in FORTRAN by Robert Kurucz (Castelli 2005). The program takes the equivalent width that has been measured for a selected atomic absorption line in a high-resolution spectrum, and computes an abundance for that species, based on a selected model atmosphere and initial set of atomic abundances for hydrogen, helium and the metals that are input into the program. The program also requires atomic line information relevant to the atomic transition associated with the line (such a energy levels and degeneracies, oscillator strengths and damping constants). This is provided by the Vienna Atomic Line Database (VALD), an atomic and molecular database for astrophysics (Heiter

et al. 2008), which allows relative populations and opacities at various depths within the appropriate model atmosphere to be formulated. The result is a value for the abundance of the species associated with the absorption line.

1.4 Stratification in Ap Stars and Departure from the Standard Model Atmosphere

As a result of abundance analyses of Ap stars over the years, several characteristics of elemental stratification have emerged (where different ions of the same element are formed at different atmospheric layers), which are summarised below from analyses by Ryabchikova et al. (2003):

- Observation of an ionisation disequilibrium in abundance studies. In certain analyses, derived abundance values for different ions of the same species are not consistent, implying that in stratified atmospheres they are formed at different layers within the atmosphere. For example, iron accumulation in deep layers, which are hotter, is seen in certain cases to lead to higher Fe II abundances (Ryabchikova et al. 2004). See Fig. 1.11

- An inability to fit the core and the wing of the hydrogen Balmer spectral lines using the same abundance profile, known as the core–wing anomaly (Cowley et al. 2001). For example in Przybylski's star – HD 101065, attempts have been made to model the H_α line profile by increasing the temperature at intermediate atmospheric layers (Kochukhov et al. 2002), though an explanation as to the cause of the effect remains inconclusive. Studies of HD 166473 have shown a similar effect (Kurtz et al. 2003); see Fig. 1.12.

- High–excitation lines of the ionized iron peak elements in certain cases are shown to be significantly different from the mean calculated for the element as a whole. This is ascribed to deviation from conditions of local thermodynamic equilibrium (LTE).

- A disagreement between the abundances derived from strong and weak lines of the same ion. This arises from the increased concentration of an element in deeper atmospheric layers, causing strong lines to weaken and weak lines to be enhanced.

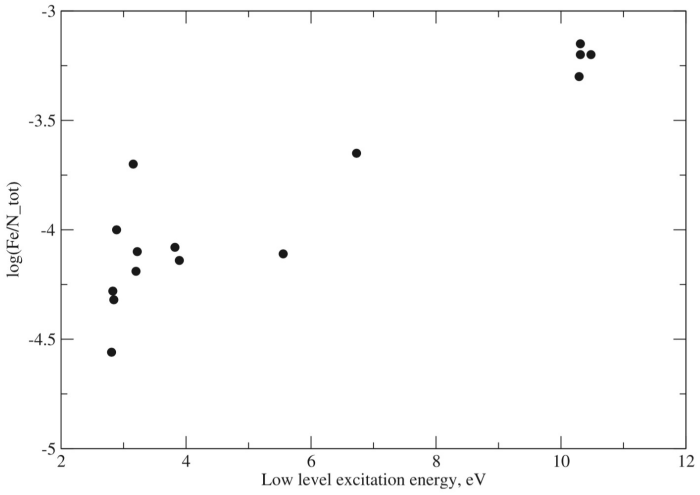

Figure 1.11: Fe II abundance for 33 Lib (HD 137949) derived from individual lines with different low level excitation energies (Ryabchikova et al. 2004).

In general, the majority of abundance analyses of Ap stars have tended to include only a handful of objects in each investigation. Adelman (1973) performed an analysis of 21 cool Ap stars of low projected rotational velocity ($<10\,\mathrm{km\,s^{-1}}$) in the effective temperature T_{eff} range 8 100–10 550 K. The iron abundance was found to increase with effective temperature, with similar abundance dependencies found for

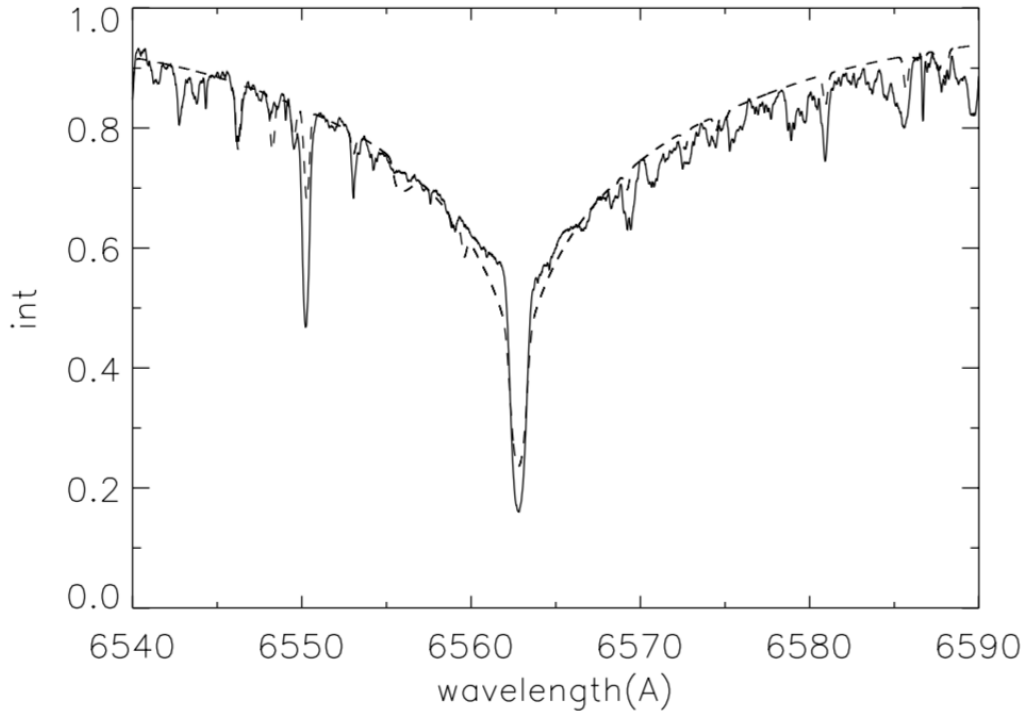

Figure 1.12: The H_α line of HD 166473 showing the core-wing anomaly. This anomaly manifests itself as a narrow central core to the line typical of a stellar atmosphere with an effective temperature near 5 500 K with broad wings more typical of an effective temperature of about 7 700 K (Cowley et al. 2001; Kochukhov et al. 2002). The dotted line is a synthetic spectrum generated using SYNTH (Piskunov 1992) with $T_{\rm eff} = 7\,700$ K for HD 166473, clearly demonstrating the abnormally narrow and deep line core (Kurtz et al. 2003).

Cr, Mn, Nd and Gd. The paper includes the measured absorption line wavelengths, equivalent widths, associated oscillator strengths, atomic data, together with derived abundances, for each Ap star, allowing a means to compare how the IDL routines described in this thesis perform in measuring equivalent widths automatically and generating associated abundances.

Freyhammer et al. (2008) discovered 17 sharp–lined magnetic Ap stars showing resolved Zeeman components from which magnetic fields in the range 3–30 kG were derived. Furthermore, abundance analyses of elements Fe, Cr, Nd, Pr and Eu were performed using fundamental parameters derived on the basis of photometric studies (Martinez 1993), and utilising FEROS spectra which were part of the dataset also used as the basis of this work.

The discovery of oscillations in HD 101065 by Kurtz (1978) led to the classification of a new sub–group of chemically peculiar objects: the rapidly oscillating Ap (roAp) stars. These stars typically have an effective temperature $T_{\rm eff}$ in the range 6 400–8 400 K, somewhat cooler than the non–oscillating Ap stars, though with some temperature overlap between the two groups (Ryabchikova et al. 2004). Comparative abundance analyses of six roAp and six Ap stars by Ryabchikova et al. (2001) consistently showed an anomaly apparent only from the roAp spectra with regard to the derived abundances of the Nd II–Nd III and Pr II–Pr III rare earth species. In each case, the abundance derived from the second ion was in the region of 1.5–2 dex higher than that derived from the first, a phenomenon known as the rare earth element (REE) ionisation disequilibrium anomaly (Ryabchikova et al. 2004). Of the six Ap stars, two of them; HD 62140 and HD 115708, also showed this anomaly, and the argument was put forward that these two may in fact be pulsating stars. The other four Ap stars showed virtually no sign of this REE ionisation disequilibrium. The same REE disequilibrium was also seen in roAp stars HD 101065 (Cowley et al. 2000), HD 122970 (Ryabchikova et al. 2000) and HD 213637 (Kochukhov 2003).

Ryabchikova et al. (2000) suggested that in the cooler roAp stars the REE anomaly may be the result of stratification.

Ryabchikova et al. (2004) considered the abundance analyses for 23 Ap stars, 13 cooler roAp stars and 4 roAp candidates, across the temperature range from 6 400 K to 10 000 K. A plot of abundance differences of the first and second ions of Nd and Pr versus T_{eff} show a marked drop from around 1.5 dex for the roAp stars, to a negligible value for the Ap stars, with a transition temperature around 8100 K, suggesting that the rare earth element anomaly may be a distinguishing feature that separates roAp and Ap stars; See Fig. 1.13. However, Kurtz et al. (2011) showed that the low-amplitude roAp star KIC 10195926 does not have strongly overabundant rare earth elements, hence no apparent disequilibrium between ionization stages. One of the objectives of this research is to test whether rare earth element ionization disequilibrium is a signature of the pulsating roAp stars, or instead is correlated with T_{eff}. Analysis over such a large survey of Ap targets has allowed us to come to some conclusions about this.

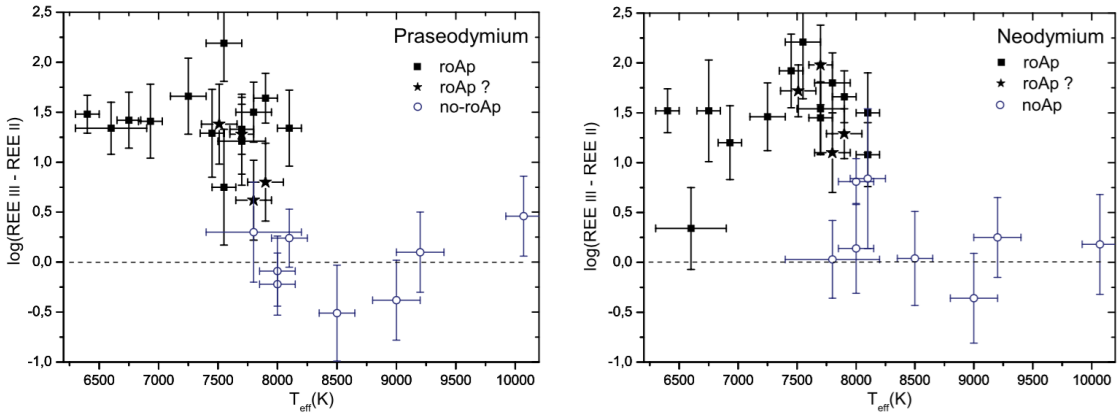

Figure 1.13: Dependence of the Pr (left panel) and Nd (right panel) anomaly on temperature (Ryabchikova et al. 2004)

Chapter 2

Model Atmospheres and Abundance Analysis

2.1 Introduction

Model atmospheres are mathematical constructions; they are a set of equations that attempt, using the laws of physics, approximations and boundary conditions, to derive the physical conditions of an internal stellar atmosphere, based on the fundamental parameters that are determined from astronomical observation, such as effective temperature $T_{\rm eff}$, surface gravity $\log g$, luminosity, metallicity. By the early 1920s, the mathematical tools for modelling stellar interiors had been developed, though there were still two major barriers to a quantitative treatment. Firstly, opacities of the stellar components were poorly understood, since the theory of quantum states and interaction of radiation with matter had not been developed. Secondly, the source of the energy carried away in starlight was unknown. The publication of Eddington's Internal Constitution of the Stars in 1926 circumvented some of these limitations through physical reasoning combined with mathematical analysis (Eddington 1926). 'The Physics of Stellar Atmospheres'' (Unsöld 1938)

demonstrated significant progress on the question of calculated opacities, and just over a decade later, the first computational model atmospheres began to appear (Strömgren 1948; Pecker 1951). These models incorporated the principles of hydrostatic and radiative equilibrium, and while conservation of radiative flux was beyond the computational capabilities of the time, the introduction of the concept of local thermodynamic equilibrium (LTE) by Schwarzschild earlier in 1914 simplified the calculations (Menzel & Milne 1966). The resulting classical models provided a basis for a qualitative understanding of spectral classification and an approximate determination of the fundamental parameters $T_{\rm eff}$ and $\log g$, but were not capable of modelling absorption lines. In 1950, Chandrasekar's book titled Radiative Transfer (Chandrasekhar 1950) provided some powerful techniques for handling monochromatic radiation in atmospheres, whilst further publications summarised the extent of development of the mathematical techniques, and physical theory (Kourganoff 1952; van der Riet Woolley & Stibbs 1953). The widespread introduction of the computer in the 1960s greatly assisted in the development of more complex stellar models. The ATLAS grid of model atmospheres for a range of stellar conditions, still widely used, was first introduced in 1970 (Kurucz 1970) with the simplification of plane parallel atmospheres, and the handling of opacity via the opacity distribution function, where the model is split into sections and the absorption probabilities are simplified into a single function.

The original code was then significantly modified and enhanced over the years. The NEMO model atmospheres employed in this research (Heiter et al. 2002) comprises several sets of grids of model stellar atmospheres computed with modified versions of the ATLAS code. Each individual set consists of several grids of models with different metallicities. The individual sets differ from each other and from previous ones essentially in the physics used for the treatment of the convective energy transport, in the higher vertical resolution of the atmospheres and in a finer grid in

the $(T_{\rm eff}/\log g)$ plane.

2.2 The Working Model Atmosphere

The development of a working stellar model atmosphere requires the ability to calculate the pressure, temperature, density and the energy distribution of photons at each location within the star. For the simplest models, the approach is as follows: firstly, one calculates the flow of radiation through the stellar atmosphere, for a star of given assumed atmospheric structure. Then, having calculated the radiation flux through each layer of the star, the assumed atmospheric structure is corrected to ensure that energy transfer at each stratum within the star is conserved. This structure is then used to correct the radiation field, and the process is repeated iteratively until a self-consistent structure for the model atmosphere is found. The process is illustrated schematically in Fig. 2.1.

For the classical models such as ATLAS, and NEMO; in order to facilitate this process, a number of assumptions and simplifications are made:

- Plane-parallel geometry. Since only the outer regions of a star are of interest in stellar modelling, then if the thickness of the atmosphere is assumed to be small compared to the radius of the star, all of the physical quantities being calculated then depend only on the geometric depth within the atmosphere. This also allows the surface gravity g to be assumed to be constant within the stellar atmosphere.

- Spherical symmetry. There are assumed to be no granulations or spots on the stellar surface; there are no magnetic fields.

- The atmosphere is in hydrostatic equilibrium. In other words, at every point within the stellar model, the surface gravity is balanced by the external pressure caused by the energy release due to nuclear reactions.

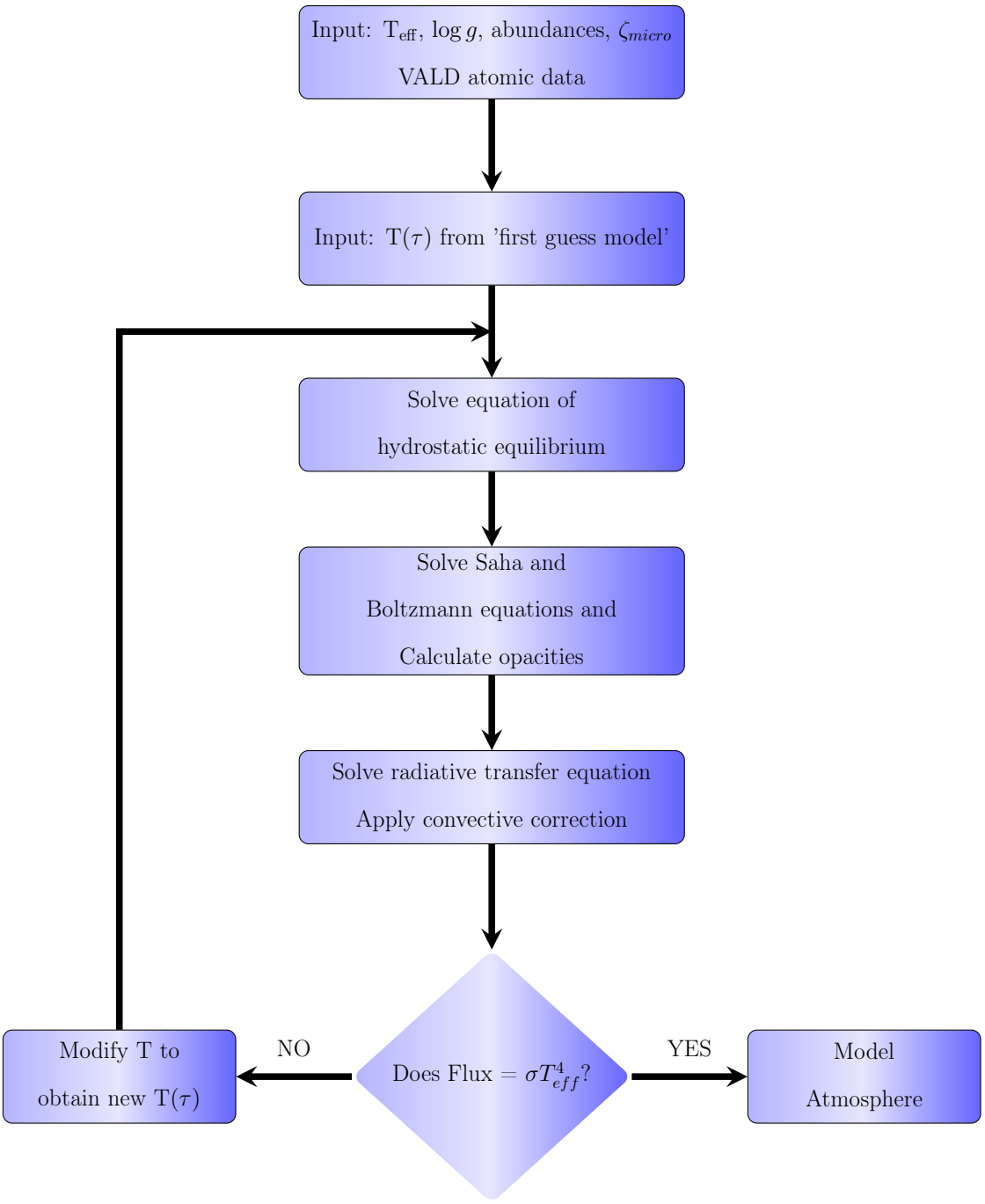

Figure 2.1: Flowchart showing the derivation of a simple stellar model.

- Energy transport is assumed to take place only via radiation or convection.
- Local thermodynamic equilibrium is assumed. This allows the calculated temperature and number density of particles to be used to solve the Saha equation

to give the ionisation fraction of each species. The Boltzmann equation can then be solved to obtain the populations of species within each populated energy level, leading on to a derivation of the opacity applicable to each layer.

- The atmosphere is time independent; that is to say, no evolutionary processes are considered in the model.
- There are no sources or sinks of energy. Thus the total flux at each layer within the atmosphere is constant.

Classical model atmospheres are typically fully constrained by the luminosity L, the radius R, and the metallicity [Fe/H]. A further parameter, the microturbulence, denoted by ζ_{micro}, representing a Gaussian distribution of small-scale velocities of convective elements along the line of sight is often included. L and R are typically replaced by the effective temperature $T_{\rm eff}$ and the log of the surface gravity $\log g$. Surface gravity determines the pressure profile within the stellar atmosphere via the equation of hydrostatic equilibrium, whereas the effective temperature determines the integrated flux at the stellar surface.

Stellar atmospheric models typically comprise sets of tables for each combination of these four parameters, specifying the temperature, pressure and density as a function of optical depth. Typically, stellar model atmospheres are divided into 70–100 layers, such that the optical depth is sampled from approximately 10^{-8} to 10^{3}. A discussion of the physical concepts in such a model now follows, based on derivations and formulae to be found in Gray (2005); LeBlanc (2010).

2.3 The Equation of Hydrostatic Equilibrium

In a stellar atmosphere, the gravitational force acting on the plasma at a given location due to the weight of material above it is balanced by the pressure gradient at the point. Consider the volume of the stellar atmosphere depicted in Fig. 2.2.

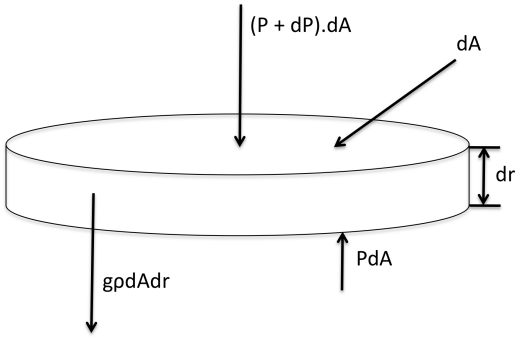

Figure 2.2: The forces acting on a mass element of stellar atmosphere of thickness dr and area dA.

Assuming the star to have spherical symmetry, and that the net force acting on the volume is zero (i.e. at equilibrium), then the difference in force between the upper and lower surfaces of the volume may be expressed as:

$$P(r)\,dA - [P(r) + dP(r)]\,dA - \rho(r)\,dA\,dr\,g(r) = 0$$

where P(r) is the gas pressure on the surface of the element of area dA; $\rho(r)$ is the gas density, and g(r) is the acceleration due to gravity in the direction $-$r, all as a function of the distance r from the centre of the star.
Rearranging, we obtain the equation of hydrostatic equilibrium:

$$\frac{dP(r)}{dr} = -\rho(r)\,g(r)$$

We know that the optical depth τ_ν as a function of optical frequency ν , and distance through the medium r is related to the density ρ and the opacity κ_ν by the expression

$d\tau_\nu = \kappa_\nu \, \rho \, dr$, so this allows us to re-write the hydrostatic equation as:

$$\frac{dP(r)}{d\tau_\nu} = \frac{g}{\kappa_\nu}$$

Once the pressure dependency with depth is known, then the number density of particles at a particular depth may be calculated for a particular assumed local temperature. This can in turn be used to solve the Saha equation to give the ionisation fractions of species present, and the Boltzmann equations are then solved to determine the populations of each of the energy levels of these species. From this the monochromatic opacity spectrum can be calculated, using opacity data loaded into the model. The solution of this equation is crucial to the development of a working model stellar atmosphere.

2.4 The Radiative Transfer Equation

For a beam of radiation of specific intensity I_ν crossing an element of matter (such as a region of stellar atmosphere) of area dA and thickness ds, and of monochromatic opacity k_ν (frequency–dependent), between the solid angles Ω and Ω + dΩ, the energy loss dE_ν (due to absorption or scattering) between the frequencies ν and $\nu + \mathrm{d}\nu$ during time dt is given by:

$$dE_\nu(\text{lost}) = k_\nu \rho I_\nu d\Omega \, d\nu \, dt \, dA \, ds$$

This situation is illustrated schematically in Fig. 2.3. Similarly, we may derive an equation for the energy gained as the beam traverses the element of atmosphere, due in this case to emission or scattering into the beam. In this case, we denote an emissivity coefficient (also frequency dependent) j_ν. In this case:

$$dE_\nu(\text{gained}) = j_\nu \rho d\Omega \, d\nu \, dt \, dA \, ds$$

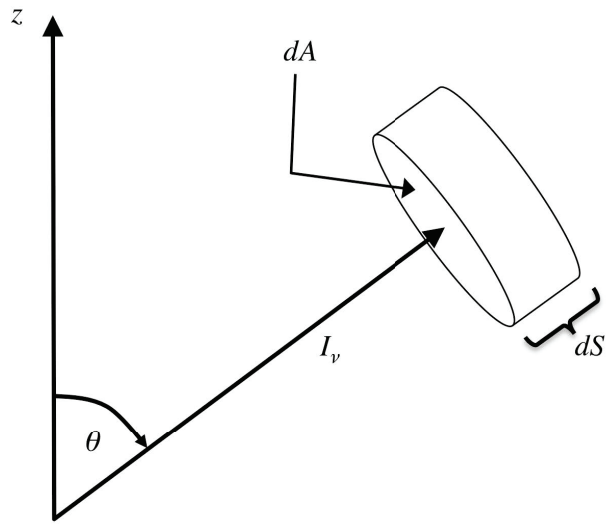

Figure 2.3: Schematic diagram illustrating a beam of radiation defined by the specific intensity I_ν at an angle θ with respect to the direction of the observer z incident perpendicular to the surface dA of an element of volume $dAdS$.

Subtraction of the two gives the net energy emitted:

$$dE_\nu(\text{emitted}) = -j_\nu \rho d\Omega \, d\nu \, dt \, dA \, ds + k_\nu \rho I_\nu d\Omega \, d\nu \, dt \, dA \, ds$$

We also introduce the variable $u = cos\,\theta$ to take account of the fact that the path length ds through the element will be greater than dz when $\theta > 0$. Thus since ds = dz/u we can rearrange the above equation to give:

$$\frac{u}{\rho}\frac{dI_\nu}{dz} = -k_\nu I_\nu + j_\nu$$

which is known as the radiative transfer equation. This equation relates the first term, the variation of specific intensity as it traverses the path, to the radiation subtracted by absorption processes (the first term on the right hand side), and radiation added by emission and scattering processes. It is the solution of this equation for the

conditions and geometry of a stellar atmosphere which allows a model atmosphere to be created, by building up the depth dependence of the physical variables such as temperature T, ρ, electron density, which define the structure of a stellar atmosphere.

If we then replace the distance z, which represents the geometric depth through the stellar atmosphere, with a variable τ called the optical depth, defined such that:

$$d\tau_\nu = -k_\nu \rho dz$$

then rearranging:

$$u\frac{dI_\nu}{d\tau_\nu} = I_\nu - \frac{j_\nu}{k_\nu}$$

The specific intensity is now expressed as a function of optical depth. Optical depth is a measure of the opaqueness of a medium at a given frequency; it is nil at the surface of a star, increasing with geometric depth. Regions where τ is < 1 are said to be optically thin; the mean free path of the photons between scattering/absorption events is said to be large. On the other hand, regions where τ is $\gg 1$ are said to be optically thick and the photon mean free path is considerably reduced. If we also define a source function S_ν as the ratio of the emissivity and absorption opacity:

$$S_\nu = \frac{j_\nu}{k_\nu}$$

then we can re-write the radiative transfer equation as (Gray 2005, chap. 7):

$$u\frac{dI_\nu}{d\tau_\nu} = I_\nu - S_\nu$$

It is the solution of this equation for the geometry of a star which allows model atmospheres to be constructed, and which we use for the abundance analysis process. In particular, a profile of the temperature dependence with depth, within the

atmosphere will allow the determination of physical conditions in that region. In order to accomplish this, some basic assumptions are made:

- Local thermodynamic equilibrium is maintained throughout the atmosphere. That is to say, the populations of the atomic energy levels and of the ionic species are determined, at least at a local level, solely by collisions within the plasma. This allows Maxwell–Boltzmann and Saha equations to be used to calculate the relative distribution of these species, both in terms of the population of the energy levels with an ion (Maxwell-Boltzmann), and the distribution of ions within each element (Saha), which in turn have a profound effect on the opacity functions used within the model. It also allows the radiative region to be treated as a blackbody, such that the source function in the above equation can be represented by the Planck function B_T, where:

$$B_T \, d\nu = \frac{2h\nu^3}{c^3} \frac{1}{e^{\frac{h\nu}{kT}} - 1} d\nu$$

  where in this case, k is the Boltzmann constant, not the opacity.

- In stellar plasmas, the frequency dependence of the opacity is extremely complex in nature. In practice, a compromise is often reached whereby a Rosseland opacity is calculated, which also uses empirical data from the measured radiative opacities of atomic species; these are fed into the model atmosphere.

- Other mechanisms of energy transfer, such as convection, are ignored in the first instance. The contribution of energy transfer via such processes is built into the model at a later stage via a 'mixing–length' formula.

- The radiative flux is at equilibrium. That is to say, the integrated flux F, which is an integration of the specific intensity over the whole sphere, for a given spherical shell within the atmosphere, is the same as for any other shell, deeper or shallower within the shell. Is is given by Stefan's Law for a black body:

$$F = \sigma T_{\text{eff}}^4$$

  where σ is the Stefan-Boltzmann constant.

- Evolutionary effects are ignored. In other words, the equations are assumed to be time-independent.

From this the variation of temperature in a model star with optical depth can be derived (Gray 2005):

$$T(\tau) = \left[\frac{3}{4}\left(\tau + \frac{2}{3}\right)\right]^{\frac{1}{4}} T_{\text{eff}}$$

A further simplification in the derivation of a model atmosphere may be made by assuming that the opacity is frequency-independent, known as the grey atmosphere or grey case. Rigorous solutions of the grey case (Chandrasekhar 1957) lead to an equation of the same form:

$$T(\tau) = \left[\frac{3}{4}\left(\tau + q(\tau)\right)\right]^{\frac{1}{4}} T_{\text{eff}}$$

where $q(\tau)$ is a slowly varying function ranging from 0.577 at $\tau = 0$ to 0.710 at $\tau = \infty$. A comparison of the temperature profile of a grey atmosphere in comparison with a model atmosphere with $\mathrm{T_{eff}} = 10\,000\,\mathrm{K}$, $\log g = 4.0$ and solar abundances is shown in Fig. 2.4.

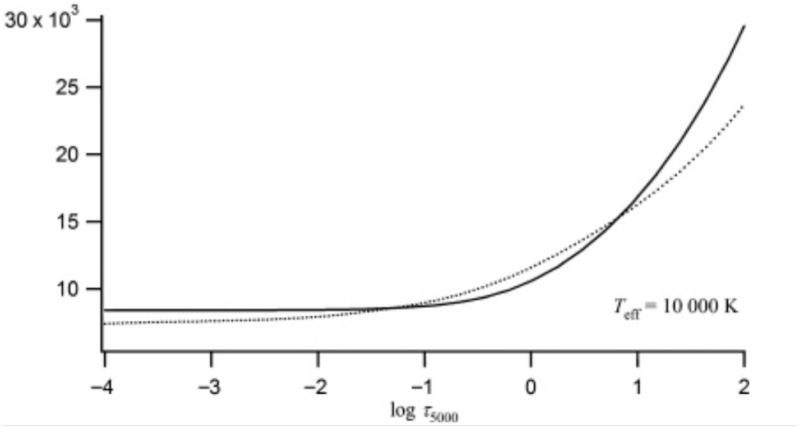

Figure 2.4: Temperature profile of an atmospheric model with $T_{\rm eff} = 10\,000$ K, $\log g = 4.0$ and solar abundances (solid lines) compared with the one for a grey atmosphere (dotted line), as a function of the optical depth τ calculated at 5000 Å. (LeBlanc 2010).

Enhancements to this approach are achieved by treating each wavelength separately and calculating its own emission coefficient and opacity. This approach then allows the calculation of the populations and energy states of the constituent stellar particles through application of the principle of Local Thermodynamic Equilibrium, and application of the Saha and Stefan–Boltzmann equations.

2.5 The Treatment of Convection in Stellar Models

The plasma within a stellar atmosphere is subject to macroscopic currents. Convection within this region may be modelled if certain limitations and assumptions are made. Under certain conditions, transport of energy via convection may occur via the displacement of a plasma cell either towards or away from the stellar surface. Cool stars, including Ap stars, have deep convective envelopes that extend for a significant proportion of the stellar radius, up into the bottom of the photosphere, and the convection process occurs because a moving cell of plasma may contain an

excess or deficit of energy compared to the surrounding material, resulting in energy transfer through the medium. Key to the energy transfer process is that the plasma cell must have sufficient optical density to prevent loss of energy by radiative means. In situations where the radiative flux, or the opacity or both, are very large, this leads to a significant temperature gradient, and when the temperature gradient exceeds a certain value, the onset of convection occurs. The point at which this process occurs theoretically is known as the Schwarzschild Criterion (Schwarzschild 1906), and makes the assumptions that the plasma cell behaves adiabatically (i.e. no heat transfer occurs between the plasma cell and the surrounding plasma). Fig. 2.5 schematically illustrates a cell of plasma rising adiabatically within the stellar atmosphere. If a plasma cell is displaced within the photosphere by a distance Δr, then the cell will continue to rise to the surface, so long as the density of the cell is lower than that of the surrounding medium. If pressure equilibrium is maintained between the cell contents and its surroundings during its ascension upwards, then the density within the cell during this displacement will decrease. If this density decreases at a faster rate with respect to displacement r than that of the surrounding medium, then the buoyancy of the cell is maintained and convection occurs.

The density change within the cell $\Delta\rho_{cell}$ may be expressed as :

$$\Delta\rho_{\mathrm{cell}} = \left(\frac{d\rho}{dr}\right)_{\mathrm{adi}} \Delta r < 0$$

where $\left(\frac{d\rho}{dr}\right)_{\mathrm{adi}}$ represents the density gradient during the adiabatic process. Simultaneously, the density of the surrounding medium changes over the same distance by $\Delta\rho_{\mathrm{avg}}$.

$$\Delta\rho_{\mathrm{avg}} = \left(\frac{d\rho}{dr}\right)_{\mathrm{rad}} \Delta r < 0$$

where $\left(\frac{d\rho}{dr}\right)_{\mathrm{rad}}$ represents the density gradient of the surrounding medium that is

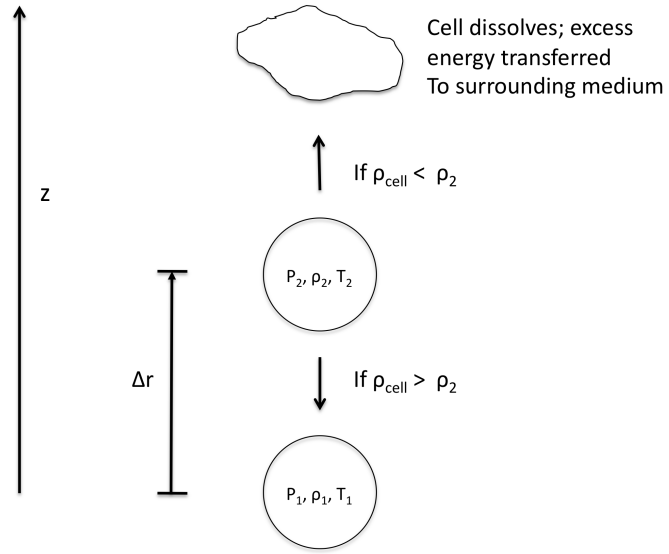

Figure 2.5: Schematic view of the convection process

in radiative equilibrium. This leads to the criterion that onset of convection may be expressed as :

$$\left(\frac{d\rho}{dr}\right)_{\text{adi}} < \left(\frac{d\rho}{dr}\right)_{\text{rad}}$$

When an ideal gas expands adiabatically, the thermodynamic gas law relates the gas pressure P to the density ρ by the following relation:

$$P \propto \rho^{\gamma} \tag{2.1}$$

where

$$\gamma = \frac{C_p}{C_v}$$

defines the ratio of the specific heat capacities of the gas at constant pressure C_p, and constant volume C_v. From Eq. (2.1) it can be seen that for an adiabatic ideal gas, the pressure is proportional to a power of the density i.e. $\ln \mathrm{P} \propto \ln \rho$, so we can replace (2.1) with:

$$\left(\frac{d\ln\rho}{dr}\right)_{\text{adi}} < \left(\frac{d\ln\rho}{dr}\right)_{\text{rad}} \tag{2.2}$$

Differentiating (2.1) with respect to r we obtain:

$$\left(\frac{d\ln\rho}{dr}\right)_{\text{adi}} = \frac{1}{\gamma}\left(\frac{d\ln P}{dr}\right)_{\text{adi}}$$

However, in the radiative zone, the equation of state follows the ideal gas law and gives the relation $P \propto \rho T$. Rearranging and differentiating with respect to r yields:

$$\left(\frac{d\ln\rho}{dr}\right)_{\text{rad}} = \left(\frac{d\ln P}{dr}\right)_{\text{rad}} - \left(\frac{d\ln T}{dr}\right)_{\text{rad}}$$

and the Schwarzschild convection criterion (2.2) may be rearranged:

$$\frac{1}{\gamma}\left(\frac{d\ln P}{dr}\right)_{\text{adi}} < \left(\frac{d\ln P}{dr}\right)_{\text{rad}} - \left(\frac{d\ln T}{dr}\right)_{\text{rad}} \tag{2.3}$$

As the cell ascends, the pressure in the cell is assumed to be the same as the surroundings; hence:

$$\left(\frac{d\ln P}{dr}\right)_{\text{adi}} = \left(\frac{d\ln P}{dr}\right)_{\text{rad}}$$

and equation (2.3) may be written as:

$$\left(\frac{1}{\gamma} - 1\right)\left(\frac{d\ln P}{dr}\right)_{\text{rad}} < -\left(\frac{d\ln T}{dr}\right)_{\text{rad}}$$

or rearranging:

$$\left(\frac{\gamma-1}{\gamma}\right) < \frac{\left(\frac{d\ln T}{dr}\right)_{\text{rad}}}{\left(\frac{d\ln P}{dr}\right)_{\text{rad}}} = \left(\frac{d\ln T}{d\ln P}\right)_{\text{rad}} = \bigtriangledown_{\text{rad}}$$

where $\bigtriangledown_{rad}$ denotes the temperature gradient in the radiative zone. As stated previously, for the cell expanding adiabatically, $P \propto \rho^{\gamma}$, or $T \propto P^{\frac{\gamma-1}{\gamma}}$ and so the temperature gradient for an adiabatic process (within the cell) can be written:

$$\bigtriangledown_{adi} = \left(\frac{d\ln T}{d\ln T}\right)_{\rm adi} = \left(\frac{\gamma-1}{\gamma}\right)$$

Finally, the Schwarzschild criterion for convection can be summarised:

$$\bigtriangledown_{\rm rad} > \bigtriangledown_{\rm adi} = \left(\frac{\gamma-1}{\gamma}\right)$$

For an ideal monatomic gas, $\gamma = \frac{5}{3}$ and $\bigtriangledown_{\rm adi} = 0.4$, so the Schwarzschild criterion is $\bigtriangledown_{\rm rad} > 0.4$. In hot stars ($\rm T_{eff} > 10\,000\,K$), $\gamma \sim \frac{5}{3}$ and convection tends to be negligible. For cooler stars, γ tends to be much smaller, promoting the onset of convection.

If we take the gas law in the form $P = (\rho/\mu)kT$ where μ is the mean molecular weight, then we can write:

$$\left(\frac{d\ln\rho}{d\ln P}\right)_{\rm avg} = 1 + \frac{d\ln\mu}{d\ln P} - \frac{d\ln T}{d\ln P}$$

2.5.1 The Mixing-Length Theory

The Schwarzschild criterion provides a basis for the conditions under which convection can occur. However, it says nothing about how efficient this is as an energy transport process. The flux Φ carried by convection by a cell may be expressed in terms of the temperature excess ΔT of the cell over and above its surroundings, the specific heat capacity at constant pressure C_p, the cell density ρ, and the upward velocity v of the cell (Gray 2005):

$$\Phi = \rho\, C_p\, v\, \Delta T \tag{2.4}$$

Equation (2.4) summarises the expression by which inclusion of the convection process in the modelling of stellar photospheres is done (Biermann 1932; Öpik 1950; Vitense 1953)

If $\Delta\rho$ is the average difference in density of the convective cell compared to its surroundings, then by mechanical conservation:

$$\frac{1}{2}\rho v^2 = g\Delta\rho l$$

where l is denoted as the mixing length, i.e. the distance over which the cell survives. Assuming pressure equilibrium, $\Delta\rho/\rho = \Delta T/T$ and we then have

$$v = g^{\frac{1}{2}}\, l^{\frac{1}{2}} (\Delta T/T)^{\frac{1}{2}}$$

The convective flux can then be written as:

$$\Phi = \rho\, C_p \left(\frac{gl}{T}\right)^{\frac{1}{2}} \Delta T^{\frac{3}{2}}$$

Expressed in terms of temperature gradients:

$$\Phi = \rho\, C_p \left(\frac{g}{T}\right)^{\frac{1}{2}} l^2 \left[\left(\frac{dT}{dx}\right)_{\text{cell}} - \left(\frac{dT}{dx}\right)_{\text{average}}\right]^{\frac{3}{2}} \tag{2.5}$$

The mixing length l may be thought of as the average distance travelled by a convective cell before it dissolves. The values used in the photospheric models are arbitrary, a typical value of ~ 1.5 scale height is used.

Modern atmospheric models are somewhat more sophisticated, and incorporate other effects such as turbulent mixing. It is their incorporation alongside measurements of equivalent widths of spectral absorption lines of a species that allow us to derive elemental abundances. For this survey, we have used the NEMO model atmospheres provided by the Department of Astronomy of the University of Vienna (Heiter et al. 2002). These models, derived from the earlier ATLAS models, predict a much lower level of efficiency in terms of energy transport by convection. Convective

flux is also neglected for temperatures $> 8\,600$K. The models replace Mixing Length Theory (MLT) with an approach known as Full Spectrum Turbulence (FST). A diffusion approximation is introduced to describe the convective flux, to take account of the fact that convection penetrates into neighbouring stable regions, leading to an additional term in the scale length, and is found to give a better overall agreement with observations, when compared with ATLAS models.

2.6 Theory of Curve of Growth

Analysis of absorption lines in the spectra of stars provides a wealth of information relating to the star's rotation, effective temperature, pressure, and chemical composition of the line-forming region of the atmosphere. The intensity I_λ(z) at a distance z from the origin of the radiation at 0 is given by (Gray 2005):

$$I_\lambda(z) = I_\lambda(0)e^{-\tau_\lambda} \tag{2.6}$$

where τ_λ represents the optical depth (wavelength-dependent) which is given by the expression:

$$\tau_\lambda = \int_0^s \kappa_\lambda \rho ds = \int_0^s n\sigma_\lambda ds \tag{2.7}$$

where n represents the number density of absorbing species, σ_λ is the cross–section associated with the bound-bound transition for the absorption line. If the equivalent width W_λ is then defined as the width of a rectangular strip of spectrum having the same area as the absorption line:

$$W_\lambda = \int_{-\infty}^{\infty} \frac{I_\lambda(0) - I_\lambda}{I_\lambda(0)}, \tag{2.8}$$

the cross section for absorption σ_λ in equation 2.7 can be written as:

$$\sigma_\lambda = \sigma_0.\Phi \tag{2.9}$$

where:

$$\sigma_0 = \frac{\lambda^4}{8\pi c}\frac{g_u}{g_l}a_{ul}$$

where g_u, g_l represent the degeneracy of the upper and lower transition levels respectively, and a_{ul} is the transition probability. Φ is the broadening function, defined so that if an absorption does take place in the line, $\Phi\,\mathrm{d}\lambda$ is the probability that the wavelength of the absorbed photon lies between λ and $\lambda + d\lambda$. In other words:

$$\int_{-\infty}^{\infty} \Phi_\lambda d\lambda = 1$$

The value of Φ is large near the line centre, but falls off rapidly with displacement to either side.

In stellar atmospheres, there are three main contributions to the broadening of stellar lines: natural broadening, due to the uncertainty in the upper energy level of the electronic transition; Doppler broadening, due to the relative velocities of the absorbing species, and pressure broadening, due to collisions with neutral species, typically hydrogen.

For natural broadening, for an atom at rest, we have:

$$\phi_\lambda = \frac{1}{\pi}\frac{\delta_k}{{\delta_k}^2 + [\lambda - \lambda_0]^2} \tag{2.10}$$

where δ_k is the radiation damping constant given by:

$$\delta_k = \frac{\lambda^2}{4\pi c}\sum_{E_r < E_k} a_{kr}.$$

Thus, the radiation damping constant is inversely proportional to the lifetime of the upper level k.

Pressure broadening also produces a damping profile and produces an increase in the effective damping constant by δ_p given approximately by:

$$\delta_p = \frac{v}{\mu} = \sqrt{\frac{2kT}{m}} n\sigma_c$$

where μ_k is the mean free path, n is the number density and σ_c is the collisional cross–section.

Doppler broadening occurs as a result of the thermal motion of the absorbing species and results in a Maxwellian distribution of velocities:

$$\Phi(v) = \frac{1}{\sqrt{\pi} b_{th}} exp\left[-\frac{(v - v_0)^2}{b_{th}^2}\right] \tag{2.11}$$

where the Doppler width b_{th} is related to the temperature via:

$$b_{th} = \sqrt{\frac{2kT}{m}}$$

Bulk convective motions in the photosphere in regions having different velocities may also give rise to macroturbulence which may be represented distribution of velocities represented by a value b_{macro}. Macroturbulence does not alter the equivalent width, i.e. the area that a line takes up. In contrast, microturbulence is caused by small cells of motion in the photosphere such that photons encounter regions of different velocity, introducing an additional Doppler broadening represented by b_{micro}. The total Doppler broadening may then be represented as a combination of b values as follows:

$$b_{\rm tot}^2 = b_{\rm th}^2 + b_{\rm macro}^2 + b_{\rm micro}^2.$$

If Doppler broadening is now included, we get:

$$\Phi_\lambda = \frac{1}{\pi} \int_{-\infty}^{\infty} \frac{\delta_k'}{{\delta_k'}^2 + [\lambda - \lambda_0(1 + \frac{v}{c})]^2} . \Psi(v)\, dv \tag{2.12}$$

Generally $\delta'_k \ll b$. However, their respective dependencies on wavelength are not the same; the probability of the absorption occurring due to Doppler broadening falls off from the line centre more rapidly than that due to natural broadening. Thus absorption lines tend to have a Doppler core and damping wings.

The complete expression for the line optical depth at wavelength λ is obtained by combining equations to give:

$$\tau_\lambda = N\sigma_0\phi_\lambda \otimes \Psi(v)$$

where N, the column density, which measures the number density of absorbers in a cylinder of unit cross–section, is given by:

$$N = \int_0^x nx\, dx$$

and where the convolution of the Doppler and natural broadening, known as the Voigt function, is given by Eq. (2.12).

These various contributions to the line width are shown in Fig. 2.6. The variation of equivalent width (EQW) of a spectral line with abundance, for a given absorbing species is dependent on the optical depth of the line. There are three phases during line growth. For weak lines, the Doppler core of the line dominates and the equivalent width is proportional to abundance A (1). At greater optical depth, the line depth approaches a maximum value, and the line saturates (2). In this region the equivalent width only depends weakly on abundance.Finally, as the optical depth increases still further, absorption in the line wings become significant, and the equivalent width becomes more strongly dependent on the abundance (3). This behaviour is illustrated above as a 'curve of growth' in Fig. 2.7. In practice, weak lines are used in the analysis since the effect of abundance on equivalent width is optimal.

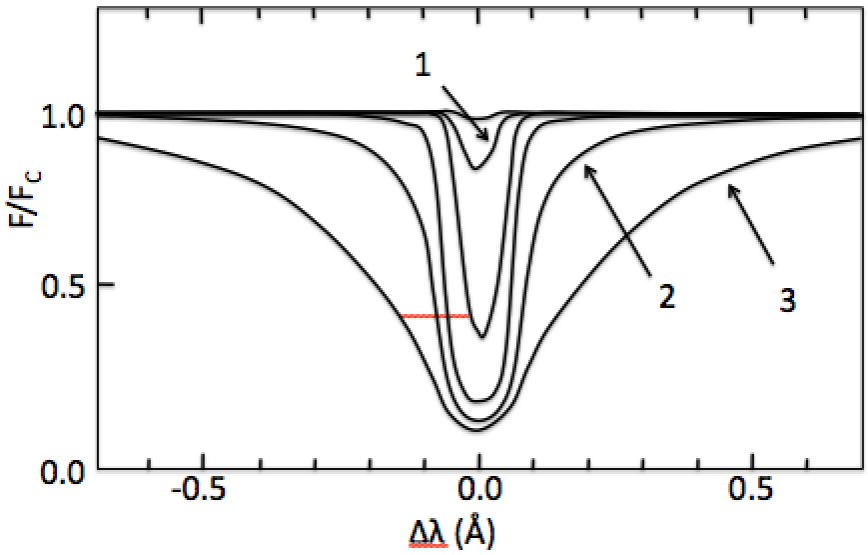

Figure 2.6: The variation of equivalent width (EQW) of a spectral line with abundance. The Doppler core of the line dominates for weak lines (1). At greater optical depth, the line saturates, (2). Finally, as the optical depth increases still further, absorption in the line wings become the dominating influence on EQW (3). (Gray 2005)

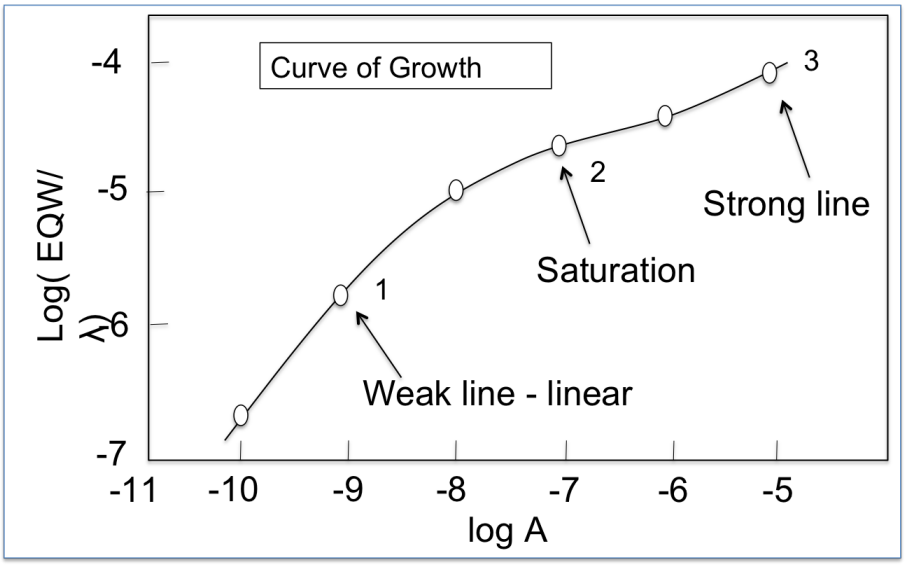

Figure 2.7: A schematic curve of growth representing the the effect on EQW as abundance increases as described in Fig. 2.6 (Gray 2005)

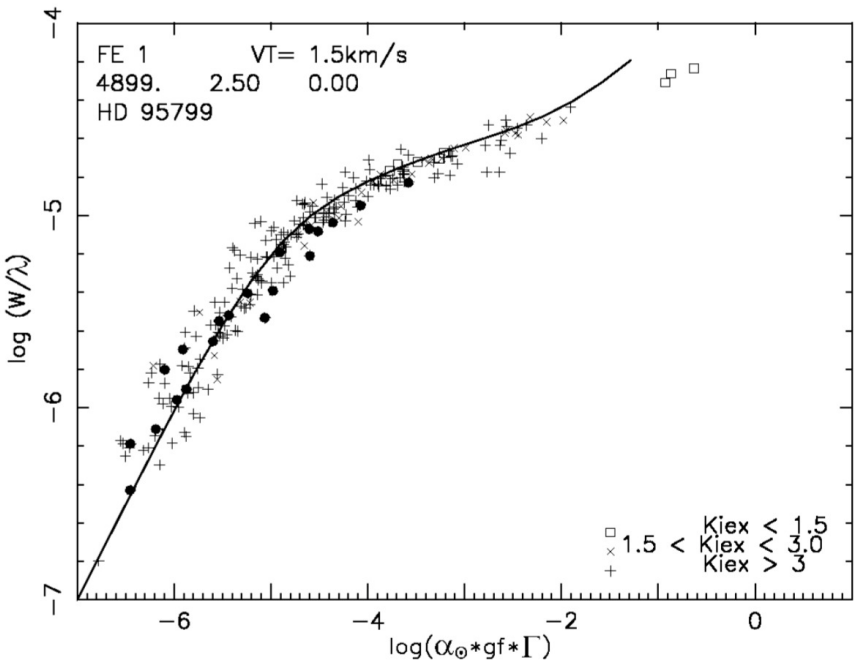

Figure 2.8: Curve of growth of Fe lines for the star HD 95799. Different symbols indicate three ranges of excitation potential. The Fe II lines are represented by filled circles. The full line is a theoretical curve of growth. $\alpha_{\odot}$ is the solar abundance of the element, gf the line transition probability of the line, and Γ is a function of the element and of the stellar model (Castilho et al. 2000)

An example of the experimental curve of growth for Fe II lines for star HD 95799 is shown in Fig. 2.8 (Castilho et al. 2000).

2.7 WIDTH Abundance Analysis Routine

WIDTH is a FORTRAN routine developed by Robert Kurucz for the determination of stellar abundances derived from measured equivalent widths. The program is described in detail by Castelli (2005). For each absorption line selected for analysis in the spectrum of interest, the routine takes the following as input:

- the measured equivalent width and observed wavelength;

- the element associated with the transition and its electronic state;
- physical parameters relating to the transition; oscillator strength; energy level and total electronic angular momentum of the lower and upper levels involved in the transition, together with damping constants. These values are derived from the VALD database (Heiter et al. 2008) for the transition involved, and then supplied to the WIDTH routine.

Data relating to the model atmosphere appropriate to the effective temperature T_{eff} and the log of the surface gravity $\log g$ of the star (derived from Strömgren photometry) are also input to the routine, along with a value for the microturbulence and convective mixing length. The routine then internally computes atomic and molecular number densities, continuous opacities, continuous surface intensities and fluxes, line absorption coefficients, line profiles and equivalent widths. This compares the input measured equivalent width (EQW) with the one computed internally, and then adjusts the abundances until the EQWs match. The WIDTH program makes extensive use of the ATLAS routines to compute appropriate model atmospheres (Nesvacil et al. 2003) which are used in the abundance calculation to calculate the surface fluxes, the surface specific intensities, the continuous absorption coefficients and line opacity. An example input parameter deck for WIDTH is shown in Appendix A. Extensive use is made of the WIDTH program in this research project to derive abundances from the absorption lines of the spectra being analysed. This is described in more detail in the following chapter.

2.8 Magnetic Fields and Star Spots in Ap Stars

The atmospheres of the magnetic Ap stars are characterised by inhomogeneous concentrations of chemical elements over their surface, under the influence of a strong

magnetic field, typically ranging in strength from a few hundred gauss, up to 34.4 kG in the case of Babcock's star HD 215441 (Babcock 1960), the strongest magnetic field yet measured. Magnetic fields can affect elemental stratification through two effects; Zeeman splitting, and the interaction of the magnetic field with the diffusing ions. In the Zeeman effect, the magnetic field causes degenerate energy levels in an ion/atom to be split, with the sub–levels separated by an energy ΔE:

$$\Delta E = \frac{ge\hbar B}{2mc}$$

where e is the electron charge, B is the strength of the magnetic field, m is the mass of the electron. Each energy level is therefore split into 2J + 1 non-degenerate sub-levels characterised by quantum number M. The Landé factor g is evaluated from the expression:

$$g = 1 + \frac{J(J+1) + S(S+1) - L(L+1)}{2J(J+1)}$$

where S, L and J represent the spin–, orbital– and combined angular momentum of the quantum state, respectively (Russell-Saunders or LS coupling is assumed; a reasonable approximation for light atoms). This effect, known as the Zeeman effect, may lead to the splitting of single absorption lines in a spectrum, and such a Zeeman pattern the number of components, relative spacing and intensity depend on the Landé factor, while the scale of the overall pattern is related to the strength of the magnetic field. A set of comparative plots showing the Zeeman splitting of the Fe II line at 6149.2 Å for a selection of the FEROS spectra is shown in Fig. 2.9. Analysis of these effects in 78 Vir (Babcock 1947c) and α^2 CVn (Babcock 1947a) and other stars led Babcock, and independently Stibbs, to propose the oblique rotator model (See see Fig. 1.2). Later observations of periodic spectral and radial velocity variations by Deutsch (1956) reinforced the link between the magnetic fields of these Ap stars, and the spectral anomalies identified in the absorption spectra. Furthermore, selection

rules in place restrict the electronic transitions to those where $\Delta M = 0, \pm 1$, with the resulting lines falling into one of three groups. The lines due to transitions $\Delta M = 0$ (π components) are distributed symmetrically around the unsplit line formed in the absence of a field. The two groups of lines formed by transitions with $\Delta M = \pm 1$ (σ components) are shifted symmetrically about the unsplit line, with transitions of $\Delta M = +1$ on one side and transitions of $\Delta M = -1$ on the other side. The polarisation properties of these σ and π components can be used to give information regarding the orientation of the magnetic field; circular polarisation from the σ components is sensitive to the longitudinal (line-of-sight) component of the magnetic field, whereas linear polarisation (from σ and π components) provide information regarding the transverse component of the magnetic field. Analysing the relative degree of polarisation across line profiles using a polarimeter allows the polarisation state to be represented as a Stokes vector $[I, Q, U, V]$, where I represents the total specific intensity of light in the beam. Q and U describe the linear polarisation of the beam and V describes the circular polarisation of the beam, with each parameter as a temporal average. Spectroscopic and spectropolarimetric observations are repeated in order to resolve the time-dependent phenomena such as rotational modulation. This technique has been used to map horizontal abundance distributions over the stellar surface and reconstruct the surface magnetic field topologies of Ap and Bp stars (Wade et al. 2000; Kochukhov et al. 2010; Rusomarov et al. 2013; Silvester et al. 2014). The cyclic variability of the Zeeman signatures detected over time can be attributed to the off-axis magnetic field being carried around by rotation as described by the oblique rotator model. By modelling the these signatures it becomes possible to recover the parent magnetic topology of the star using tomographic techniques. The technique of combining Zeeman spectropolarimetry and Doppler imaging is called Zeeman-Doppler Imaging (ZDI) (Semel 1989).An example of the technique is

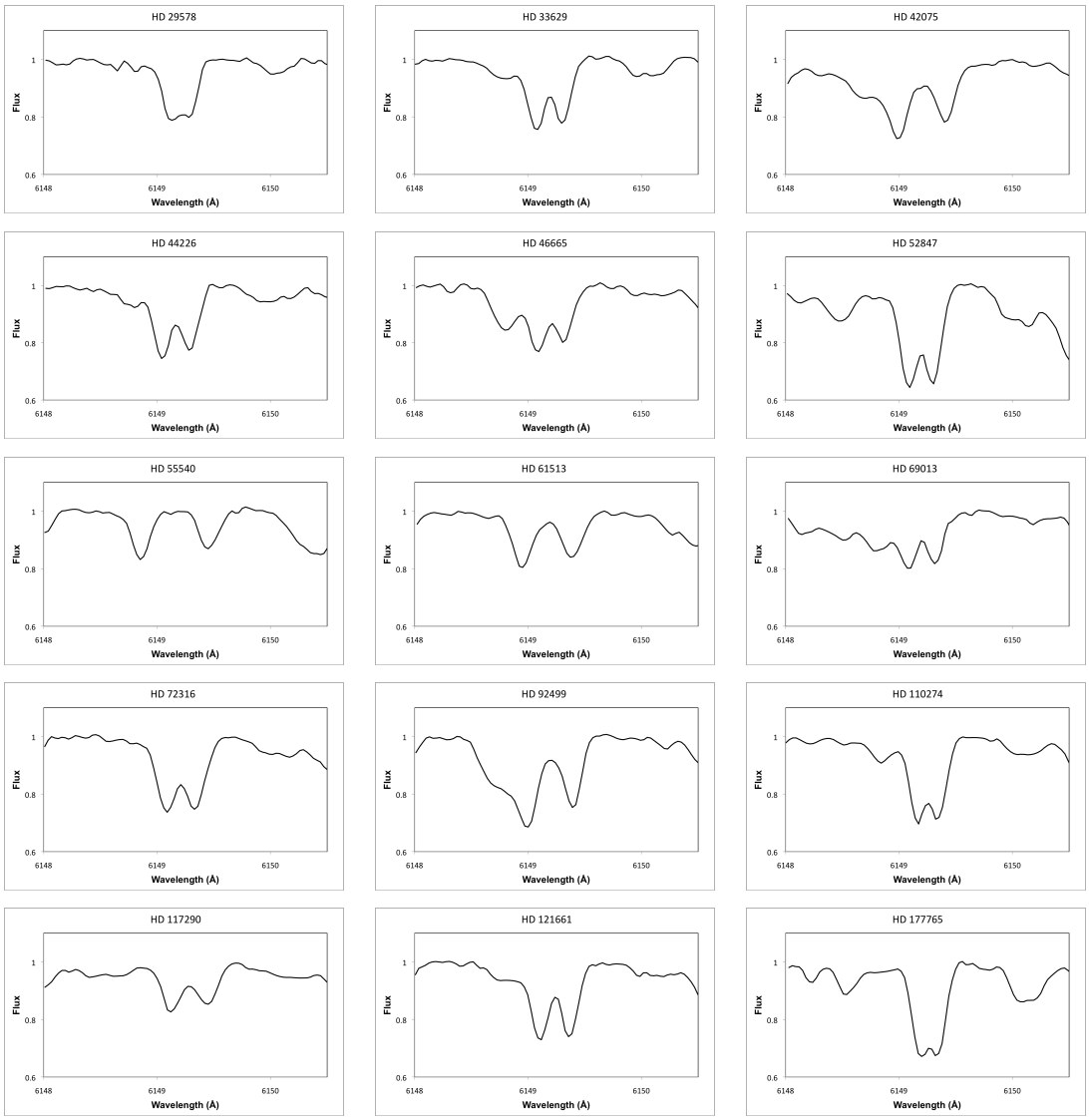

Figure 2.9: Comparison plots showing the magnetically resolved Zeeman splitting of the Fe II line at 6149.2 Å for a selection of the FEROS spectra. The degree of splitting is related to the strength of the magnetic field modulus

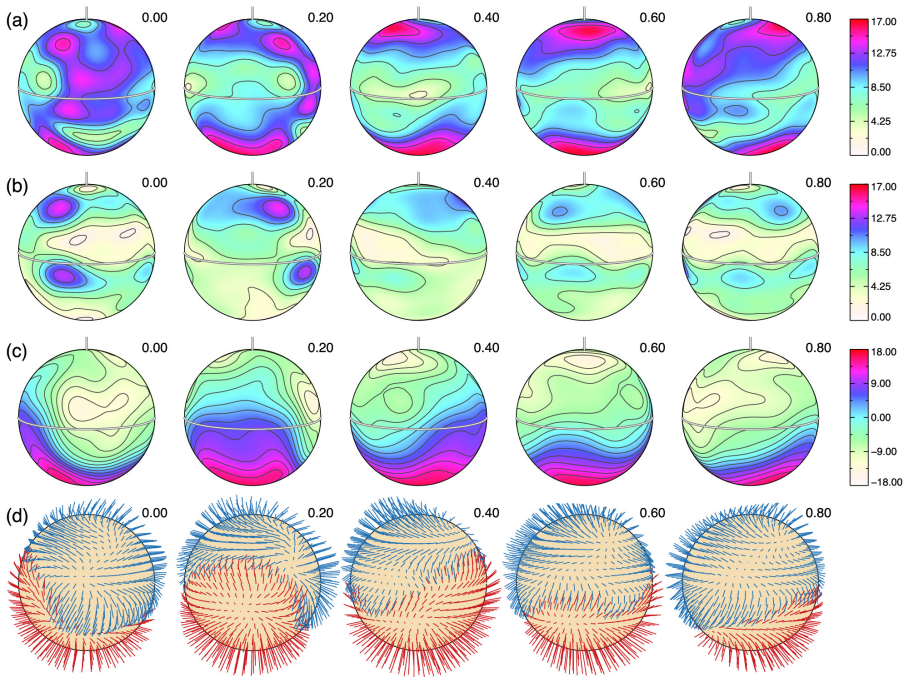

Figure 2.10: Surface magnetic field distribution of Ap star HD 32633 derived using Stokes IQUV computed with INVERS10 (Piskunov & Kochukhov 2002) using a spherical harmonic description of the field topology. The spherical plots (at an inclination angle of $i = 180°$) show distributions of (a) the field modulus, (b) the horizontal field, (c) the radial field and (d) the field orientation. Each column corresponds to a different phase of rotation (0.0, 0.2, 0.4, 0.6 and 0.8) and the colour bars on the right side indicate the magnetic field strength in kG (Silvester et al. 2015)

illustrated in Fig. 2.10.

The abundance anomalies observed in the atmospheres of Ap stars have been explained on the basis of atomic diffusion processes. Quantitative calculations have also been carried out to determine the effect of magnetic field geometry on the atomic diffusion of magnetic Ap stars. For example, Michaud et al. (1981) constructed theoretical magnetic dipole and quadrupole field geometries based on the oblique rotator model to generate synthetic line profiles for 53 Cam and compared them with observed magnetic field generations, assuming simple turbulence properties and vertical radiative acceleration. More recently, Alecian & Stift (2010) have also performed computations based on radiative acceleration of selected elements modelled the 2-D distributions in magnetic atmospheres, resulting in a grid of horizontal and vertical abundance distributions for 16 metals across a range of $T_{\rm eff}$ and magnetic field strengths in stars with a dipolar magnetic field geometry.

As well as the anomalous surface distribution of chemical abundances, Ap stars are also characterised by unusual energy distributions in their spectra; an effect known as line blanketing. The magnetic field effects changes in the atmospheric structure, affecting energy transport, diffusion processes, with magnetic intensification of certain spectral lines, leading to a redistribution of energy in the spectrum, with the UV flux of Ap stars depressed compared to 'normal' stars with a similar flux distribution in the visible region of the spectrum (Leckrone 1973). Kochukhov et al. (2005) computed model atmospheres for Ap stars to take account of magnetic line blanketing, and show that that the effect is most pronounced for stars at the cooler end of the effective temperature range.

Chapter 3

Automating the Abundance Analysis Process

3.1 Introduction

The abundance analysis of the high–resolution absorption spectrum of a star, through the inspection and measurement of the equivalent widths of the atomic absorption lines of the atomic species under consideration across the spectral range, can be a time–consuming process. One typical approach combines the fundamental parameters of the star (the effective temperature $T_{\rm eff}$, the log of the surface gravity $\log g$, and metallicity), usually derived by some independent means such as spectrophotometry, in combination with an appropriate model atmosphere and alongside the characteristics of the electronic transitions within the spectral range (oscillator strength, lower and upper atomic energy levels and term symbols representing the total angular momentum of the atomic state, taken together with damping constants) to create a synthetic spectrum. The abundances are then modified until there is an optimal match between the synthetic and observed spectrum.

A second classical approach takes the equivalent widths (EQWs) measured for

each identified line in the observed spectrum belonging to the ion or ions whose abundances are to be determined, along with the characteristics of the electronic transition, in tandem with the fundamental parameters of the star and an appropriate model atmosphere to derive the relationship between EQW and abundance, and arrive at an average abundance for each of the ions of interest.

This chapter describes our initial approach in using a software package to perform the abundance analysis, and the subsequent development and application of a series of routines written in the IDL programming language to form a semi–automated approach to the abundance analysis process; specifically the inspection of a collection of high–resolution spectra collected on an echelle spectrograph spanning several years to derive a set of abundances for Iron (Fe I and Fe II), and the Rare Earth Elements (REE) Neodymium Nd II / Nd III and Praseodymium Pr II / Pr III.

3.2 The FEROS Observational Survey Data

The survey forming the basis of this thesis is based on a data set of high–resolution spectra collected by Christian Nitschelm of Antagofasta University, Chile, in collaboration with myself, Lars Freyhammer and Vladimir Elkin, as members of Don Kurtz' group at the University of Central Lancashire. The spectral targets were, in turn, selected from an earlier survey, the Cape Survey (Martinez 1993) which was intended as a basis for asteroseismological studies of roAp objects, drawn from the SrCrEu Ap stars of the Michigan Spectral Catalogue. The spectra span the period from 2007 February to 2010 February. For consistency, all of the spectra were recorded on the same spectrograph; ESO's Fibre–fed, cross-dispersed Extended Range, Echelle Spectrograph (FEROS) mounted on the 2.2–m Max Planck Gesellschaft (MPG) telescope based at La Silla, Chile. The opto–mechanical layout of the FEROS spectrograph is shown in Fig. 3.1.

The spectrograph has an accessible spectral wavelength range of 3500–9200 Å

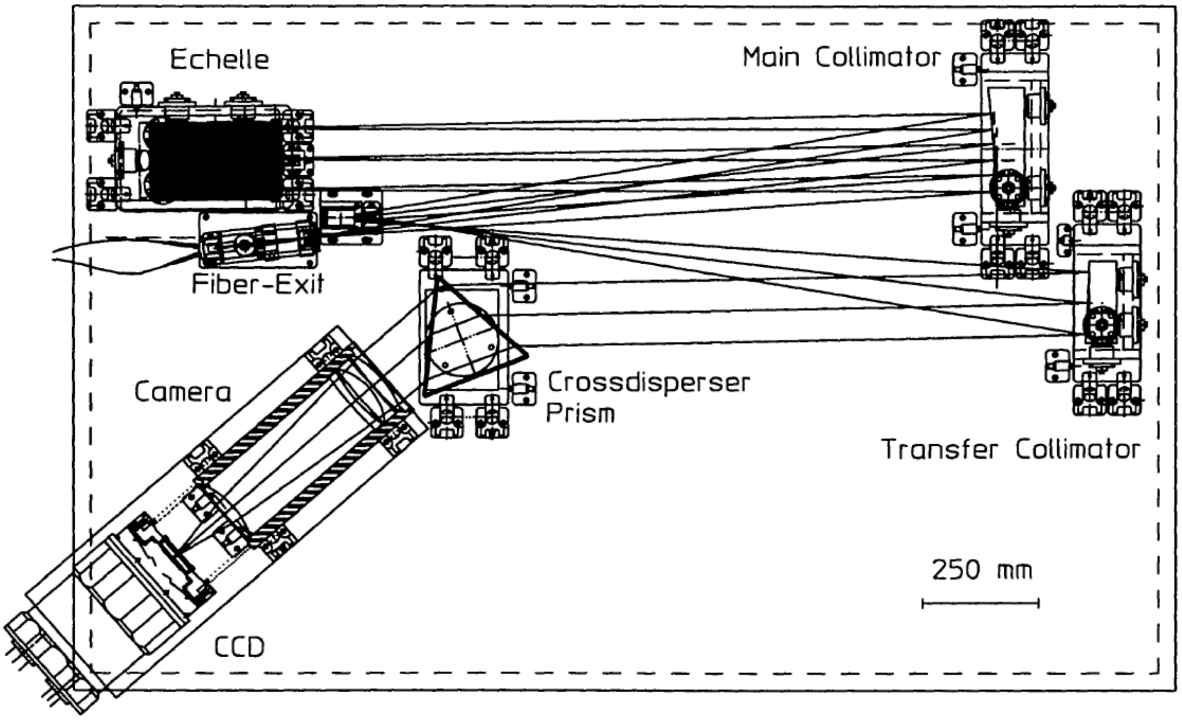

Figure 3.1: The opto-mechanical layout of the FEROS Echelle Spectrograph (Stahl et al. 1999)

and an optical resolution (in the red region of the spectrum) of $R = 48\,000$. In all, some 435 spectra were collected relating to 352 target stars. The spectra were all recorded using a stellar fibre (1.8 arcsec aperture) and an exposure time ranging from 108–2400 s, based on the signal counts measured in the continuum. Each spectrum typically spans the range $\sim$ 3660–9200 Å, with a measured signal-to-noise ratio in the range of 100–400. The spectra were reduced to 1–D with the Data Reduction Software (DRS) pipeline software provided by ESO using the standard calibration data (bias, flatfield and Thorium–Argon wavelength reference spectra). The spectra were then normalized to unity continuum level. Each spectrum has a timestamp in MJD format. The complete list of spectra is given in Appendix B. With the exception of spectra recorded in 2010, all spectra were collected and reduced by

other members of the Kurtz group. Sample spectra from the FEROS dataset are shown in Fig. 3.2 for HD 92499 and in Fig. 3.3 for HD 40765.

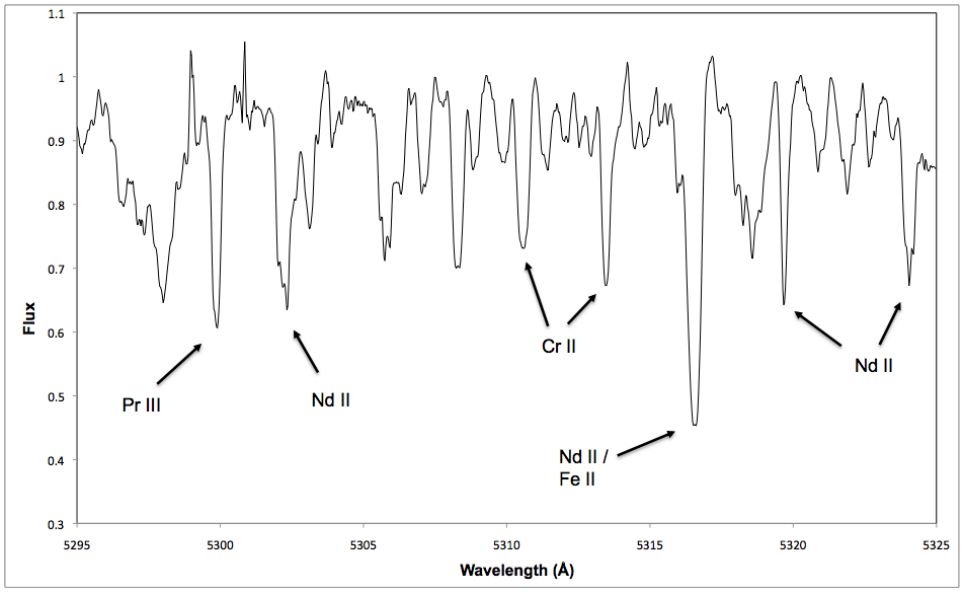

Figure 3.2: Sample of spectrum of Ap star HD 92499 between 5295–5325 Å

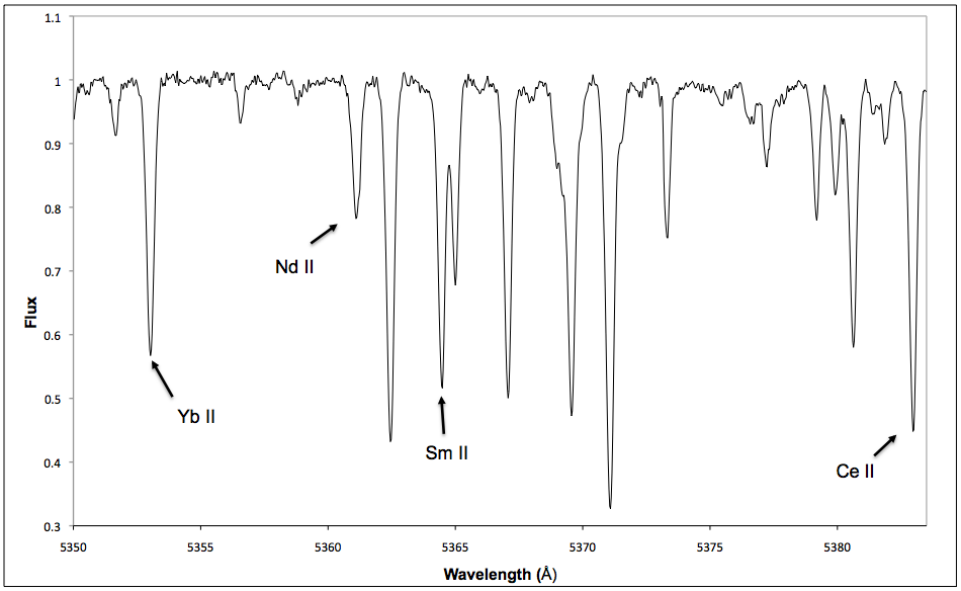

Figure 3.3: Sample of spectrum of Ap star HD 40765 between 5350–5383 Å

3.3 The Core Wing Anomaly

The core wing anomaly (CWA) refers to the anomalous hydrogen Balmer line profiles apparent in the spectra of several Ap stars at the cooler end of the temperature range. The phenomenon is most clearly seen in the H_α profile, but is also see in H_β and and consists of a noticeably abrupt transition from the broad Stark wings indicative of an effective temperature range 7000–8000 K, to a narrow Doppler core more representative of temperatures around 6000 K or less. This is in contrast to the Balmer line profiles of normal A and F stars, in which a smooth transition from Stark wings to Doppler core is is observed (Gardiner et al. 1999), and on this basis such lines have provided useful diagnostic evidence for the thermal structure of the atmospheres of these 'normal' stars. On the other hand, Przybylski's star (HD 101065), an Ap star, was known to exhibit the characteristics of the CWA (Wegner 1976; Przybylski 1979) and it has subsequently been observed in a number of other objects, for example HD 166473, HD 137949 (33 Lib), HD 217522, HD 965 alongside HD 101065 (Cowley et al. 2001); see Fig 3.4. The anomaly points to an abnormal atmospheric structure, and attempts have been made to explain the phenomenon in both qualitative and quantitative terms, considering possible effects of elemental diffusion processes and magnetic fields, and developing models incorporating line blanketing, and modifying boundary temperatures in the intermediate model atmospheric layers (Kochukhov et al. 2002). However, a comprehensive explanation of the phenomenon is not yet available. We performed a basic review of the FEROS collection of spectra on which this work is based, to determine by visual inspection of the H_α line profiles, which stars were candidates demonstrate the CWA phenomenon. Of the 352 stars examined in this way, 23 of the cooler stars were shown to exhibit the CWA phenomenon, in the effective temperature range $5\,900\,\mathrm{K} < \mathrm{T_{eff}} < 8\,000\,\mathrm{K}$. The stars exhibiting this anomaly in marked in the last column of Appendix B with the symbol ‡.

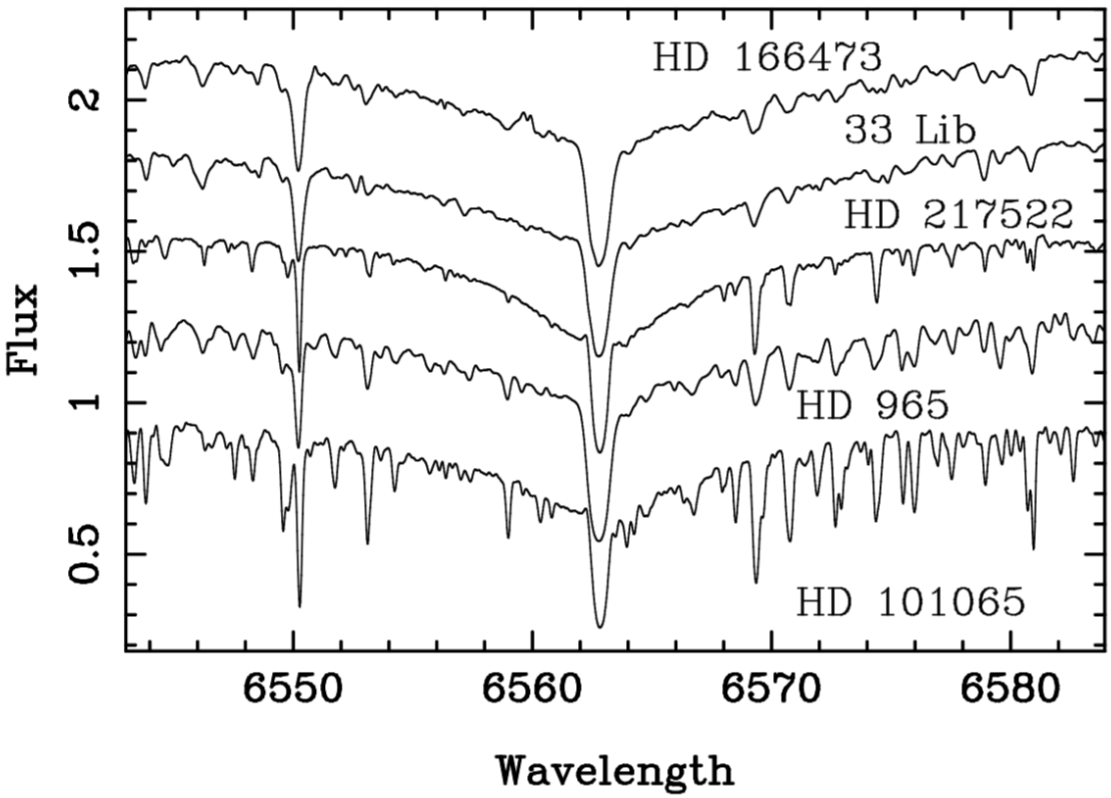

Figure 3.4: The H_α profiles of five Ap stars (wavelength in angstroms) showing the core wing anomaly (CWA). The spectra stacked above HD 101065 have been displaced by 0.4, 0.6, 1.0 or 1.3 flux units (Cowley et al. 2001)

3.4 Determination of Fundamental Parameters T_{eff} and $\log g$

The fundamental parameters T_{eff} and $\log g$ for each of the target stars in the survey were derived using the results of Strömgren and H_β photometry provided by Martinez (Martinez 1993). Strömgren photometry was designed specifically for B-, A- and F- stars, and is calibrated for normal stars in the spectral range (Crawford 1975, 1978, 1979) and also has a number of standard stars available (Crawford & Barnes 1969; Crawford et al. 1970; Crawford & Barnes 1974).

A fortran program, TEMPLOGG (Kupka & Bruntt 2001) takes the visual magnitude V of the star along with the Strömgren indices ((b-y), m_1, c_1, β) for each of the survey stars in turn to derive values for T_{eff} and $\log g$. The program is designed for 'normal' stars from spectral types B0 I to G5 V and is based on the calibration grids developed by Moon & Dworetsky (1985) relating to the calibration of values of β and c_1 with T_{eff} and $\log g$. There are two grids; one for the range of T_{eff} up to 8500 K, and the other for values above 8500 K. The grids for these two sets of ranges are shown in Figs 3.5 and 3.6, respectively.

The result is a set of values for T_{eff} and $\log g$ for each of the stars in our survey. These values are then used in order to determine the most appropriate model atmosphere to use when calculating the abundances derived from the measured equivalent widths.

One of the caveats with regard to the application of Strömgren photometry to Ap stars is the fact that the afore-mentioned line blanketing causes the continuum flux distributions to deviate significantly from those of normal stars. In the cooler Ap stars the c_1 index is depressed relative to a normal star of equivalent luminosity, leading to a higher apparent value of $\log g$. In addition, the prominent abundance anomalies represented as abundance spots on the stellar surface lead to photometric

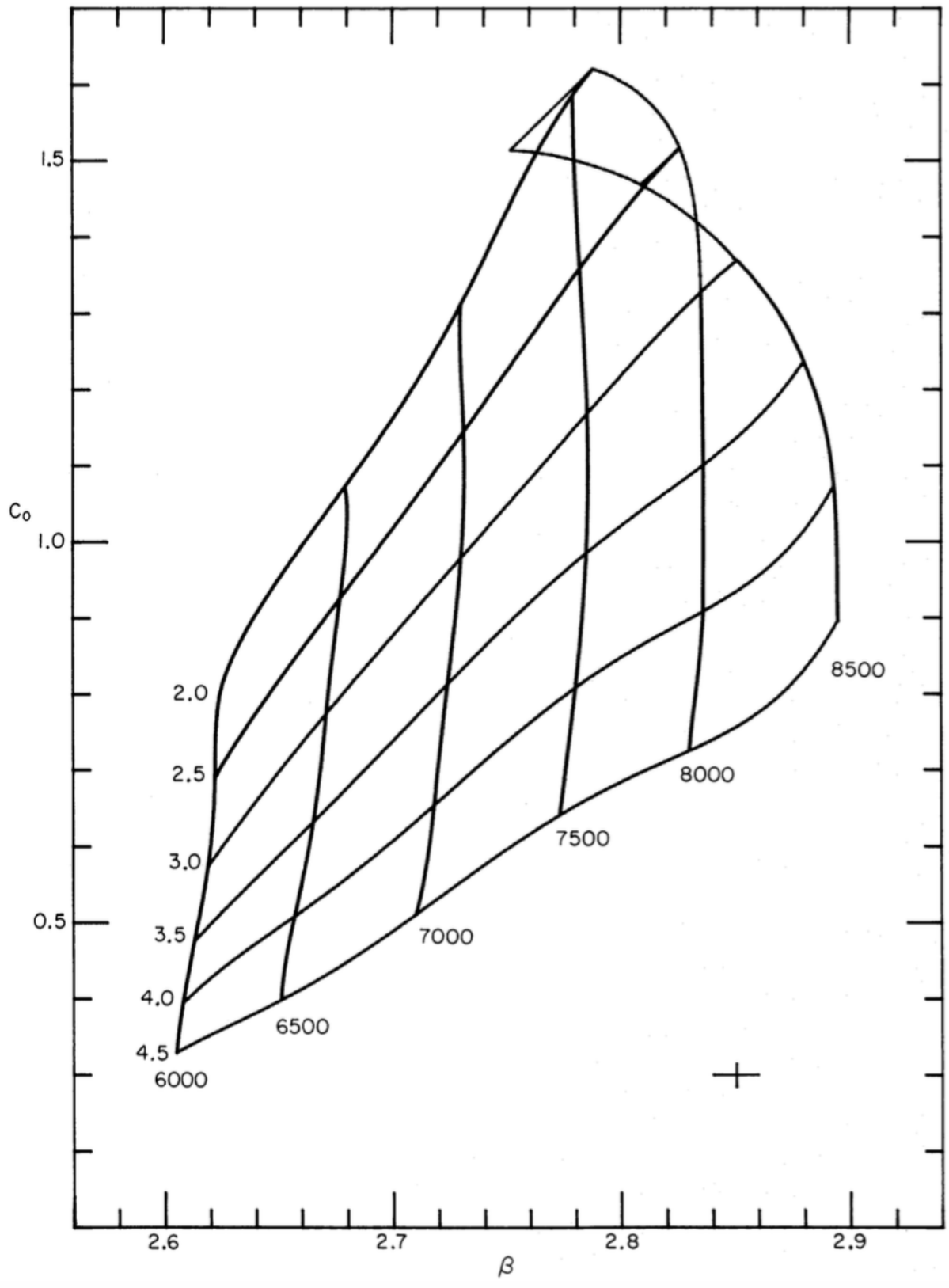

Figure 3.5: Relationship between Strömgren indices β and c_0 for stars with T_{eff} $< 8500\,K$ (Moon & Dworetsky 1985)

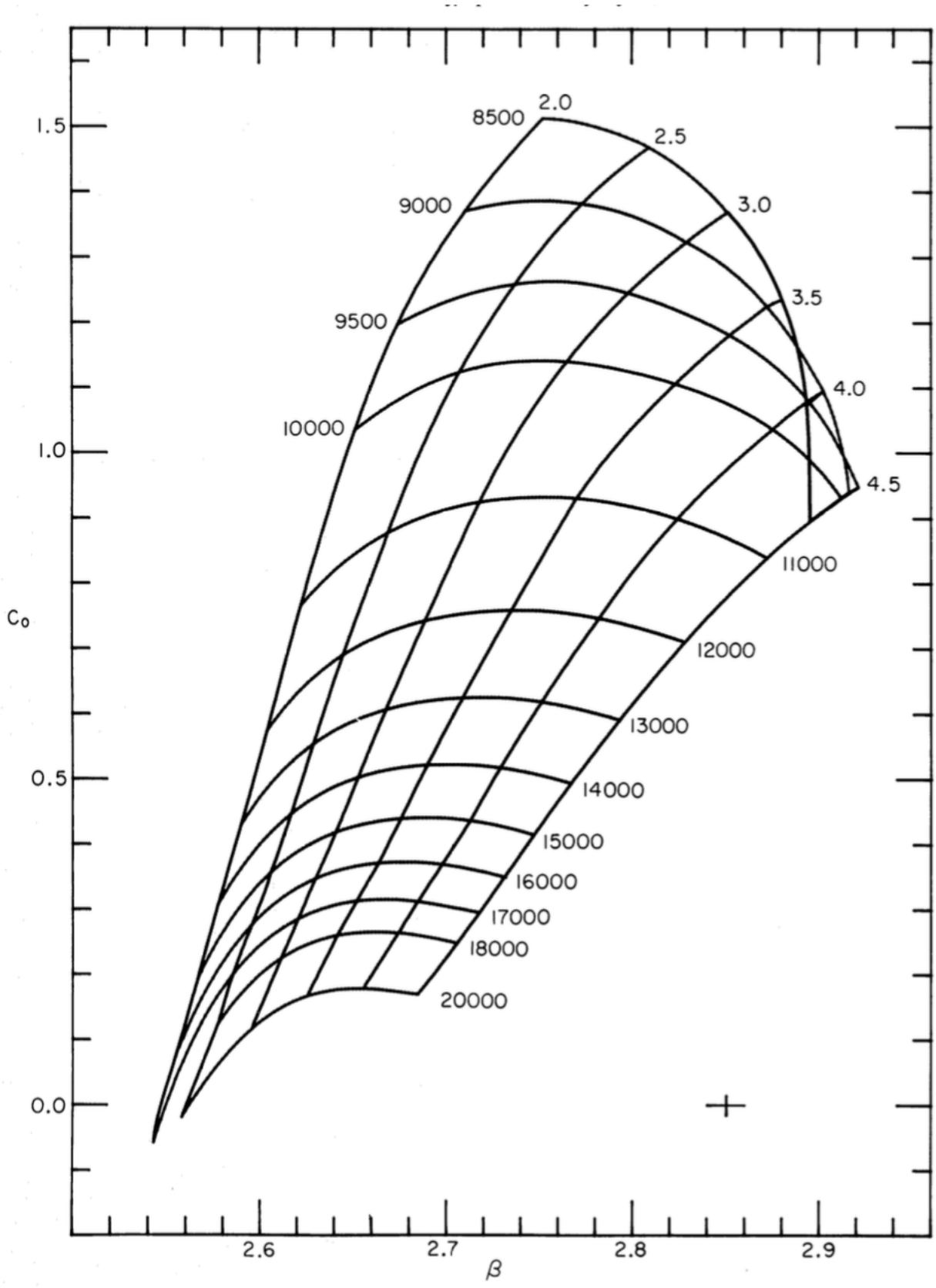

Figure 3.6: Relationship between Strömgren indices β and c_0 for stars with $T_{eff} >$ 8500 K (Moon & Dworetsky 1985)

variability with rotational phase. As an example, Dukes & Adelman (2018) analysed the time-resolved Strömgren photometry of eight Ap stars to determine the u, v, b and y amplitudes. The amplitudes for HD 49713 and HD 171263 are shown in Fig. 3.7. Since the *ubvy* values are using alongside the β parameter to determine the fundamental parameters $T_{\rm eff}$, $\log g$ for the star, then it is clear that the values determined in this way will vary depending on where in the rotation period the original spectra were recorded.

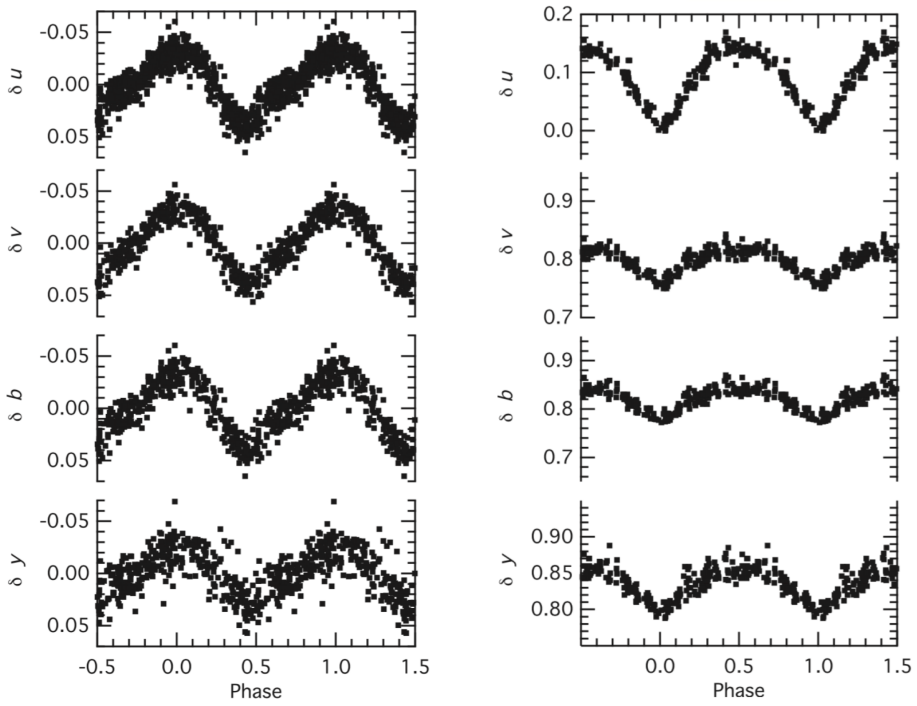

Figure 3.7: Strömgren differential *uvby* photometry of HD 49713 (left) and HD 171263 (right) as a function of phase

This chapter describes two different approaches to the problem of performing a semi–automated abundance analysis of the FEROS spectra for the Ap stars of interest to us. The first makes use of the VWA software package, as described in the following section. This approach was found to have some limitations when applied to the spectra and abundance determination of Ap stars, and so a second approach was

developed to build and use a set of routines written in Interactive Data Language (IDL) to prepare the spectra for further processing via ATLAS and WIDTH.

3.5 VWA Abundance Analysis

The VWA software package (the abbreviation is derived from its functionality in potentially determining, from an absorption spectrum, the $v\,sin\,i$ of the stellar object, wavelength displacement due to radial velocity and abundance analysis) is a set of routines written in IDL and developed for the semi–automatic abundance analysis of stellar spectra (Bruntt et al. 2002).

VWA takes the fundamental parameters of the star ($T_{\rm eff}$, $\log g$ and metallicity) as input to derive a model atmosphere using modified versions of the ATLAS code (Kurucz 1993; Smalley & Kupka 1997). The abundance analysis is facilitated by the use of atomic line data across the spectral range of the spectrum of interest. The complete line list is extracted from the Vienna Atomic Line Database (VALD) (Heiter et al. 2008) and is refined in a three–stage process. Firstly, for each VALD line within the spectral range of interest, the degree of blending with the neighbouring atomic line for the fundamental parameters in question is considered. The degree of blending, i.e. the threshold below which it is considered acceptable is selected by the user, and on the basis of this, a subset of the VALD lines are selected for further analysis. Secondly, VWA analyses the observed spectrum in the region around each selected line. A Voigt profile is fitted to the observed spectrum, and the line is selected or rejected by VWA based on the closeness of fit based on a series of selectable criteria: the degree of asymmetry between the left– and right– hand part of the observed line; the minimum depth of the profile; the maximum value of 'goodness of fit' (χ^2) for the profile and spectral line. Finally, the user is presented with an array of plots of the observed spectra around each selected line, and each line may then be interactively selected for, or rejected from, further processing. An

example of this is shown for HD 24355 in Fig. 3.8. The final result is a list of lines to be used for the abundance analysis. An abundance determination is made for each of the selected lines by computing a synthetic spectrum using the program SYNTH (Valenti & Piskunov 1996), adjusting the abundance of the element in question until the equivalent widths of the computed and observed spectrum match. Furthermore, for stars of low $v \sin i$, it is possible to constrain the parameters $T_{\rm eff}$, $\log g$, metallicity, microturbulence ζ_{micro} by adjusting these values until any correlation between measured EQWs for lines of the same element, and the elemental abundance, and/or correlation between measured EQW and the excitation potential of the lower transition level, is removed.

3.5.1 VWA Abundance Analysis of the Solar-Type Star HD 43587

In order to test the applicability of VWA to a semi–automated abundance analysis of the Ap stars in our data set, the technique was first applied to an analysis of the solar–type star HD 43587. The absence of elemental stratification and other peculiarities in the atmospheres of such stars when compared with those of Ap stars, means that the standard stellar models used in our approach are likely to be more representative of their physical environment, and this should make abundance analysis simpler as a result, facilitating a simpler evaluation of our technique before we go on to analyse the more complex Ap stars. COROT (COnvection, ROtation and planetary Transits) was a space mission aimed at conducting exo–planet and asteroseismology research (Baglin et al. 2001). As part of the mission, a number of bright target stars were selected for study, particularly with a view to the determination of their fundamental parameters and metallicity, and HD 43587 was originally identified as one of these targets. Its slow rotation ($v \sin i < 7\,\mathrm{km\,s^{-1}}$), solar–like composition and absence of apparent peculiarity in the Strömgren indices made it

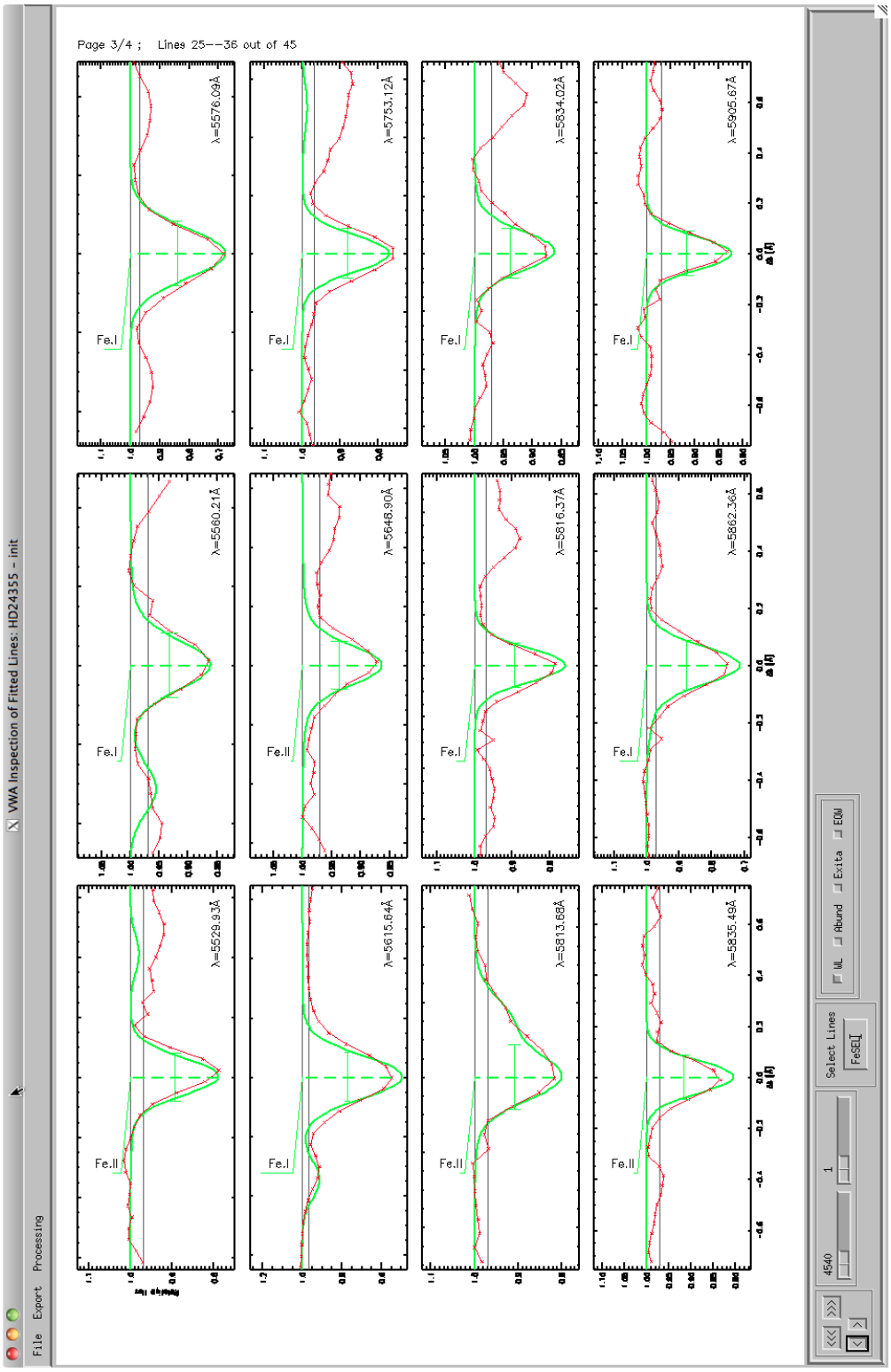

Figure 3.8: A selection of synthetic (green) and observed (red dotted) Fe I lines superimposed on one another by VWA for stellar object HD 24355 in the spectral wavelength range 5529–5905 Å.

a strong candidate for their purposes. An abundance analysis on some of the target stars including HD 43587 had already been undertaken (Bruntt et al. 2004) based on spectra collected on the ELODIE echelle spectrograph attached to the 1.93–m telescope at the Observatoire de Haute–Provence (OHP) (R = 45 000). However, for our analysis, a normalised echelle spectrum of the same target in the wavelength range 3780–6320 Å taken on the HARPS (High Accuracy Radial velocity Planet Searcher) attached to the 3.6–m telescope at La Silla (R = 115 000) was made available (Roxburgh 2011).

Preliminary matching with a synthetically generated spectrum was carried out in VWA using a SYNTH–generated model, and adjusted for radial offset and macroturbulence v_{macro}. A sample fit is shown in Fig. 3.9. VWA was then used to select a number of Fe I and Fe II lines based on minimised blending, and the selection was modified for each step in a range of values of $T_{\rm eff}$, $\log g$ and microturbulence ζ_{micro}. The fit between actual and synthetically–generated lines was examined, and where the fit was good, the line under inspection was selected for further processing; the others were rejected. The list of iron lines selected in the analysis of HD 43587 is given in Appendix C.1. Plots were then generated in VWA to show the correlation of Fe I and Fe II abundance with equivalent width (EQW) and excitation potential (χ_E) of the lower level involved in the absorption, respectively. The values of $T_{\rm eff}$, $\log g$ and microturbulence ζ_{micro} were then continually adjusted until the correlation for each of these relations was minimised, to derive the values for this star; see Fig. 3.10.

The fundamental parameter values derived are shown in Table 3.1. Also shown in the table for comparison are the fundamental parameters for HD 43587 derived by Bruntt et al. (2004) using the VWA technique, as well as those derived by Sousa (2011) using the same HD 43587 HARPS spectrum used in this work, but employing an analysis using the MOOG code (Sneden 1973) based on the equivalent widths

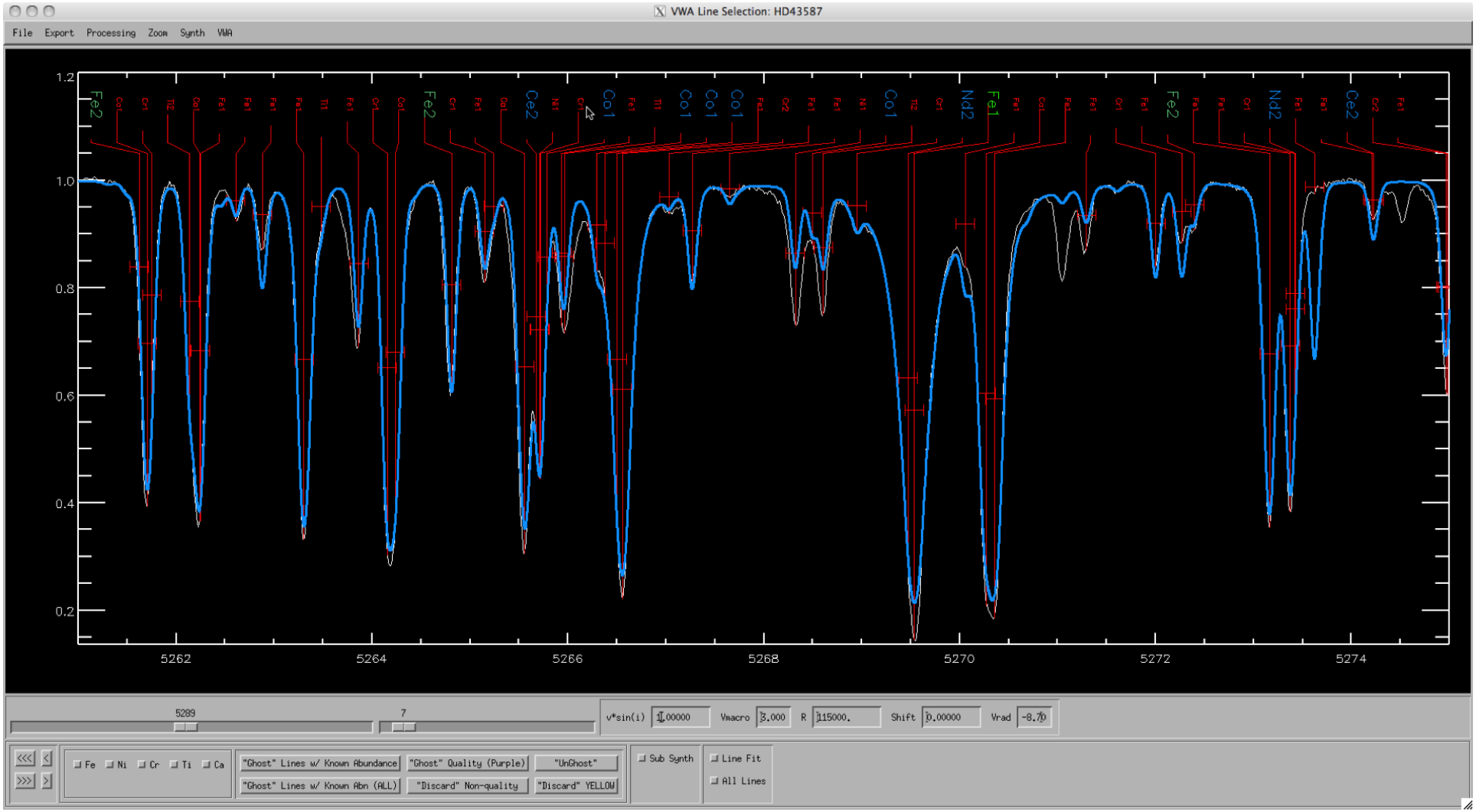

Figure 3.9: A sample of the spectrum of HD 43587 in the wavelength range $6490 - 6634$ Å. The synthetic spectrum (blue line) generated by SYNTH is shown superimposed over the observed spectrum (white line). An identification of the spectral lines is also shown

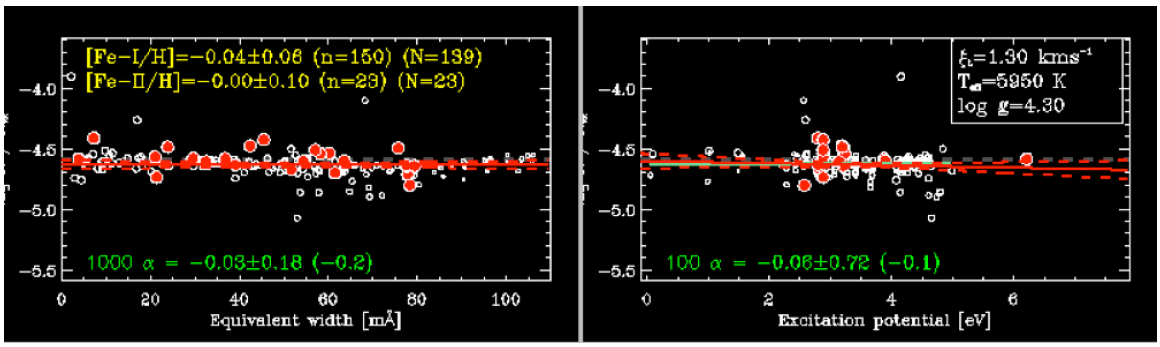

Figure 3.10: VWA plots of iron abundance vs. EQW (LHS), and iron abundance vs. excitation potential (RHS), for star HD 43587 based on fundamental parameters $T_{\rm eff} = 5950\,{\rm K}$, $\log g = 4.3$, microturbulence $\zeta_{micro} = 1.3\ {\rm km\,s^{-1}}$. Fe I (empty white circles), Fe II (filled red circles).

Table 3.1: Table comparing fundamental parameters derived for HD 43587 resulting from three different studies. The column $n(Fe\,{\rm I})\,/\,n(Fe\,{\rm II})$ indicates the respective number of Fe I / Fe II lines involved in the analysis.

$T_{\rm eff}$ (K)	$\log g$	[Fe/H]	$\zeta_{micro}(km\,s^{-1})$	$n(Fe\,{\rm I})\,/\,n(Fe\,{\rm II})$	Reference
5950 ± 20	4.3 ± 0.1	$+0.02 \pm 0.08$	1.30 ± 0.05	139/23	This work
5937 ± 10	4.38 ± 0.02	-0.01 ± 0.01	1.18 ± 0.01	256/35	(Sousa 2011)
5870 ± 60	4.20 ± 0.15	-0.09 ± 0.11	–	206/23	(Bruntt et al. 2004)

of Fe I and Fe II weak lines, by imposing excitation and ionization equilibrium as described by Sousa et al. (2008, 2011). As can be seen there is, in general, good agreement between the fundamental parameters derived in our analysis and those completed by Sousa (2011) and Bruntt et al. (2004). The result was used to corroborate the fundamental parameters for HD 43587 in the analysis by Boumier et al. (2014).

3.5.2 VWA Abundance Analysis of Ap Star HD 188136

In order to explore the applicability of VWA to our investigations further, specifically to the timely analysis of the data set of FEROS Ap spectra, an iron abundance analysis was attempted for HD 188136, a metal-rich variable δ Scuti star (Kurtz 1980; Wegner 1981). HD 188136 shows significant spectral peculiarities (Wegner 1981) with a very strong Sr II line at 4077 Å and shows a rare earth enhancement lying somewhere between the cool Ap stars and Przybylski's star, HD 101065. The spectrum used for our analysis (MJD 53892.431728) was taken using the UVES spectrograph mounted at the ESO VLT telescope at Paranal, Chile (Dekker et al. 2000). The spectral range was 3600−9460 Å. The spectrum was normalised using the RAINBOW component of VWA. The fundamental parameters adopted by Wegner for his abundance analysis are given in Table 3.2.

Table 3.2: Fundamental parameters adopted for HD 188136 (Wegner 1981).

$T_{\rm eff}$ (K)	$\log g$	[Fe/H]	$\zeta_{micro}(km\,s^{-1})$
7050 ± 300	3	+0.6	2.68

With these values as a starting point for our analysis, VWA was used to select a number of unblended Fe I / Fe II lines in the UVES spectrum, and the selected lines were reviewed manually to compare the fit with synthetically generated lines, in a similar manner to the analysis of HD 43587. Lines accepted for further processing at this point were then processed by VWA to generate an iron abundance for each line, and the fundamental parameters. $T_{\rm eff}$, $\log g$ and microturbulence ζ_{micro} were then continually adjusted until a best attempt at minimising the correlation of abundance with equivalent width and excitation potential respectively was completed. A grid of parameter values in the range $6\,600\,{\rm K} < T_{\rm eff} < 7\,600\,{\rm K}$; $3.0 < \log g < 3.9$; $1.0 < \zeta_{micro} < 3.0$ km s^{-1} was employed in this process. However, in the case of HD 188136,

removal of such correlation was difficult to achieve, and the best fit still showed a significant correlation in all cases; see Fig. 3.11. The list of iron lines selected in the analysis of HD 188136 is given in Appendix C.2.

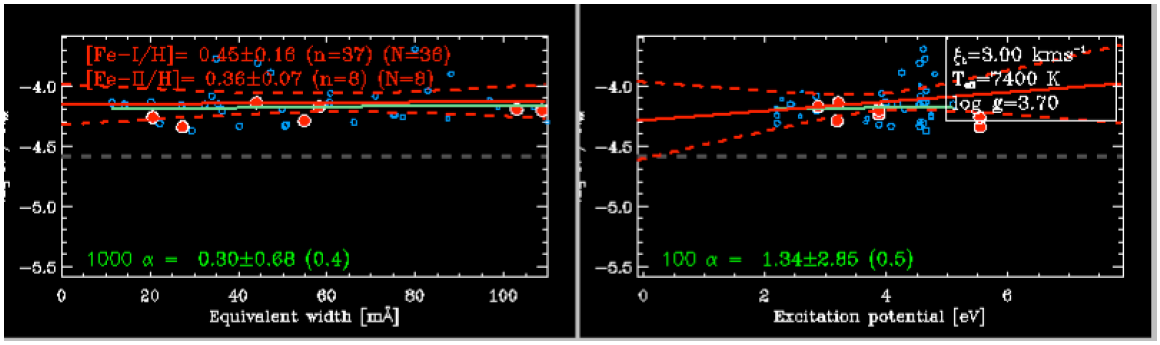

Figure 3.11: VWA plots of iron abundance vs. EQW (LHS), and iron abundance vs. excitation potential (RHS), for star HD 188136 based on fundamental parameters $T_{\rm eff} = 7400\,{\rm K}$, $\log g = 3.7$, microturbulence $\zeta_{micro} = 3.0\ {\rm km\,s^{-1}}$. Fe I (empty blue circles), Fe II (filled red circles)

The difficulty in removing the correlation may well be due to aspects of abundance stratification in the atmosphere of HD 188136. In any case, it is clear that the manual intervention required in the application of VWA does not easily lend itself to the efficient processing of the large number of spectra that we have at our disposal, so an alternative approach, based on developing a semi–automated process for abundance analysis, was developed.

3.6 An Approach to Semi–automating the Abundance Analysis Process

An alternative approach to semi–automate the abundance analysis process using a set of routines, written in the IDL programming language, was developed to calculate the equivalent width for each one of a pre–determined set of spectral lines for each

spectrum, processed along with an appropriate model atmosphere by the WIDTH program (Castelli 2005) to generate a relative abundance for that line within each spectrum. The programs are listed in Appendix D. The process was broken down as follows:

Each high–resolution spectrum within the collection was processed in turn; in each case the H_α line was cross-correlated with a synthetically–generated H_α line to determine any wavelength correction that must be applied to the spectrum due to radial velocity or instrumental variations. For each of the set of selected lines, the spectrum was analysed further at the corrected wavelength to determine whether there was a matching line in the spectrum, and if so, whether the line profile was deemed to be sufficiently well–defined and un–blended to warrant further consideration. The routine determined whether a line profile minimum existed within a certain wavelength offset either side of the laboratory line wavelength, and if so, measured the profile flux change as a function of distance either side of the minimum to ensure that the line profile was well defined. Specifically, a spectral window $\pm$ 0.15 Å either side of the corrected wavelength of the line was defined, and the minimum normalised flux value within this range was determined; lines with a normalised flux value greater than 0.97 were rejected from further processing. For each line that was not rejected, the wavelength of this minimum flux value was determined, and the flux increase either side of this wavelength was measured in order to calculate a value for the full–width at half–minimum (FWHM) flux. Only lines that reached the full-width at half-minimum (FWHM) flux threshold within a range of 1.25 Å either side of the centroid determined earlier were considered suitable for further processing. These limits imposed on the normalised flux value and on the FWHM centroid offset were designed to compensate for noisy continuum and blending, respectively, and were found to result in adequate comparison between the EQWs measured by the routine,

and by hand. Approximately 30% of spectral lines were rejected at this stage, either because the line was considered too weak, or too broad, suggesting that the line may be affected by blending.

A simple factoring term was applied to the FWHM value in order to generate a total value for the baseline width. This value was then used as a basis for calculating an equivalent width for the line, by integration of the absorption line profile across the baseline, assuming a continuum level at a normalised flux level of 1.0. In order to determine an appropriate value for the factoring term, the equivalent widths for a randomly selected set of lines of various line strengths, and taken from various spectra in the survey, were manually calculated using the line profile integration facilities within ESO's Munich Image Data Analysis System (MIDAS) (Banse et al. 1983; Grosbøl & Ponz 1990), and compared with the equivalent widths calculated by the routine for the same lines, using a selection of factoring terms from 2.0–2.3. A value of 2.0 corresponds to a representation of the line profile as a simple inverted isosceles triangle, routinely used to derive a simple estimate of line equivalent width based on the FWHM, and a reasonable approximation for weak lines where stark broadening and resultant absorption in the wings of the line profile is less pronounced. The results of these comparisons are shown in Fig. 3.12. The most consistent agreement between the two processes for calculating the equivalent width were found when a factoring term of 2.0 was used as measured by the correlation r^2 fit. In practice this means that the full width of our spectral lines at the continuum is calculated to be twice the value at the FWHM level. This factoring value was then used in further comparisons between the automated routine and the manual MIDAS approach to ensure a consistency in derivation of the equivalent widths of spectral lines. The equivalent width of the Nd III line at 6145.068 Å was determined manually via the MIDAS technique, and also via the automated routine, for a sample of 120

spectra within the survey. The resulting scatter plot of EQWs determined by these two methods is illustrated in Fig. 3.12. It can be seen that the EQWs calculated by these two methods are in good agreement across the survey sample.

The equivalent width for a spectral line calculated by the routine was then combined with atomic line data provided by the Vienna Atomic Line Database (VALD) (Heiter et al. 2008) to generate a data file for input to the WIDTH program for processing, together with an appropriate model atmosphere selected from the Vienna New Model Grid of Stellar Atmospheres (NEMO) (Heiter et al. 2002). Strömgren H_β photometry, using the photometric measurements for each of the stars given by Martinez (1993), was used to determine an appropriate value for the effective temperature $T_{\rm eff}$ and $\log g$. For all stars, the $\log g$ value selected was constrained between 3.6 and 4.2, such that any values determined photometrically to be less than the minimum or greater than the maximum value were corrected to be at the low end or high end of this range, respectively. The m_1 and c_1 indices are strongly affected by line blocking in Ap stars. It is clear that the c_1 index is not a good indicator of $\log g$ in these objects (Martinez 1993). Because studies of Ap stars have all concluded that the stars lie between just post–ZAMS (Zero Age Main Sequence) and TAMS (Terminal Age Main Sequence), and because we do not have a good estimate of $\log g$ from the Strömgren photometry, it was deemed a reasonable constraint to keep the search for atmospheric models in this range. From these values of $T_{\rm eff}$ and $\log g$, the choice of model atmosphere was made, using a nominal value for the microturbulence of 2 $\mathrm{km\,s^{-1}}$. Using these parameters, WIDTH was used to calculate an abundance from each line. The abundances were then averaged for each element/ion combination, within a spectrum, and in the case where multiple spectra exist for a target object, averaged across the spectra to give a final abundance value for each ion species for each programme object.

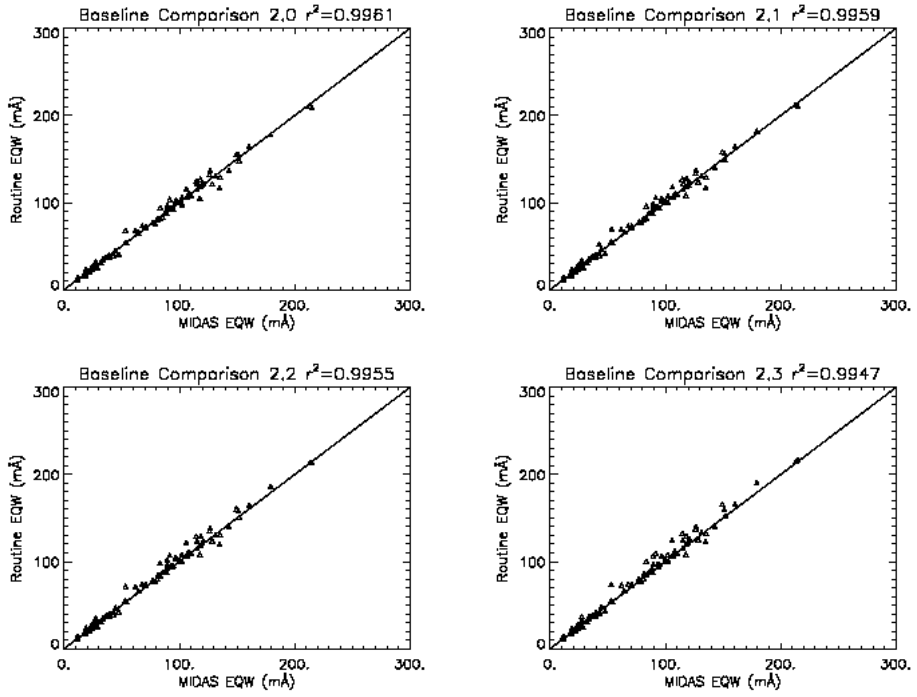

Figure 3.12: Comparison of equivalent widths for a selection of spectral lines measured manually (x axis) versus those calculated by the automated routines (y axis) for a selection of baseline factor terms, ranging from 2.0 (top left) to 2.3 (bottom right), with correlation r^2 of 0.996, 0.9959, 0.9955 and 0.9947, resepctively. A factor of 2.0 appear to represent the best match between manual and automated calculation. This figure shows that, within the constraints of the lines chosen for analysis, the automated routine reproduces manual equivalent width measurements well.

3.7 Selection of Spectra and Individual Line Selection

In order to minimise the effects of line blending, an upper limit was placed on the measured rotational velocity $v \sin i$ value for spectra that were to be incorporated into the analysis. For this purpose, strong Fe I lines at 5434.523 Å and 5576.088 Å were selected and their measured FWHM values for each spectrum as measured by the automated routine were compared with an interpolated empirical relationship between FWHM and $v \sin i$ for the same lines generated synthetically for a range of $v \sin i$ values using the SYNTH program (Piskunov 1992); see Fig. 3.13. This gave a measured value of $v \sin i$ for each object; only spectra which had an average $v \sin i < 40\,\mathrm{km\,s^{-1}}$ were included for further analysis. The spectra thus selected are indicated in the final column in the table in Appendix B with a tick. Around 70% of the original spectra were eliminated from further analysis at this stage.

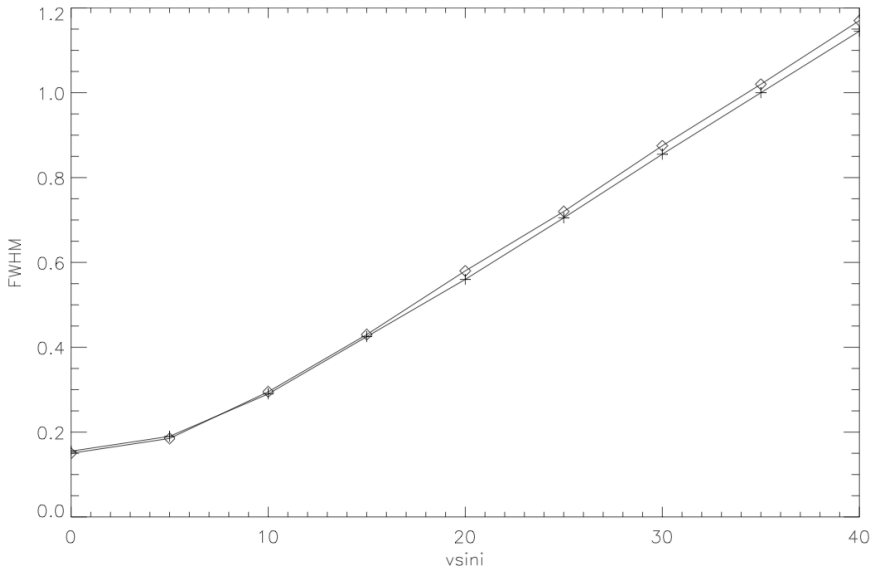

Figure 3.13: Correlation plots of FWHM with $v \sin i$ for a pair of strong synthetically-generated Fe I lines at 5434.523 Å (plusses) and 5576.088 Å (diamonds)

Given the significant proportion of FEROS spectra that were excluded from further analysis at this point, an analysis was done of the distribution of approximate $v \sin i$ values across the FEROS spectra; a histogram showing the results is shown in Fig. 3.14. It can been that a significant number of spectra; just over 50, or around 15 % of the total number of stars have a $v \sin i$ value in the range 50–60 $\mathrm{km\,s^{-1}}$. Therefore in any future studies it may be appropriate to increase the cutoff value of $v \sin i$ in order to reduce the number of spectra rejected from further analysis.

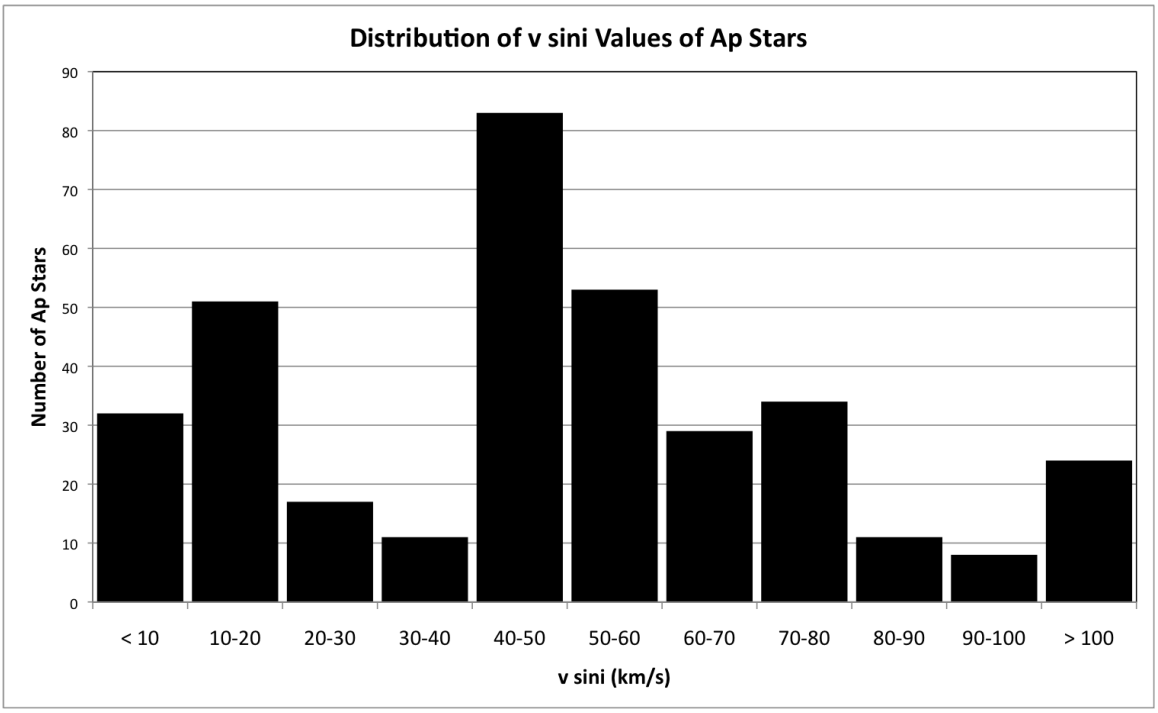

Figure 3.14: The observed distribution of $v \sin i$ for the collection of Ap stars in the FEROS dataset as interpolated from the measured equivalent widths of the strong Fe I lines at 5434.523 Å and 5576.088 Å across the range of samples

3.8 Testing the Automation Process

In order to test the validity of this automation process, the calculation of the equivalent width and the calculation of an abundance using the atmospheric model selected

were tested against alternative established approaches. Specifically, we wanted to make certain that the equivalent widths measured by the semi-automated routine compared favourably with those measured 'by hand' . We also wanted to ensure that the WIDTH Fortran program derived chemical abundances correctly for nominated lines based on the measured equivalent widths.

3.8.1 Comparison of Equivalent Width Measurements with MIDAS

In order to compare the equivalent widths derived by the semi–automated routines with those measured by hand, a small number of stars for which $v \sin i$ was determined by the process to be less than $40\,\mathrm{km\,s^{-1}}$ were selected, and for each star, a number of unblended absorption lines were then chosen for a number of ions, covering the spectral range 5010–6168 Å, and ranging in EQW from 10–324 mÅ. The specific lines chosen are listed in Appendix E.1. For each of the lines, the semi–automated routine was used to calculate the EQW, using the logic previously described. At the same time, the spectrum in question was loaded into MIDAS, which was then used to measure the EQW of each line independently by hand. The EQWs measured by the two methods were then compared by plotting as an x–y scatter plot; see Fig. 3.15. The plot shows good agreement between the two methods, with a correlation r^2 of 0.99, allowing a degree of confidence that, at least in the case of well-defined, unblended lines such as these, the semi–automated routine is able to satisfactorily measure equivalent widths.

3.8.2 Verification of WIDTH Routine Abundance Derivations

We also needed to ensure that the derived equivalent widths were being handled correctly by the WIDTH routine in deriving associated abundances. To this end, we needed some published data relating to measured EQWs for specific transitions

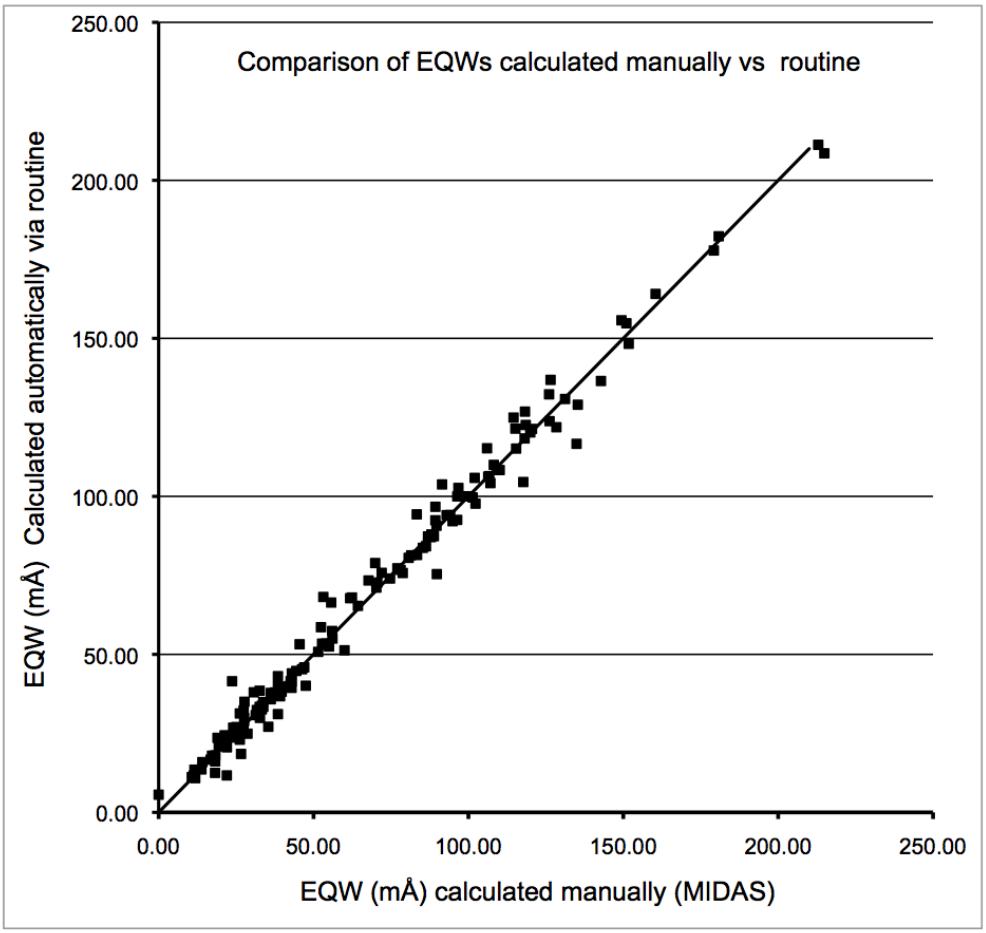

Figure 3.15: X–Y scatter plot comparing the EQWs for a number of selected lines measured both by hand using MIDAS (x–axis) and by the semi–automated routine (y–axis), with a correlation r^2 of 0.99. The straight line represents X=Y

and derived abundances. The data on Ap stars published by Adelman (1973) were used for this purpose. The EQWs and derived abundances for a selected number of transitions were chosen from the Adelman paper. The EQWs and associated atomic transition data obtained from VALD (oscillator strengths, damping constants, excitation potentials of the ground and upper states and degeneracy) were then fed into the WIDTH routine, and the resulting derived abundances were then compared with those published by Adelman (1973). The specific lines chosen are listed in Appendix E.2. The result of this is shown in Fig. 3.16. Again, there is acceptable agreement with the abundances derived by the WIDTH routine that we use in our analysis, and those in Adelman's paper. There is a suggestion that at the higher abundances the routines may be slightly underestimating the abundance relative to Adelman, but we don't believe that such a small correction to the measured EQWs justifies reworking the automation algorithm on this basis. The comparison overall allows us to have confidence in the final abundances that we derive using our semi–automated routines.

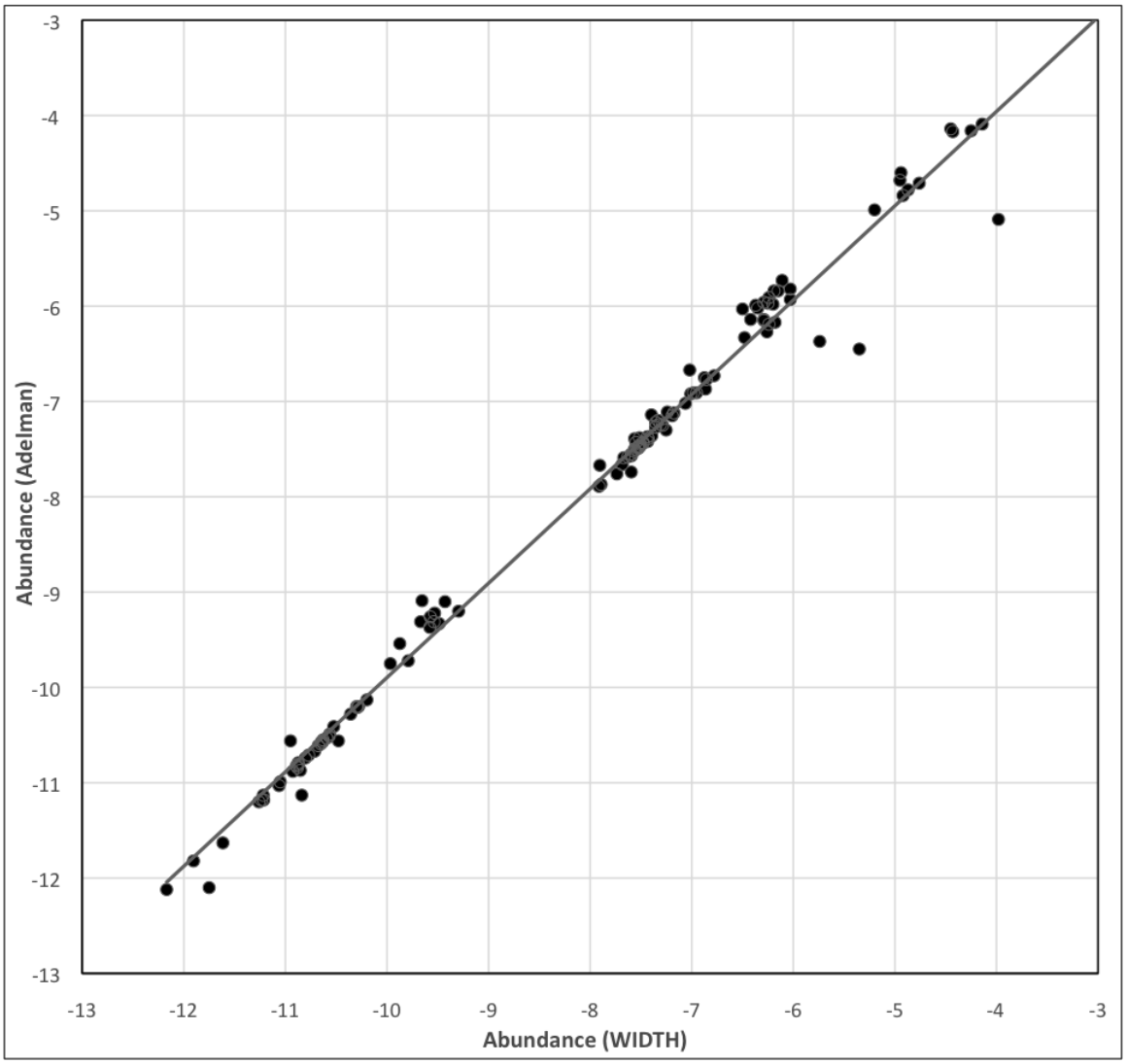

Figure 3.16: X–Y scatter plot comparing the abundances derived by the WIDTH routine used in our analysis, with those published by Adelman (1973). The straight line represents X=Y

Chapter 4

Iron Abundance of Ap Stars

The relatively high abundance of iron in stars with solar metallicity tends to result in a lowering of the efficiency of radiative diffusion processes, so that radiative acceleration for Fe is typically not as pronounced in the Ap stars as for other elements. However, the effects are still present to the extent that in most cases, Fe is overabundant in the Ap stars. Some significant examples of under-abundance exist however, including that of the celebrated Przybylski's star, HD 101965 (Przybylski 1977). Furthermore, the relatively high abundance of Fe in stellar atmospheres, combined with the significant number of excited electronic states attainable during electronic transitions in stellar atmospheres, leads, in general, to a large number of relatively strong lines in the stellar atmosphere for A–F stars, and this is reflected in the absorption spectrum. The proliferation of such lines in the spectra of Ap stars, and spectral resolution of line profiles in slow rotators lends itself to further investigation of Fe abundance in our large sample of Ap stars.

Despite the interest in chemically peculiar stars over the years, there are few abundance surveys of Ap stars that comprise more than a handful of target objects at one time. In one of the earliest abundance surveys of Ap stars, Adelman (1973) performed an elemental abundance analysis of 21 cool Ap stars in the effective temperature range $8\,100\,\mathrm{K} \leqslant \mathrm{T_{eff}} \leqslant 10\,550\,\mathrm{K}$. Abundances were derived by curve-of-growth

analysis using the absorption lines of the ion species of interest. Spectroscopic lines used in the study were measured within the ranges 3850–3870 Å and between 3968–4650 Å. Comprising studies on 24 different elements in total, an abundance analysis of Fe I and Fe II ions formed part of the results. The list of target stars studied and their fundamental parameters and derived abundances are given in Table 4.1. Adelman used the ATLAS model atmosphere program along with an early version of WIDTH to generate a curve of growth for each ion of interest. Zeeman magnetic broadening was treated to first approximation as a pseudo–microturbulence velocity particular to each line. Approximate values for the fundamental parameters $T_{\rm eff}$ and log g were derived from UBV photometry and then modified by ensuring that the abundances derived from Fe I and Fe II lines agreed.

A much later survey (Ryabchikova et al. 2004) performed an abundance survey for a number of ions including Fe I and Fe II on a combination of four rapidly oscillating Ap (roAp) stars together with nine Ap stars, using spectra from a number of different telescopes and spectrometers. The ATLAS package was used to construct solar–type model atmospheres, and the fundamental parameters were in some cases derived from spectrophotometric observations, in other cases, taken from the literature. The VWA software package was used in combination with WIDTH to perform a basic abundance analysis; this was then refined by generating the spectrum synthetically using SYNTH, and modifying the abundances until a match between this and the observed spectrum was obtained. The list of stars along with their type, fundamental parameters and derived Fe abundances from this study is shown in Table 4.2.

Freyhammer et al. (2008) performed an abundance analysis of 17 magnetic Ap stars with magnetic field moduli in the range 3–30 kG, based on some of the spectra also used in this work. Abundance estimates were derived for Fe, as well as Cr, Nd, Pr and Eu, by using ATLAS model atmospheres and SYNTHMAG (Piskunov 1999),

Table 4.1: List of stars for which abundances were calculated by Adelman (1973)

Star	$T_{\rm eff}$ (K)	$\log g$	$A_{Fe\,\textsc{i}}$	$A_{Fe\,\textsc{ii}}$
HD 2453	10 300	4.0	−3.01	−2.90
HD 5797	9550	4.0	−2.61	−2.65
HD 8441	10 150	4.0	−3.36	−3.37
HD 12288	10 500	4.0	−3.32	−3.19
HD 18078	10 000	4.0	−3.01	−3.00
HD 22374	9400	4.0	−3.60	−3.66
HD 50169	10 100	4.0	−3.08	−2.99
HD 81009	9200	4.0	−4.06	−4.09
HD 89069	9900	4.0	−3.31	−3.35
HD 110066	10 000	4.0	−2.95	−2.90
HD 111133	10 550	4.0	−3.37	−3.19
HD 118022	9950	4.0	−2.76	−2.89
HD 137909	9700	4.0	−3.10	−3.08
HD 137949	8800	4.0	−3.43	−3.51
HD 165474	9100	4.0	−4.02	−3.95
HD 176232	8100	4.0	−4.20	−4.12
HD 191742	8800	4.0	−3.28	−3.37
HD 192678	10 350	4.0	−2.95	−2.84
HD 201601	8100	4.0	−3.99	−4.05
HD 204411	9500	4.0	−3.33	−3.32
HD 216533	10 300	4.0	−3.45	−3.39

Table 4.2: List of stars for which abundances have been calculated by Ryabchikova et al. (2004)

Star	Type	$T_{\rm eff}$ (K)	$\log g$	$A_{Fe\,\rm I}$	$A_{Fe\,\rm II}$
HD 137949	roAp	7550	4.3	−4.30	−4.10
HD 176232	roAp	7550	4.0	−4.25	−4.14
HD 12098	roAp	7800	4.3	−4.30	−4.2
HD 60435	roAp	8100	4.2	−4.27	−4.30
HD 75445	Ap	7700	4.3	−4.55	−4.33
HD 29578	Ap	7800	4.2	−4.03	−3.93
HD 116114	Ap	8000	4.1	−4.20	−4.18
HD 137909	Ap	8000	4.3	−3.92	−3.66
HD 18610	Ap	8100	4.0	−3.81	−3.87
HD 188041	Ap	8500	4.5	−3.98	−3.63
HD 110066	Ap	9000	4.3	−3.35	−2.83
HD 212385	Ap	9200	4.4	−3.81	−3.73
HD 183806	Ap	10 070	3.7	−3.37	−3.53

a variation of the SYNTH code incorporating effects of magnetic Zeeman splitting. The list of stars along with fundamental parameters and derived Fe abundances in this study is shown in Table 4.3.

Ghazaryan et al. (2018) compiled existing published information on several hundred peculiar stars comprising AmFm, HgMn and ApBp stars. This included 188 ApBp objects in an effective temperature range from 6 400 K $\leqslant$ $\rm T_{eff}$ $\leqslant$ 16 600 K, and included 104 stars for which Fe abundances were compiled, in the range 6 930 K $\leqslant$ $\rm T_{eff}$ $\leqslant$ 14 700 K. The data also incorporated the survey studies conducted by Adelman, Ryabchikova et al. and Freyhammer et al. referred to earlier. By the

Table 4.3: List of stars for which abundances have been calculated by Freyhammer et al. (2008)

Star	$T_{\rm eff}$ (K)	$\log g$	$A_{Fe\,\textsc{i}}$	$A_{Fe\,\textsc{ii}}$
HD 33629	7570	4.00	−4.29	−4.37
HD 42075	7590	4.00	−4.55	−4.24
HD 44226	8060	4.00	−3.79	−4.09
HD 46665	8050	4.00	−4.99	−4.43
HD 47009	8280	4.00	−4.76	−4.52
HD 52847	8060	4.00	−4.24	−3.57
HD 55540	8230	4.00	−5.02	−4.34
HD 69013	7470	4.00	−4.71	−4.70
HD 72316	8050	4.00	−4.59	−4.09
HD 75049	9700	4.00	−4.30	−4.04
HD 88701	8080	4.00	−4.96	−4.01
HD 92499	7810	4.00	−4.59	−4.35
HD 96237A1	7930	4.00	−4.71	−4.71
HD 96237A2	7800	4.00	−4.24	−4.15
HD 110274	8130	4.00	−4.57	−4.25
HD 117290	8230	4.00	−4.33	−4.28
HD 121661	8230	4.00	−4.52	−3.98
HD 135728A	8060	4.00	−3.36	−3.35
HD 135728B	8060	4.00	−4.30	−4.30
HD 143487	6930	4.00	−5.90	−4.70

nature of the compilation itself, the data collated by the various researchers was generated from a number of different instrumental sources, and employed a variety

of abundance analysis techniques in order to derive the Fe abundance results. A plot of the Fe abundances published is shown in Fig. 4.1

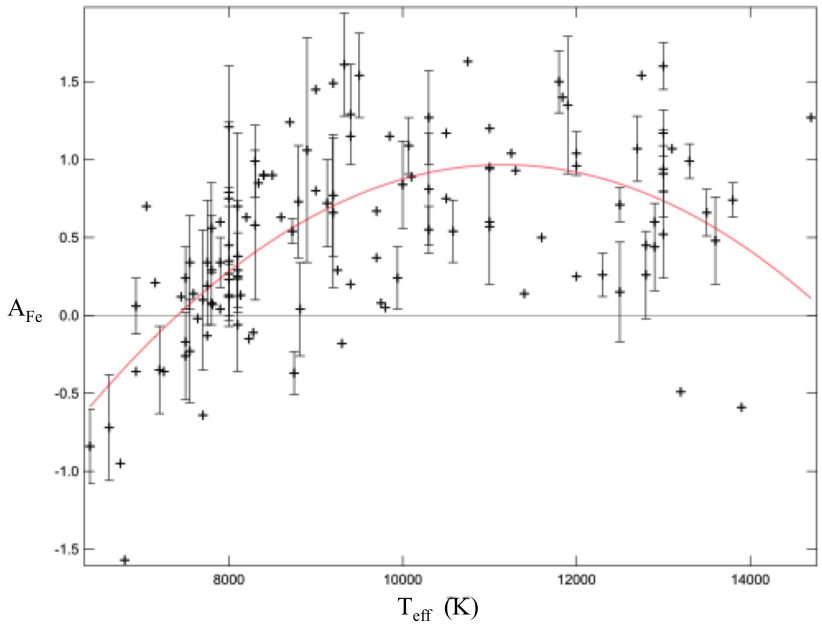

Figure 4.1: Fe abundances A_{Fe} relative to solar (horizontal black line) in ApBp stars vs. effective temperature T_{eff}. The red solid curve is a polynomial fit showing the correlation of A_{Fe} and T_{eff} (Ghazaryan et al. 2018).

4.1 Method

The selection of Fe I and Fe II lines to use in this analysis of the collection of spectra, was performed by visual inspection of the spectrum of the star HD 82989 using VWA in the spectral wavelength range of 4000–6700 Å. The fundamental parameters of the star are listed with the others in this study in Appendix B. The effective temperature T_{eff} of 6 744 K derived by TEMPLOGG based on the spectrophotometry of Martinez (1993) places it at the cool end of the range of effective temperatures in our sample, and together with a slow effective rotation estimated to be $v \sin i \ll 40\,\mathrm{km\,s^{-1}}$,

makes it a good candidate for identifying suitable non–blended Fe I and Fe II lines for further analysis of the spectra in our sample; see Fig. 4.2. The radial offset of the spectrum was calculated by adjusting the spectral offset of the spectrum until the H_α line was superimposed on the same line generated synthetically at the laboratory wavelength for H_α. This offset was then applied across the whole spectrum. Line identification data was provided as input to VWA from VALD, and the Fe I and Fe II lines were selected by inspection on the basis of minimal blending with other lines in the spectrum. A sample of the resultant line list is shown in Table 4.4, with the complete list given in Appendix F.1. The selected Fe lines then formed the basis of the automated abundance analysis for Fe I and Fe II by feeding each of the lines into WIDTH along with the atomic line data from VALD and the measured equivalent widths for each star measured by the semi–automated routine as described in chapter 3.

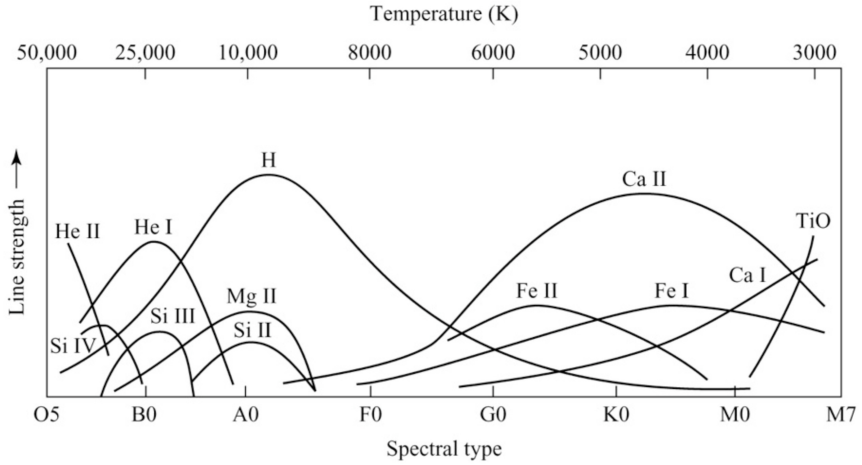

Figure 4.2: Approximate line intensity as a function of effective temperature T_{eff} for several ion specifies, including Fe I and Fe II based on calculations by Payne (1925).

Table 4.4: A sample of the Fe I / Fe II line list used in the Fe abundance analysis in this work. The complete line list is given in Appendix F.1. For each line, $\log(gf)$ represents the oscillator strength; E_i, E_f the initial and final energy levels of the transition in eV; J_i, J_f the J degeneracy (combined spin–orbit coupling) of initial and final levels; gl represents the Landé factor, and γ_r, γ_s and γ_w represent the radiative–, Stark–, and Van der Waals broadening, respectively (Heiter et al. 2008)

Ion	Wl[A]	log(gf)	E_i[eV]	J_i	E_f[eV]	J_f	gl	γ_r	γ_s	γ_w
Fe I	4613.203	−1.67	3.292	0	5.978	1	0.01	7.88	−5.16	−7.158
	4619.288	−1.12	3.602	3	6.286	2	1.7	8.18	−5.86	−7.26
	4643.463	−1.147	3.654	2	6.323	2	1.84	8.36	−5.07	−7.245
	4678.846	−0.833	3.602	3	6.251	4	1.3	8.15	−5.02	−7.279
	4691.412	−1.523	2.99	4	5.632	4	1.05	7.31	−6.22	−7.682
	4707.275	−1.08	3.241	3	5.874	4	1.08	7.88	−5.27	−7.203
	4878.211	−0.888	2.885	0	5.426	1	3	8.18	−5.41	−7.255
	4903.31	−0.926	2.882	1	5.41	2	2.24	8.18	−5.41	−7.259
Fe II	4075.954	−4.792	2.544	2.5	5.585	1.5	1.27	8.56	−6.6	−7.796
	4273.326	−3.303	2.704	1.5	5.605	0.5	2.16	8.56	−6.53	−7.873
	4296.572	−2.933	2.704	1.5	5.589	2.5	0.58	8.47	−6.53	−7.881
	4303.176	−2.511	2.704	1.5	5.585	1.5	1.43	8.56	−6.53	−7.875
	4384.319	−3.684	2.657	5.5	5.484	4.5	0.67	8.47	−6.53	−7.886
	4385.387	−2.582	2.778	0.5	5.605	0.5	1.33	8.56	−6.53	−7.875
	4416.83	−2.602	2.778	0.5	5.585	1.5	0.77	8.56	−6.53	−7.875

4.2 Results of the automation process

A plot of the Fe I abundance ($\log N/N_{\rm tot}$) of the survey stars as a function of effective temperature ($T_{\rm eff}$ increasing from right–to–left) calculated by the automated routine is shown in Fig. 4.3 (asterisks). For comparison, the Fe I abundances calculated

by Adelman (1973) for a selection of 21 cool Ap stars are also plotted (red open squares); for a selection of Ap and roAp stars derived by Ryabchikova et al. (2004) (green open diamonds), and for the Ap stars surveyed by Freyhammer et al. (2008) (blue open triangles). The Fe abundance relative to solar abundance is shown as a horizontal dotted line. It can be seen that in all three sets of data, there is a correlation of higher Fe I abundance with effective temperature, with a correlation r^2 of 0.81 for the FEROS data.

The abundances for the Fe II ions as a function of effective temperature are shown in Fig. 4.4 (black asterisks). In the same figure, the Fe II abundances derived by Adelman (1973) are also plotted for the same selection of roAp stars (red open squares), and for comparison, the Fe II abundances for the same collection of stars as derived by Ryabchikova et al. (2004) (green open diamonds), and for the Ap stars surveyed by Freyhammer et al. (2008) (blue open triangles). The Fe abundance relative to solar abundance is again shown as a horizontal dotted line. Again, there is a correlation of higher Fe II abundance with increasing effective temperature, though it appears less pronounced than the correlation in Fe I, with a correlation r^2 of 0.61 for the FEROS plot.. A plot of Fe I versus Fe II abundance for this subset of Ap stars is presented in Fig. 4.5. A correlation of increasing Fe II abundance with Fe I abundance can be seen.

A sample of the Fe I and Fe II abundances in tabular form are shown in Table 4.5, with the complete list shown in Appendix F.2. The columns $SE_{Fe\,I}$, $SE_{Fe\,II}$ represent, for each star, the standard error (SE) of the derived abundance, in the cases where several absorption lines have been used to calculate an average Fe abundance, as given by:

$$SE = \frac{\sigma}{\sqrt{n_{\rm elem}}}$$

where σ is the standard deviation of the average of the derived abundances, n_{elem} is the number of absorption lines contributing to the average abundance. The columns $n_{Fe\,I}$, $n_{Fe\,II}$ represent the number of Fe I , Fe II lines respectively, contributing to the derived abundance.

Table 4.5: A sample list of stars for which Fe I / Fe II abundances have been calculated in this work, where columns $A_{Fe\,I}$, $A_{Fe\,II}$ show the derived abundances; $SE_{Fe\,I}$, $SE_{Fe\,II}$, the standard error, and $n_{Fe\,I}$, $n_{Fe\,II}$, the number of Fe I / Fe II lines contributing to the analysis. For comparison, the Fe solar abundance is −4.52 (Anders & Grevesse 1989). The complete list is given in Appendix F.2.

Star	$T_{\rm eff}$ (K)	$A_{Fe\,I}$	$SE_{Fe\,I}$	$n_{Fe\,I}$	$A_{Fe\,II}$	$SE_{Fe\,II}$	$n_{Fe\,II}$
HD 2883	6269	−5.27	0.04	55	−4.63	0.16	29
HD 5823	7176	−4.60	0.08	58	−4.40	0.15	28
HD 8783	8250	−3.97	0.08	62	−4.19	0.16	30
HD 23207	8064	−3.89	0.10	63	−3.83	0.15	30
HD 23715	7625	−3.83	0.06	63	−3.68	0.14	31
HD 26726	8008	−3.40	0.14	58	−3.35	0.17	27
HD 29578	7554	−4.63	0.07	65	−4.44	0.15	30
HD 30849	5889	−5.21	0.09	63	−4.30	0.14	30
HD 31973	8203	−4.13	0.09	60	−4.32	0.18	30
HD 33629	7321	−4.03	0.08	62	−4.09	0.22	29

4.2.1 Effects of Microturbulence

The microturbulence effect manifests itself in abundance analysis studies in a broadening of the line profile as the light passes through cells that are in turbulent motion on a scale that is small compared to the mean free path of the photon. We may

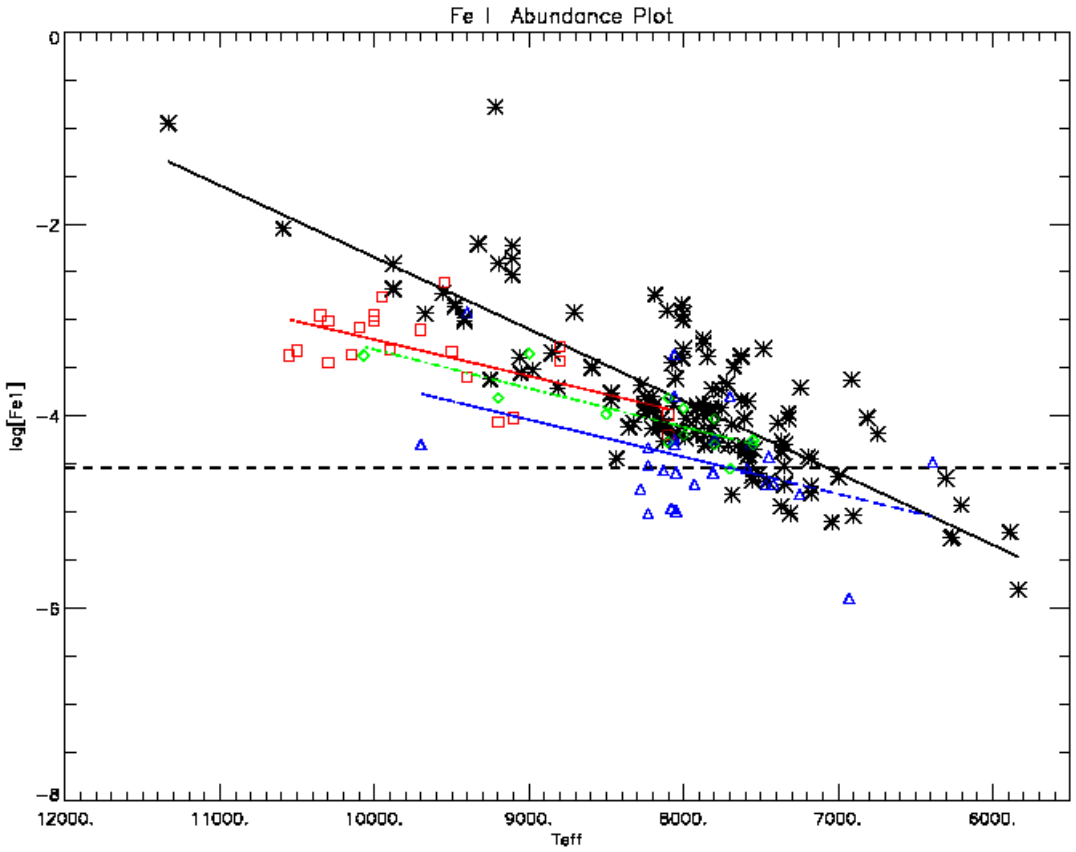

Figure 4.3: Plot of the Fe I abundance (log $N/N_{\rm tot}$) as a function of stellar effective temperature $T_{\rm eff}$ increasing to the left as in an HR–Diagram). A linear regression fit is also shown with a correlation $r^2 = 0.81$ (solid black line). For comparison, the plot also shows the Fe I abundances derived by Adelman (1973) for a selection of cool Ap stars (red open squares), for a selection of Ap and roAp stars derived by Ryabchikova et al. (2004) (green open diamonds), and for the Fe I abundances for a collection of Ap stars derived by Freyhammer et al. (2008) (blue open triangles). The solar abundance is represented by the horizontal dashed line. This result is significant, and represents the most comprehensive Fe abundance survey of Ap stars to date, compiled using spectra all originating from the same spectrograph

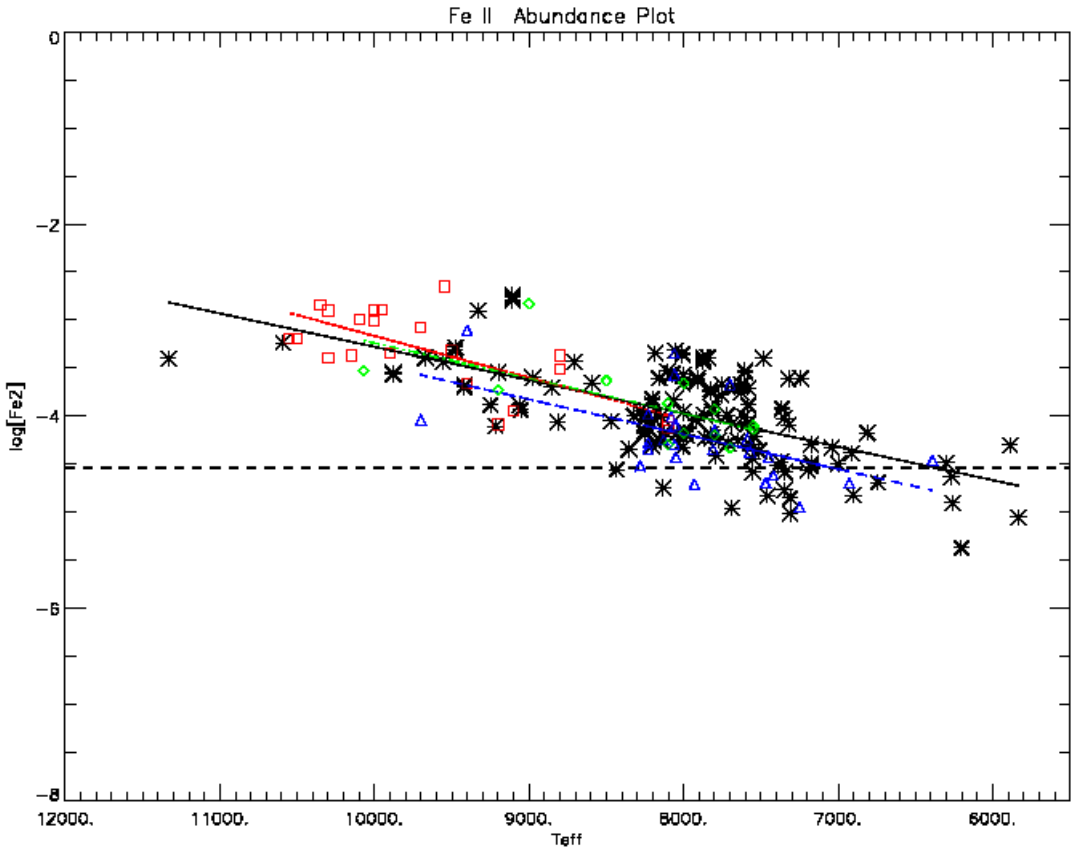

Figure 4.4: Plot of the Fe II abundance (log $N/N_{\rm tot}$) as a function of stellar effective temperature $T_{\rm eff}$ increasing to the left as in an HR Diagram). A linear regression fit is also shown with a correlation $r^2 = 0.61$ (solid black line). For comparison, the plot also shows the Fe II abundances derived by Adelman (1973) for a selection of cool Ap stars (red open squares), for the Fe II abundances for a collection of Ap and roAp stars derived by Ryabchikova et al. (2004) (green open diamonds), and for the Fe II abundances for a collection of Ap stars derived by Freyhammer et al. (2008) (blue open triangles). Linear regression fits for the open squares (dotted, $r^2 = 0.72$); open diamonds (dashed, $r^2 = 0.56$) and open triangles (dash-dot, $r^2 = 0.67$) are also shown. The solar abundance is represented by the horizontal dashed line.

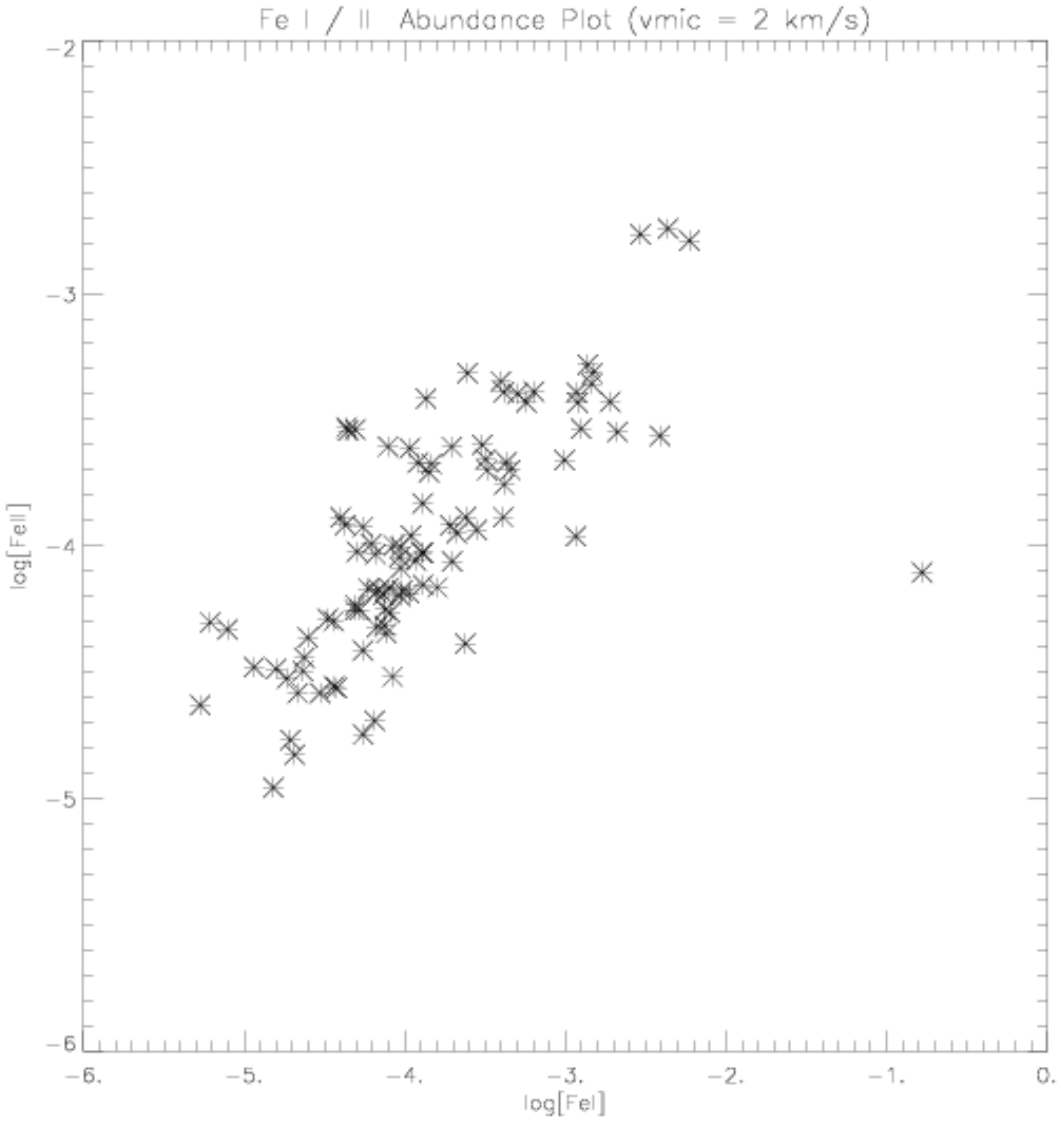

Figure 4.5: Plot of Fe I abundance (log $N/N_{\rm tot}$, x-axis) versus Fe II abundance (log $N/N_{\rm tot}$, y-axis) derived for the Ap stars selected for $v \sin i < 40\,{\rm km\,s^{-1}}$, and for microturbulence $\zeta_{micro} = 2\,{\rm km\,s^{-1}}$

therefore expect to see effects of microturbulence in our sample of spectra, and so to that end, the analysis was repeated using NEMO models and WIDTH simulation based on values for the microturbulence ζ_{micro} of $0\,\mathrm{km\,s^{-1}}$ and $4\,\mathrm{km\,s^{-1}}$, respectively. The abundances for the Fe I ions, and for Fe II ions, as a function of effective temperature for $\zeta_{micro} = 0\,\mathrm{km\,s^{-1}}$ and $4\,\mathrm{km\,s^{-1}}$ are shown in Fig. 4.6. As before, in the same figure, the Fe abundances derived by Adelman (1973) (red open squares), Ryabchikova et al. (2004) (green open diamonds), and Freyhammer et al. (2008) (blue open triangles) are also shown. Plots of the Fe abundance as a function of stellar effective temperature for values of microturbulence ζ_{micro} of $0\,\mathrm{km\,s^{-1}}$, $2\,\mathrm{km\,s^{-1}}$ and $4\,\mathrm{km\,s^{-1}}$ are shown in Fig. 4.7. One can see from this that the derived abundances are enhanced or reduced by around 0.5–0.8 dex for a decrease or increase of $2\,\mathrm{km\,s^{-1}}$, respectively.

4.2.2 Effects of Magnetic Splitting

As discussed earlier in Section 2.8, the Zeeman effect is a manifestation of the effect of the magnetic field which causes degenerate energy levels in an ion/atom to be split,with the sub–levels separated by an energy which is proportional to the Landé factor g associated with the lines involved. The effect is to act as a de-saturation mechanism in a similar way to microturbulence, and so we decided to repeat the analysis using subsets of the original Fe I / Fe II lines at the lower and upper ends of the range of Landé factors. The distribution of Landé factors of the original sample of Fe lines is shown in Fig. 4.8

On the basis of this distribution, we decided to repeat the Fe abundance analysis for Fe I and Fe II lines with Landé factors < 1.00, and then again, only using lines with Landé values > 1.50. The resulting plots of abundances are shown in Fig. 4.9.

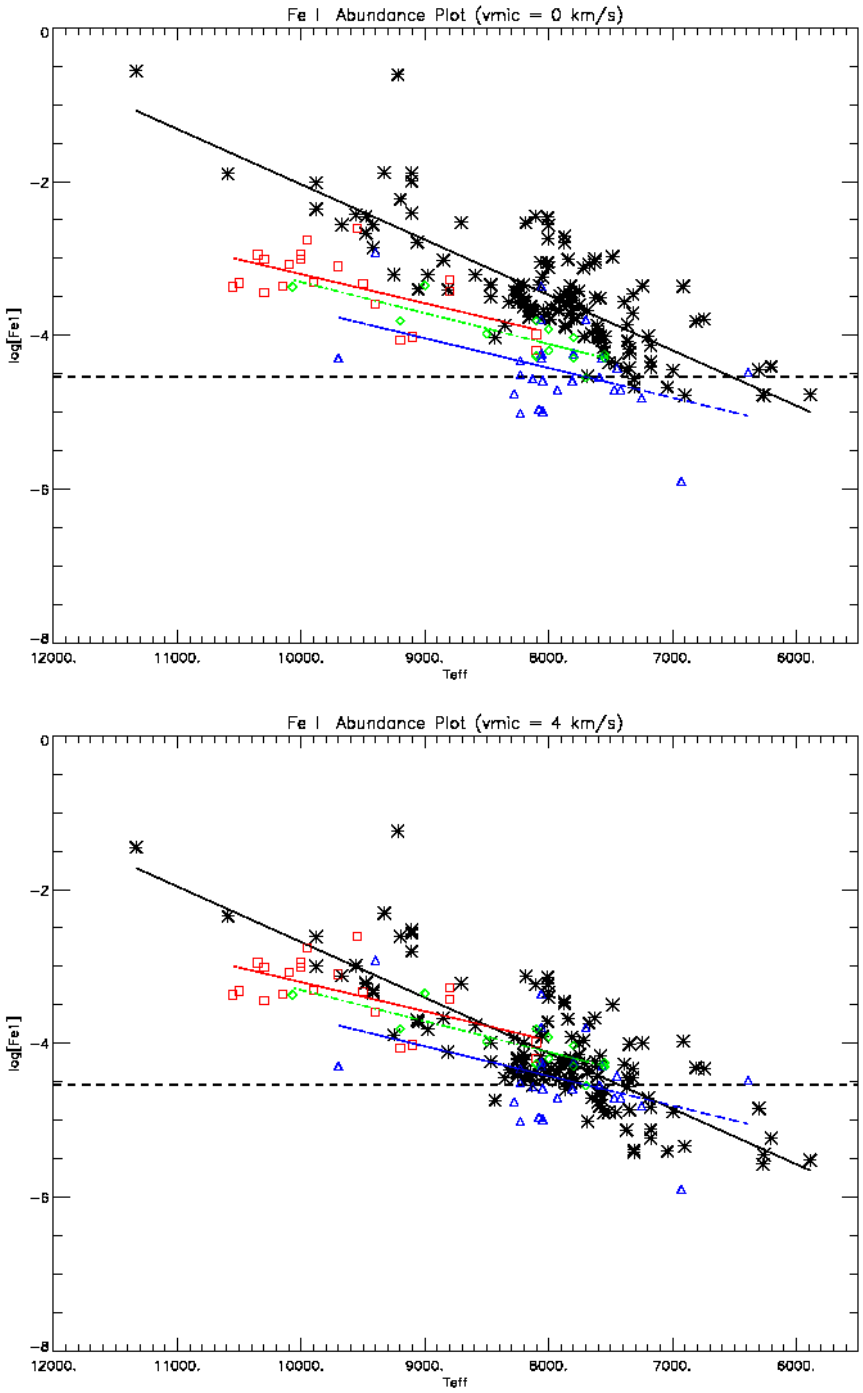

Figure 4.6: Plots of the Fe I abundance (log $N/N_{\rm tot}$) as a function of stellar effective temperature $T_{\rm eff}$ for values of microturbulence ζ_{micro} of $0\,{\rm km\,s^{-1}}$ (upper plot) and $4\,{\rm km\,s^{-1}}$ (lower plot). The Fe abundances derived by Adelman (1973), Ryabchikova et al. (2004) and Freyhammer et al. (2008) are plotted as described in Fig. 4.3

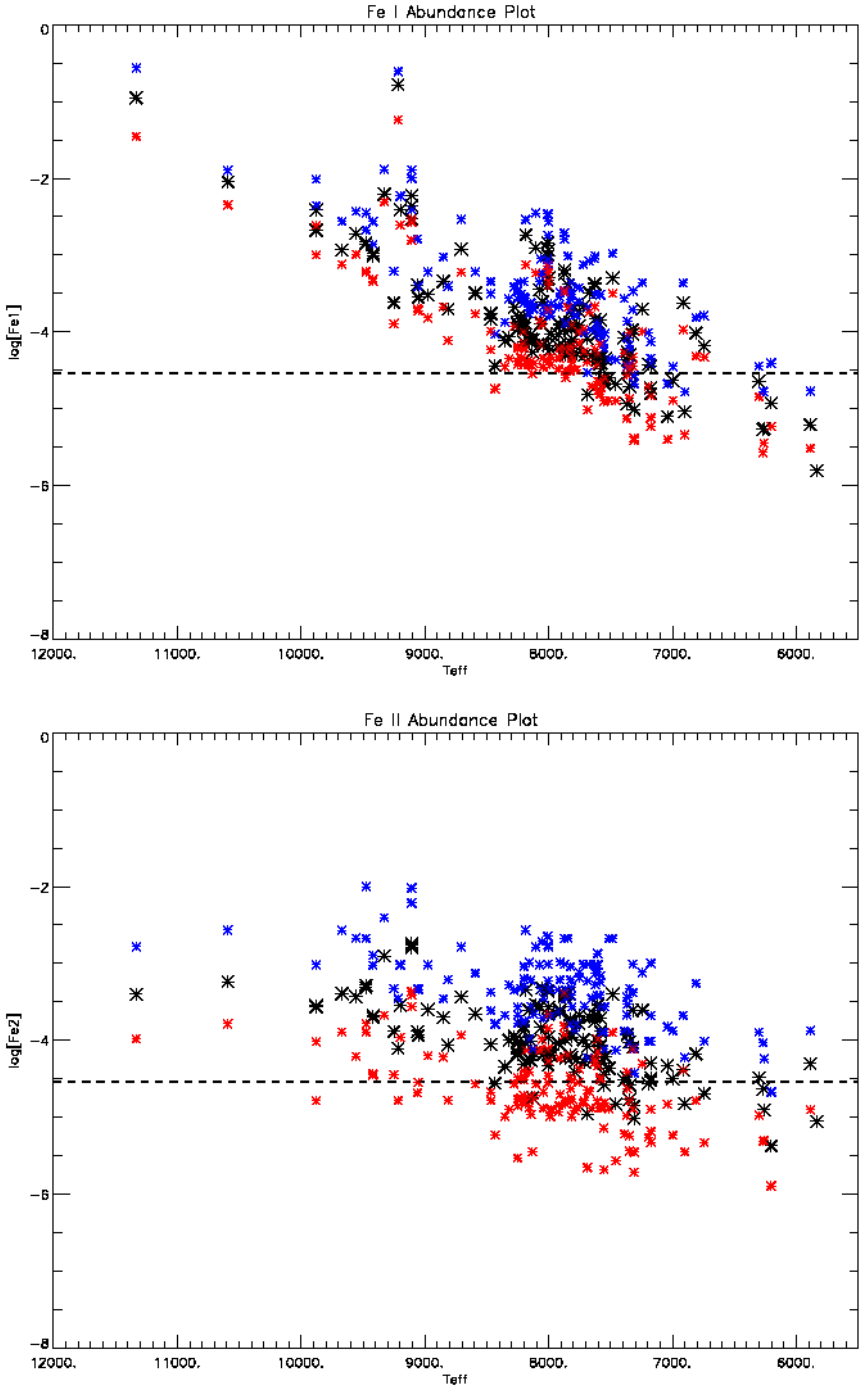

Figure 4.7: Plots of the Fe abundance (log $N/N_{\rm tot}$) as a function of stellar effective temperature $T_{\rm eff}$ for values of microturbulence ζ_{micro} of $0\,{\rm km\,s^{-1}}$ (blue), $2\,{\rm km\,s^{-1}}$ (black) and $4\,{\rm km\,s^{-1}}$ (red) for Fe I (upper plot) and Fe II (lower plot)

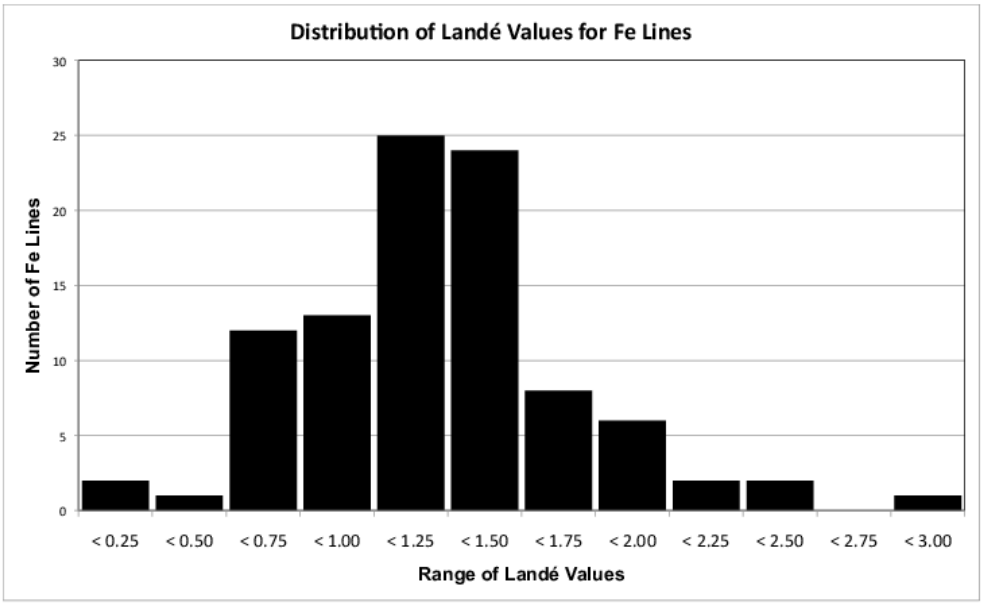

Figure 4.8: Distribution of Landé values g for the sample of Fe I / Fe II lines used in the original abundance analysis

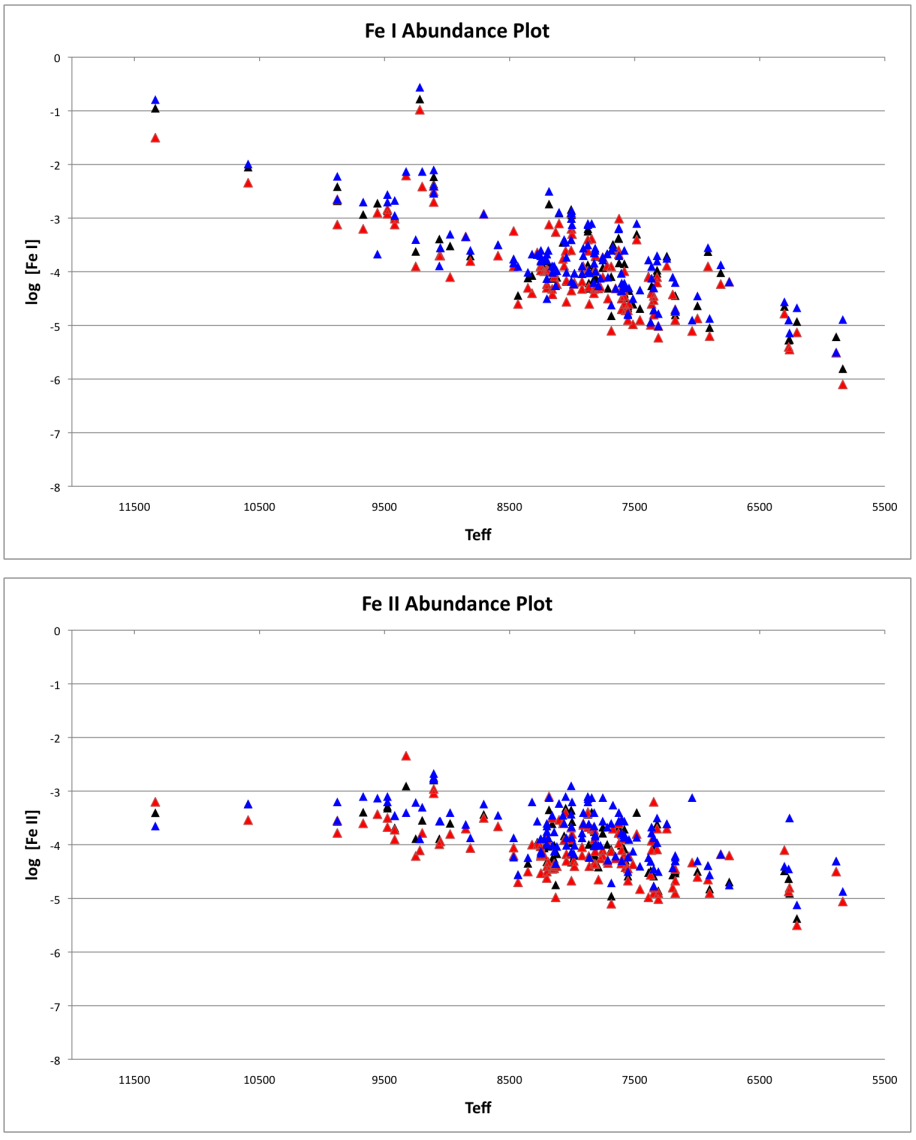

Figure 4.9: Plots of the Fe abundance (log $N/N_{\rm tot}$) as a function of stellar effective temperature $T_{\rm eff}$ for the original line list (black), for a subset of lines with Landé values > 1.50 (red), and for a subset of lines with Landé values < 1.00 (blue), for Fe I (upper plot) and Fe II (lower plot)

4.3 Discussion

While the correlation is less steep than for Fe I, the Fe II abundance clearly increases with increasing T_{eff} in our results, and this trend is clearly evident in both Fig. 4.3 and Fig. 4.4, a trend that is also borne out in the earlier surveys mentioned previously. We can also see from Fig. 4.1 that the recent composite analysis by Ghazaryan et al. (2018) also shows a similar abundance relationship with T_{eff} over the temperature range common to both studies. While there is good agreement in the absolute Fe abundance values at lower temperatures, there is a marked deviation in our results towards significantly higher abundance values at the higher T_{eff} range, particularly in respect of Fe I abundance. Possible reasons for this departure will be explored in the next section. Interestingly, the long controversy about the Fe abundance in HD 101065, Przybylski's star, which has been resolved with acceptance that Fe is deficient in the spectrum of this star, can now be seen to be consistent with the lower Fe abundances at the cool end of the range of Ap stars. With the progression from overabundant to under-abundant Fe as a function of T_{eff}, we expect that the coolest Ap stars will show deficient Fe abundances. We believe that the correlation is real, and that it is present in previous, independent studies. The trend of decreasing Fe I and Fe II abundance with increasing microturbulence as shown in Fig. 4.7 is illustrative of the fact that the effect of microturbulence on saturated transitions is to remove the saturation to a degree by broadening the spectral lines, thus increasing the equivalent widths associated with the transitions more than they might otherwise be if microturbulence were not present. This in turn implies that a reduced number of ions are required in order to result in a given EQW for an increased microturbulence, resulting in a lower derived abundance. Similarly, the effect of the magnetic splitting of some of the lines, resulting in de-saturating transitions and altering the derived abundances has been demonstrated. This implies that we have to be mindful of the line lists that are selected for abundance analysis in this way.

4.4 Conclusion and caveats

As can be seen in Fig. 4.3 and Fig. 4.4, the overall trend of increasing Fe abundance with T_{eff} as derived by the semi-automated abundance routines shows a similar trend to that shown in previous studies. In addition, at the cooler end of the T_{eff} range, there is generally good agreement between the abundances derived by this method and with the earlier surveys. However, there is a marked difference at higher temperatures in that the Fe abundances derived by the routines are significantly higher; in the range of 1–2 dex, particularly in the case of Fe I. This may be due to any one of a number of simplifications inherent in the way the routines process the absorption lines:

- Blending and departure from a Voigt absorption profile. For well–defined unblended line profiles of slowly rotating stars ($v \sin i \ll 40\,\mathrm{km\,s^{-1}}$), comparison between the EQW as measured by the routine (where the full width at half maximum (FWHM) is factored up to specify the baseline) to that measured by hand using MIDAS compares well in such circumstances. However, for lines that diverge from a Voigt profile, this approximation is likely to break down. Also, unlike the technique of generating a synthetic spectrum, the semi–automated routines make no attempt to consider blended lines. Indeed, all lines are deemed to be unblended. However, as rotation increases, the ability to determine unblended lines decreases, as the line profile widens and the baseline increases, increasing with it the chance of line overlap. Furthermore, as we have seen, the discarding of spectra with sample lines deemed to have an apparent rotational velocity greater than $40\,\mathrm{km\,s^{-1}}$ leads to elimination of a significant number of spectra ($> 70\,\%$) from further analysis. It may be that this process of selection is too simplistic.

- Magnetic effects. Unlike some of the earlier surveys, where techniques such

as SYNTHMAG are used to reproduce the magnetic splitting synthetically, the semi-automated routines make no attempt to compensate for magnetic splitting (Zeeman) effects, which in some cases for certain objects with high magnetic fields (HD 75049, for example) can have a profound effect on the line profile of certain lines; see Section 2.8. Hence to a first approximation, the Landé factor characterises magnetic sensitivity of a line and the value of the Landé factor may be used as an indicator of how likely the transition is to exhibit Zeeman splitting. The Landé factors for each transition are available from the VALD database. Selection of transitions with low Landé values may reduce the impact of magnetic splitting on the abundance analysis. We have shown that selection of subsets of lines of low or high Landé value can have an effect on the derived abundances from this study of around 0.2–0.3 dex.

- Uniform microturbulence. In order to simplify the analysis process the automated routines apply a uniform value for the microturbulence of $2\,\mathrm{km\,s^{-1}}$, in contrast to some of the earlier analyses which attempt greater granularity in the application of microturbulence on a line–by–line basis to simulate magnetic line broadening. Fig. 4.7 shows that derived abundances are sensitive to the level of microturbulence modelled, suggesting that a more flexible approach to the inclusion of microturbulence on a line-by-line or star-by-star basis may be preferable.

Despite these limitations, we believe this approach provides a simple way of analysing a significant number of spectra leading to a consistent approach and an associated minimisation in systematic error of the resulting derived abundances.

Chapter 5

Neodymium and Praseodymium Abundance of Ap Stars

The separation of chemical species in the atmospheres of Ap stars under the competitive effects of gravitation, and radiative levitation (Michaud et al. 2015) leads to the elemental stratification effects observed in the absorption spectra of these objects. In particular, the rare earth elements (REE) are extremely enhanced compared to solar abundances, and can rightly be seen as a signature of Ap objects. This phenomenon has been known for some time (Hack 1976; Cowley 1980) and can be explained as a consequence of the considerable number of populated electronic energy levels of these ions and the high number density of associated absorption lines at the flux maximum for the effective temperatures of the stars in question, which promotes radiative levitation towards the upper levels of the stellar atmosphere. This in turn is due to the fact that electronic structure of the REE ion gives rise to a considerable number of potential energy levels as outer–shell electrons are promoted amongst the higher s– p– d– and f– atomic orbitals levels, with associated splitting of degenerate levels due to couple of spin– (S) and orbital angular– (L) momenta; see Fig. 5.1.

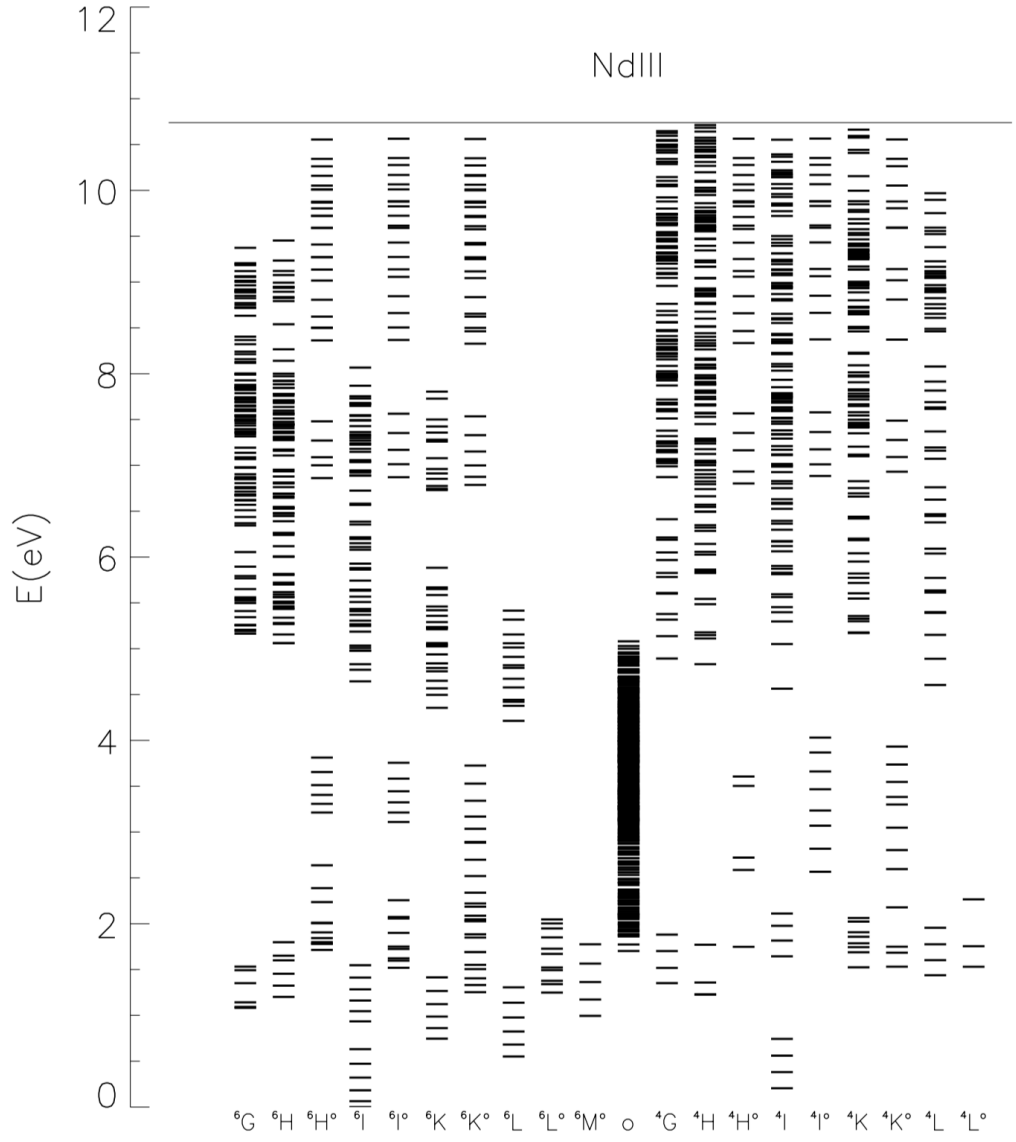

Figure 5.1: Energy levels of the Nd III ion. The term symbols corresponding to the various electronic configurations are shown along the x–axis. The column labelled 'o' corresponds to energy levels that have not been identified (Mashonkina et al. 2005)

CHAPTER 5

5.1 REE Ionisation Disequlibria and Temperature Dependence

There are several potential indicators of elemental stratification in the stellar atmosphere that may become apparent (where different ions of the same element are formed at different atmospheric layers) when conducting abundance analyses. These were introduced in Chapter 1, and include ionisation disequilibrium; the core–wing anomaly; departure from conditions of local thermodynamic equilibrium (LTE), and discrepancies in the abundances derived from strong and weak lines of the same ion (Ryabchikova et al. 2003). An earlier abundance analysis by Ryabchikova et al. (2001) of 6 Ap and 6 roAp stars, all of similar $T_{\rm eff}$, reported that, based on line intensities in the spectra for Nd and Pr, the abundances derived for Nd III and Pr III were significantly higher, by around 2 dex, than those of the corresponding Nd II and Pr II ions in the case of the roAp stars, whereas no such anomaly was seen in the comparative Ap stars. The same phenomenon has also been reported elsewhere (Cowley et al. 2000; Ryabchikova et al. 2000; Kochukhov 2003). One of the questions arising from this observation was whether the observed disequilibria might be a spectroscopic signature of the onset of roAp pulsation phenomena. To address this question, a later abundance study including a greater number of targets was conducted by Ryabchikova et al. (2004) for 23 Ap stars, 13 cooler roAp stars and 4 roAp candidates. This analysis was discussed in the previous chapter in the context of our Fe I and Fe II abundance results. However, the analysis comprises derived abundances for 32 elements in total, including the rare earth ion species for elements Ce, Pr, Nd, Sm, Eu, Gd, Tb, Dy, Er, Yb and Lu. The spectra for the analysis were collected at four different facilities; the European Southern Observatory in Chile (ESO), the South African Astronomical Observatory (SAAO), the

Canada–France–Hawaii Telescope (CFHT) and the Crimean Astrophysical Observatory (CrAO). The initial fundamental parameters were derived from TEMPLOGG using Strömgren photometry (Hauck & Mermilliod 1998; Martinez 1993).

A plot of abundance differences of the first and second ions of Nd and Pr versus T_{eff} show a marked drop from around 1.5-2 dex for the roAp stars, to a negligible value for the Ap stars; see Fig. 5.2. The roAp and Ap stars in their study occupy different temperature ranges. The roAp stars are cooler than the group of Ap stars, with a transition temperature around 8 100 K, leading the authors to suggest that the rare earth element anomaly may be a distinguishing feature that separates roAp and Ap stars.

A much later study (Ryabchikova & Romanovskaya 2017) derived abundances for REE elements Ce, Nd, Pr and Eu for 26 magnetic Ap stars in the effective temperature range $7\,000\,\mathrm{K} \leqslant T_{eff} \leqslant 10\,000\,\mathrm{K}$. The spectra originated from three different sources: the UVES (UV and Visual Echelle Spectrograph) at ESO VLT in Chile, the ESPaDOnS (Echelle SpectroPolarimetric Device for the Observation of Stars) spectrograph at the Canada–French–Hawaii Telescope CHFT, and the FEROS spectrograph at La Silla. Again the REE anomaly is observed, decreasing with increasing T_{eff}, except for Eu. The Nd disequilibrium is shown to decrease with increasing magnetic field strength at the cool end of the T_{eff} range. One of the objectives of this research is to test whether rare earth element ionisation disequilibrium is indeed a signature of the pulsating roAp stars, or instead is simply correlated with T_{eff}. Analysis over such a large survey of Ap targets in our study has allowed us to come to some conclusions about this.

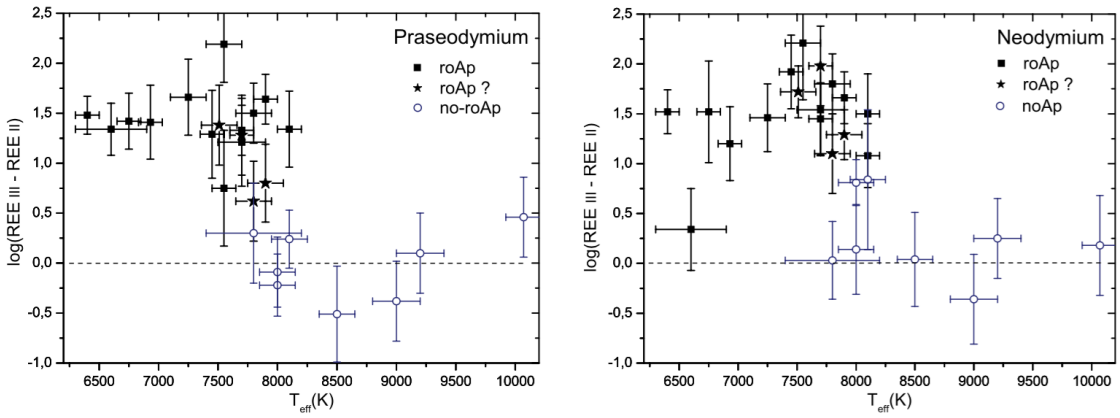

Figure 5.2: Dependence of the Pr (left panel) and Nd (right panel) anomaly on temperature (Ryabchikova et al. 2004)

5.2 Method

The method of approach taken in deriving the Fe I / Fe II abundances in our survey is described in more detail in section 4.1. A similar approach was employed in deriving the Nd II / Nd III and Pr II / Pr III abundances; only the differences will be described here. The Nd / Pr line list used in this analysis was compiled from a number of sources, including preceding studies (Adelman 1973; Mashonkina et al. 2005, 2009), along with observation of suitable lines in the spectrum of HD 82989 using VWA, and the atomic parameters were then extracted from the VALD database. A sample line list is shown in Table 5.1; the complete table is given in Appendix G.1. As before with the Fe analysis, the selected Nd / Pr lines were then used in the automated abundance analysis for Nd II / Nd III and Pr II / Pr III by feeding the equivalent width measured for each for each line and for each star into WIDTH along with formatted atomic line data from VALD as described in Chapter 3. The resulting abundances were then collated and averaged for further evaluation.

Table 5.1: Sample of the Nd II / Nd III / Pr II / Pr III line list used in the Pr / Nd abundance analysis in this work. The complete list is given in Appendix G.1. For each line, $\log(gf)$ represents the oscillator strength; E_i, E_f the initial and final energy levels of the transition in eV; J_i, J_f the J degeneracy (combined spin–orbit coupling) of initial and final levels; gl represents the Landé factor, and γ_r, γ_s and γ_w represent the radiative–, Stark–, and Van der Waals broadening, respectively. (Heiter et al. 2008)

Ion	Wl[A]	log(gf)	E_i[eV]]	J_i	E_f[eV]	J_f	gl	γ_r	γ_s	γ_w
Nd II	4061.080	0.550	0.471	7.5	3.524	8.5	1.07	0.000	−5.327	0.000
	4706.543	−0.710	0.000	3.5	2.634	2.5	0.61	0.000	0.000	0.000
	4811.342	−1.015	0.064	4.5	2.640	3.5	0.77	0.000	0.000	0.000
	5033.507	−0.470	1.136	9.5	3.599	8.5	1.09	0.000	0.000	0.000
	5063.722	−0.620	0.976	8.5	3.423	7.5	1.15	0.000	0.000	0.000
	5077.154	−1.047	0.823	7.5	3.264	6.5	0.73	0.000	0.000	0.000
Nd III	4796.500	−1.650	0.141	5.0	2.725	6.0	1.54	0.000	0.000	0.000
	5286.753	−1.900	0.631	8.0	2.976	7.0	1.50	0.000	0.000	0.000
	5294.113	−0.690	0.000	4.0	2.341	4.0	0.62	0.000	0.000	0.000
	5633.554	−2.220	0.141	5.0	2.341	4.0	1.43	0.000	0.000	0.000
	5677.179	−1.450	0.631	8.0	2.815	7.0	1.60	0.000	0.000	0.000
	5845.020	−1.180	0.631	8.0	2.752	9.0	1.10	0.000	0.000	0.000
Pr II	4368.334	−0.393	0.000	4.0	2.837	5.0	1.79	0.000	0.000	0.000
	4405.825	−0.392	0.550	8.0	3.363	8.0	1.20	0.000	0.000	0.000
	4672.087	−0.781	0.216	5.0	2.869	6.0	1.56	0.000	0.000	0.000
Pr III	6071.085	−2.360	0.359	6.5	2.400	6.5	1.11	0.000	0.000	0.000
	6090.010	−0.820	0.359	6.5	2.394	5.5	1.05	0.000	0.000	0.000
	6160.233	−0.980	0.173	5.5	2.185	4.5	0.89	0.000	0.000	0.000
	6161.194	−1.140	1.549	5.5	3.561	4.5	1.31	0.000	0.000	0.000
	6706.703	−1.640	0.552	7.5	2.400	6.5	1.48	0.000	0.000	0.000

5.3 Results of the automation process

A plot of the Nd II and Nd III abundances ($\log N/N_{\rm tot}$) of the survey stars as a function of effective temperature ($T_{\rm eff}$ increasing from right–to–left) derived by the automated routine is shown in Fig. 5.3. Whilst there is no apparent strong correlation of Nd III abundance with $T_{\rm eff}$ (lower plot), there does appear to be a strong correlation of Nd II abundance with $T_{\rm eff}$ (upper plot), with a 'goodness of fit' value of r^2=0.79.

A plot of the Pr II and Pr III abundances ($\log N/N_{\rm tot}$) as a function of effective temperature $T_{\rm eff}$ is similarly shown in Fig. 5.4. Again, although there is no apparent correlation of Pr III abundance with $T_{\rm eff}$ (lower plot), there does appear to be a strong correlation of Pr II abundance with $T_{\rm eff}$ (upper plot), with a 'goodness of fit' value in this case of r^2=0.65.

Finally, plots showing the abundance difference between the III and II ion states are shown in Fig. 5.5 for Nd (upper plot) and Pr (lower plot). These plots also indicate the stars that are known from the literature to be roAp stars; these stars are also marked in the last column of Appendix B with the symbol 'r' . Comparison with the results of Ryabchikova et al. (2004) in Fig. 5.2 show a similar trend of increasing disequlibrium with $T_{\rm eff}$, so that the cooler stars show an overabundance of the III ion up to 2 dex, and with the overabundance decreasing with increasing $T_{\rm eff}$. Unlike Ryabchikova et al., our results show a slight under-abundance of the III ion with respect to II at the hottest effective temperatures. A sample list of stars for which Nd II / Nd III and Pr II / Pr III abundances have been calculated is shown in Table 5.2; the complete list is given in Appendix G.2.

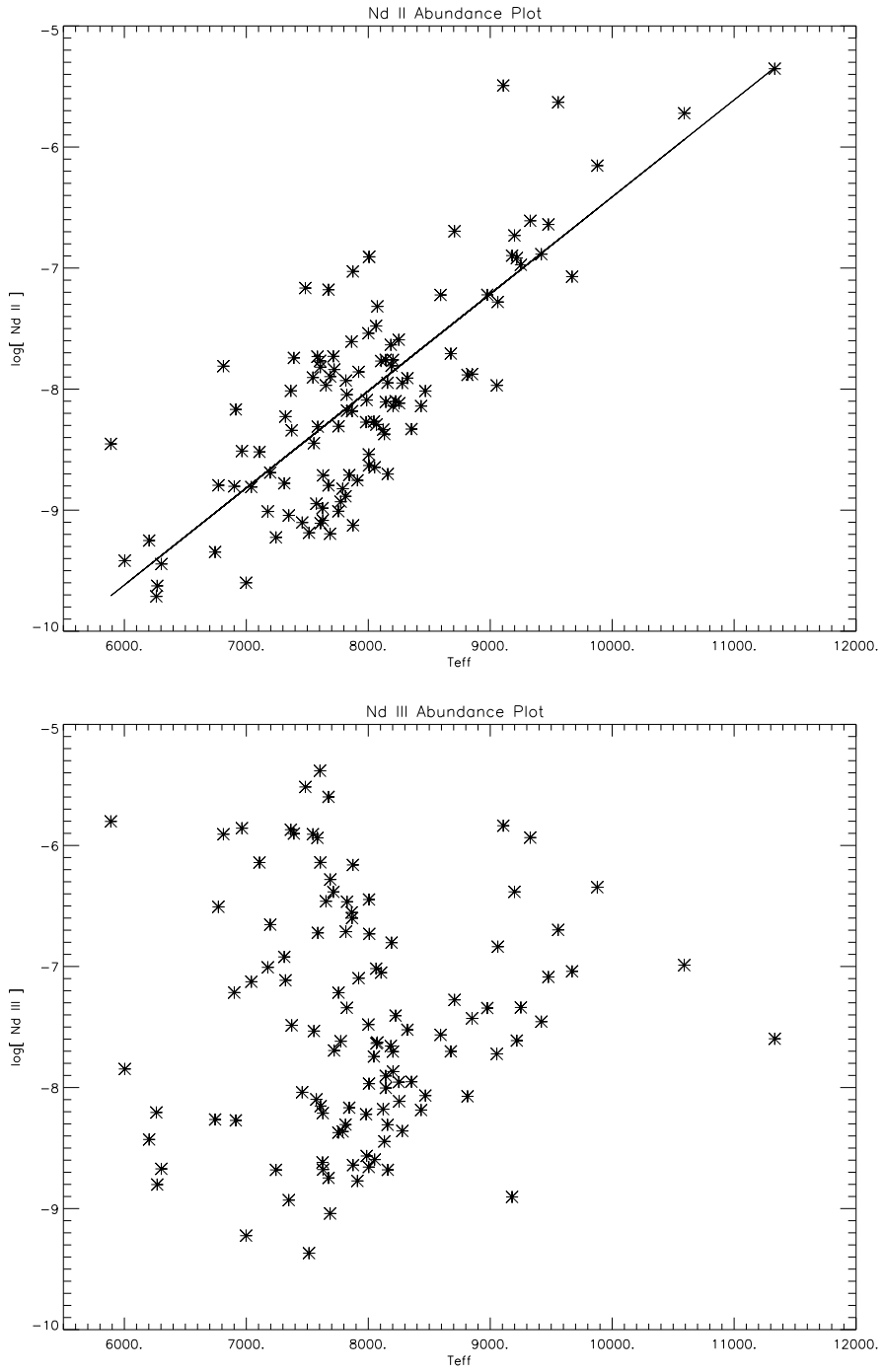

Figure 5.3: Plot of the Nd abundance (Nd II: upper figure; Nd III: lower figure), showing (log N/$N_{\rm tot}$) as a function of increasing stellar effective temperature $T_{\rm eff}$. A linear regression fit is also shown on the Nd II plot with a correlation $r^2 = 0.79$ (solid black line)

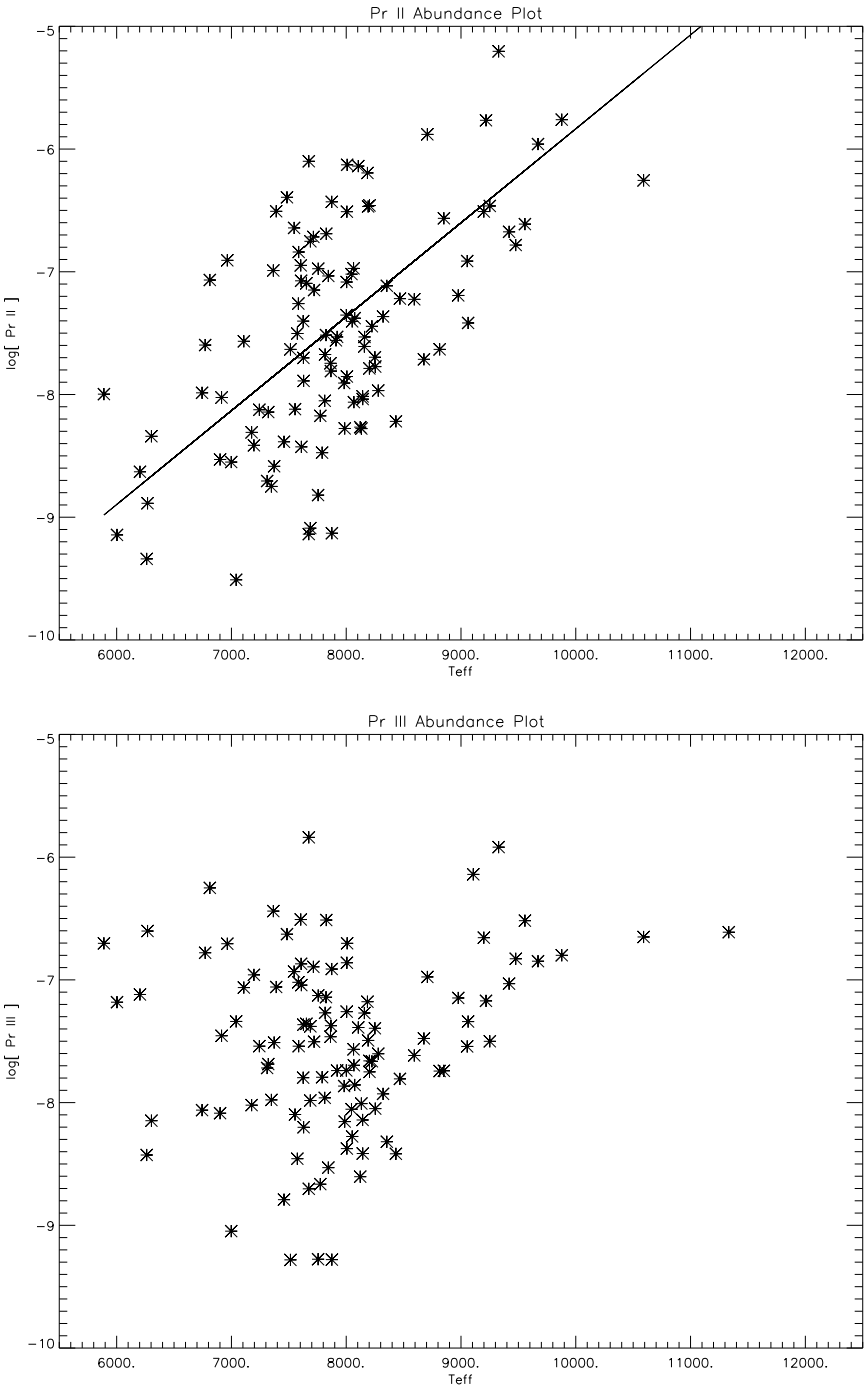

Figure 5.4: Plot of the abundance (Pr II: upper figure; Pr III: lower figure), showing (log N/$N_{\rm tot}$) as a function of increasing stellar effective temperature $T_{\rm eff}$. A linear regression fit is also shown on the Pr II plot with a correlation $r^2 = 0.65$ (solid black line)

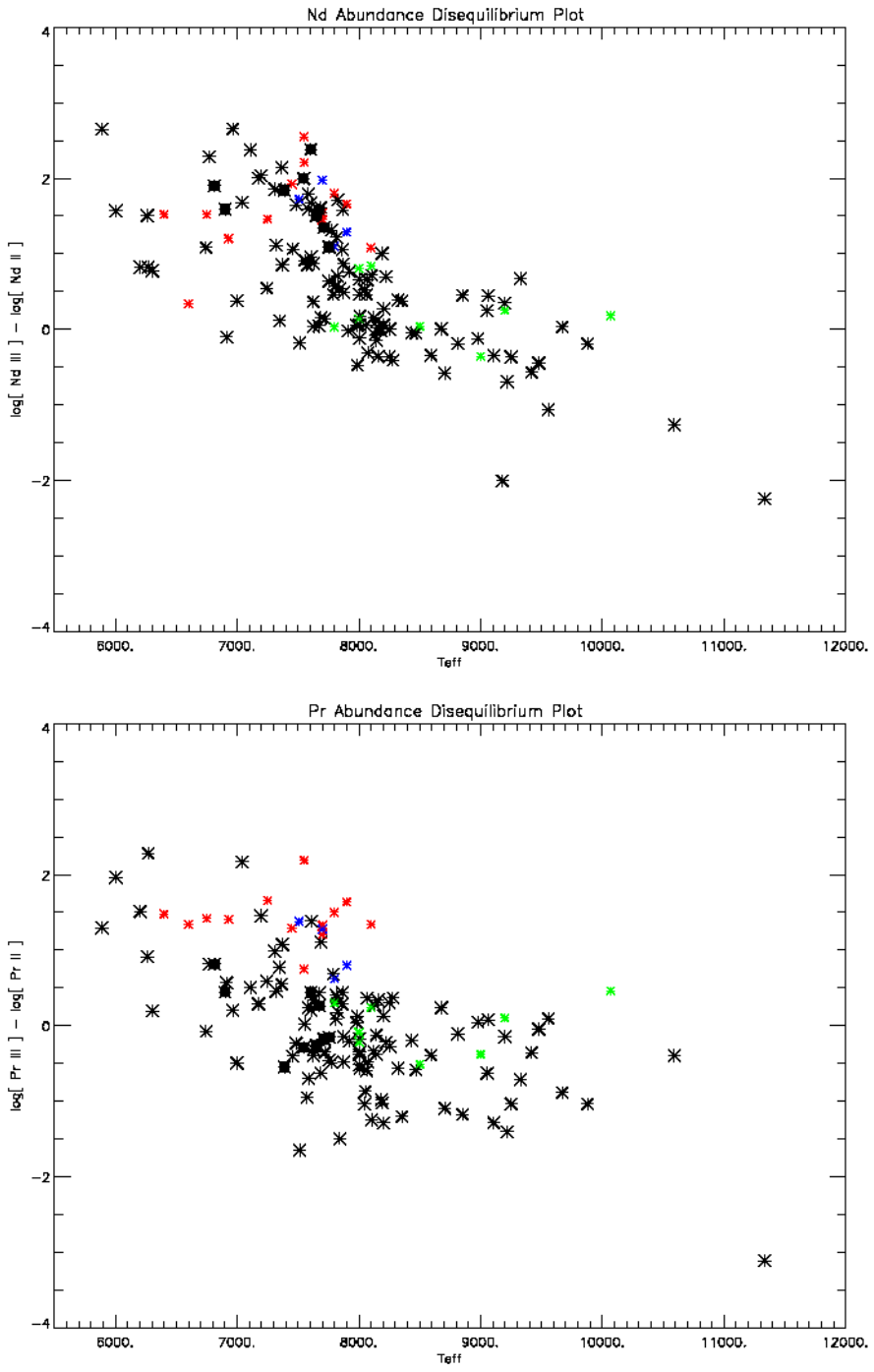

Figure 5.5: Plot of the elemental abundance disequilibrium (Nd: upper figure; Pr: lower figure) showing (log $[N\,\mathrm{III} - N\,\mathrm{II}]/N_{\mathrm{tot}}$) as a function of increasing stellar effective temperature $\mathrm{T_{eff}}$. Confirmed roAp stars from the FEROS results are shown as black squares. The Nd / Pr disequilibrium results derived by Ryabchikova et al. (2004) are also shown, for roAp stars (red asterisks), roAp candidates (blue asterisks) and non-roAp (green asterisks)

Table 5.2: A sample list of stars for which Nd II / Nd III and Pr II / Pr III abundances have been calculated in this work, where columns A_{ion} show the derived abundances for each ion species, and n_{ion} the number of lines contributing to the analysis. The complete list is given in Appendix G.2

Star	$T_{\rm eff}$ (K)	$A_{Nd\,II}$	$n_{Nd\,II}$	$A_{Nd\,III}$	$n_{Nd\,III}$	$A_{Pr\,II}$	$n_{Pr\,II}$	$A_{Pr\,III}$	$n_{Pr\,III}$
HD 2883	6269	−9.62	11	−8.80	2	−8.89	10	−6.60	1
HD 5823	7176	−9.01	10	−7.01	11	−8.31	8	−8.02	3
HD 8783	8250	−7.59	7	−7.96	9	−7.69	9	−7.39	3
HD 23207	8064	−7.48	9	−7.02	10	−6.97	5	−7.57	10
HD 23715	7625	−8.98	6	−8.62	5	−7.40	7	−7.80	1
HD 26726	8008	−6.91	10	−6.73	9	−6.13	7	−6.70	3
HD 29578	7554	−8.45	6	−7.53	11	−8.12	10	−8.10	5
HD 30849	5889	−8.45	9	−5.80	9	−7.80	8	−6.70	5
HD 31973	8203	−8.14	5	−7.87	9	−6.46	5	−7.75	3
HD 33629	7321	−8.23	13	−7.11	11	−8.14	9	−7.69	5

5.4 Discussion

Although the correlation for Pr is less steep and less pronounced than for Nd, we can see that the disequlibrium effect increases perceptibly with increasing $T_{\rm eff}$ in our results; this trend is shown in Fig. 5.5, a trend that is also observed in the survey by Ryabchikova et al. (2004) referred to previously. In the latter paper, the authors go on to make the case for REE disequlibrium as an indication of the onset of roAp pulsation below $\sim 8\,100$ K, with roAp and Ap stars occupying differing areas of the temperature range. From the objects in our FEROS data that are known to be roAp objects, Fig. 5.5 shows that for the Nd data, the FEROS roAp stars exhibit increasing disequilibrium with lower $T_{\rm eff}$ in line with the observations of Ryabchikova et al. (2004). The Pr disequilibrium plot is less equivocal in this regard. In the main,

the roAp stars in our FEROS data do not show an increased disequilibrium effect with lower $T_{\rm eff}$. However, our more extensive survey comprising a significantly greater number of Ap objects, and using a dataset of spectra all collected on the same FEROS spectrograph, suggests that REE disequilibrium may instead be characteristic of all cool Ap stars below a certain $T_{\rm eff}$. There are roAp stars that do not show strong Pr and Nd disequilibium effects, but do so in the case of the ion Ce II. There is another, KIC 10195926, that shows little overabundance of rare earth elements at all. However, Kurtz et al. (2011) showed that the low-amplitude roAp star KIC 10195926 does not have strongly overabundant rare earth elements, and hence no apparent disequilibrium between ionisation stages. The Nd and Pr disequilibria are strongly correlated with $T_{\rm eff}$ so that the roAp stars, which only appear for lower $T_{\rm eff}$ in the range for Ap stars, almost all show the disequilibria. This is neither necessary, or sufficient. It is simply that the Nd and Pr disequilibria are a proxy in this case for $T_{\rm eff}$, and the roAp stars have a restricted range of $T_{\rm eff}$. Therefore, we believe that the disequilibria are not a signature for roAp pulsations. If disequilibria had been a necessary condition for roAp pulsations, that would indicate that those pulsations needed the atmospheric structure that arises from the stratification.

5.5 Conclusion and caveats

We believe that the analysis of Pr and Nd abundances over a large number of stars in our survey shows a significant REE disequlibrium effect in the cooler Ap stars, and that it it more likely to be subject to a transitional $T_{\rm eff}$ value, rather than acting as a signature of roAp pulsation as has been suggested in earlier studies. Extending our survey to include additional REE ion pairs in the future may allow us to investigate this effect in other ion species. Having said that, the simplifications in the analysis in the case of the Fe I / Fe II discussed at the end of Chapter 4, namely: elimination of a significant proportion of the available spectra based on a

simple $v \sin i$ test on one absorption line; no consideration of magnetic or potential blending effects, or departure from a Voigt absorption profile; the application of a standard microturbulence value across all spectra, are all also applicable in this case. Another potential limitation of our approach is the application of a single line list across the whole $T_{\rm eff}$ range. Nd and Pr line intensities diminish significantly at higher effective temperatures in this survey, so it may be more appropriate to introduce different line lists for differing ranges of $T_{\rm eff}$. This, and other possible improvements to our approach will discussed in the next chapter.

Chapter 6

Conclusions and Future Work

The semi-automated routines provide an efficient method of analysing the collection of spectra we have and provide an overview of derived abundances for ion species of choice. The results provide a sound basis for a more detailed investigation by more time-intensive manual techniques. There are some limitations to the approach, and considerations for improvement that are worthy of further discussion and evaluation.

6.1 Temperature-dependent line lists

The current implementation of the semi-automated abundance routines uses a single line list to derive abundances for all spectra forming part of the analysis, independent of the T_{eff} of the stellar object being analysed. However, the temperature has a profound effect on the distribution of the ions among the ionic states, and the occupancy of the excited states of the ion(s) of interest, and therefore has a significant effect on the equivalent width (EQW) of a line profile; see Fig. 4.2. Therefore, in order to try to maximise the number of lines of suitable EQW across the range of T_{eff} values, one approach would be to define different line list sets for different ranges of T_{eff}, and use the automation logic to apply the line list appropriately. Synthetic spectra may be used to simulate the line depths for an absorption line at

different values of $T_{\rm eff}$, to establish the dependency of one on the other, and allow by inspection, selection of the most appropriate line(s) to use for a particular $T_{\rm eff}$. Alternatively, inspection of Ap spectra corresponding to a range of $T_{\rm eff}$ values may yield the best lines to use for each temperature range. This approach comes with some caveats. Firstly, we need to avoid selecting the strongest lines in order to avoid saturation (corresponding to the central region of Fig. 1.10), so we may need to restrict the acceptable EQW to a certain threshold level (an EQW $< 100\,$mA, say). We also need to be aware that a line chosen for use on the basis of a lack of blending at one $T_{\rm eff}$, may be subject to blending at another $T_{\rm eff}$ by proximity in terms of wavelength with other lines that may come into prominence, thus rendering that line unsuitable for selection at the latter temperature. Even at a given $T_{\rm eff}$, Ap stars have individual and distinct peculiarities, making automation of the abundance analysis process more difficult.

6.2 More sophisticated approach to spectral evaluation

The mechanism for the selection of suitable spectra for additional processing is described in Section 3.7. In brief, the EQWs for two specific Fe I lines are measured for each spectrum, and converted to a nominally averaged $v \sin i$ value by interpolation of the relationship between EQW and $v \sin i$ for the same lines generated synthetically under the same fundamental conditions. Only spectra which have an average estimated $v \sin i$ value $< 40\,{\rm km\,s^{-1}}$ are subsequently included for further analysis. This simple approach has some limitations. For example, if one or other of the actual lines is not particularly strong in the spectrum being assessed, possibly due to the $T_{\rm eff}$ of the object under consideration, as discussed in the previous section, then the spectrum may be prematurely discounted from the analysis, and indeed our present

approach currently leads overall to around 70% of spectra being eliminated from further analysis at this stage. One option may be to increase the number of target lines used for the $v \sin i$ assessment; lines for which a significant proportion may be expected to remain prominent over the T_{eff} range of the target stars. Accepting the spectrum for further analysis when, say any two or three of the lines are assessed to represent a $v \sin i$ value $< 40\,\mathrm{km\,s^{-1}}$ should allow an increased proportion of the spectra to be included in the analysis without compromising the integrity of the survey.

6.3 Minimising magnetic effects

The program SYNTHMAG (Piskunov 1999) can be used to generate synthetic spectra taking into account the Zeeman splitting of spectral lines susceptible to the presence of the strong magnetic field typically associated with Ap stars. The abundances are adjusted until an acceptable fit between synthetic and observed spectrum is reached. However, this iterative process is complex and does not lend itself particularly well to an efficient automated abundance survey of a large number of spectra. The extent of splitting is determined by the strength of the magnetic field, and also the susceptibility to splitting of the energy levels associated with the transition as measured by the Landé factor g which characterises the angular momentum of an atom, as described in Section 4.4. One way to try and mitigate the effect of this Zeeman splitting would be to limit the selection of lines comprising the line list to those associated with only a small Landé factor. This parameter is available for review when selecting lines in the VALD database, facilitating the selection of lines with only a small Landé factor.

6.4 Extending the abundance analysis to other elements

This work has focused on surveying the abundances of Fe and Nd / Pr ion species. However, this approach may be extended to incorporate other ions, such as the iron peak and other rare earth elements. The technique is only limited in this regard by the extent to which suitably strong unblended lines in the spectral region of this survey 3600 - 9460 Å can be identified and line data extracted from the VALD database in order to build the input parameters for the WIDTH routine. To illustrate the benefit our approach may bring to investigating the abundances of other elements; the recent compilation of abundance analyses by Ghazaryan et al. (2018) comprised 188 ApBp stars with published Ce abundances for 77 of them taken from 32 contributing papers, including references for 27 Ce abundances from one paper referred to in the previous chapter; Ryabchikova & Romanovskaya (2017), with the remainder extracted from among the 31 other papers. Even in the former paper, the spectra originated from several different sources. A potential advantage in a survey using our technique is that all spectra were recorded on the one (FEROS) instrument, so that it should be possible to undertake a Ce abundance analysis from our data set while minimising the systematic errors associated with observations from multiple sources.

6.5 Conclusions

Using our semi-automated approach, we have analysed 137 spectra relating to 111 Ap objects, taken from a base of 435 spectra relating to 352 stars. We derived Fe I / Fe II abundances, demonstrating a similar trend to that shown in earlier studies, of increasing abundance of Fe I and Fe II with increasing T_{eff}.

In the case of Nd II / Nd III and Pr II / Pr III abundances, our survey, based on a significantly greater number of Ap objects than in earlier studies, and using a dataset of spectra all collected on the same FEROS spectrograph, shows a significant REE disequlibrium effect in the cooler Ap stars, demonstrating what we believe to be a transitional T_{eff} effect rather than a signature of roAp pulsation. We believe that there are still some significant enhancements to be made to our technique; that the approach is sound, and can be extended relatively easily to incorporate other element species of interest.

References

Adelman, S. J. 1973, ApJS, 26, 1

Alecian, G. & Stift, M. J. 2010, A&A, 516, A53

Aller, L. H., Appenzeller, I., Baschek, B., et al., eds. 1982, Landolt-Börnstein: Numerical Data and Functional Relationships in Science and Technology - New Series " Gruppe/Group 6 Astronomy and Astrophysics " Volume 2 Schaifers/Voigt: Astronomy and Astrophysics / Astronomie und Astrophysik " Stars and Star Clusters / Sterne und Sternhaufen, 54

Anders, E. & Grevesse, N. 1989, Geochim. Cosmochim. Acta, 53, 197

Árnadóttir, A. S., Feltzing, S., & Lundström, I. 2010, A&A, 521, A40

Babcock, H. W. 1947a, PASP, 59, 112

Babcock, H. W. 1947b, PASP, 59, 260

Babcock, H. W. 1947c, ApJ, 105, 105

Babcock, H. W. 1960, ApJ, 132, 521

Baglin, A., Auvergne, M., Catala, C., Michel, E., & COROT Team. 2001, in ESA Special Publication, Vol. 464, SOHO 10/GONG 2000 Workshop: Helio- and Asteroseismology at the Dawn of the Millennium, ed. A. Wilson & P. L. Pallé, 395–398

Banse, K., Crane, P., Grosbol, P., et al. 1983, The Messenger, 31, 26

Belopolsky, A. 1913, Astronomische Nachrichten, 196, 1

Biermann, L. 1932, ZAp, 5, 117

Boumier, P., Benomar, O., Baudin, F., et al. 2014, A&A, 564, A34

Bruntt, H., Bikmaev, I. F., Catala, C., et al. 2004, A&A, 425, 683

Bruntt, H., Catala, C., Garrido, R., et al. 2002, A&A, 389, 345

Cannon, A. J. & Pickering, E. C. 1901, Annals of Harvard College Observatory, 28, 129

Carquillat, J.-M. & Prieur, J.-L. 2007, MNRAS, 380, 1064

Castelli, F. 2005, Memorie della Societa Astronomica Italiana Supplementi, 8, 44

Castilho, B. V., Gregorio-Hetem, J., Spite, F., Barbuy, B., & Spite, M. 2000, A&A, 364, 674

Chandrasekhar, S. 1950, Radiative transfer.

Chandrasekhar, S. 1957, An introduction to the study of stellar structure.

Cowley, C. R. 1980, Vistas in Astronomy, 24, 245

Cowley, C. R., Hubrig, S., Ryabchikova, T. A., et al. 2001, A&A, 367, 939

Cowley, C. R., Ryabchikova, T., Kupka, F., et al. 2000, MNRAS, 317, 299

Crawford, D. L. 1958, ApJ, 128, 185

Crawford, D. L. 1975, AJ, 80, 955

Crawford, D. L. 1978, AJ, 83, 48

Crawford, D. L. 1979, AJ, 84, 1858

Crawford, D. L. & Barnes, J. V. 1969, AJ, 74, 818

Crawford, D. L. & Barnes, J. V. 1974, AJ, 79, 687

Crawford, D. L., Glaspey, J. W., & Perry, C. L. 1970, AJ, 75, 822

Dekker, H., D'Odorico, S., Kaufer, A., Delabre, B., & Kotzlowski, H. 2000, in Proc. SPIE, Vol. 4008, Optical and IR Telescope Instrumentation and Detectors, ed. M. Iye & A. F. Moorwood, 534–545

Deutsch, A. J. 1956, PASP, 68, 92

Dukes, Robert J., J. & Adelman, S. J. 2018, PASP, 130, 044202

Eddington, A. S. 1926, The Internal Constitution of the Stars

Freyhammer, L. M., Elkin, V. G., Kurtz, D. W., Mathys, G., & Martinez, P. 2008, MNRAS, 389, 441

Gardiner, R. B., Kupka, F., & Smalley, B. 1999, A&A, 347, 876

Ghazaryan, S., Alecian, G., & Hakobyan, A. A. 2018, MNRAS, 480, 2953

Golay, M., ed. 1974, Astrophysics and Space Science Library, Vol. 41, Introduction to astronomical photometry

Gray, D. 2005, The Observation and Analysis of Stellar Photospheres (The Edinburgh Building, Cambridge CB2 8RU,UK: Cambridge University Press)

Gray, R. O. 1988, AJ, 95, 220

Gray, R. O. & Corbally, J., C. 2009, Stellar Spectral Classification

Grosbøl, P. & Ponz, D. 1990, in Acquisition, Processing and Archiving of Astronomical Images, ed. G. Longo & G. Sedmak, 111–123

Guthnick, P. & Prager, R. 1914, Photoelektrische untersuchungen an spektroskopischen Doppelsternen und an Planeten

Hack, M. 1976, in IAU Colloq. 32: Physics of Ap Stars, ed. W. W. Weiss, H. Jenkner, & H. J. Wood, 255–+

Hauck, B. & Mermilliod, M. 1998, A&AS, 129, 431

Heiter, U., Barklem, P., Fossati, L., et al. 2008, Journal of Physics Conference Series, 130, 012011

Heiter, U., Kupka, F., van't Veer-Menneret, C., et al. 2002, A&A, 392, 619

Henry, G. W. & Fekel, F. C. 2005, AJ, 129, 2026

Hui-Bon-Hoa, A., LeBlanc, F., Hauschildt, P. H., & Baron, E. 2002, A&A, 381, 197

Kiess, C. C. 1917, Popular Astronomy, 25, 656

Kochukhov, O. 2003, A&A, 404, 669

Kochukhov, O., Bagnulo, S., & Barklem, P. S. 2002, ApJ, 578, L75

Kochukhov, O., Khan, S., & Shulyak, D. 2005, A&A, 433, 671

Kochukhov, O., Makaganiuk, V., & Piskunov, N. 2010, A&A, 524, A5

Kourganoff, V. 1952, Basic methods in transfer problems; radiative equilibrium and neutron diffusion

Kupka, F. & Bruntt, H. 2001, Journal of Astronomical Data, 7, 8

Kurtz, D. W. 1978, Information Bulletin on Variable Stars, 1436, 1

Kurtz, D. W. 1980, MNRAS, 193, 29

Kurtz, D. W., Cunha, M. S., Saio, H., et al. 2011, MNRAS, 414, 2550

Kurtz, D. W., Elkin, V. G., & Mathys, G. 2003, MNRAS, 343, L5

Kurucz, R. L. 1970, SAO Special Report, 309

Kurucz, R. L. 1993, IAU Commission on Close Binary Stars, 21, 93

Landstreet, J. D. 2009, in EAS Publications Series, Vol. 39, EAS Publications Series, ed. C. Neiner & J.-P. Zahn, 1–20

LeBlanc, F. 2010, An Introduction to Stellar Astrophysics

Leckrone, D. S. 1973, ApJ, 185, 577

Lockyer, N. & Baxendall, F. E. 1906, Proc. Roy. Soc. London A, 77, 550

Ludendorff, H. 1907, Astronomische Nachrichten, 176, 327

Martinez, P. 1993, PhD thesis, , University of Cape Town, SA, (1993)

Mashonkina, L., Ryabchikova, T., & Ryabtsev, A. 2005, A&A, 441, 309

Mashonkina, L., Ryabchikova, T., Ryabtsev, A., & Kildiyarova, R. 2009, A&A, 495, 297

Maury, A. C. & Pickering, E. C. 1897, Annals of Harvard College Observatory, 28, 1

Menzel, D. H. & Milne, E. A. 1966, Selected papers on the transfer of radiation

Michaud, G. 1970, ApJ, 160, 641

Michaud, G., Alecian, G., & Richer, J. 2015, Atomic Diffusion in Stars

Michaud, G., Megessier, C., & Charland, Y. 1981, A&A, 103, 244

Moon, T. T. & Dworetsky, M. M. 1985, MNRAS, 217, 305

Morgan, W. W. 1931a, ApJ, 73, 104

Morgan, W. W. 1931b, ApJ, 74, 24

Morgan, W. W. 1933, ApJ, 77, 330

Napiwotzki, R., Schoenberner, D., & Wenske, V. 1993, A&A, 268, 653

Nesvacil, N., Stütz, C., & Weiss, W. W. 2003, in Astronomical Society of the Pacific Conference Series, Vol. 298, GAIA Spectroscopy: Science and Technology, ed. U. Munari, 173–+

Öpik, E. J. 1950, MNRAS, 110, 559

Payne, C. H. 1925, PhD thesis, RADCLIFFE COLLEGE.

Pecker, J. C. 1951, L'Astronomie, 65, 57

Piskunov, N. 1999, in Astrophysics and Space Science Library, Vol. 243, Polarization, ed. K. N. Nagendra & J. O. Stenflo, 515–525

Piskunov, N. & Kochukhov, O. 2002, A&A, 381, 736

Piskunov, N. E. 1992, in Physics and Evolution of Stars: Stellar Magnetism, ed. Y. V. Glagolevskij & I. I. Romanyuk, 92–+

Preston, G. W. 1974, ARA&A, 12, 257

Przybylski, A. 1977, MNRAS, 178, 71

Przybylski, A. 1979, New Zealand Journal of Science, 22, 429

Roxburgh, I. 2011, personal communication

Rusomarov, N., Kochukhov, O., Piskunov, N., et al. 2013, A&A, 558, A8

Ryabchikova, T., Nesvacil, N., Weiss, W. W., Kochukhov, O., & Stütz, C. 2004, A&A, 423, 705

Ryabchikova, T., Wade, G. A., & LeBlanc, F. 2003, in IAU Symposium, Vol. 210, Modelling of Stellar Atmospheres, ed. N. Piskunov, W. W. Weiss, & D. F. Gray, 301–+

Ryabchikova, T. A. & Romanovskaya, A. M. 2017, Astronomy Letters, 43, 252

Ryabchikova, T. A., Savanov, I. S., Hatzes, A. P., Weiss, W. W., & Handler, G. 2000, A&A, 357, 981

Ryabchikova, T. A., Savanov, I. S., Malanushenko, V. P., & Kudryavtsev, D. O. 2001, Astronomy Reports, 45, 382

Schwarzschild, K. 1906, Nachrichten von der Königlichen Gesellschaft der Wissenschaften zu Göttingen. Math.-phys. Klasse, 195, p. 41-53, 195, 41

Semel, M. 1989, A&A, 225, 456

Silvester, J., Kochukhov, O., & Wade, G. A. 2014, MNRAS, 444, 1442

Silvester, J., Kochukhov, O., & Wade, G. A. 2015, MNRAS, 453, 2163

Smalley, B. & Kupka, F. 1997, A&A, 328, 349

Smith, K. C. 1996, Ap&SS, 237, 77

Sneden, C. 1973, PhD thesis, University of Texas

Sousa, S. 2011, personal communication

Sousa, S. G., Santos, N. C., Israelian, G., et al. 2011, A&A, 526, A99

Sousa, S. G., Santos, N. C., Mayor, M., et al. 2008, A&A, 487, 373

Stahl, O., Kaufer, A., & Tubbesing, S. 1999, in Astronomical Society of the Pacific Conference Series, Vol. 188, Optical and Infrared Spectroscopy of Circumstellar Matter, ed. E. Guenther, B. Stecklum, & S. Klose, 331

Stibbs, D. W. N. 1950, MNRAS, 110, 395

Strömgren, B. 1948, AJ, 53, 107

Strömgren, B. 1956, Vistas in Astronomy, 2, 1336

Unsöld, A. 1938, Annales d'Astrophysique, 1, 376

Valenti, J. A. & Piskunov, N. E. 1996, in Astronomical Society of the Pacific Conference Series, Vol. 108, M.A.S.S., Model Atmospheres and Spectrum Synthesis, ed. S. J. Adelman, F. Kupka, & W. W. Weiss, 175

van der Riet Woolley & Stibbs, D. W. N. 1953, The outer layers of a star

Vitense, E. 1953, ZAp, 32, 135

Wade, G. A., Donati, J.-F., Landstreet, J. D., & Shorlin, S. L. S. 2000, MNRAS, 313, 823

Wegner, G. 1976, MNRAS, 177, 99

Wegner, G. 1981, ApJ, 247, 969

Appendices

Appendix A

Example WIDTH Input Deck

The important features of this example input deck are as follows:

1. VTUR statement. This reflects the number of micro-turbulence values to compute for (in this example, 1, with a value of 2.00 $\mathrm{km\,s^{-1}}$).

2. LINE statement. This introduces the atomic data for the line, including wavelength (in nm), equivalent width (in pm), log(gf), spin-orbit term J and energy level (in $\mathrm{cms^{-1}}$) for the lower and upper levels of the transition, a code to represent the element atomic number + charge, and the broadening terms.

3. The remaining statements from TEFF downwards represent the model atmosphere to be used for the analysis (including $\mathrm{T_{eff}}$, log g, initial abundances).

```
VTUR
1 2.00
LINE 1.361 406.7978 HD184343
406.7978 -0.472 4.0 25898.000 4.0 50474.000 26.00
406.7978 151 8.36 -5.04 -7.27
LINE 1.996 407.1737 HD184343
407.1737 -0.022 2.0 12969.000 2.0 37520.000 26.00
```

APPENDIX A

```
407.1737 151 8.07 -6.24 -7.75

LINE 14.67 417.8862 HD184343

417.8862 -2.500 2.5 20833.000 3.5 44755.000 26.01

417.8862 152 8.47 -6.54 -7.88

END

TEFF 11500.  GRAVITY 4.00000 LTE

TITLE [>Z 0.0 V 2.0 C CGM,OFF R -6.875,0.125,72 <]

OPACITY IFOP 1 1 1 1 1 1 1 1 1 1 1 1 0 1 0 0 0 0 0

CONVECTION OFF 1.00 TURBULENCE OFF 0.00 0.00 0.00 0.00

ABUNDANCE SCALE 1.00000 ABUNDANCE CHANGE 1 0.91100 2 0.08900

ABUNDANCE CHANGE 3 -10.88 4 -10.89 5 -9.44 6 -3.48 7 -3.99 8 -3.11

ABUNDANCE CHANGE 9 -7.48 10 -3.95 11 -5.71 12 -4.46 13 -5.57 14 -4.49

ABUNDANCE CHANGE 15 -6.59 16 -4.83 17 -6.54 18 -5.48 19 -6.92 20 -5.68

ABUNDANCE CHANGE 21 -8.94 22 -7.05 23 -8.04 24 -6.37 25 -6.65 26 -4.37

ABUNDANCE CHANGE 27 -7.12 28 -5.79 29 -7.83 30 -7.44 31 -9.16 32 -8.63

ABUNDANCE CHANGE 33 -9.67 34 -8.69 35 -9.41 36 -8.81 37 -9.44 38 -9.14

ABUNDANCE CHANGE 39 -9.80 40 -9.44 41 -10.62 42 -10.12 43 -20.00 44 -10.20

ABUNDANCE CHANGE 45 -10.92 46 -10.35 47 -11.10 48 -10.18 49 -10.38 50 -10.04

ABUNDANCE CHANGE 51 -11.04 52 -9.80 53 -10.53 54 -9.81 55 -10.92 56 -9.91

ABUNDANCE CHANGE 57 -10.82 58 -10.49 59 -11.33 60 -10.54 61 -20.00 62 -11.04

ABUNDANCE CHANGE 63 -11.53 64 -10.92 65 -12.14 66 -10.94 67 -11.78 68 -11.11

ABUNDANCE CHANGE 69 -12.04 70 -10.96 71 -11.28 72 -11.16 73 -11.91 74 -10.93

ABUNDANCE CHANGE 75 -11.77 76 -10.59 77 -10.69 78 -10.24 79 -11.03 80 -10.95

ABUNDANCE CHANGE 81 -11.14 82 -10.19 83 -11.33 84 -20.00 85 -20.00 86 -20.00

ABUNDANCE CHANGE 87 -20.00 88 -20.00 89 -20.00 90 -11.92 91 -20.00 92 -12.51

ABUNDANCE CHANGE 93 -20.00 94 -20.00 95 -20.00 96 -20.00 97 -20.00 98 -20.00

ABUNDANCE CHANGE 99 -20.00
```

APPENDIX A

```
READ DECK6 72 RHOX,T,P,XNE,ABROSS,ACCRAD,VTURB

4.52567945E-07 6589.9 4.470E-03 2.289E+09 2.947E-01 1.227E+02 2.000E+05

6.03889282E-07 6614.0 5.965E-03 3.029E+09 2.932E-01 1.212E+02 2.000E+05

8.07035339E-07 6628.0 7.972E-03 4.012E+09 2.907E-01 1.192E+02 2.000E+05

1.08021854E-06 6648.0 1.067E-02 5.314E+09 2.884E-01 1.170E+02 2.000E+05

1.44698933E-06 6676.9 1.430E-02 7.034E+09 2.869E-01 1.167E+02 2.000E+05

1.93864249E-06 6706.9 1.915E-02 9.300E+09 2.855E-01 1.170E+02 2.000E+05

2.59678195E-06 6744.9 2.565E-02 1.228E+10 2.849E-01 1.175E+02 2.000E+05

3.47584212E-06 6786.4 3.433E-02 1.620E+10 2.849E-01 1.179E+02 2.000E+05

4.64498971E-06 6835.5 4.588E-02 2.134E+10 2.861E-01 1.165E+02 2.000E+05

6.19446987E-06 6889.0 6.119E-02 2.804E+10 2.884E-01 1.152E+02 2.000E+05

8.23796021E-06 6948.5 8.138E-02 3.677E+10 2.924E-01 1.140E+02 2.000E+05

1.09188834E-05 7012.2 1.079E-01 4.808E+10 2.979E-01 1.126E+02 2.000E+05

1.44195059E-05 7079.1 1.425E-01 6.267E+10 3.049E-01 1.098E+02 2.000E+05

1.89727112E-05 7147.7 1.875E-01 8.142E+10 3.130E-01 1.047E+02 2.000E+05

2.48746210E-05 7216.1 2.459E-01 1.054E+11 3.227E-01 1.011E+02 2.000E+05

3.24926373E-05 7284.3 3.213E-01 1.359E+11 3.340E-01 9.887E+01 2.000E+05

4.22851953E-05 7352.9 4.182E-01 1.746E+11 3.472E-01 9.612E+01 2.000E+05

5.48176114E-05 7421.4 5.423E-01 2.234E+11 3.626E-01 9.433E+01 2.000E+05

7.07728700E-05 7490.7 7.003E-01 2.848E+11 3.809E-01 9.339E+01 2.000E+05

9.09664566E-05 7561.4 9.003E-01 3.615E+11 4.024E-01 9.326E+01 2.000E+05

1.16380801E-04 7634.6 1.152E+00 4.570E+11 4.274E-01 9.155E+01 2.000E+05

1.48209915E-04 7708.1 1.467E+00 5.752E+11 4.561E-01 8.949E+01 2.000E+05

1.87880409E-04 7781.1 1.860E+00 7.206E+11 4.892E-01 8.844E+01 2.000E+05

2.37060032E-04 7853.9 2.348E+00 8.987E+11 5.276E-01 8.827E+01 2.000E+05

2.97702216E-04 7926.9 2.949E+00 1.116E+12 5.720E-01 8.892E+01 2.000E+05

3.72111333E-04 8000.2 3.686E+00 1.379E+12 6.229E-01 8.936E+01 2.000E+05
```

4.63032309E-04 8072.6 4.587E+00 1.697E+12 6.811E-01 9.005E+01 2.000E+05

5.73712071E-04 8142.9 5.684E+00 2.079E+12 7.473E-01 9.123E+01 2.000E+05

7.08062924E-04 8212.3 7.015E+00 2.536E+12 8.219E-01 9.220E+01 2.000E+05

8.70718484E-04 8278.5 8.627E+00 3.080E+12 9.066E-01 9.436E+01 2.000E+05

1.06707027E-03 8343.1 1.057E+01 3.728E+12 1.003E+00 9.745E+01 2.000E+05

1.30344820E-03 8407.6 1.291E+01 4.498E+12 1.112E+00 1.007E+02 2.000E+05

1.58730278E-03 8469.9 1.572E+01 5.407E+12 1.237E+00 1.048E+02 2.000E+05

1.92735570E-03 8530.9 1.909E+01 6.479E+12 1.378E+00 1.099E+02 2.000E+05

2.33380856E-03 8590.9 2.310E+01 7.740E+12 1.539E+00 1.160E+02 2.000E+05

2.81860904E-03 8650.2 2.789E+01 9.220E+12 1.722E+00 1.232E+02 2.000E+05

3.39580682E-03 8709.8 3.359E+01 1.096E+13 1.930E+00 1.315E+02 2.000E+05

4.08236231E-03 8774.3 4.037E+01 1.300E+13 2.165E+00 1.392E+02 2.000E+05

4.89865510E-03 8836.5 4.841E+01 1.540E+13 2.429E+00 1.483E+02 2.000E+05

5.86822926E-03 8899.1 5.796E+01 1.820E+13 2.729E+00 1.593E+02 2.000E+05

7.01794435E-03 8963.8 6.926E+01 2.148E+13 3.072E+00 1.723E+02 2.000E+05

8.37808810E-03 9033.1 8.262E+01 2.533E+13 3.467E+00 1.877E+02 2.000E+05

9.98249039E-03 9109.1 9.835E+01 2.986E+13 3.926E+00 2.058E+02 2.000E+05

1.18682651E-02 9198.8 1.168E+02 3.524E+13 4.462E+00 2.258E+02 2.000E+05

1.40767958E-02 9300.1 1.384E+02 4.159E+13 5.088E+00 2.488E+02 2.000E+05

1.66575869E-02 9418.8 1.635E+02 4.913E+13 5.809E+00 2.735E+02 2.000E+05

1.96721670E-02 9555.3 1.928E+02 5.803E+13 6.631E+00 3.007E+02 2.000E+05

2.31939039E-02 9713.1 2.269E+02 6.853E+13 7.567E+00 3.311E+02 2.000E+05

2.73152866E-02 9897.5 2.667E+02 8.087E+13 8.604E+00 3.644E+02 2.000E+05

3.21765986E-02 10113.8 3.134E+02 9.534E+13 9.660E+00 3.953E+02 2.000E+05

3.80079450E-02 10365.5 3.694E+02 1.123E+14 1.064E+01 4.191E+02 2.000E+05

4.51287735E-02 10654.8 4.375E+02 1.323E+14 1.153E+01 4.401E+02 2.000E+05

5.39740619E-02 10990.9 5.220E+02 1.559E+14 1.226E+01 4.567E+02 2.000E+05

```
6.52156856E-02 11380.6 6.292E+02 1.842E+14 1.270E+01 4.629E+02 2.000E+05

7.99242356E-02 11827.8 7.695E+02 2.192E+14 1.277E+01 4.561E+02 2.000E+05

9.95961297E-02 12342.2 9.574E+02 2.634E+14 1.263E+01 4.469E+02 2.000E+05

1.26425638E-01 12936.6 1.214E+03 3.205E+14 1.223E+01 4.293E+02 2.000E+05

1.63585555E-01 13605.4 1.570E+03 3.958E+14 1.172E+01 4.092E+02 2.000E+05

2.15461023E-01 14373.0 2.068E+03 4.958E+14 1.118E+01 3.891E+02 2.000E+05

2.87586049E-01 15222.4 2.762E+03 6.291E+14 1.079E+01 3.719E+02 2.000E+05

3.86652045E-01 16168.2 3.716E+03 8.047E+14 1.055E+01 3.589E+02 2.000E+05

5.20153032E-01 17192.5 5.004E+03 1.030E+15 1.052E+01 3.536E+02 2.000E+05

6.98859653E-01 18316.5 6.728E+03 1.312E+15 1.047E+01 3.486E+02 2.000E+05

9.38574635E-01 19538.6 9.042E+03 1.663E+15 1.041E+01 3.447E+02 2.000E+05

1.25897570E+00 20874.3 1.214E+04 2.095E+15 1.043E+01 3.438E+02 2.000E+05

1.68314322E+00 22327.4 1.623E+04 2.624E+15 1.054E+01 3.469E+02 2.000E+05

2.24265372E+00 23904.0 2.163E+04 3.268E+15 1.066E+01 3.478E+02 2.000E+05

2.97675791E+00 25615.2 2.872E+04 4.050E+15 1.090E+01 3.543E+02 2.000E+05

3.93018970E+00 27465.5 3.791E+04 4.988E+15 1.123E+01 3.612E+02 2.000E+05

5.14722342E+00 29465.7 4.963E+04 6.087E+15 1.188E+01 3.770E+02 2.000E+05

6.67832384E+00 31629.3 6.435E+04 7.355E+15 1.262E+01 3.933E+02 2.000E+05

8.57053879E+00 33957.7 8.253E+04 8.791E+15 1.382E+01 3.917E+02 2.000E+05

PRADK 2.3677E+01

BEGIN ITERATION 5 COMPLETED

END

STOP
```

Appendix B

List of FEROS Stellar Spectra used in Abundance Analysis

Table B.1: List of spectra used in the analysis. In the last column: ✓ denotes selected for further processing; ‡ denotes evidence of Core Wing Anomaly

Star	Dec	RA	Date of observations	Exposure	$T_{\rm eff}$	$\log g$	Spectral	Minimum λ	Maximum λ	$v \sin i$	
				sec	K	cgs	Type	Å	Å	$km\,s^{-1}$	
HD 2202	−50.8426514	6.4025278	2008-08-08T09:30:31	321	6543	4.21	F6	3659.7342	9199.7442	41	
HD 2883	−61.3525200	7.8560572	2008-08-08T09:52:17	946	6269	4.79	F8	3659.9806	9199.9906	15	✓
HD 2957	−13.4899197	8.1663771	2008-08-09T07:28:03	371	9327	4.08	A2	3659.7458	9199.7558	55	
HD 2957	−13.4898005	8.1667538	2008-08-09T07:38:39	600	9327	4.08	A2	3659.7242	9199.7342	55	
HD 3988	−83.0401764	9.6698570	2008-08-08T08:56:02	321	7674	3.74	A9	3660.7706	9200.7806	15	✓
HD 3988	−83.0393906	9.6722689	2008-08-09T09:02:26	540	7674	3.74	A9	3660.9678	9200.9778	15	✓
HD 3988	−83.0400085	9.6650162	2008-08-12T07:02:01	600	7674	3.74	A9	3661.0814	9201.0914	15	✓
HD 3988	−83.0400238	9.6631441	2008-08-13T07:07:22	700	7674	3.74	A9	3660.9680	9200.9780	15	✓
HD 5823	−11.9527302	14.8945646	2009-07-09T09:29:45	1200	7176	4.17	F2	3660.2778	9200.2878	19	✓‡
HD 5823	−11.9359703	14.8980064	2008-08-10T08:15:16	1200	7176	4.17	F2	3660.0645	9200.0745	19	✓‡
HD 5823	−11.9374199	14.8970051	2008-08-12T06:32:59	1500	7176	4.17	F2	3660.0855	9200.0955	19	✓‡
HD 7676	−34.1486092	19.96836	2007-02-07T00:35:53	286	7778	4.77	A9	3659.6722	9199.6822	76 ‡	
HD 8700	−73.6061172	20.6813698	2009-07-09T09:52:58	1200	9460	4.00	A2	3659.2118	9199.2218	45	
HD 8783	−72.3308716	20.9428101	2008-08-08T10:11:40	180	8250	3.87	A7	3659.6698	9199.6797	18	✓
HD 8783	−72.3302307	20.9450111	2008-08-09T09:15:35	300	8250	3.87	A7	3659.6706	9199.6806	18	✓
HD 8783	−72.3308716	20.9430523	2008-08-10T07:52:07	300	8250	3.87	A7	3659.6693	9199.6793	18	✓

Table B.1

Star	Dec	RA	Date of observations	Exposure	$T_{\rm eff}$	$\log g$	Spectral	Minimum λ	Maximum λ	$v \sin i$	
				sec	K	cgs	Type	Å	Å	$km\,s^{-1}$	
HD 9050	−14.0355997	22.2155361	2008-08-09T07:53:58	664	7486	3.91	F0	3659.7033	9199.7133	56	
HD 11090	−67.4899902	26.5976868	2009-07-10T09:06:35	1200	7944	4.65	A8	3659.1128	9199.1228	> 100	
HD 11346	−74.1030579	26.9097347	2009-07-10T09:30:49	1200	7899	3.94	A8	3659.6680	9199.6779	46	
HD 14944	−77.2110291	34.5991669	2008-08-10T08:38:41	1200	7815	3.33	A8	3659.3839	9199.3939	> 100	
HD 16002	−73.2658310	37.3614769	2008-08-09T08:32:43	664	7919	3.68	A8	3659.5842	9199.5942	52	
HD 16145	−17.2920494	38.7503166	2008-08-10T08:00:56	250	8663	3.81	A5	3659.7302	9199.7402	59	
HD 19712	−1.7008899	47.5545502	2009-02-05T00:50:04	300	10947	4.44	A0	3659.5058	9199.5158	66	
HD 19712	−1.6966500	47.5604172	2008-08-10T08:08:38	200	10947	4.44	A0	3659.5976	9199.6076	66	
HD 19712	−1.6971101	47.5604858	2008-08-12T07:17:08	350	10947	4.44	A0	3659.6188	9199.6288	66	
HD 20505	−59.2029610	48.7239761	2009-02-05T01:00:02	1100	8884	4.11	A4	3660.1902	9200.2002	43	
HD 20880	−73.5593719	48.9680634	2009-02-06T00:53:32	345	8062	3.88	A8	3659.9313	9199.9413	83	
HD 20880	−73.5592880	48.9672966	2009-02-07T00:45:39	345	8062	3.88	A8	3659.9337	9199.9437	83	
HD 20880	−73.5549622	48.9730797	2008-08-10T09:03:12	400	8062	3.88	A8	3659.9566	9199.9666	83	
HD 20880	−73.5543823	48.9785614	2008-08-11T07:05:08	900	8062	3.88	A8	3659.9281	9199.9381	83	
HD 20880	−73.5549164	48.9745140	2008-08-12T07:27:26	550	8062	3.88	A8	3659.8897	9199.8997	83	
HD 21799	−2.0154600	52.6696053	2009-07-11T09:19:50	1200	7108	4.00	F2	3660.1303	9200.1403	23	✓‡
HD 22032	−4.6524000	53.2825890	2009-07-11T09:44:55	1100	6964	4.00	F3	3659.7406	9199.7506	15	✓‡
HD 22378	−2.3746300	53.9924278	2010-02-01T01:09:26	1200	9471	4.00	A2	3659.5432	9199.5532	43	

Table B.1

Star	Dec	RA	Date of observations	Exposure	$T_{\rm eff}$	$\log g$	Spectral	Minimum λ	Maximum λ	$v \sin i$	
				sec	K	cgs	Type	Å	Å	$km\,s^{-1}$	
HD 22488	−66.7349777	53.1503487	2008-08-10T09:13:55	250	6988	3.56	F3	3659.6433	9199.6533	94	
HD 23207	−18.7162704	55.6699905	2008-08-10T09:50:00	250	8064	4.32	A7	3659.9407	9199.9507	13	✓
HD 23715	−24.0474300	56.6116791	2007-02-07T00:44:19	1100	7625	4.09	A9	3660.1093	9200.1193	17	✓
HD 24212	−79.5965729	55.1764526	2009-07-13T09:45:20	1200	9277	4.00	A2	3660.1296	9200.1395	76	
HD 24786	−21.8528004	58.8833084	2009-07-10T09:53:41	1200	8386	4.00	A6	3659.2114	9199.2213	47	
HD 24786	−21.8375702	58.8874512	2008-08-12T07:40:54	1200	8386	4.00	A6	3659.2139	9199.2239	47	
HD 26726	−24.8159409	63.1785202	2009-07-16T09:43:09	1200	8008	4.84	A8	3659.4034	9199.4134	39	✓‡
HD 26726	−24.7991409	63.1782684	2008-08-12T08:04:35	1200	8008	4.84	A8	3659.3581	9199.3681	39	✓‡
HD 27211	−52.1727219	63.7929878	2009-02-05T01:24:12	1000	9936	4.19	A1	3659.4490	9199.4590	73	
HD 27211	−52.1674004	63.8003616	2008-08-10T09:27:02	1200	9936	4.19	A0	3659.4970	9199.5070	73	
HD 27285	−19.8854599	64.4357758	2008-08-12T08:27:58	1200	7731	3.97	A9	3659.9626	9199.9726	51	
HD 27463	−60.9579086	64.0464478	2009-02-06T01:10:16	200	9064	4.22	A3	3659.5232	9199.5332	66	
HD 27463	−60.9578896	64.0460815	2009-02-06T01:46:21	200	9064	4.22	A3	3659.4306	9199.4406	66	
HD 27463	−60.9533615	64.0541916	2008-08-10T09:21:16	120	9064	4.22	A3	3659.4857	9199.4957	66	
HD 27463	−60.9545097	64.0543747	2008-08-12T09:54:08	300	9064	4.22	A3	3659.5062	9199.5162	66	
HD 27472	−61.0937500	64.0791779	2009-02-05T01:45:12	1000	7553	3.89	A9	3659.7568	9199.7668	48	
HD 28430	−40.1975594	66.8404694	2007-02-10T01:00:29	240	7914	3.87	A8	3658.3958	9198.4058	72	
HD 29578	−54.6297417	69.0924530	2009-02-06T01:54:24	500	7554	4.15	A9	3659.4127	9199.4227	<10	✓

Table B.1

Star	Dec	RA	Date of observations	Exposure	$T_{\rm eff}$	$\log g$	Spectral	Minimum λ	Maximum λ	$v \sin i$	
				sec	K	cgs	Type	Å	Å	$km\,s^{-1}$	
HD 29578	−54.6253204	69.1021347	2008-08-09T08:48:29	600	7554	4.15	A9	3659.8504	9199.8604	<10	✓
HD 30335	−44.4267311	71.0980988	2009-02-05T02:06:40	1200	8465	4.10	A6	3659.3641	9199.3741	41	
HD 30374	−75.1130219	69.6827621	2009-02-07T00:56:29	1100	8077	3.83	A7	3659.5405	9199.5505	58	
HD 30849	−49.1781693	72.1276093	2009-02-06T02:05:49	800	5889	5.57	G1	3659.8918	9199.9018	12	✓‡
HD 31225	−20.7742195	73.2845078	2008-08-10T09:57:14	160	8088	3.73	A7	3660.0168	9200.0268	69	
HD 31225	−20.7751007	73.2853012	2008-08-12T10:12:36	300	8088	3.73	A7	3659.9956	9200.9056	69	
HD 31973	−44.6269302	74.4346695	2007-02-07T01:05:33	1200	8203	4.07	A7	3659.5161	9199.5261	27	✓
HD 33011	−15.7881298	76.6302032	2009-02-05T02:33:40	1100	7443	4.02	F0	3659.7500	9199.7600	55	
HD 33629	−33.7861786	77.4971619	2009-02-06T02:22:51	900	7321	4.24	F1	3658.8753	9198.8853	<10	✓
HD 33629	−33.7766991	77.5054779	2007-02-07T01:28:08	800	7321	4.24	F1	3658.8762	9198.8862	<10	✓
HD 34205	−15.0975504	78.7621994	2007-02-07T01:43:50	900	8143	4.09	A7	3659.3605	9199.3705	<10	✓
HD 34514	−20.8316402	79.2985458	2007-02-07T02:02:03	900	9417	3.93	A2	3659.2663	9199.2763	44	
HD 35361	−75.1139069	78.8886642	2009-02-05T02:56:15	1100	7638	3.40	A9	3659.8511	9199.8612	>100	
HD 36964	−24.3447895	83.5473862	2009-02-07T01:19:33	1100	7862	4.21	A8	3659.6117	9199.6217	>100	
HD 37308	−17.0134106	84.2057953	2007-02-07T02:19:31	350	7672	3.85	A9	3660.0635	9200.0734	79	
HD 38719	−56.9210396	86.0570602	2008-08-12T10:03:23	350	8906	3.93	A4	3659.5482	9199.5583	43	
HD 39575	−26.2977295	88.0741043	2009-02-06T02:41:39	308	10725	4.38	A0	3659.4638	9199.4738	50	
HD 40277	−70.4896774	87.8004684	2009-02-06T02:50:39	473	8348	4.42	A6	3659.1666	9199.1766	75	

Table B.1

Star	Dec	RA	Date of observations	Exposure	$T_{\rm eff}$	$\log g$	Spectral	Minimum λ	Maximum λ	$v \sin i$	
				sec	K	cgs	Type	Å	Å	$km\,s^{-1}$	
HD 40765	−30.6720200	89.8962555	2009-02-05T03:18:54	1100	6914	3.92	F3	3657.9398	9197.9497	24	✓
HD 40886	−27.8844795	90.0989990	2007-02-08T00:40:26	240	10106	4.21	A0	3659.8362	9199.8462	>100	
HD 41385	−20.8654995	90.9724960	2007-02-07T02:27:31	1100	7826	4.63	A8	3659.5179	9199.5279	13	✓
HD 41511	−16.4907093	91.2226028	2009-02-06T03:02:34	200	7106	2.20	F2	3656.1171	9196.1271	>100	
HD 41613	−77.8564606	88.8723068	2009-02-06T03:10:32	1100	7816	3.92	A8	3659.1055	9199.1155	53	
HD 41757	−24.9182091	91.4884109	2007-02-08T00:48:19	300	9103	3.45	A3	3660.7478	9200.7578	84	
HD 42075	−26.6181393	91.8861923	2007-02-07T02:47:58	800	7365	4.34	F0	3659.8283	9199.8383	<10	✓
HD 42075	−26.6212196	91.9038086	2007-02-10T01:31:00	800	7365	4.34	F0	3659.8502	9199.8602	<10	✓
HD 42605	−12.7403498	92.7642975	2007-02-07T03:03:33	600	8191	4.26	A7	3659.3715	9199.3815	26	✓
HD 42777	−20.4969501	92.9377060	2007-02-07T03:16:05	900	9787	4.49	A1	3659.5318	9199.5418	64	
HD 43226	−71.1298218	92.0610962	2009-02-06T03:35:20	900	8152	4.45	A7	3659.3841	9199.3940	42	
HD 43901	−47.8268089	94.0304871	2007-02-08T00:55:53	240	7982	4.04	A8	3659.6281	9199.6381	<10	✓
HD 44226	−25.3426704	94.8754272	2010-02-02T01:33:01	1500	7816	4.35	A8	3658.9507	9198.9607	<10	✓
HD 44226	−25.3256702	94.8775253	2007-02-07T03:34:17	1100	7816	4.35	A8	3659.0700	9199.0800	<10	✓
HD 44290	−14.1943598	95.1008377	2007-02-07T03:55:20	286	10014	4.18	A0	3658.9949	9199.4900	>100	
HD 44550	−20.0455894	95.3666611	2009-02-07T01:42:13	1100	6557	3.42	F6	3658.8314	9198.8414	>100	
HD 45698	−37.0987511	96.7747421	2007-02-08T01:03:06	300	8214	4.45	A7	3659.8278	9199.8378	46	
HD 45870	−.0515594	97.3029327	2009-02-07T02:04:05	1100	9400	3.95	A2	3660.0921	9200.1021	93	

Table B.1

Star	Dec	RA	Date of observations	Exposure	$T_{\rm eff}$	$\log g$	Spectral	Minimum λ	Maximum λ	$v \sin i$	
				sec	K	cgs	Type	Å	Å	$km\,s^{-1}$	
HD 45961	−17.3713493	97.4479523	2007-02-07T04:03:54	1100	8062	3.97	A7	3659.3265	9199.3365	49	
HD 46649	−16.6223907	98.4548264	2009-02-07T02:25:53	1100	9188	4.14	A3	3659.5967	9199.6067	64	
HD 46665	−22.6937294	98.4039612	2007-02-07T04:24:22	1200	9062	4.37	A4	3659.4554	9199.4654	<10	✓
HD 47009	−13.7609301	98.9348373	2010-02-02T02:01:44	1500	8106	4.22	A7	3659.0489	9199.0589	43	
HD 47009	−13.7455301	98.9355316	2007-02-07T04:46:32	800	8106	4.22	A7	3659.0743	9199.0843	43	
HD 49686	−36.2240295	101.9661407	2009-02-07T02:47:18	1100	8175	3.84	A7	3659.8272	9199.8371	66	
HD 50031	−14.2278900	102.6520004	2009-02-07T03:10:00	1100	8390	4.50	A6	3660.1408	9200.1508	73	
HD 50143	−21.9125595	102.7186737	2009-02-07T03:32:57	1100	7549	4.36	A9	3659.2700	9199.2800	47	
HD 50620	−47.3367691	102.8788834	2009-02-08T00:51:02	1100	8321	4.31	A6	3659.2483	9199.2583	11	✓
HD 50627	−77.7871704	100.8930817	2010-01-31T01:20:24	1200	7755	4.08	A9	3659.7758	9199.7858	51	
HD 50861	−59.3092194	102.7697678	2009-02-06T03:55:27	1100	7679	3.82	A9	3659.8706	9199.8806	>100	
HD 51203	−30.0762100	103.7686081	2010-01-31T01:45:19	1200	7583	4.45	A9	3660.0548	9200.0648	35	✓
HD 51203	−30.0768299	103.7701111	2010-02-02T01:03:34	1500	7583	4.45	A9	3660.0842	9200.0942	35	
HD 52280	−65.72708	103.9237671	2009-02-08T01:13:59	1100	8731	3.97	A5	3660.3029	9200.3129	64	
HD 52539	−16.4508305	105.2206726	2009-02-05T03:41:39	1100	11075	4.39	B9	3659.0577	9199.0677	47	
HD 52599	−27.1281700	105.1733856	2007-02-07T05:02:13	360	7790	3.78	A9	3659.1333	9199.1433	15	✓
HD 52696	−19.2066593	105.3480377	2009-02-05T04:05:08	570	8132	3.74	A7	3659.1869	9199.1969	<10	✓
HD 52847	−23.1198406	105.4235992	2010-02-02T02:30:10	600	7874	4.81	A8	3659.6876	9199.6976	15	✓

Table B.1

Star	Dec	RA	Date of observations	Exposure	$T_{\rm eff}$	$\log g$	Spectral	Minimum λ	Maximum λ	$v \sin i$	
				sec	K	cgs	Type	Å	Å	$km\,s^{-1}$	
HD 52847	−23.1040096	105.4250259	2007-02-07T05:10:42	300	7874	4.81	A8	3659.6655	9199.6755	15	✓
HD 54087	−15.8794899	106.7134781	2007-02-07T05:18:02	1100	7123	3.25	F2	3659.5860	9199.5960	67	
HD 54399	−61.8537712	106.1178055	2009-02-05T04:19:43	1100	7950	3.71	A8	3659.6003	9199.6103	52	
HD 55540	−21.0639191	108.1090851	2007-02-07T05:44:14	1100	9107	4.39	A3	3658.8215	9198.8315	24	✓
HD 55540	−21.0618706	108.1115570	2007-02-08T04:07:16	1200	9107	4.39	A3	3658.8701	9198.8801	24	✓
HD 55540	−21.0653801	108.1227188	2007-02-10T01:08:28	1100	9107	4.39	A3	3658.8213	9198.8313	24	✓
HD 55719	−40.5143394	108.0410080	2010-02-02T02:43:38	400	9054	3.91	A3	3660.0526	9200.0626	$<$10	✓
HD 56026	−63.9684410	107.7087631	2009-02-08T01:36:24	1100	7887	3.89	A8	3660.0541	9200.0641	91	
HD 56350	−53.6760902	108.3794556	2009-02-06T04:18:10	200	11849	4.20	B9	3659.5106	9199.5206	$>$100	
HD 56882	−46.3710518	109.1441422	2010-02-02T02:54:28	600	8101	4.30	A7	3659.9865	9199.9965	48	
HD 56882	−46.3527603	109.1428528	2007-02-08T01:10:39	320	8101	4.30	A7	3660.0158	9200.0258	48	
HD 56981	−72.0132828	108.1073532	2009-02-08T01:58:04	1100	5621	5.51	G3	3659.8234	9199.8334	45	
HD 57040	−53.4352684	109.1425095	2007-02-08T01:18:31	900	7484	5.29	F0	3659.6365	9199.6465	21	✓
HD 57964	−37.4898987	110.4606705	2007-02-08T01:35:52	1200	7672	4.38	A9	3659.4515	9199.4615	41	
HD 58868	−35.6007881	111.4502106	2009-02-08T02:20:43	1100	8156	4.37	A7	3659.2979	9199.3079	62	
HD 58939	−52.9101601	111.2129517	2009-02-08T02:47:12	1200	8434	3.76	A6	3659.4809	9199.4909	53	
HD 59164	−26.2338104	111.9049149	2007-02-08T01:58:43	360	9076	3.77	A3	3659.7170	9199.7270	76	
HD 59437	−14.3054800	112.3138046	2007-02-08T02:08:10	900	8851	4.14	A4	3659.9722	9199.9822	14	✓

Table B.1

Star	Dec	RA	Date of observations	Exposure	$T_{\rm eff}$	$\log g$	Spectral	Minimum λ	Maximum λ	$v \sin i$	
				sec	K	cgs	Type	Å	Å	$km\,s^{-1}$	
HD 59660	−52.0849113	112.0344315	2009-02-08T03:10:58	1200	8079	3.81	A7	3659.9018	9199.9118	56	
HD 59776	−33.4135094	112.5357513	2007-02-08T02:25:49	600	6848	3.68	F4	3659.3504	9199.3604	81 ‡	
HD 60572	−34.5872116	113.4155960	2007-02-08T02:39:53	900	9461	4.44	A2	3659.6252	9199.6352	45	
HD 61513	−30.0710201	114.5904770	2009-02-08T03:36:05	1200	10509	4.45	A0	3659.2229	9199.2329	44	
HD 61731	−20.7433300	114.9500351	2009-02-08T03:59:57	1200	7867	4.76	A8	3659.3511	9199.3611	12	✓
HD 61763	−44.8456612	114.6689301	2010-02-02T03:08:16	450	9179	3.08	A3	3659.2778	9199.2878	42	
HD 62244	−24.1113205	115.5063782	2007-02-09T00:43:32	240	8593	3.81	A5	3659.1410	9199.1510	14	✓
HD 62399	−45.3167992	115.3866730	2007-02-09T00:50:57	900	9880	4.34	A0	3659.6493	9199.6593	87	
HD 62530	−16.1746807	115.9610443	2007-02-09T01:08:35	240	10424	4.05	A0	3659.4143	9199.4243	>100	
HD 62553	−22.1825008	115.9112015	2010-02-02T03:19:41	380	8275	3.90	A7	3659.9940	9200.4090	63	
HD 62556	−27.1861992	115.8584595	2009-02-05T04:44:51	300	9080	4.24	A3	3659.3607	9199.3707	43	
HD 62562	−45.0308189	115.6056290	2007-02-09T01:15:12	500	8291	4.46	A6	3659.3130	9199.3230	>100	
HD 62905	−16.9905205	116.3968582	2010-01-31T02:09:44	1100	9251	4.08	A3	3659.3349	9199.3449	19	✓
HD 62953	−15.1752501	116.4549408	2007-02-09T01:26:32	500	7720	1.92	A9	3658.5227	9198.5327	42	
HD 63728	−61.7344398	116.6328583	2007-02-10T01:46:52	646	9415	4.19	A2	3659.4296	9199.4396	68	
HD 63759	−27.8304996	117.3511581	2007-02-09T01:37:34	240	8451	3.83	A6	3659.9620	9199.9720	78	
HD 64288	−48.2376518	117.7088623	2010-01-31T02:31:43	1200	10417	4.43	A0	3660.0290	9200.0390	63	
HD 65142	−18.8977604	119.1521606	2007-02-09T01:44:20	286	9749	3.78	A1	3659.8342	9199.8442	47	

Table B.1

Star	Dec	RA	Date of observations	Exposure	$T_{\rm eff}$	$\log g$	Spectral	Minimum λ	Maximum λ	$v \sin i$	
				sec	K	cgs	Type	Å	Å	$km\,s^{-1}$	
HD 65963	−36.9173088	119.9504471	2007-02-09T01:51:34	800	9432	4.01	A2	3659.3556	9199.3656	60	
HD 67909	−53.4880905	121.8851395	2007-02-08T02:57:02	530	8066	4.23	A7	3659.7013	9199.7113	41	
HD 68013	−52.7996712	121.9805298	2007-02-08T03:14:44	900	10213	4.35	A0	3659.3221	9199.3321	48	
HD 68419	−48.3363113	122.4883499	2007-02-10T02:00:46	300	8922	4.14	A4	3659.5877	9199.5977	53	
HD 68480	−5854092	122.3531189	2010-02-02T03:30:06	800	9878	4.35	A0	3659.8058	9199.8158	19	✓
HD 68480	−57.9880409	122.3683701	2007-02-10T02:08:37	431	9878	4.35	A0	3659.7819	9199.7919	19	✓
HD 68807	−46.2113609	123.23270	2007-02-10T02:18:10	646	8946	4.31	A4	3659.5163	9199.5263	52	
HD 68998	−16.1823902	123.5707703	2007-02-09T02:07:54	350	7785	3.69	A9	3659.2161	9199.2261	51	
HD 69013	−15.7717505	123.6016922	2007-02-09T02:16:44	900	7390	5.33	F0	3659.1644	9199.1744	19	✓‡r
HD 69638	−21.6128292	124.2458191	2007-02-09T02:33:57	900	8236	4.19	A7	3659.2825	9199.2925	>100	
HD 69862	−61.8708496	123.8283310	2010-01-31T02:55:36	1200	8158	3.97	A7	3660.1823	9200.1923	11	✓
HD 70702	−51.5452194	125.2383804	2007-02-10T02:32:10	420	10875	4.65	A0	3659.5951	9199.6051	47	
HD 71058	−41.8541412	125.9141464	2007-02-10T02:41:25	900	5404	4.39	G5	3658.5718	9198.5818	>100	
HD 72316	−33.6492805	127.7212219	2010-02-02T03:47:21	750	9477	4.12	A2	3659.5366	9199.5466	54	
HD 72316	−33.6312218	127.7226715	2007-02-09T02:51:27	500	9477	4.12	A2	3659.5399	9199.5499	14	✓
HD 72801	−50.2257805	128.1421814	2010-02-01T01:33:03	1200	7679	3.83	A9	3659.7588	9199.7688	44	
HD 73101	−21.9888401	128.9425507	2007-02-09T03:02:35	900	9787	3.97	A1	3659.8290	9199.8390	94	
HD 73403	−37.9765587	129.1989288	2007-02-09T03:19:50	500	10225	4.28	A0	3659.7670	9199.7770	41	

Table B.1

Star	Dec	RA	Date of observations	Exposure	$T_{\rm eff}$	$\log g$	Spectral	Minimum λ	Maximum λ	$v \sin i$	
				sec	K	cgs	Type	Å	Å	$km\,s^{-1}$	
HD 73850	−51.1357498	129.5618439	2007-02-09T03:31:34	720	8060	4.39	A7	3660.1061	9200.1161	78	
HD 74494	−24.5240192	130.8786926	2007-02-09T03:56:01	500	10043	4.20	A0	3659.2561	9199.2661	46	
HD 74555	−38.6960907	130.8219452	2007-02-10T03:04:25	700	9249	3.97	A3	3660.1208	9200.1308	80	
HD 74629	−19.7168598	131.0991211	2010-01-31T03:21:03	1100	8354	4.10	A6	3660.0744	9200.0844	17	✓
HD 74636	−51.6694984	130.7063599	2007-02-10T03:18:58	800	9216	3.91	A3	3660.2799	9200.2899	67	
HD 74672	−28.5426006	131.0747375	2010-01-31T03:43:23	1100	8377	4.15	A6	3659.7169	9199.7269	56	
HD 75049	−50.7341118	131.3752289	2007-02-10T03:35:23	600	10431	4.47	A0	3659.5251	9199.5351	45	
HD 75049	−50.7343712	131.3776550	2007-02-10T04:02:00	900	10431	4.47	A0	3659.5706	9199.5806	75	
HD 75425	−42.0375710	132.0931854	2010-01-31T04:06:06	1100	8031	4.39	A6	3659.4477	9199.4577	75	
HD 76276	−22.9642906	133.5878906	2010-01-31T04:28:56	1200	7774	4.11	A9	3659.2452	9199.2552	<10	✓
HD 76460	−62.4648590	133.2429962	2010-01-31T04:54:01	1100	7574	3.95	A9	3659.9519	9199.9619	<10	✓
HD 76759	−13.0944700	134.4532471	2007-02-10T03:48:18	600	7852	4.07	A8	3659.7372	9199.7472	43	
HD 76877	−52.9771004	134.1496735	2010-02-01T01:58:14	1200	8006	3.91	A8	3659.7096	9199.7196	10	✓
HD 77438	−52.4648285	135.0446014	2010-02-01T02:21:36	1500	7875	4.00	A8	3659.6447	9199.6547	14	✓
HD 77609	−20.5467701	135.7776489	2007-02-10T04:26:27	211	9118	3.73	A3	3659.8655	9199.8755	58	
HD 77830	−51.8482819	135.6983643	2007-02-10T04:33:04	800	6810	3.52	F4	3659.5257	9199.5357	75	
HD 79539	−33.9246902	138.4094086	2007-02-07T06:05:04	800	8253	3.98	A7	3660.0855	9200.0955	<10	✓
HD 79976	−16.8346500	139.1565399	2007-02-07T06:20:51	286	9246	3.86	A3	3660.1324	9200.1424	80	

Table B.1

Star	Dec	RA	Date of observations	Exposure	$T_{\rm eff}$	$\log g$	Spectral	Minimum λ	Maximum λ	$v \sin i$	
				sec	K	cgs	Type	Å	Å	$km\,s^{-1}$	
HD 80249	−50.9667091	139.1736298	2010-02-01T02:50:21	1500	10837	4.47	A0	3659.6477	9199.6577	40	
HD 81076	−45.6583786	140.4893646	2010-02-01T03:18:38	1200	7353	3.01	F0	3660.0854	9200.0954	50	
HD 81289	−43.5998611	140.8330383	2007-02-07T06:49:25	360	10273	4.33	A0	3659.4942	9199.5042	72	
HD 81588	−48.4841003	141.2005768	2007-02-07T06:40:50	360	7863	4.36	A8	3659.4034	9199.4135	<10	✓
HD 81877	−40.3665695	141.7718658	2007-02-07T06:28:11	600	9614	3.98	A1	3659.7306	9199.7406	56	
HD 82038	−59.3896904	141.7353821	2010-02-01T03:53:26	1200	8030	3.76	A7	3659.6929	9199.7029	60	
HD 82417	−46.8112106	142.5683441	2007-02-08T04:30:24	900	8160	3.57	A7	3659.5596	9199.5696	15	✓
HD 82562	−36.5347519	142.9344025	2007-02-08T04:48:43	900	9188	4.03	A3	3660.1277	9200.1377	77	
HD 82749	−50.5046310	143.0661774	2007-02-10T04:48:59	900	9092	3.77	A3	3659.8824	9199.8924	45	
HD 82989	−65.4948196	143.0561981	2007-02-07T06:58:00	300	6744	3.85	F5	3659.8157	9199.8257	12	✓
HD 83181	−44.6116982	143.7913513	2007-02-09T04:08:07	900	9252	4.12	A3	3659.9256	9199.9356	46	
HD 83817	−71.7104568	144.1929016	2010-02-01T04:17:17	1000	6666	3.86	F5	3659.7889	9199.7989	>100	
HD 85284	−55.0454292	147.2170258	2010-02-01T04:37:33	1200	8814	3.74	A4	3659.8216	9199.8316	11	✓
HD 85453	−50.3364906	147.5824280	2007-02-10T05:59:06	211	12308	4.40	B9	3659.6796	9199.6896	47	
HD 85564	−50.5273285	147.7685394	2010-02-02T04:03:43	1300	7696	4.14	A9	3659.9751	9199.9851	89	
HD 86592	−12.7600098	149.7864685	2009-02-06T04:55:25	300	7823	4.79	A8	3659.6786	9199.6887	61	
HD 86976	−40.8631592	150.2412109	2007-02-09T04:25:40	240	8242	4.63	A7	3659.5486	9199.5586	48	
HD 88241	−40.4896584	152.3406677	2010-02-01T03:41:50	500	7458	3.39	F0	3659.6490	9199.6590	<10	✓

Table B.1

Star	Dec	RA	Date of observations	Exposure	$T_{\rm eff}$	$\log g$	Spectral	Minimum λ	Maximum λ	$v \sin i$	
				sec	K	cgs	Type	Å	Å	$km\,s^{-1}$	
HD 88385	−56.7494392	152.4408264	2007-02-10T05:53:23	211	9671	4.29	A1	3659.7468	9199.7568	30	✓
HD 88507	−49.6929588	152.7778625	2010-02-02T04:28:48	1300	7913	4.01	A8	3660.0804	9200.0904	62	
HD 88701	−37.5002098	153.2278900	2007-02-09T04:31:51	720	9557	4.18	A2	3659.6336	9199.6436	20	✓
HD 89075	−26.6092491	153.9842377	2010-02-02T04:54:33	500	9916	3.85	A0	3657.3789	9197.3889	51	
HD 89192	−55.5287399	153.9491882	2009-02-07T03:55:28	200	9058	4.04	A4	3659.9347	9199.9447	>100	
HD 89385	−54.4004288	154.3574219	2007-02-10T05:40:52	240	9243	4.13	A3	3659.6151	9199.6251	48	
HD 89519	−68.1457977	154.2900085	2007-02-10T05:47:00	240	9315	3.80	A2	3659.9281	9199.9381	73	
HD 89680	−47.0962486	154.9459229	2007-02-09T04:45:45	286	8112	3.69	A7	3659.5363	9199.5463	41	
HD 91087	−22.5177193	157.6257629	2007-02-09T04:52:49	900	8224	4.44	A7	3660.6623	9200.0166	10	✓
HD 91982	−50.1447487	159.0364532	2007-02-09T05:10:11	900	8177	3.92	A7	3660.3810	9200.3910	47	
HD 92499	−43.0784798	160.0112305	2007-02-07T07:07:55	600	7604	4.70	A9	3659.5266	9199.5366	<10	✓ r
HD 92499	−43.0787086	160.82550	2007-02-08T03:49:28	900	7604	4.70	A9	3659.5674	9199.5774	<10	✓ r
HD 92499	−43.0815201	160.0264587	2007-02-10T05:23:36	900	7604	4.70	A9	3659.5416	9199.5516	<10	✓ r
HD 92534	−61.5930405	159.8641663	2007-02-10T05:06:10	779	9745	4.31	A1	3659.8596	9199.8696	75	
HD 93500	−59.4639511	161.5670776	2010-02-02T07:07:09	1000	8766	3.76	A5	3660.1079	9200.1179	43	
HD 94274	−55.5131302	162.9513092	2007-02-07T08:31:03	900	9460	4.19	A2	3660.2906	9200.3006	68	
HD 94455	−80.9534683	162.3777313	2010-01-31T09:09:34	350	8105	3.72	A7	3659.6640	9199.6740	27	✓
HD 95158	−21.1674900	164.7381592	2007-02-07T07:20:25	800	7627	3.82	A9	3659.6387	9199.6487	20	✓

Table B.1

Star	Dec	RA	Date of observations	Exposure	$T_{\rm eff}$	$\log g$	Spectral	Minimum λ	Maximum λ	$v \sin i$	
				sec	K	cgs	Type	Å	Å	$km\,s^{-1}$	
HD 95491	−51.6419296	165.1203766	2007-02-07T08:15:22	800	7462	3.60	F0	3659.9870	9199.9970	48	
HD 95699	−42.5066490	165.5201263	2009-02-08T04:23:12	300	8085	3.98	A7	3659.7855	9199.7955	>100	
HD 96237	−25.0159492	166.3733978	2007-02-07T07:36:38	1100	7674	4.49	A9	3659.8823	9199.8923	12	✓ r
HD 97394	−43.6745682	167.9821777	2007-02-07T08:01:39	660	8006	4.33	A8	3659.9604	9199.9704	17	✓
HD 100357	−67.0384293	172.9674072	2007-02-08T03:32:29	800	9326	4.14	A2	3659.9092	9199.9192	76	
HD 102333	−19.39406	176.6418304	2007-02-09T05:27:38	600	8122	4.12	A7	3660.1642	9200.1742	<10	✓
HD 103302	−49.3187485	178.3774719	2007-02-08T05:06:07	240	9054	4.07	A3	3659.9927	9200.2731	63	
HD 105999	−63.3806305	182.9514465	2007-02-08T05:12:56	240	6641	3.78	F5	3659.2835	9199.2935	>100	
HD 106215	−35.3645782	183.2809448	2007-02-08T05:19:28	900	8707	3.88	A5	3660.4229	9200.4329	24	✓
HD 109426	−70.3417892	188.7845459	2010-01-31T08:51:56	1000	7831	4.02	A8	3660.1135	9200.1235	43	
HD 109989	−41.8482399	189.8309174	2007-02-07T08:48:21	700	8047	4.11	A7	3659.8963	9199.9063	64	
HD 110072	−34.3760796	189.9500122	2007-02-10T06:04:45	1200	7196	4.88	F2	3659.3357	9199.3457	16	✓
HD 110274	−58.9217682	190.3427887	2007-02-07T09:02:37	900	7921	4.36	A8	3660.0619	9200.0719	<10	✓
HD 110274	−58.9249382	190.3589935	2007-02-10T07:42:57	900	7921	4.36	A8	3660.1031	9200.1131	<10	✓
HD 110446	−56.8720589	190.6353149	2007-02-07T09:19:58	1100	8563	3.74	A6	3659.7856	9199.7956	61	
HD 114035	−85.5831909	198.6548309	2010-02-02T07:27:43	650	9807	3.98	A5	3660.4752	9200.4852	41	
HD 115220	−38.3656807	199.0462494	2007-02-09T05:40:12	286	8004	4.19	A8	3659.9277	9199.9377	18	✓
HD 115285	−68.0433197	199.4080505	2007-02-10T06:40:00	240	7964	3.54	A8	3660.6519	9200.6619	63	

Table B.1

Star	Dec	RA	Date of observations	Exposure	$T_{\rm eff}$	$\log g$	Spectral	Minimum λ	Maximum λ	$v \sin i$	
				sec	K	cgs	Type	Å	Å	$km\,s^{-1}$	
HD 115440	−76.4404221	199.9302673	2010-02-02T07:41:53	600	7041	4.43	F3	3659.6941	9199.7041	26	✓‡
HD 116423	−68.1946182	201.3053894	2010-02-02T07:54:54	750	7372	3.98	F0	3659.6742	9199.6842	13	✓‡
HD 116729	−37.2282219	201.5150146	2007-02-08T05:37:16	800	8416	4.51	A6	3659.5453	9199.5553	45	
HD 116763	−53.4713287	201.6884766	2007-02-10T06:27:32	600	9093	3.83	A3	3660.4701	9200.4801	51	
HD 117227	−47.4170189	202.4082184	2007-02-08T05:52:58	800	7795	4.02	A8	3659.7134	9199.7234	>100	
HD 117290	−49.1316414	202.5238495	2007-02-08T06:08:31	900	8046	4.22	A7	3660.5442	9200.5542	11	✓
HD 117290	−49.1346207	202.5453491	2007-02-10T08:36:05	900	8046	4.22	A7	3660.5918	9200.6018	11	✓
HD 117691	−63.4950714	203.3600159	2007-02-08T06:25:42	1100	7243	3.36	F1	3659.9366	9199.9466	17	✓
HD 119308	−35.2942085	205.7839203	2008-08-11T22:54:47	400	9396	4.20	A2	3660.1297	9200.1397	41	
HD 119308	−35.2939491	205.7829590	2008-08-11T23:05:41	800	9396	4.20	A2	3660.1459	9200.1559	41	
HD 119308	−35.2938004	205.7808685	2008-08-12T00:14:59	600	9396	4.20	A2	3660.0645	9200.0745	41	
HD 119308	−35.2773819	205.7737274	2008-08-12T23:19:21	300	9396	4.20	A2	3660.1202	9200.1302	41	
HD 121276	−51.7150688	208.9143219	2007-02-09T05:47:27	900	7020	4.03	F3	3659.7114	9199.7214	52	
HD 121661	−62.7214203	209.6443024	2007-02-10T06:46:16	350	8976	4.29	A4	3659.8073	9199.8173	14	✓
HD 121788	−30.0744495	209.5490875	2007-02-08T06:46:24	660	7348	3.63	F0	3658.5701	9198.5801	12	✓
HD 121788	−30.0742798	209.5475922	2007-02-09T06:04:43	660	7348	3.63	F0	3661.6880	9201.6980	12	✓
HD 121788	−30.0772209	209.5659485	2007-02-10T08:00:03	660	7348	3.63	F0	3660.4265	9200.4365	12	✓
HD 121840	−62.0511589	209.9123230	2007-02-09T06:18:26	900	8052	3.98	A7	3660.3483	9200.3583	15	✓

Table B.1

Star	Dec	RA	Date of observations	Exposure	$T_{\rm eff}$	$\log g$	Spectral	Minimum λ	Maximum λ	$v \sin i$	
				sec	K	cgs	Type	Å	Å	$km\,s^{-1}$	
HD 122525	−53.7183914	210.9617310	2007-02-08T07:00:01	450	8279	3.88	A7	3660.4786	9200.4886	14	✓
HD 122569	−40.0482597	210.8930206	2007-02-08T07:10:07	530	9238	4.11	A3	3660.1253	9200.1353	52	
HD 122659	−17.2997303	210.9010468	2007-02-10T06:54:23	600	9218	3.99	A3	3660.0482	9200.0582	16	✓
HD 123627	−70.1809387	212.9549103	2008-08-11T23:59:22	600	8316	3.88	A6	3659.9376	9199.9477	55	
HD 123627	−70.1653824	212.9463959	2008-08-12T23:59:33	400	8316	3.88	A6	3659.9211	9199.9311	55	
HD 124437	−66.1928101	214.0349731	2007-02-08T07:21:10	600	7772	3.61	A9	3660.3175	9200.3275	52	
HD 125467	−66.3250809	215.5635071	2007-02-08T07:33:59	500	8087	4.24	A7	3659.9363	9199.9463	54	
HD 126297	−44.6666603	216.4398041	2007-02-09T06:35:57	1100	7687	3.82	A9	3660.3608	9200.3708	<10	✓
HD 126365	−14.0860596	216.3421326	2007-02-10T07:07:17	286	6648	4.17	F5	3661.3137	9201.3237	49	
HD 126936	−45.1018906	217.4431305	2007-02-08T07:45:06	1200	6749	3.72	F5	3659.9287	9199.9387	>100	
HD 128649	−42.7609596	219.8171997	2007-02-09T06:56:38	900	9631	4.38	A1	3660.2345	9200.2445	44	
HD 129189	−72.0776062	221.3238831	2008-08-13T00:08:52	650	9455	4.28	A2	3659.6621	9199.6721	97	
HD 130336	−66.5294266	222.6760406	2008-08-12T01:01:07	800	10760	4.36	A0	3659.7897	9199.7997	77	
HD 131141	−35.3786888	223.1990051	2007-02-08T08:12:30	1200	7844	4.35	A8	3659.6272	9199.6372	15	✓
HD 132205	−55.0383797	224.9742432	2008-08-13T02:05:49	700	7653	4.70	A9	3660.3597	9200.3697	12	✓ r
HD 132673	−70.8371277	226.1351013	2008-08-11T00:24:31	600	7848	4.01	A8	3660.4388	9200.4488	63	
HD 132968	−66.8253174	226.3359222	2008-08-13T00:59:39	600	8048	3.50	A7	3659.9338	9199.9438	47	
HD 135297	−0.3666000	228.5719452	2008-08-11T23:35:17	600	9561	3.99	A1	3660.7958	9200.8058	51	

Table B.1

Star	Dec	RA	Date of observations	Exposure	$T_{\rm eff}$	$\log g$	Spectral	Minimum λ	Maximum λ	$v \sin i$	
				sec	K	cgs	Type	Å	Å	$km\,s^{-1}$	
HD 135297	−0.3665300	228.5721893	2008-08-12T23:31:22	300	9561	3.99	A1	3660.8045	9200.8145	51	
HD 135396	−65.6107101	229.5624847	2008-08-12T00:29:10	750	6998	3.48	F3	3660.5097	9200.5197	<10	✓
HD 135480	−77.7112427	230.6090851	2008-08-10T00:23:43	600	8429	4.23	A6	3659.9951	9200.5102	46	
HD 135480	−77.6963730	230.6008606	2008-08-13T00:37:18	750	8429	4.23	A6	3659.9975	9200.7500	46	
HD 135728	−31.4563293	229.3897247	2007-02-08T08:35:13	500	7798	3.93	A8	3661.1402	9201.1502	45	
HD 135728	−31.4622192	229.3925476	2008-08-08T01:20:40	400	7798	3.93	A8	3660.4704	9200.4804	45	
HD 135728	−31.4461708	229.3820038	2008-08-13T00:22:28	700	7798	3.93	A8	3660.1477	9200.1577	45	
HD 135815	−41.1203499	229.6308136	2007-02-08T08:45:45	900	7987	3.67	A8	3660.4993	9200.5093	25	✓
HD 137160	−55.0233994	231.6833954	2008-08-12T00:45:45	600	7896	3.89	A8	3660.3467	9200.3567	47	
HD 137581	−51.0250702	232.2113190	2008-08-12T01:41:07	1200	8126	3.55	A7	3659.7632	9199.7732	>100	
HD 137802	−67.1401367	232.9830017	2008-08-12T01:17:34	1200	8109	4.54	A7	3660.2830	9200.2930	56	
HD 137848	−41.0695992	232.4308167	2007-02-08T09:03:02	1100	8510	3.85	A6	3660.0535	9200.0635	48	
HD 138426	−19.4044609	233.1334534	2007-02-10T07:14:06	350	8433	4.13	A6	3660.3202	9200.0131	<10	✓
HD 138927	−43.8827095	234.1885834	2007-02-09T07:13:43	720	7514	3.79	F0	3660.1196	9200.1296	15	✓
HD 139474	−75.9237976	236.3165741	2008-08-10T00:40:08	799	9350	4.05	A2	3659.9172	9199.9272	60	
HD 139631	−40.0809784	235.1606598	2007-02-09T07:28:02	420	7952	3.84	A8	3660.2341	9200.2441	50	
HD 140220	−44.1021309	236.0105133	2008-08-13T01:10:41	250	7908	3.40	A8	3660.2990	9200.3090	53	
HD 140748	−68.1232986	237.4382324	2008-08-11T01:44:10	1000	8144	4.14	A7	3660.4885	9200.4985	<10	✓

Table B.1

Star	Dec	RA	Date of observations	Exposure	$T_{\rm eff}$	$\log g$	Spectral	Minimum λ	Maximum λ	$v \sin i$	
				sec	K	cgs	Type	Å	Å	$km\,s^{-1}$	
HD 141317	−49.3578300	237.6150665	2008-08-12T02:16:45	800	7837	3.82	A8	3660.6286	9200.6386	76	
HD 141317	−49.3409500	237.6067505	2008-08-13T01:47:23	900	7837	3.82	A8	3660.6088	9200.6188	97	
HD 142823	−49.1004715	239.6800842	2008-08-13T01:17:55	750	7986	4.20	A8	3659.7940	9199.8040	97	
HD 143487	−30.9140091	240.4095612	2007-02-09T07:37:09	900	6812	5.19	F4	3660.4847	9200.4947	13	✓‡r
HD 143654	−51.5497589	241.82550	2008-08-12T02:34:57	800	8380	4.13	A6	3661.1090	9201.1190	65	
HD 144748	−25.1249294	242.0636902	2007-02-09T07:59:56	400	8302	3.87	A6	3660.7696	9200.7796	57	
HD 146631	−52.1951714	244.9109497	2009-07-17T02:13:57	1200	7629	3.70	A9	3659.4754	9199.4854	18	✓
HD 146971	−9.6113796	244.8460236	2008-08-13T01:33:03	650	8589	3.95	A5	3659.8941	9199.9041	51	
HD 147105	−25.3919792	245.1843414	2007-02-08T09:23:30	660	8109	4.04	A7	3659.8557	9199.8657	72	
HD 148593	−14.5873404	247.4004822	2008-08-08T00:03:17	730	7714	4.61	A9	3660.7664	9200.7764	<10	✓‡r
HD 149250	−70.1589432	249.7759705	2008-08-13T02:22:58	1300	9326	4.15	A2	3660.6032	9200.6132	43	
HD 150035	−27.2833309	249.8569946	2007-02-09T08:09:03	500	8096	3.78	A7	3660.4568	9200.4668	71	
HD 150862	−25.2139301	251.1599884	2007-02-09T08:19:31	720	6203	4.98	F8	3661.8984	9201.9084	<10	✓
HD 151860	−54.1516800	253.2026215	2008-08-13T02:48:35	1100	6901	4.23	F4	3659.8964	9199.9064	<10	✓‡r
HD 152387	−46.7204208	253.7880554	2008-08-13T03:32:32	1000	8616	3.86	A5	3660.5415	9200.5515	55	
HD 153149	−17.4653606	254.5644684	2007-02-09T08:33:28	900	8354	4.52	A6	3660.4213	9200.4312	83	
HD 153183	−72.3933487	256.0833740	2008-08-11T01:23:12	1000	7813	3.70	A8	3660.2610	9200.2710	26	✓
HD 153953	−51.5682297	256.2802429	2009-07-13T06:30:25	1100	7567	3.65	A9	3660.3871	9200.3971	57	

Table B.1

Star	Dec	RA	Date of observations	Exposure	$T_{\rm eff}$	$\log g$	Spectral	Minimum λ	Maximum λ	$v \sin i$	
				sec	K	cgs	Type	Å	Å	$km\,s^{-1}$	
HD 154253	−60.7716904	256.9932251	2009-07-13T06:51:41	1000	8021	4.39	A8	3660.4520	9200.4620	64	
HD 154308	−33.0528297	256.5180969	2007-02-09T08:50:33	500	8236	4.19	A7	3660.6318	9200.6418	73	
HD 154645	−42.6924095	257.1397095	2007-02-09T09:01:07	600	7530	3.59	A9	3660.5374	9200.5474	53	
HD 154708	−58.0260582	257.5803528	2009-07-09T06:38:29	1000	7051	4.84	F2	3660.2216	9200.2316	55 ‡	
HD 154708	−58.0266991	257.5853577	2009-07-17T01:53:12	1000	7051	4.84	F2	3659.9391	9199.9491	55 ‡	
HD 155127	−26.4545403	257.7048645	2007-02-10T07:22:10	360	7998	3.68	A8	3660.0284	9200.0384	77	
HD 155366	−49.9112396	258.3921814	2009-07-13T05:12:58	1100	8209	3.83	A7	3660.8131	9200.8231	57	
HD 156049	−57.4450302	259.6530457	2008-08-12T02:51:51	350	9737	4.13	A1	3659.8250	9199.8350	84	
HD 156808	−39.4981499	260.3244324	2007-02-09T09:13:12	350	7421	1.88	F0	3660.5208	9200.5308	55	
HD 156869	−52.9815788	260.6887817	2008-08-11T02:04:09	350	7894	3.85	A8	3660.7068	9200.7168	78	
HD 156869	−52.9838715	260.6859436	2008-08-12T03:19:06	350	7894	3.85	A8	3660.6193	9200.6293	78	
HD 157289	−61.4837914	261.5384216	2008-08-12T03:00:58	800	8112	4.14	A7	3659.9262	9199.9362	44	
HD 158205	−56.7381897	262.7846680	2008-08-12T03:45:12	350	8468	3.79	A6	3659.9220	9199.9320	22	✓
HD 158205	−56.7383118	262.7841492	2008-08-12T03:55:56	600	8468	3.79	A6	3659.8774	9199.8874	22	✓
HD 158293	−58.5870399	262.9494934	2008-08-12T04:09:04	800	8185	3.96	A7	3660.4059	9200.4159	28	✓
HD 158450	−8.0371504	262.4138184	2009-07-10T06:32:26	900	8324	4.43	A6	3660.3273	9200.3373	58	
HD 158450	−8.0200796	262.4183044	2008-08-08T00:18:21	371	8324	4.43	A6	3660.3497	9200.3597	58	
HD 159992	−62.3529282	265.4082336	2008-08-13T04:29:27	1300	10546	4.49	A0	3659.9950	9200.5023	49	

Table B.1

Star	Dec	RA	Date of observations	Exposure	$T_{\rm eff}$	$\log g$	Spectral	Minimum λ	Maximum λ	$v \sin i$	
				sec	K	cgs	Type	Å	Å	$km\,s^{-1}$	
HD 160127	−39.9557304	265.0129395	2007-02-09T09:21:13	211	8154	3.79	A7	3660.4704	9200.4804	50	
HD 160544	−18.6438198	265.3210449	2007-02-10T08:57:50	646	7929	4.22	A8	3660.6814	9200.6914	44	
HD 161423	−71.7108231	267.9506226	2009-07-17T03:43:58	1100	7688	4.82	A9	3659.5256	9199.5356	14	✓
HD 161704	−39.4279099	267.1879883	2007-02-09T09:26:42	286	6303	4.40	F8	3660.4106	9200.4206	11	✓
HD 161755	−18.3100204	267.66528	2009-07-10T06:08:49	1200	7909	4.09	A8	3660.9022	9200.9122	45	
HD 161755	−18.3118305	267.57678	2009-07-17T05:46:14	1200	7909	4.09	A8	3660.8294	9200.8394	45	
HD 161755	−18.3121490	267.58899	2009-07-18T05:56:34	2000	7909	4.09	A8	3660.8610	9200.8710	45	
HD 162316	−75.8210831	269.7082520	2009-07-17T04:06:35	1100	7607	4.89	A9	3660.3302	9200.3402	10	✓
HD 162373	−31.3519306	268.0217285	2007-02-10T09:11:26	660	8249	4.32	A7	3660.2947	9200.3047	62	
HD 163379	−50.6022911	269.6056519	2008-08-09T05:27:05	539	6790	3.24	F5	3659.0371	9199.0471	>100	
HD 163833	−42.6193199	270.0573730	2008-08-10T02:09:40	1103	9199	3.82	A3	3660.0274	9200.0374	31	✓
HD 164231	−45.6724815	270.5718689	2008-08-08T04:19:16	424	8064	4.03	A7	3660.3020	9200.3120	70	
HD 164485	−13.1488600	270.4692078	2008-0810T00:56:49	450	7444	4.04	F0	3661.0320	9201.0420	43	
HD 164821	−39.8027802	271.1853638	2009-07-09T07:18:07	1200	9861	4.00	A0	3660.3824	9200.3924	55	
HD 164827	−0.4591600	270.7407837	2008-08-08T01:02:26	871	8034	4.06	A7	3660.5717	9200.5817	87	
HD 165945	−15.5303097	272.2433777	2008-08-10T01:51:43	871	8310	4.23	A6	3660.4966	9200.5066	88	
HD 166223	−44.3208885	272.9277649	2009-07-10T06:50:29	1200	10591	3.97	A0	3659.6747	9199.6847	15	✓
HD 166469	−28.9214993	272.9683838	2009-07-09T07:09:04	350	9888	3.95	A0	3660.2070	9200.2169	73	

Table B.1

Star	Dec	RA	Date of observations	Exposure	$T_{\rm eff}$	$\log g$	Spectral	Minimum λ	Maximum λ	$v \sin i$	
				sec	K	cgs	Type	Å	Å	$km\,s^{-1}$	
HD 166808	−28.2586899	273.3583374	2008-08-08T03:29:12	799	8490	4.01	A6	3660.1873	9200.1973	44	
HD 167024	−38.8971481	273.7690125	2007-02-10T09:24:39	646	8208	4.00	A7	3660.3485	9200.3585	50	
HD 167288	−23.1207104	273.8606567	2008-08-08T02:09:28	424	6980	4.65	F3	3660.2629	9200.2728	66 ‡	
HD 167700	−24.4030495	274.3348083	2008-08-10T03:13:19	1023	8262	4.14	A7	3659.3353	9199.3453	45	
HD 168767	−26.9144592	275.6093750	2008-08-08T02:40:50	480	7951	4.01	A8	3660.1011	9200.1111	51	
HD 169380	−37.9319611	276.5024719	2009-07-10T07:14:06	1200	9328	4.40	A2	3660.1152	9200.1252	31	✓
HD 169481	−44.4795113	276.7205811	2008-08-09T05:44:51	730	8003	3.63	A8	3661.0999	9201.1099	46	
HD 169852	−31.5710297	276.9969177	2008-08-08T02:20:48	1023	8185	3.96	A7	3660.0311	9200.0411	82	
HD 171771	−21.4988499	279.3473816	2008-08-08T04:10:15	371	8195	3.99	A7	3660.6957	9200.7057	47	
HD 172626	−37.0969086	280.6867065	2009-07-10T07:38:13	1200	8074	3.95	A7	3660.0216	9200.0316	33	✓
HD 172703	−33.5141411	280.7530212	2009-07-09T07:41:50	900	9419	3.86	A2	3659.9380	9199.9480	16	✓
HD 172703	−33.4976883	280.7561035	2008-08-11T05:27:10	900	9419	3.86	A2	3659.9600	9199.9700	16	✓
HD 173562	−58.9520988	282.3461304	2008-08-11T02:42:21	300	8586	3.73	A5	3659.5889	9199.5989	60	
HD 173562	−58.9372902	282.3339539	2008-08-12T04:26:52	400	8586	3.73	A5	3659.8572	9199.8672	60	
HD 174581	−44.7960281	283.2915344	2009-07-11T06:54:02	1200	9371	4.00	A2	3660.2122	9200.2222	55	
HD 176519	−49.3269386	285.7427063	2009-07-10T08:01:09	1200	9626	4.50	A1	3659.8262	9199.8362	51	
HD 177013	−17.3118591	285.8438721	2008-08-10T04:01:00	730	7299	4.26	F1	3660.2946	9200.3046	41	
HD 177016	−20.5801392	285.8994141	2008-08-08T05:26:24	871	7720	3.79	A9	3660.0797	9200.0897	67	

Table B.1

Star	Dec	RA	Date of observations	Exposure	$T_{\rm eff}$	$\log g$	Spectral	Minimum λ	Maximum λ	$v \sin i$	
				sec	K	cgs	Type	Å	Å	$km\,s^{-1}$	
HD 177268	−34.2950287	286.3324585	2009-07-11T06:30:26	1100	8202	4.25	A7	3659.9118	9199.9218	<10	✓
HD 177268	−34.2947388	286.3343811	2009-07-17T04:29:57	1100	8202	4.25	A7	3659.9137	9199.9237	<10	✓
HD 177268	−34.2791481	286.3345337	2008-08-11T05:46:08	950	8202	4.25	A7	3659.9573	9199.9673	<10	✓
HD 177382	−28.1518097	286.3793640	2008-08-08T05:05:50	1023	7673	4.03	A9	3661.6223	9201.6323	56	
HD 177765	−26.3347893	286.7689209	2008-08-09T06:00:28	799	7756	4.47	A9	3660.0997	9200.1097	<10	✓ r
HD 178246	−13.7870302	287.0683594	2008-08-10T04:16:59	871	8046	4.34	A7	3660.2173	9200.2273	42	
HD 179902	−21.7579498	288.7612000	2009-07-11T07:17:20	1200	6771	4.00	F5	3659.8307	9199.8407	37	✓‡
HD 179902	−21.7572899	288.7620239	2009-07-17T06:20:42	2400	6771	4.00	F5	3659.8281	9199.8381	37	✓‡
HD 180055	−1.6525300	288.7630920	2009-07-16T06:58:48	1200	7506	4.00	F0	3661.5252	9201.5352	45 ‡	
HD 180303	−20.7969704	289.1728516	2009-07-11T07:40:44	1200	8677	4.00	A5	3659.6935	9199.7036	34	✓
HD 180303	−20.7966900	289.1729431	2009-07-17T07:04:11	1300	8677	4.00	A5	3659.6669	9199.6769	34	✓
HD 180303	−20.7975407	289.1729736	2009-07-18T06:57:38	2000	8677	4.00	A5	3659.7166	9199.7266	34	✓
HD 182459	−23.1553097	291.3952942	2009-07-10T08:25:18	900	9442	4.00	A2	3660.0674	9200.0774	45	
HD 183735	1.0245800	292.6929626	2009-07-16T07:21:28	1200	6713	4.00	F5	3659.5118	9199.5218	78 ‡	
HD 183836	0.1461500	292.8327332	2009-07-12T06:01:20	1100	7572	4.00	A9	3659.8999	9199.9099	43	
HD 184020	−49.7065506	293.6458740	2009-07-09T08:00:41	900	9273	4.00	A3	3660.4621	9200.4721	45	
HD 184120	−20.5013695	293.3909302	2009-07-11T08:03:40	1200	7824	4.20	A8	3659.9383	9199.9483	14	✓
HD 184120	−20.5023994	293.3912354	2009-07-18T07:35:13	2400	7824	4.20	A8	3659.9559	9199.9659	14	✓

Table B.1

Star	Dec	RA	Date of observations	Exposure	$T_{\rm eff}$	$\log g$	Spectral	Minimum λ	Maximum λ	$v \sin i$	
				sec	K	cgs	Type	Å	Å	$km\,s^{-1}$	
HD 184343	−23.3946095	293.6917725	2009-07-13T07:11:10	1200	11333	1.86	B9	3660.2437	9200.2537	22	✓
HD 185067	−1.6696000	294.3519897	2009-07-13T08:19:53	1100	7609	4.00	A9	3659.9824	9199.9924	78	
HD 185129	−15.8273296	294.5278320	2009-07-13T07:34:50	1200	8067	4.00	A7	3660.8244	9200.8344	<10	✓
HD 185204	−46.9110298	294.9985657	2008-08-10T06:07:07	1023	7586	4.62	A9	3659.8209	9199.8308	<10	
HD 185204	−46.9129906	294.9981995	2008-08-12T05:45:47	1200	7586	4.62	A9	3659.8135	9199.8235	<10	✓
HD 186038	−3.0976200	295.5160217	2009-07-13T08:41:00	1200	6003	4.00	G0	3660.1297	9200.1397	32	✓‡
HD 186041	−28.6515408	295.7703857	2008-08-08T05:45:43	799	6233	3.79	F8	3659.5690	9199.5790	46	
HD 187761	−39.4142113	298.2911987	2008-08-08T06:02:32	1103	7604	4.16	A9	3660.4655	9200.4755	57	
HD 187761	−39.4137917	298.2904358	2008-08-13T05:18:17	1600	7604	4.16	A9	3660.4355	9200.4455	57	
HD 188008	−36.5799294	298.5906677	2008-08-08T06:26:05	539	8215	4.31	A7	3660.4436	9200.4536	41	
HD 188008	−36.5807114	298.5907593	2008-08-12T04:59:55	700	8215	4.31	A7	3660.4678	9200.4778	41	
HD 188601	−22.0256996	299.1538086	2009-07-11T08:26:54	1200	7527	4.91	A9	3659.5173	9199.5273	61 ‡	
HD 188601	−22.0248108	299.1560059	2009-07-16T08:23:31	1200	7527	4.91	A9	3659.5153	9199.5253	61 ‡	
HD 188862	−12.0540895	299.3820496	2009-07-13T07:57:26	1200	8217	4.00	A7	3660.0264	9200.0364	76	
HD 189963	−6.4504800	300.7281799	2009-07-12T09:03:29	1200	8001	4.27	A8	3659.7491	9199.7591	27	✓
HD 190075	0.6811400	300.7854614	2009-07-12T07:39:48	900	8490	4.00	A6	3660.5342	9200.5442	76	
HD 190654	−78.3579178	303.7239990	2008-08-11T06:04:58	1150	6337	4.44	A1	3659.8766	9199.8866	49	
HD 190654	−78.3573074	303.7220154	2008-08-13T04:54:00	1200	6337	4.44	F8	3659.8569	9199.8669	49	

Table B.1

Star	Dec	RA	Date of observations	Exposure	$T_{\rm eff}$	$\log g$	Spectral	Minimum λ	Maximum λ	$v \sin i$	
				sec	K	cgs	Type	Å	Å	$km\,s^{-1}$	
HD 191439	−58.7849197	303.2034302	2008-08-08T06:50:35	600	9576	4.33	A1	3660.0434	9200.0534	44	
HD 191439	−58.7853699	303.2039185	2008-08-12T05:12:47	800	9576	4.33	A1	3660.0172	9200.0272	44	
HD 191695	−21.3211594	302.9880066	2009-07-11T08:50:00	1200	7311	4.38	F1	3659.8152	9199.8252	<10	✓‡
HD 191695	−21.3207607	302.9899597	2009-07-16T08:47:30	1200	7311	4.38	F1	3659.7910	9199.8010	<10	✓‡
HD 193382	−47.7451591	305.4555664	2009-07-09T08:18:51	1200	9123	4.00	A3	3660.5608	9200.5708	66	
HD 193644	−51.1936607	305.8676147	2008-08-09T06:31:18	424	6644	3.90	F5	3659.7217	9199.7317	49	
HD 193941	−52.3413696	306.2933350	2008-08-09T06:43:48	600	6331	4.50	F8	3660.0127	9200.0227	>100	
HD 194623	−26.2072296	306.8732910	2008-08-08T06:38:43	480	6554	4.22	F7	3659.8852	9199.8952	>100	
HD 194750	−43.2536087	307.2325134	2008-08-09T06:57:55	600	10816	4.30	A0	3660.0189	9200.0289	40	
HD 194750	−43.2547188	307.2336731	2008-08-12T05:29:20	800	10816	4.30	A0	3660.0200	9200.0100	40	
HD 195112	−38.5819283	307.6651306	2008-08-09T07:11:19	799	7431	4.33	F0	3660.2047	9200.2147	86 ‡	
HD 195112	−38.5812988	307.6659851	2008-08-10T06:27:16	1000	7431	4.33	F0	3660.3345	9200.3445	86 ‡	
HD 195112	−38.5820808	307.6660156	2008-08-13T06:04:59	1200	7431	4.33	F0	3660.2890	9200.2990	86 ‡	
HD 196470	−17.5207005	309.5188599	2009-07-12T08:40:16	1200	7546	4.55	F0	3659.7434	9199.7535	20	✓‡r
HD 196691	−6.1758199	309.7738647	2009-07-12T08:21:31	900	9285	4.00	A3	3660.3689	9200.3789	49	
HD 196691	−6.1777301	309.7763672	2009-07-16T09:17:37	900	9285	4.00	A3	3660.3123	9200.3223	49	
HD 200623	−35.7063408	316.3719788	2008-08-08T07:19:32	730	8239	4.34	A7	3661.1997	9201.2097	49	
HD 200623	−35.7055397	316.3722534	2008-08-10T07:06:08	900	8239	4.34	A7	3661.2001	9201.2101	49	

Table B.1

Star	Dec	RA	Date of observations	Exposure	$T_{\rm eff}$	$\log g$	Spectral	Minimum λ	Maximum λ	$v \sin i$	
				sec	K	cgs	Type	Å	Å	$km\,s^{-1}$	
HD 200623	−35.7069588	316.3717041	2008-08-13T06:28:38	1200	8239	4.34	7A1	3661.2218	9201.2318	49	
HD 201018	−37.0495987	317.75378	2008-08-08T07:35:56	424	8215	4.46	A7	3660.1461	9200.1561	95	
HD 201018	−37.0489082	317.78125	2008-08-10T07:25:49	600	8215	4.46	A7	3660.2276	9200.2376	95	
HD 201018	−37.0499687	317.76599	2008-08-13T06:51:05	800	8215	4.46	A7	3660.2720	9200.2820	95	
HD 203006	−40.8306198	320.1627197	2009-07-11T09:12:51	200	9673	4.21	A1	3660.1577	9200.1677	>100	
HD 203683	−3.3850501	320.9726562	2009-07-13T09:03:47	1200	9146	4.00	A3	3660.7438	9200.7538	62	
HD 207259	−73.1769180	327.8696899	2008-08-08T07:05:36	600	7784	4.40	A9	3659.8266	9199.8366	43	
HD 207259	−73.1761780	327.8690796	2008-08-10T06:47:30	900	7784	4.40	A9	3659.8715	9199.8815	43	
HD 207259	−73.1768188	327.8689270	2008-08-12T06:09:29	1200	7784	4.40	A9	3659.8471	9199.8571	43	
HD 209051	−6.4531002	330.1464844	2009-07-13T09:27:04	900	10520	4.00	A0	3660.4169	9200.4269	55	
HD 209605	−26.8525295	331.2879333	2008-08-08T07:46:27	1103	7720	4.24	A9	3660.3337	9200.3437	34	✓
HD 211099	−6.7548699	333.7079773	2009-07-16T08:10:20	600	10020	4.00	A0	3660.1374	9200.1474	45	
HD 214985	−20.6449909	340.5708008	2009-07-09T08:42:03	1200	10652	4.00	A0	3660.9227	9200.9327	55	
HD 215913	−2.1702001	342.1459351	2009-07-09T09:06:05	1200	6072	4.00	G0	3659.2901	9199.3001	76	
HD 215966	−34.9883003	342.3454285	2008-08-08T08:09:53	108	10013	3.75	A0	3659.5997	9199.6097	56	
HD 215966	−34.9883614	342.3455505	2008-08-08T08:15:09	180	10013	3.75	A0	3659.6035	9199.6135	56	
HD 219391	−27.1821804	348.9078369	2008-08-08T08:28:31	480	7911	4.12	A8	3659.2053	9199.2153	14	✓
HD 219391	−27.1824493	348.9079895	2008-08-13T05:48:22	800	7911	4.12	A8	3660.2619	9200.2719	14	✓

Table B.1

Star	Dec	RA	Date of observations	Exposure	$T_{\rm eff}$	$\log g$	Spectral	Minimum λ	Maximum λ	$v \sin i$	
				sec	K	cgs	Type	Å	Å	$km\,s^{-1}$	
HD 221127	−23.0613403	352.3632202	2008-08-08T08:39:32	730	6262	4.94	F8	3659.5472	9199.5572	<10	✓
HD 221531	−11.9909096	353.2276306	2008-08-08T08:20:43	273	6431	4.50	F7	3659.7601	9199.7701	53	
HD 222638	−57.4827614	355.6084290	2008-08-08T09:04:26	480	9543	4.37	A1	3660.0796	9200.0896	72	
HD 222638	−57.4827614	355.6087341	2008-08-10T07:38:49	600	9543	4.37	A1	3660.0814	9200.0914	72	
HD 222925	−61.9178314	356.2849121	2008-08-08T09:16:16	664	5836	2.95	G1	3660.8018	9200.8118	35	✓

Appendix C

Tables for Chapter 3

Table C.1: Fe I / Fe II abundance lines used in the analysis of HD 43587

Ion	Wavelength	Abundance
Fe I	4112.3185	−4.71
	4114.4450	−4.64
	4120.2060	−4.74
	4132.8990	−4.66
	4136.5210	−4.64
	4136.9970	−4.73
	4168.9416	−4.68
	4184.8910	−4.75
	4217.5456	−4.60
	4220.3410	−4.69
	4387.8910	−4.71
	4454.3800	−4.70
	4485.6750	−4.66
	4502.5909	−4.64

APPENDIX C

Table C.1

Ion	Wavelength	Abundance
Fe I	4517.5240	−4.63
	4551.6470	−4.63
	4556.9240	−4.69
	4566.5140	−4.58
	4587.1276	−4.64
	4602.0000	−4.64
	4602.9410	−4.69
	4630.1200	−4.66
	4635.8460	−4.65
	4661.5344	−4.64
	4661.9700	−4.70
	4678.8450	−4.66
	4704.9480	−4.68
	4728.5457	−4.82
	4741.5290	−4.69
	4745.8000	−4.77
	4779.4390	−4.62
	4787.8269	−4.64
	4799.4060	−4.64
	4800.6490	−4.86
	4807.7080	−4.63
	4839.5440	−4.73
	4882.1430	−4.70
	4892.8589	−4.63
	4907.7318	−4.63

APPENDIX C

Table C.1

Ion	Wavelength	Abundance
Fe I	4917.2290	−4.64
	4924.7695	−4.80
	4938.8130	−4.60
	4962.5719	−4.69
	4986.2226	−4.63
	5029.6176	−4.65
	5049.8190	−4.61
	5054.6420	−4.64
	5067.1496	−4.60
	5068.7650	−4.62
	5126.1920	−4.70
	5141.7390	−4.68
	5162.2729	−4.68
	5187.9142	−4.70
	5194.9410	−4.56
	5198.7110	−4.63
	5217.3890	−4.63
	5228.3760	−4.60
	5242.4910	−4.64
	5250.6450	−4.64
	5253.4610	−4.63
	5257.6550	−4.66
	5281.7900	−4.58
	5288.5247	−4.60
	5365.3990	−4.66

APPENDIX C

Table C.1

Ion	Wavelength	Abundance
Fe I	5367.4660	−4.62
	5379.5740	−4.64
	5383.3690	−4.60
	5389.4790	−4.63
	5393.1670	−4.62
	5409.1330	−4.66
	5410.9098	−4.60
	5424.0680	−4.61
	5434.5230	−4.52
	5441.3387	−4.64
	5445.0420	−4.61
	5461.5499	−4.60
	5464.2796	−4.63
	5466.9870	−4.60
	5472.7090	−4.63
	5473.9000	−4.65
	5491.8315	−4.67
	5522.4460	−4.62
	5543.9357	−4.63
	5562.7060	−4.71
	5565.7040	−4.89
	5567.3910	−4.56
	5569.6180	−4.55
	5576.0888	−4.62
	5586.7559	−4.58

APPENDIX C

Table C.1

Ion	Wavelength	Abundance
Fe I	5607.6637	−4.62
	5608.9723	−4.66
	5615.6439	−4.53
	5624.0220	−4.64
	5624.5420	−4.62
	5633.9460	−4.68
	5635.8220	−4.59
	5638.2620	−4.64
	5641.4340	−4.58
	5646.6840	−4.61
	5651.4690	−4.58
	5652.3180	−4.61
	5661.3450	−4.57
	5677.6840	−4.59
	5678.3788	−4.58
	5679.0229	−4.65
	5691.4970	−4.60
	5696.0890	−4.56
	5701.5440	−4.65
	5705.4640	−4.59
	5717.8329	−4.64
	5731.7620	−4.61
	5742.9600	−4.60
	5760.3440	−4.64
	5775.0806	−4.65

APPENDIX C

Table C.1

Ion	Wavelength	Abundance
Fe I	5855.0760	−4.58
	5871.3040	−3.90
	5880.0272	−4.61
	5905.6710	−4.62
	5916.2470	−4.58
	5984.8150	−4.90
	5987.0650	−4.86
	6005.5420	−4.26
	6007.9600	−5.07
	6027.0509	−4.65
	6065.4820	−4.58
	6078.4910	−4.85
	6085.2580	−4.59
	6098.2440	−4.62
	6127.9060	−4.61
	6136.6150	−4.56
	6137.6910	−4.61
	6157.7280	−4.67
	6165.3600	−4.62
	6187.3980	−4.74
	6200.3129	−4.61
	6230.7220	−4.56
	6380.7430	−4.64
	6408.0180	−4.72
	6469.1920	−4.50

APPENDIX C

Table C.1

Ion	Wavelength	Abundance
Fe I	6475.6240	−4.10
	6494.9800	−4.54
	6593.8700	−4.63
	6609.1100	−4.64
	6625.0220	−4.52
	6646.9310	−4.54
	6704.4800	−4.62
	6705.1010	−4.74
	6710.3160	−4.54
	6732.0649	−4.59
	6745.9560	−4.76
Fe II	4178.8620	−4.81
	4508.2880	−4.71
	4515.3390	−4.65
	4576.3400	−4.70
	4620.5210	−4.67
	4993.3580	−4.64
	5197.5770	−4.50
	5234.6250	−4.65
	5256.9380	−4.74
	5284.1090	−4.54
	5414.0730	−4.58
	5425.2570	−4.48
	5534.8470	−4.55
	5991.3760	−4.61

APPENDIX C

Table C.1

Ion	Wavelength	Abundance
Fe II	6084.1110	−4.49
	6149.2580	−4.59
	6239.3660	−4.42
	6247.5570	−4.61
	6369.4620	−4.57
	6432.6800	−4.43
	6446.4100	−4.59
	6456.3830	−4.60
	6516.0800	−4.52

Table C.2: Fe I / Fe II abundance lines used in the analysis of HD 188136

Ion	Wavelength	Abundance
Fe I	5731.7620	−3.88
	5752.0320	−3.80
	5816.3730	−4.31
	5859.5860	−4.31
	5905.6710	−4.35
	5934.6530	−4.04
	5952.7160	−4.15
	5984.8150	−4.23
	6003.0100	−4.31
	6024.0490	−3.94

APPENDIX C

Table C.2

Ion	Wavelength	Abundance
Fe I	6027.0509	−4.31
	6093.6430	−4.14
	6096.6500	−4.15
	6098.2440	−3.19
	6129.5820	−4.04
	6170.5040	−3.88
	6336.8230	−4.24
	6380.7430	−4.13
	6411.6470	−4.26
	6419.9420	−4.20
	6752.7050	−4.13
	6810.2570	−4.31
	6842.6790	−3.76
	6843.6480	−4.16
	6855.1610	−4.07
	6858.1450	−3.66
	7445.7490	−4.03
	7491.6470	−4.15
	6084.1110	−4.28
Fe II	6113.3220	−4.13
	6147.7410	−4.21
	6149.2580	−4.156
	6238.3920	−3.98
	6369.4620	−4.14
	6383.7220	−4.34

APPENDIX C

Table C.2

Ion	Wavelength	Abundance
Fe II	6416.9190	−4.16
	6442.9550	−4.20

Appendix D

Program Listing of IDL Abundance Analysis Routines

D.1 PROGRAM calc_eqw.pro

```
PRO calc_eqw
;#########################################################################
;
; Name: calc_eqw
;
; Version:  5
;
; Last modified:   2 Feb 2015
;
; Purpose: To measure EQWs
;
; Inputs: line list, input FITS files, VALD data
;
; Outputs: Formatted WIDTH output files,
;
; Parameters: None
;
;#########################################################################

;initialisation

logg_in = '9.9'
vmicro_in='4'
model='cgm'
; ======================================
```

```
default9 , wavestart , 3600.
default9 , endwave, 30000.
default9 , orderstep , 100.
default9 , logg_in ,4.
default9 , box_width, 20000L
default9 , n, 0L
default9 , vsini ,0.
;default9 , model,'cgm'
 banner1 = '
    ++++++++++++++++++++++++++++++++++++++++++++++++++++++++++++++++++++++++
    '
;

;================================
; set up limiting Halpha parms
;
;================================
halpha_lab = 6562.852D
halpha_min = 6556.000D
halpha_max =  6568.000D
flux_cap =1.5D
min_flux_threshold = 0.97
min_hw_value = 1.25
vsini_stor=fltarr(20)


base_factor=2.0 ;specifies factor x fwhm to calc eqw wl
   range
lw_lim = .15D   ; linewidth limit to restrict Halpha match
   calculation

timestamp=string(strmid(systime(0),8,2),format='(i2.2)') $
          + strmid(systime(0),4,3)+strmid(systime(0),22,2) $
          + '_'+strmid(systime(0),11,8)

;================================
; set up base file/directory
; naming constructs
;================================

; set here value for base files

logg_in = String(logg_in, Format='(f3.1)')
logg_str = logg_in
vmicro_in = strtrim(String(vmicro_in, Format='(a)'),2)
remchar,string(logg_str),'.'

base_output='/Users/mph/Feros_all/output/'
width_script = '/Users/mph/ATLAS/documentation/
   atlas_cookbook/width_script'
```

APPENDIX D

```
final_output = base_output + timestamp + '_g' + string(
    logg_str) + '_v' + strcompress(string(vmicro_in) + '_' +
    model)
;final_output = base_output + timestamp + '_v' + strcompress
    (string(vmicro))


width_output = final_output + '/width_output'
;print,'width output =',width_output
flux_min_output = final_output + '/flux_min_output'
extract_output = final_output + '/extract_output'

;input files

;model_path = '/Users/mph/ATLAS/nemo/mlt/vmicro_2/p00/' ;
    location of model atmosphere
alpha_file = '/Users/mph/Feros_all/temp/halpha_template.prf'
     ; location oh Halpha synth line

list2s_file = '/Users/mph/Feros_all/datafiles/star_filename'
star_teff_file = '/Users/mph/Feros_all/datafiles/star_teff'
sellib_file = '/Users/mph/vwadata/
    vald_grid_sellib_REE_04MAY10.idl'
line_file_name = '/Users/mph/Feros_all/datafiles/eqw_lines'
datadir = '/Users/mph/Feros_all/datafiles/'

; WIDTH input file
w_filename = datadir +  'width.dat'
input_file_path = '/Users/mph/Feros_all/'
file_mask = '/*.fits'

;
;create output directory
;

spawnrob,'cd ' + base_output

spawnrob,'mkdir ' + final_output

; create log file for flux min decision

openw,3,flux_min_output

;=============================================
; read in grevasp file to resolve
; atomic numbers for each element
; for WIDTH
;=============================================
```

APPENDIX D

```
import_grevasp, grevasp

; restore the sellib file containing VALD data


restore,sellib_file


;=============================================
; read in the table of Teffs,
; loggs etc - format:
;=============================================

 ;Object     Gr  Teff     logg  V0    E(b-y) D(m0)  Tol.
    Iter. Warning
 ;  2202     7   6543   4.21   8.37 -0.007  0.001 1.19E-06  38

readcol, star_teff_file,star_teff_obj,star_teff_gr,
   star_teff_teff,$
star_teff_logg,star_teff_v0,star_teff_E,star_teff_D,
   star_teff_tol,star_teff_iter,$
format='a,a,a,a,a,a,a,a,a',/silent

;=============================================
; read in the table of FITS spectra filenames
; and catalog numbers etc
;=============================================

readcol, list2s_file,list2s_catalog_num,list2s_fits_file,$
list2s_hdname,format='a,a,a',/silent


file_ct=n_elements(list2s_catalog_num)

print, 'Total number of files to process : ', file_ct


for ff=0,file_ct -1 do begin


  teff_found = 0



  print,'File now being processed :',list2s_fits_file(ff)

  ; ok we now need to retrieve some Teff,
  ; logg data assoc with this file

  for k = 0,n_elements(star_teff_obj) - 1 do begin
```

```
    if star_teff_obj(k) eq list2s_catalog_num(ff) and
       teff_found eq 0 then begin

      ;the HD  number has been found in star_teff.min - can
          assign Teff, logg

      teff = star_teff_teff(k)
      logg = star_teff_logg(k)

      teff_found = 1

      output_star = 'HD' + string(star_teff_obj(k))
    endif

  endfor ; number of Teff entries in star_teff.min

if teff_found eq 0 then begin
  print, 'No Teff data found for ',list2s_fits_file(ff)
  openu,5, width_output,/append
  printf,5,'++ No Teff/logg info available for :',$
  list2s_fits_file(ff),format='(a,a)'
  close,5
  goto, jump1

endif



;=============================================================
;construct complete file name to retrieve from
;input directory
;=============================================================

file_name_array = input_file_path + list2s_fits_file(ff)

;=============================================================
;build spectrum from fits file
;=============================================================

flux = readfits(file_name_array, header)

n = n_elements(flux)

w  = where(strmatch(header,'CRVAL1*'),c)
w1 = where(strmatch(header,'CDELT*'),c)
w2 = where(strmatch(header,'CRPIX1*'),c)


x  = strsplit(header(w), ' ', /extract)
```

```
x1 = strsplit(header(w1), ' ', /extract)
x2 = strsplit(header(w2), ' ', /extract)
ref_pix = double(x2(2))
pixel_0 = double(x(2))
pixel_increment = double(x1(2))

begl =  0.000D
endl =  0.000D


obs_alpha_flux_min = 0.000D
obs_alpha_wl_min = 0.000D
obs_flux_min = 0.000D
obs_wl_min = 0.000D
specshift = 0.000

line_corr_wl = 0.000D
wllim = 1.0000D
wllim_min = 0.000D
wllim_max = 0.000D


alpha_ll = 0.0D
alpha_ul = 0.0D
obs_ll = 0.0D
obs_ul = 0.0D
combi_ll = 0.0D
combi_ul = 0.0D

wllim_left = dblarr(300)
wllim_right = dblarr(300)
flipper = intarr(1000)


wave = pixel_0  + pixel_increment * (findgen(n) -ref_pix)
;print,'pixel incr ',pixel_increment

wuse = where(wave ge wavestart and  wave le endwave, cuse)
wave = wave(wuse)
flux = flux(wuse)
n = n_elements(wave)

;print,' %% This is your wavelength range: '
;print,min(wave)
;print,max(wave)

obs = dblarr(2,n)
obs2 = dblarr(2,n)
obs3 = dblarr(2,n)
```

```
wl_use=dblarr(2,n)
obs_alpha=dblarr(2,n)
alpha_use=dblarr(2,n)
obs_use=dblarr(2,n)
for i=0L,n-1 do begin
  obs(0,i) = wave(i)
endfor

for i=0L,n-1 do begin
  obs(1,i) = flux(i)
endfor


;now find the min point of the spectrum within the h alpha
    range

obs_use = where((obs(0,*) ge halpha_min) and $
                                (obs(0,*) le halpha_max) and
                                   $
                    (obs(1,*) le flux_cap ),b99)

inter_obs=dblarr(2,b99)

inter_obs(0,*) = obs(0,obs_use)
obs_ll = inter_obs(0,0)
obs_ul = inter_obs(0,b99-1)
import_alpha,alpha_file,obs_alpha ; read in the Halpha
    line
alpha_use = where((obs_alpha(0,*) ge halpha_min) and $
                                (obs_alpha(0,*) le
                                   halpha_max) and $
                    (obs_alpha(1,*) le flux_cap ),c99)

inter_alpha=dblarr(2,c99)
inter_alpha(0,*) = obs_alpha(0,alpha_use)
alpha_ll = inter_alpha(0,0)
alpha_ul = inter_alpha(0,c99-1)

; now find the common wl range between observed spectrum
    and Halpha

combi_ll = alpha_ll < obs_ll
combi_ul = alpha_ul > obs_ul
final_obs = where((obs(0,*) ge combi_ll) and $
                    (obs(0,*) le combi_ul ),b98)

final2_obs = dblarr(2,b98)
xx=dblarr(2,b98)
final2_obs(0,*) = obs(0,final_obs)
```

```
final2_obs(1,*) = obs(1,final_obs)
final_alpha = where((obs_alpha(0,*) ge combi_ll) and $
                    (obs_alpha(0,*) le combi_ul ),c98)

final2_alpha = dblarr(2,c98)

final2_alpha(0,*) = obs_alpha(0,final_alpha)
final2_alpha(1,*) = obs_alpha(1,final_alpha)
xx(1,*)=interpol(final2_alpha(1,*),final2_alpha(0,*),
   final2_obs(0,*))
xx(0,*) = final2_obs(0,*)

bb = n_elements(xx(0,*))

lag = intarr(2*bb-3)
result = dblarr(2*bb-3)

for i=0,2*bb-4 do begin
  lag(i) = i-bb+2
endfor

result = c_correlate(final2_obs(1,*),xx(1,*),lag)

;plot, final2_obs(0,*),final2_obs(1,*),col=200,/ynozero
;oplot, xx(0,*),xx(1,*),col=200,psym=0

dd = where(result eq max(result))

specshift= lag(dd) * pixel_increment

;print,'H alpha spectral shift:',specshift

;*******************************************
;  ok we have the radial velocity correction
;  now read in the selected linelist
;*******************************************

spawnrob,'cp ' + line_file_name + ' ' + final_output


readcol, line_file_name,input_wl,input_elem,input_elem_ion
   ,$
input_loggf,input_elow, input_jlow,input_eupper,
   input_jupper,$
input_gl,input_gr,input_gs,input_gw, $
format='d,a,a,f,f,f,f,f,f,f,f,f',/silent

nlines = n_elements(input_wl)
```

```
; now to write this line information to the output file
;print,nlines

if ff eq 0 then begin
  openu,5, width_output,/append
  printf,5,banner1,format='(a)'
      printf,5,'++          Spectral lines processed in this
          run :
      printf,5,'++              ', format='(a)'
      printf,5,banner1,format='(a)'
      printf,5,'++Elem/Ion     Wl.          Elow      Jlow
         Eupper     Jupper  loggf gammal gammar gammas
         gammaw    '

  for ll=0L,nlines-1 do begin

    printf,5,'LL ',input_elem(ll),input_elem_ion(ll),
       input_wl(ll),$
    input_elow(ll), input_jlow(ll),$
    input_eupper(ll),input_jupper(ll),input_loggf(ll),
       input_gl(ll),$
    input_gr(ll),input_gs(ll),input_gw(ll),$
    format='(a3,a3,a2,f12.4,f12.3,f5.1,f12.3,f5.1,f6.3,f6
       .3,f6.3,f6.3,f6.3)'

  endfor

  close,5
endif ; only print lines fist time around

eqw_factor = dblarr(nlines)

nobs = n_elements(obs(0,*))
obs_corr = fltarr(2,nobs)

; correct for H alpha offset

for i=0L,nobs-1 do begin
  obs_corr(0,i) = obs(0,i) + specshift
  obs_corr(1,i) = obs(1,i)
endfor

wl_step = median(obs_corr(0,1:nobs-1) - obs_corr(0,0:nobs
   -2)) ; typical WL step

wl_lim = wl_step * 2.0

fwhm = dblarr(2,nobs); WL + measured fwhm!
fwfm = dblarr(2,nobs) ;
```

```
   cnt = 0L ; fwhm counter

;#################################################################
;
; ok now we build the WIDTH parameter file
;
;#################################################################
     openw,1,w_filename

   card='VTUR'
   printf,1,card,format = '(a)'
   nvt = 1
    ; microturbulence
    vts = vmicro_in

   printf,1, nvt,vts,format='(i5,3f5.2)'

   vsini_stor(*) = 0
   vsini_line_num = 0
   ;for i=11,11 do begin

   for i=0,nlines-1 do begin

   ;for i=0,3 do begin

     ;*****************************************************
     ; ok we now need to extract some line data for the
     ; linelist line
     ;
     ;*****************************************************

     ; we need:
     ; element - line input
     ; ion - line input
     ; wl - line input
     ; jlow - lower energy J value - line input
     ; elow - line input
     ; jupper - upper energy J value - line input
     ; eupper - upper energy J value - line input
     ; loggf - from sellib
     ; code - constructed from atomic list file and ion
     ; nelion - calclated from code
     ; gammar - from sellib
     ; gammas - from sellib
     ; gammaw - from sellib
     ; eqw - calculated here
     ; HDname - constructed here
     ;
```

```
output_loggf = input_loggf(i)
output_gammar  = input_gr(i)
output_gammas  = input_gs(i)
output_gammaw  = input_gw(i)
; read in the rest of the line data
output_wl = input_wl(i) / 10    ; wl for WIDTH
   specified in nm
output_jlow = input_jlow(i)
output_jupper = input_jupper(i)
output_elow = input_elow(i) * 8062.4   ; convert eV to
   cm-1
output_eupper= input_eupper(i) * 8062.4   ; convert eV
   to cm-


; lets get the atomic number from file

 mat1 = where(input_elem(i)  eq grevasp.elem,cs)

 if cs ne 1 then begin
   print, ' error with atomic data'
   stop
 endif else begin

   zz = grevasp(mat1).egre07
   code=0.00D
   a = float(input_elem_ion(i)) - 1
   output_code = ZZ + a/100
   output_nelion=((zz-1) * 6) + input_elem_ion(i)

 endelse ; atomic number found

plot_dir_name = output_star + '_' + string(input_wl(i))
   + '_' + string(ff) + '.jpg'
plot_dir_name = strcompress(plot_dir_name,/remove_all)

out_jpg = base_output + timestamp + '/' + plot_dir_name


;+++++++++++++++++++++++++++++++++++++++++++++++++++++++++++++++++++++++

; ok here's the logic for finding each line:
;
; construct a window of range +/- lw_lim before and
   after each line
; currently lw_lim = 0.15 A
; find the minimum flux within this region
; check whether this flux is above a minimum value,
; currently = 0.97
```

```
    ; if greater than this, set eqw=0
    ; if less than this,
    ; locate the wl of the min flux, move each side of this
      to
    ; find the fwhm of the line
    ; if the move to either side of the line goes too far,
      currently
    ; 1.25 either side, then reject the line


    obs_use = where(obs_corr(0,*) ge input_wl(i) - lw_lim
      and $
    obs_corr(0,*) le input_wl(i) + lw_lim, c99)

  ; print,'window min',input_wl(i) - lw_lim

  ;print,'window max',input_wl(i) + lw_lim

  ; print,'input wl',input_wl(i)
   ; print,'obs use ',obs_use
   ;print,'obs corr ',obs_corr(*,obs_use)
       n_use=n_elements(obs_use)
   obs_flux_min = where ( obs_corr(1,obs_use) eq min(
      obs_corr(1,obs_use)),c)


    ; check to see whether line has a minimum flux; if not,
      set eqw to zero and report the fact

       if obs_corr(1,obs_use(obs_flux_min(0))) gt
          min_flux_threshold then begin

       eqw_factor(i) = 0
       output_eqw = 0

       printf, 3, 'Filename = ',list2s_fits_file(ff),'Line
          WL =',input_wl(i),$
       'Flux =',obs_corr(1,obs_use(obs_flux_min(0))), 'Min
          Threshold =',min_flux_threshold, $
       'Reason: flux below threshold'

       print,'The following line does not have minimum flux
          level, eqw set to zero: '
       print,'Filename = ', list2s_fits_file(ff)
       print,'Line WL = ',input_wl(i)
       print,'Flux = ',obs_corr(1,obs_use(obs_flux_min(0)))
       print,'Min Threshold = ',min_flux_threshold
```

```
    ; if vsini_line(i) eq 'Y' then begin
     ;   vsini_stor(vsini_line_num) = 0.0
      ; vsini_line_num = vsini_line_num + 1
      ; print,' flux too low '
    ;  print,'vsinilinenum =',vsini_line_num

     ;endif


endif else begin


 cwl = obs_flux_min(0)

 cwl=obs_use(cwl)


 ; go left:

 ex = 0 & k = 0
 hw1 = -1. & hw2 = -1.



 while ex eq 0 and cwl+k gt 0 do begin

  hw1 = -1.

  k = k - 1

  if (1.-obs_corr(1,cwl+k))/(1.-obs_corr(1,cwl)) le 0.5
      then begin
    hw1 = obs_corr(0,cwl) - obs_corr(0,cwl+k)   ; half
        width, left part
    ex = 1 ; exit loop!
  endif
 endwhile

; go right:
 ex = 0 & k = 0

 while ex eq 0 and cwl+k lt (nobs-1) do begin
   hw2 = -1.
   k = k + 1
```

```
    if (1.-obs_corr(1,cwl+k))/(1.-obs_corr(1,cwl)) le
       0.5 then begin
     hw2 = obs_corr(0,cwl+k) - obs_corr(0,cwl)     ; half
        width, right part
     ex = 1 ; exit loop!
    endif
  endwhile



  fwhm(0,i) = obs_corr(0,cwl)
  fwhm(1,i) = hw1 + hw2

  ;
     ************************************************************

  ;
  ; At this point, can calculate a vsini for each of the
      two iron lines at 5434, 5576,
  ; and write out to a vsini file
  ;
  ;
     ************************************************************


  ;if vsini_line(i) eq 'Y' then begin

    get_vsini,input_wl(i),fwhm(1,i),vsini

   ; print,'vsini line num ',VSINI_LINE_NUM

    vsini_stor(vsini_line_num) = vsini

    vsini_line_num = vsini_line_num + 1

   ; print,' vsini_stor ',vsini_stor
   ; print,'vsini =',vsini

    ; print,' initially ok '
    ;  print,'vsinilinenum =',vsini_line_num


    ;print,'i,fwhm, vsini =',i,fwhm(1,i),vsini
;  endif

  wllim_left(i) = obs_corr(0,cwl) - (base_factor*hw1)
     wllim_right(i) = obs_corr(0,cwl) + (base_factor*hw2
        )
;print, 'wllim ', wllim_left(i) , wllim_right(i)
; now calculate EQW
```

```
wlim99 = where(obs_corr(0,*) ge wllim_left(i) and $
                    obs_corr(0,*) le wllim_right(i), c99)
                       ;


; Dont Include the data point just before and just
    after

if c99 ge 1 then begin
  wlim = lonarr(c99) & wlim = wlim99
  cc = c99

endif

if cc ge 3 then begin
  output_eqw = total( (1. - obs_corr(1,wlim)) * $
  ( obs_corr(0,wlim(1:cc-1)) - obs_corr(0,wlim(0:cc-2))
      ) ) * 100. ; EQW in pAA.

      eqw_factor(i) = output_eqw

endif

;+++++++++++++++++++++++++++++++
;
; Add an extra check here - if
; search for fwhm goes too far from centroid, then
; set eqw to zero
;
;+++++++++++++++++++++++++++++++

if hw1 gt min_hw_value or hw2 gt min_hw_value  then
   begin

  eqw_factor(i) = 0
  output_eqw = 0

  printf, 3, 'Filename = ',list2s_fits_file(ff),'Line
     WL =',input_wl(i),$
  'Flux =',obs_corr(1,obs_use(obs_flux_min)), 'Min
     Threshold =',min_flux_threshold, $
  'Reason: extended too far to find fwhm'

  print,'Have had to extend too far to find fwhm - eqw
     set to zero : '
  print,'Filename = ', list2s_fits_file(ff)
  print,'Line WL = ',input_wl(i)
  print,'Flux = ',obs_corr(1,obs_use(obs_flux_min))
```

```
        print, 'hw1/hw2 = ',hw1,' / ',hw2
        ;if vsini_line(i) eq 'Y' then begin

          ;   vsini_stor(vsini_line_num-1) = 0.0

      ;print,' problem - line too wide '
       ;      print,'vsinilinenum =',vsini_line_num

        ; endif
      endif
       ;print, 'input wl :',input_wl(i)
       ;print,'Flux = ',obs_corr(1,obs_use(obs_flux_min))
       ; print,'min wl = ',obs_corr(*,obs_use(obs_flux_min))
      ;print,'hw1/hw2 = ',hw1,' / ',hw2


    endelse

      ;print,'output eqw ',output_eqw


      ; ok we now have an EQW for the line.... now need to
         construct the WIDTH input file

      card='LINE'
      printf,1,card,output_eqw,output_wl,output_star,format='
         (a4,f10.2,f10.4,1x,a50)'


      printf,1, output_wl,output_loggf,output_jlow,
         output_elow,output_jupper,$
             output_eupper,output_code,$
             format='(f10.4,f7.3,f5.1,f12.3,f5.1,f12.3,f9.2)'

      printf,1,output_wl,output_nelion,output_gammar,
         output_gammas,output_gammaw,$
        format='(f10.4,i4,f6.2,f6.2,f6.2)'

endfor   ; end processing lines for each data file
card='END'
printf,1,card,format='(a)'

; construct the model atmosphere file
; most appropriate for this
;


ggg = float(teff)
```

```
  if ggg ge 10000 then interval = 500 $
  else interval = 200



  teff_low = (floor(ggg/interval)*interval)
  teff_high = (ceil(ggg/interval)*interval)


  if (ggg-teff_low) le (teff_high - ggg) then teff_output =
     teff_low $
  else teff_output = teff_high


  ; hhh = float(logg_in)*100

  ; apply limits to logg

   hhh = float(logg)*100

  if hhh gt 420 then hhh = 420

  if hhh lt 360 then hhh = 360



  logg_low = (floor(hhh/20)*20)
  logg_high = (ceil(hhh/20)*20)

  if (hhh-logg_low) le (logg_high - hhh) then logg_output =
     logg_low $
  else logg_output = logg_high
  ;
  ;
  ;
  ;
  ; modify to us logg input to script
  ;
  ;
  ;


if logg_in ne '9.9' then begin
    ;print,'logg not 9.9'
    hhh = float(logg_in)*100

    ;print, 'h here ',hhh


    logg_output = uint(float(logg_in)*100)
```

```
    hhh = uint(hhh)
endif


  ; ok construct the filename from this
  ;
  ;print,'v micro in',vmicro_in
  ;if teff_output gt 8600 or vmicro_in eq '8' $
  ;then model_suffix = strcompress('_' + vmicro_in + 'p00r.
     mod',/remove_all) $
  model_suffix = strcompress('_' + vmicro_in + 'p02.mod',/
     remove_all)

  if teff_output ge 10000 then model_prefix = 'T' else
     model_prefix = 'T0'

 model_path =  '/Users/mph/ATLAS/nemo/' + model + '/vmicro_'
     + string(vmicro_in) + '/p02/'
 model_path = strcompress(model_path,/remove_all)

  model_file = model_prefix + string(teff_output) + 'G' +
     string(logg_output) + model_suffix
  ;else model_file = 'T0' + string(teff_output) + 'G' +
     string(logg_output) + '_2p00.mod'
  model_file = strcompress(model_file,/remove_all)

  model_filename = model_path + model_file

  ;
  ; need to check whether model file exists:
  ;

  ff1 = file_search(model_filename,count=ccf)


  if ccf ne 1 then begin

    print,' *** Model atmosphere not found: ' +
       model_filename

    openu,5, width_output,/append
    printf,5,'++ Model Atmosphere -' + model_file + ' for
       vmicro ' +  vmicro_in + ' not found '
    ;list2s_fits_file(ff),format='(a,a)'
    close,5
    close,1
    goto, jump1
```

```
endif


OPENR, 4, model_filename
; Define a string variable:
AF = ''
; Loop until EOF is found:
WHILE ~ EOF(4) DO BEGIN
   ; Read a line of text:
  READF, 4, AF
   ; Print the line:
   if strmid(AF,0,5) ne 'BEGIN' then PRINTF,1, AF,format='(
      a)'
ENDWHILE

printf,1,'MOLECULES ON',format='(a)'
printf,1,'READ MOLECULES',format='(a)'
printf,1,'OPACITY ON HLINES',format='(a)'
printf,1,'BEGIN',format='(a)'
printf,1,'END',format='(a)'
printf,1,'STOP',format='(a)'

; Close the file:
CLOSE, 4

;openw,2,'/Users/mph/playground/eqw_out'

;for g = 0, nlines-1 do begin
;    print, input_wl(g),eqw_factor(g),format = '(f10.3,f10
   .2)'
;    printf,2,input_wl(g),eqw_factor(g),format = '(f10.3,
   f10.2)'
;endfor

;close,2
close,1


width_dir_name = output_star + '_' + string(ff) + '
   _width_input'


;width_file = base_output + timestamp + '/' +
   width_dir_name
width_file = final_output + '/' + width_dir_name
width_file = strcompress(width_file,/remove_all)
spawnrob,'cp '+w_filename+' '+width_file
```

```
;+++++++++++++++++++++++++++++++++++++++++++++++++++++++++++++
;  output header information into the width_output file
;
;+++++++++++++++++++++++++++++++++++++++++++++++++++++++++++++


openu,5, width_output,/append
printf,5,banner1,format='(a)'
printf,5,'++          Filename       :  ', list2s_fits_file(
    ff),format='(a,a)'
printf,5,'++          File Number    :  ',string(ff),format='
    (a,i3)'
printf,5,'++          Star           : ', output_star,format=
    '(a,a)'
printf,5,'++          Spectral shift: ', specshift,format='(
    a,f6.4)'
printf,5,'++          Teff           : ', teff,format='(a,a)'
printf,5,'++          logg           : ', logg_in,format='(a,
    f4.2)'
printf,5,'++          Model          : ', model_file,format='
    (a,a)'

;print, 'vsini_line num',vsini_line_num

;for vv = 0, vsini_line_num - 1 do begin

;   printf,5,'++          Vsini at ' + string(uint(input_wl(
    vv))) + '    : ', $
;   string(vsini_stor(vv)),format='(a,a-)'

;   print, 'here ',vsini_stor(vsini_line_num)
 ;    print,' hree vsini_stor ',vsini_stor

;endfor


printf,5,banner1,format='(a)'

close,5

;
; at this point, call the WIDTH routine with
; the parameter file
;
spawnrob, width_script + ' >> '+ width_output

jump1: continue
```

```
  endfor    ; end processing data files

;+++++++++++++++++++++++++++++++++++++++
;
; now produce extract file with important
; details from width_output file
;
;+++++++++++++++++++++++++++++++++++++++

openr,5,width_output
openw,6,extract_output

; Define a string variable:
AF = ''
; Loop until EOF is found:
WHILE ~ EOF(5) DO BEGIN
    ; Read a line of text:
    READF, 5, AF
    ; Print the line:
    if strmid(AF,0,2) eq '++' or $
    strmid(AF,0,2) eq 'LL' or $
    strmatch(AF,'*HD*') $
    then begin
      if strmatch(AF,'*HD*') and strmid(AF,0,2) ne '++' then
         begin

        vva = string(double(strmid(AF,79,9))*10)
        ;print, ' vva =',vva
        wlmatch = where(float(input_wl) eq vva,bb)

        if bb ne 1 then stop
        ;print,'wl mtch ',input_wl(wlmatch)
        ;input_elem(ll),input_elem_ion(ll),input_wl(ll)

        strput,AF,input_elem(wlmatch),70
        strput,AF,input_elem_ion(wlmatch),73
      endif
     PRINTF,6, AF,format='(a)'
    endif
ENDWHILE

close,3
close,5
close,6

print, 'OK you can or format the output via the command'

print,'  format_abund,"'+final_output+'/'+'"   '

END
```

D.2 PROGRAM format_abund.pro

```
PRO format_abund,input_dir,eqw_out=eqw_out

;#########################################################################
;
; Name: format_abund.pro
;
; Version:    4
;
; Last modified:    2 Jun 2017
;
; Purpose: Formats the WIDTH output
;
; Inputs:  WIDTH output files
;
; Outputs: IDL database structure containing
;          abundance results
;
; Parameters: input directory
;
;
;#########################################################################

default9, eqw_out, 0
spec_abund_eqw=fltarr(500,10,30)
spec_abund_avg=fltarr(500,10,30)
spec_abund_stdev=fltarr(500,10,30)
spec_abund_error=fltarr(500,10,30)
spec_abund_avg(*) = -99.

print,eqw_out

suff_pos = strpos(input_dir,'_g')
suffix = strmid(input_dir,suff_pos,12)

;input_file = strcompress(input_dir + '/extract_output' +
   suffix)
input_file = strcompress(input_dir + '/extract_output')

output_file = input_dir + '/abund_output'
output_str = input_dir + '/abund_struct_v5'
a=strarr(7)


nlines=0
file_ct = 0

;
;create the abund_db abundance database structure
```

```
;

abund_db = replicate({star:'', filename:'',filenum:'',teff:'
    ', logg:'', model:'',$
                        elem_tot:strarr(300),wl:fltarr(300),
                           eqw:fltarr(300), abund:fltarr(300)
                           },500)


;
;create the star_db star database structure
;


star_db = replicate({star:'',teff:'', logg:'', model:'',
    elem_tot:strarr(30),abund_eqw:fltarr(30),abund_avg:fltarr
    (30),abund_stdev:fltarr(30),abund_error:fltarr(30)},500)


; prime the abundances with -99.0 to signify null value

abund_db(*).abund(*) = -99.0
star_db(*).abund_avg(*) = -99.0

line_arr = fltarr(300)

;
;open the WIDTH output file and parse the data for each line
    for each
; spectrum
;

openr,1,input_file
bb=''
cc=''
AF = ''
  ; Loop until EOF is found:
  WHILE ~ EOF(1) DO BEGIN
    line_ct = 0
    ; Read a line of text:
    READF, 1, AF
    ; Print the line:
    if strmid(AF,0,2) eq 'LL' then begin
      line_arr(nlines) = float(strcompress(strmid(AF,11,9)))
      openu,2,output_file,/append
      printf,2,AF
      close,2
      nlines=nlines+1

    endif
```

```
if strmid(AF,10,8) eq 'Filename' then begin

    abund_db(file_ct).filename=strcompress(strmid(AF
        ,26,100))
endif

if strmid(AF,10,11) eq 'File Number' then begin

    abund_db(file_ct).filenum=strcompress(strmid(AF
        ,26,4))
endif
  if strmid(AF,10,4) eq 'Star' then begin
   abund_db(file_ct).star=strcompress(strmid(AF,26,10))
  endif

      if strmid(AF,10,4) eq 'Teff' then begin
   abund_db(file_ct).teff=strcompress(strmid(AF,26,5))
  endif
   if strmid(AF,10,4) eq 'logg' then begin
   abund_db(file_ct).logg=strcompress(strmid(AF,26,4))
  endif
  if strmid(AF,10,5) eq 'Model' then begin
   abund_db(file_ct).model=strcompress(strmid(AF,26,20))
  endif


  if strmid(AF,0,1) eq '0' then begin
    line_ct = 0
    a(*) = ''
    a = strsplit(AF,/extract)

    abund_db(file_ct).wl(line_ct) = double(a(4))

    abund_db(file_ct).elem_tot(line_ct) = string(a(2)) +
        string(a(3))



    abund_db(file_ct).eqw(line_ct) = 10*float(a(9))
    if a(9) le 0.00 then begin
      abund_db(file_ct).abund(line_ct) = -99.0
    endif else begin

      print,'float ',float(a(8))
      abund_db(file_ct).abund(line_ct) = float(a(10))
    endelse
    for i = 1,nlines-1 do begin
```

```
            line_ct = line_ct+1
            READF, 1, AF
            a(*) = ''
            a = strsplit(AF,/extract)


            abund_db(file_ct).elem_tot(line_ct) = string(a(2))
                + string(a(3))

            abund_db(file_ct).wl(line_ct) = double(a(4))
            abund_db(file_ct).eqw(line_ct) = 10*float(a(9))
            if a(9) le 0.00 then begin
            abund_db(file_ct).abund(line_ct) = -99.0
            endif else begin
            abund_db(file_ct).abund(line_ct) = float(a(10))
            endelse
          endfor
          file_ct = file_ct + 1
        endif

    ENDWHILE


close,1
print,file_ct


;
; Save the abund_db database for data extraction/plotting
    later
;



;ok now need to get number of unique element ions

b = UNIQ(abund_db(0).elem_tot)

elem_ion = abund_db(0).elem_tot(b)
elem_ion2 = where(elem_ion ne '',n)
elem_ion2 = elem_ion(elem_ion2)

print,n_elements(elem_ion2)


; now generate the average abundance for each element and
    for each star
```

APPENDIX D

```
dd = UNIQ(abund_db.star)

star_names = abund_db(dd).star

print,' nelements star name',n_elements(star_names)

star_2 = where(star_names ne '',mm)

star_2 = star_names(star_2)

print,' nelements star_2',n_elements(star_2)

;
for i = 0, n_elements(star_2) -1 do begin


;
; create star_db data as a summary per star
;


  match_star = where(abund_db.star eq star_2(i),nnn)
  star_db(i).star = abund_db(match_star(0)).star
  star_db(i).teff = abund_db(match_star(0)).teff
  star_db(i).logg = abund_db(match_star(0)).logg
  star_db(i).model = abund_db(match_star(0)).model
  print,'match ',match_star

  for j = 0, nnn-1 do begin

   ; for each spectrum for that star


     for k = 0,n_elements(elem_ion2) -1 do begin

      star_db(i).elem_tot(k) = elem_ion2(k)

     ; for each unique element/ion within that spectrum

       match_elem = where(abund_db(match_star(j)).elem_tot
          eq elem_ion2(k) and $
                          abund_db(match_star(j)).abund ne
                             -99.0,ooo)


      ; print,'match elem ',match_elem
```

```
        if ooo ge 1 then begin
        print,' i j k ',i,j,k
        spec_abund_eqw(i,j,k) = mean(abund_db(match_star(j)).
           eqw(match_elem))
        spec_abund_avg(i,j,k) = mean(abund_db(match_star(j)).
           abund(match_elem))
        spec_abund_stdev(i,j,k) = stddev(abund_db(match_star(
           j)).abund(match_elem))

        if ooo gt 1 then begin

          ; need to correct the error bars by dividing the
             std dev. by the sqrt(number obs -1)

          spec_abund_error(i,j,k) = stddev(abund_db(
             match_star(j)).abund(match_elem))/(sqrt(ooo-1))

        endif else begin

          spec_abund_error(i,j,k) = spec_abund_stdev(i,j,k)

        endelse


        print,spec_abund_avg(i,j,k)

        endif else begin
         print,' i j k ',i,j,k
         spec_abund_eqw(i,j,k)  = -99.
         spec_abund_avg(i,j,k)  = -99.
         print,spec_abund_avg(i,j,k)
        endelse


      endfor   ; element within spectrum


    endfor     ; each spectrum within star



endfor ; each star

for ii = 0, n_elements(star_2) -1 do begin
for kk = 0, n_elements(elem_ion2) -1 do begin

  s = where(spec_abund_avg(ii,*,kk) gt -99.0,bnm)
```

```
    print, 'bnm = ',bnm
    print,spec_abund_avg(ii,*,kk)
    print, 's =',s

   if bnm gt 0 then begin

   star_db(ii).abund_eqw(kk) = mean(spec_abund_eqw(ii,s,kk))
   star_db(ii).abund_avg(kk) = mean(spec_abund_avg(ii,s,kk))
   star_db(ii).abund_stdev(kk) = mean(spec_abund_stdev(ii,s,
      kk))
    star_db(ii).abund_error(kk) = mean(spec_abund_error(ii,s,
       kk))
    print,' mean ',mean(spec_abund_avg(ii,s,kk))

   endif else begin

   star_db(ii).abund_eqw(kk) = 0.
   star_db(ii).abund_avg(kk) = -99.

   endelse

endfor
endfor

save,filename=output_str,abund_db,star_db

print, 'OK you can or plot the output via the command'


print,'  plot_abund_v5,"'+input_dir+'"' + ',El'


END
```

D.3 PROGRAM plot_abund.pro

```
PRO plot_abund,input_dir,elem

;#############################################################################
;
; Name: plot_abund
;
; Version: V5
;
; Last modified: 12 Oct 2015
;
; Purpose: To plot results from IDL structure database
;
; Inputs: stars matching vsini criteria
;         results database
;
; Outputs: results plot
;
; Parameters: input_dir ocation of results
;             elem element to plot
;
;#############################################################################


; initialisation

default9,line,0
default9,avg,0
default9,elem,''


star_teff=dblarr(520)
star_name = strarr(520)
star_eqw = fltarr(520)
star_abund = fltarr(520)
star_stdev = fltarr(520)
star_error = fltarr(520)
star_fe1_avg=dblarr(520)
star_fe2_avg=dblarr(520)
star_filename = strarr(520)
adel_teff_fe = fltarr(520)
adel_abund_fe1 = fltarr(520)
adel_abund_fe2 = fltarr(520)
b_abundance_fe1=fltarr(520)
ap_abundance_fe1=fltarr(520)
ry_abundance_fe1=fltarr(520)
b_abundance_fe2=fltarr(520)
ap_abundance_fe2=fltarr(520)
```

```
ry_abundance_fe2=fltarr(520)

b_teff_f=intarr(520)
ap_teff_f=intarr(520)
ry_teff_f=intarr(520)

input_str = input_dir + '/abund_struct_v5'

restore,input_str

; extract the model from the database

base_model = star_db(0).model

if strtrim(base_model) eq '' then stop


;extract vtur,metallicity from base model name

mod_vtur = strmid(base_model,strpos (base_model,'_') + 1,1)
mod_metal = strmid(base_model,strpos (base_model,'_') + 3,2)

x = where(star_db(0).elem_tot eq elem,d)

  if d ne 1 then begin
    print,'Element ' + elem + ' not found in structure or
       defined twice'
      print, 'd = ',d
    stop
  endif

; input comparative data files

b_file = '/Users/mph/Feros_all/List_of_B_abundances_input'
ap_file = '/Users/mph/Feros_all/List_of_aP_abundances_input'
ry_file = '/Users/mph/Feros_all/List_of_aP_abund_Ryab_input'
infil_adelman = '/Users/mph/Feros_all/
   List_of_Fe_Abundances_Adelman'

readcol, infil_adelman,adel_teff,adel_abundance_fe1,
   adel_abundance_fe2,format='a,a,a', $
/silent, SKIPLINE=1

readcol,b_file, b_star,b_abundance,b_teff,b_logg,$
format='a,a,a,a',/silent , SKIPLINE=1

readcol,ap_file, ap_star,ap_abundance_fe1,ap_abundance_fe2,
   ap_teff,ap_logg,$
format='a,a,a,a,a',/silent , SKIPLINE=1
```

APPENDIX D

```
readcol,ry_file, ry_star,ry_abundance_fe1,ry_abundance_fe2,
   ry_teff,ry_logg,$
format='a,a,a,a,a',/silent, SKIPLINE=1


;ap_abundance_fe1=float(strcompress(ap_abundance_fe1))
;ap_abundance_fe2=float(strcompress(ap_abundance_fe2))
;b_abundance_f=float(strcompress(b_abundance))
;ry_abundance_fe1=float(strcompress(ry_abundance_fe1))
;ry_abundance_fe2=float(strcompress(ry_abundance_fe2))

;b_teff_f = uint(b_teff)
;ap_teff_f = uint(ap_teff)
;ry_teff_f = uint(ry_teff)


; read in stars satisfying vsini criterion

;infile = '/Users/mph/Feros_all/List_of_good_stars'
;readcol, infile,star_obj,format='a'
;n_stars = n_elements(star_obj)


; now include the list of stars whose spectra conform to the
    vsini
; criteria

vsini_instruc = '/Users/mph/Feros_all/output/17Aug11_18
   :10:48_g99_v2_mcgm/abund_struct_v3'

restore,vsini_instruc

qq =  where(abund_db.vsini_ok eq '1'B, ccc)
aaa = uniq(abund_db(qq).star)
print, 'number of spectra with vsini = ok ',ccc

nst = n_elements(aaa)

;openw,2,output_file

;for i = 0,n_stars-1 do begin
for i = 0,nst-1 do begin
  w = where(strcompress(star_db.star) eq abund_db(qq(aaa(i))
     ).star,c)


  print, 'c = ',abund_db(qq(aaa(i))).star
```

```
   if c lt 1 then begin

     print,'Star ' + abund_db(qq(aaa(i))).star + ' not found
        in structure'

     stop

          ;print,'Star ' + star_obj(i) + ' not found in
             structure'

   endif


   star_name(i) = star_db(w).star

   star_teff(i) = float(star_db(w).teff)
   star_eqw(i) = star_db(w).abund_eqw(x)
   star_abund(i) = star_db(w).abund_avg(x)
   star_stdev(i) = star_db(w).abund_stdev(x)
    star_error(i) = star_db(w).abund_error(x)

;print,'star name/teff/eqw/abund/stdev/error ', i,star_name(
    i),uint(star_teff(i)),star_eqw(i),star_abund(i),
    star_stdev(i),star_error(i)


endfor

;
set_plot,'ps'

;set up plot file

ps_file_out = input_dir + '/plot_'+elem+'.ps'
device,/landscape,filename=ps_file_out,ysize=19,xsize=25

;device,filename='/Users/mph/UCLAN /Disequilibrium Paper/' +
     elem + '_v'+ mod_vtur + '_p' + mod_metal + '_abundance.
    ps',ysize=9,xsize=12,$
;encapsulated=eps, /helvetica,/isolatin1, landscape=0,/color
    , FONT_SIZE = 6

nz = where(star_teff gt 0)
nz2 = where(star_abund(nz) gt -99.0)


  ; For Nd/Pr plots
   ;
```

```
; plot,star_teff(nz2),star_abund(nz2) ,psym=1,xrange
   =[12000,5500],yrange=[-12,-4],$
title= elem + ' Abundance Plot', XTICKFORMAT='(F6.0)',
   symsize=0.5,$
   xtitle='Teff', ytitle=strcompress('log[' + elem + ']',/
      remove_all)


col = getcolor(/load)
title1 = elem + ' Abundance Plot ' + ' vtur= ' + mod_vtur +
    ' metal= '+ mod_metal

plot,star_teff(nz2),star_abund(nz2) ,psym=1,xrange
   =[12500,5500],yrange=[-8,0],$
 title= title1 , XTICKFORMAT='(F6.0)', symsize=1.5,$
    xtitle='Teff', ytitle=strcompress('log[' + elem + ']',/
       remove_all)



 ; oploterr,star_teff(nz),star_abund(nz),star_error(nz)
 print, 'error =',star_error(nz)
; plot solar abundance line

for tt = 1, n_elements(nz2) - 1 do begin

print,'star name/teff/eqw/abund ', i,star_name(nz2(tt)),
   uint(star_teff(nz2(tt))),star_eqw(nz2(tt)),star_abund(
   nz2(tt))

endfor



xsolar = [ 13000,4000]
ysolar = [-4.54,-4.54]

oplot,xsolar,ysolar,thick=2,linestyle=2

result = linfit(star_teff(nz2),star_abund(nz2), YFIT=yfit)
    ;oplot, star_teff(nz),yfit, thick=2
    print,' num elements stars ',n_elements(star_teff(nz2))


 r_sq = correlate(star_teff(nz2),star_abund(nz2))

print,'Result Correlation coeff ',elem , ' : ',r_sq

; 4       Diamond
```

```
; 5       Triangle
; 6       Square

if elem eq 'Fe1' or  elem eq 'Fe2' then begin
  if elem eq 'Fe1'  then begin
     oplot, adel_teff,adel_abundance_fe1,psym=6,col=col.red
     result_adel_fe1 = linfit(float(adel_teff),float(
        adel_abundance_fe1), YFIT=yfit_adel_fe1)
     oplot, adel_teff,yfit_adel_fe1, thick=2,linestyle=1,col
        =col.red

     oplot, ap_teff,ap_abundance_fe1,psym=5,col=col.blue
      result_ap_fe1 = linfit(float(ap_teff),float(
         ap_abundance_fe1), YFIT=yfit_ap_fe1)
     oplot, ap_teff,yfit_ap_fe1, thick=2,linestyle=2,col=col
        .blue



        oplot, ry_teff,ry_abundance_fe1,psym=4,col=col.green
          result_ry_fe1 = linfit(float(ry_teff),float(
             ry_abundance_fe1), YFIT=yfit_ry_fe1)
     oplot, ry_teff,yfit_ry_fe1, thick=2,linestyle=3,col=col
        .green

    r_sq_adel_fe1 = correlate(float(adel_teff),float(
       adel_abundance_fe1))
        print,'Adel Correlation coeff ',elem , ' : ' ,
           r_sq_adel_fe1

    r_sq_ap_fe1 = correlate(float(ap_teff),float(
       ap_abundance_fe1))
         print,'Ap Correlation coeff ',elem , ' : ' ,
            r_sq_ap_fe1

     r_sq_ry_fe1 = correlate(float(ry_teff),float(
        ry_abundance_fe1))
         print,'Ry Correlation coeff ', elem , ' : ',
            r_sq_ry_fe1

  endif else begin


     oplot, adel_teff,adel_abundance_fe2,psym=6,col=col.red

     result_adel_fe2 = linfit(float(adel_teff),float(
        adel_abundance_fe2), YFIT=yfit_adel_fe2)
     oplot, adel_teff,yfit_adel_fe2, thick=2,linestyle=1,col
        =col.red
```

```
      oplot, ap_teff,ap_abundance_fe2,psym=5,col=col.blue

            result_ap_fe2 = linfit(float(ap_teff),float(
               ap_abundance_fe2), YFIT=yfit_ap_fe2)
      oplot, ap_teff,yfit_ap_fe2, thick=2,linestyle=2,col=col
         .blue

      oplot, ry_teff,ry_abundance_fe2,psym=4,col=col.green

        result_ry_fe2 = linfit(float(ry_teff),float(
           ry_abundance_fe2), YFIT=yfit_ry_fe2)
      oplot, ry_teff,yfit_ry_fe2, thick=2,linestyle=3,col=col
         .green

    print, 'ry ', ry_teff,ry_abundance_fe2

       r_sq_adel_fe2 = correlate(float(adel_teff),float(
          adel_abundance_fe2))
        print,'Adel Correlation coeff ',elem, ' : ',
           r_sq_adel_fe2

    r_sq_ap_fe2 = correlate(float(ap_teff),float(
       ap_abundance_fe2))
         print,'Ap Correlation coeff ',elem, ' : ',
            r_sq_ap_fe2

     r_sq_ry_fe2 = correlate(float(ry_teff),float(
        ry_abundance_fe2))
         print,'Ry Correlation coeff ', elem, ' : ',
            r_sq_ry_fe2

  endelse

endif


device,/close


END
```

Appendix E

E.1 List of absorption lines used in comparing the derivation of EQWs using MIDAS and IDL semi−automated approach

Table E.1: List of Absorption Lines for Comparison of MIDAS vs IDL Routine

			Measured EQW	
Star	Ion	λ (Å)	MIDAS (mÅ)	Routine (mÅ)
HD6655	Fe I	5141.739	78.10	76.75
	Fe I	5162.273	131.20	130.81
	Fe I	5194.941	115.40	115.12
	Fe I	5217.389	102.30	97.70
	Fe I	5234.625	94.10	94.13
	Cr I	5296.691	80.70	80.55
	Fe I	5334.847	39.20	36.75
	Ti II	5336.771	78.80	75.75
	Ca I	5342.695	24.20	25.76
	Mn I	5377.637	42.90	39.41

APPENDIX E

Table E.1

			Measured EQW	
Star	Ion	λ (Å)	MIDAS (mÅ)	Routine (mÅ)
	Fe I	5386.333	25.10	25.14
	Cr I	5409.784	128.40	121.88
	Mn I	5420.355	54.00	53.50
	Ni I	5435.855	42.60	41.53
	Fe I	5461.550	21.20	22.28
	Ni I	5468.100	10.70	11.17
	Fe I	5496.561	11.80	10.83
	Ni I	5593.733	37.80	37.18
HD2883	Ti II	5129.152	119.97	120.24
	Fe I	5266.555	108.19	109.97
	Nd II	5302.270	135.31	129
	Cr II	5313.563	33.79	33.42
	Ce II	5367.435	86.95	87.33
	Fe I	5383.369	99.80	100.03
	Ti II	5418.751	37.45	37.95
	Fe I	5446.871	160.42	164.07
	Fe I	5462.960	118.26	126.82
	Nd II	5485.696	18.24	16.14
	Ce II	5503.061	39.34	39.27
	Y II	5509.895	70.59	72.72
	Fe I	5543.936	27.42	32.27
	Si I	5645.613	17.22	17.93
	Ce II	5691.463	16.78	16.69
	La II	5769.057	33.76	34.9

APPENDIX E

Table E.1

			Measured EQW	
Star	Ion	λ (Å)	MIDAS (mÅ)	Routine (mÅ)
	Fe I	5806.717	25.90	26.91
	Fe I	5952.716	47.49	40.08
HD126365	Fe I	5052.17	179.23	177.8
	Fe I	5365.192	106.01	115.22
	Fe I	5415.192	102.02	105.85
	Fe I	5506.778	91.49	103.78
	Fe I	6024.049	61.81	67.78
	Ce II	6102.762	151.75	148.28
	Fe I	6400.000	118.14	118.33
	Fe I	4430.614	134.91	116.63
	Mn I	4462.031	214.90	208.55
	Sm II	4476.480	126.04	132.29
	Nd II	4497.256	120.52	121.34
	Pr II	4550.083	323.97	331.43
	Zr II	4613.946	81.53	81.34
	Ce II	4714.831	114.57	124.93
	Cr II	4954.806	44.43	44.76
	Gd II	5031.273	67.75	73.39
	Fe I	5072.672	92.96	94.06
	Fe I	5133.681	106.40	106.26
HD2957	Ni I	5010.022	88.84	87.39
	Ce II	5145.836	96.77	102.67
	Tl II	5185.902	151.01	154.77
	Fe II	5234.625	126.52	136.86

APPENDIX E

Table E.1

Star	Ion	λ (Å)	Measured EQW MIDAS (mÅ)	Measured EQW Routine (mÅ)
	Fe I	5253.461	89.34	96.7
	Fe II	5256.938	149.41	155.72
	Tm II	5305.863	212.94	211.25
	Tm II	5420.792	115.16	121.44
	La II	5482.268	96.41	99.98
	Nd II	5581.590	77.07	77.25
	Ca I	5604.939	53.16	68.17
	Fe I	5615.644	89.33	92.43
	Cr I	5746.412	83.41	81.45
	Cr I	5787.918	83.32	94.31
	Cr II	5854.192	94.89	92.14
	Cr II	5886.239	88.04	87.95
	Ce II	6010.675	28.68	24.9
	Sm II	6168.341	70.28	71.12
HD3988	Fe I	5044.210	31.32	30.77
	Fe II	5061.734	64.33	65.35
	Fe I	5094.948	24.06	23.69
	Ti II	5211.530	19.06	154.82
	Gd II	5303.434	33.33	33.75
	Fe I	5373.698	27.61	29.89
	Mn I	5399.499	27.4	26.26
	Ti II	5418.751	18.31	18.08
	Yb II	5426.875	24.05	26.81
	Tm II	5475.783	36.18	36.47

Table E.1

Star	Ion	λ (Å)	Measured EQW MIDAS (mÅ)	Routine (mÅ)
	Tm II	5488.762	27.61	28.92
	Ce II	5505.244	18.99	23.58
	Ti I	5514.343	31.9	30.91
	Fe I	5562.706	22.02	20.58
	Ni I	5593.733	11.3	11.68
	Nd II	5741.27	20.03	20.93
	Fe I	5827.875	11.54	13.51
	Ti I	5922.109	20.89	20.96
	Ce II	5216.863	85.28	83.71
	Cr II	5237.329	142.79	136.51
	Cr II	5246.768	101.36	99.66
	Fe II	5260.259	117.71	104.54
	Fe I	5281.79	52.75	53.39
	Cr II	5310.686	110.1	108.33
	Fe I	5324.178	106.73	106.41
	Cr II	5334.869	96.37	92.56

E.2 List of absorption lines used in comparing the derivation of abundances using WIDTH vs the Adelman (1973) data

APPENDIX E

Table E.2: List of absorption lines selected for comparison of WIDTH vs Adelman (1973)

			Abundance	
Ion	λ (Å)	W_λ (mÅ)	A_{WIDTH}	$A_{Adelman}$
Mg I	4571.09	28	−4.87	−4.78
	4702.99	141	−4.95	−4.68
	4167.27	127	−4.76	−4.71
Mg II	4481.33	182	−4.25	−4.16
	3850.39	13	−4.14	−4.09
	4427.99	8	−4.43	−4.17
Al I	3944.01	163	−6.5	−6.03
	3961.52	140	−7.02	−6.67
Si II	3856.02	91	−4.94	−4.6
	3862.59	61	−5.2	−4.99
	3853.66	35	−4.92	−4.84
	4130.89	18	−3.98	−5.09
	4128.07	47	−4.45	−4.14
Ca I	4226.73	278	−6.03	−5.82
	4425.44	89	−6.19	−5.84
	4434.96	99	−6.37	−5.99
	4435.69	79	−6.24	−5.91
	4455.89	86	−6.11	−5.73
	4283.01	89	−6.29	−5.96
	4289.36	78	−6.42	−6.14
	4298.99	86	−6.15	−5.84
	4302.53	110	−6.35	−6.02

APPENDIX E

Table E.2

			Abundance	
Ion	λ (Å)	W_λ (mÅ)	A_{WIDTH}	$A_{Adelman}$
	4318.65	89	−6.25	−5.97
	4578.55	40	−6.29	−6.15
	4581.40	42	−6.48	−6.33
	4585.87	68	−6.2	−5.98
	4094.93	27	−6.26	−6.27
	4092.63	25	−6.18	−6.17
	3875.80	19	−5.35	−6.45
	3753.34	19	−5.74	−6.37
	4526.93	40	−6.29	−6.14
	4355.09	37	−6.24	−6.19
	4685.27	21	−6.03	−5.93
Sc II	4246.83	131	−9.655	−9.09
	4354.61	31	−9.295	−9.2
	4374.46	87	−9.531	−9.22
	4415.56	75	−9.574	−9.26
	4420.66	6	−9.579	−9.37
	4431.37	13	−9.487	−9.33
	4294.77	35	−9.538	−9.31
	4314.08	86	−9.874	−9.54
	4320.74	71	−9.967	−9.75
	4325.01	91	−9.429	−9.1
	4670.40	46	−9.669	−9.31
Ti I	4656.47	19	−7.193	−7.15
	4681.91	7	−7.913	−7.89

APPENDIX E

Table E.2

			Abundance	
Ion	λ (Å)	W_λ (mÅ)	A_{WIDTH}	$A_{Adelman}$
	3962.85	7	−7.737	−7.76
	3964.27	17	−7.252	−7.3
	3998.64	72	−7.397	−7.14
	4008.93	38	−6.983	−6.91
	3924.53	19	−7.509	−7.47
	3929.88	7	−7.892	−7.87
	3947.77	13	−7.685	−7.66
	4533.24	59	−7.562	−7.39
	4534.78	48	−7.549	−7.43
	4555.49	17	−7.394	−7.36
	4548.76	18	−7.517	−7.47
	4518.02	19	−7.516	−7.47
	4272.44	6	−6.856	−6.77
	4274.58	6	−7.669	−7.59
	4286.00	31	−7.307	−7.24
	4287.41	14	−7.525	−7.49
	4289.06	4	−7.01	−6.92
	4298.66	39	−7.356	−7.27
	4300.56	52	−7.355	−7.22
	4305.91	52	−7.514	−7.38
	4723.17	6	−6.875	−6.75
	4427.09	15	−7.628	−7.58
	4186.12	5	−7.594	−7.57
	4617.27	17	−7.534	−7.48

APPENDIX E

Table E.2

			Abundance	
Ion	λ (Å)	W_λ (mÅ)	A_{WIDTH}	$A_{Adelman}$
	4623.10	10	−7.525	−7.47
	4639.36	7	−7.567	−7.52
	4639.94	2	−7.595	−7.74
	4645.19	2	−7.595	−7.55
	4650.02	11	−6.78	−6.73
	4496.15	11	−7.174	−7.12
	4284.99	12	−6.953	−6.91
	4449.14	20	−7.437	−7.37
	4450.90	15	−7.503	−7.45
	4453.71	6	−7.525	−7.48
	4417.27	7	−7.429	−7.39
	4282.70	13	−7.24	−7.11
	3862.82	8	−7.332	−7.2
	3869.27	3	−7.434	−7.42
	3873.20	2	−7.905	−7.67
	4015.37	3	−7.482	−7.44
	4017.77	5	−7.288	−7.25
	4002.47	8	−7.062	−7.02
	4200.75	5	−6.865	−6.87
	4742.79	11	−7.179	−7.12
	4758.12	9	−7.479	−7.43
	4759.17	9	−7.563	−7.5
Pr II	3964.82	3	−11.616	−11.63
Nd II	4061.09	25	−10.874	−10.79

APPENDIX E

Table E.2

			Abundance	
Ion	λ (Å)	W_λ (mÅ)	A_{WIDTH}	$A_{Adelman}$
	4177.32	29	−10.524	−10.41
	4303.58	27	−10.853	−10.87
	4358.17	3	−11.218	−11.13
	4368.63	3	−10.713	−10.67
	3990.10	14	−10.565	−10.49
	3952.20	11	−10.594	−10.53
	3851.66	9	−11.236	−11.18
	4021.34	8	−11.261	−11.2
	4446.38	7	−10.651	−10.59
	4385.66	4	−10.95	−10.56
	4462.99	9	−10.89	−10.82
	4075.12	18	−10.28	−10.2
	4338.69	7	−10.478	−10.56
	3879.55	4	−11.214	−11.18
	3880.78	6	−11.063	−11.03
	3900.21	15	−10.882	−10.84
	3901.84	10	−10.927	−10.88
	3994.68	10	−10.804	−10.74
Sm II	4704.39	6	−10.198	−10.13
	4452.72	6	−10.676	−10.61
	4035.11	5	−10.633	−10.57
	4434.32	9	−10.645	−10.57
	4262.67	3	−11.051	−10.99
	4523.9	2	−10.875	−10.81

APPENDIX E

Table E.2

			Abundance	
Ion	λ (Å)	W_λ (mÅ)	A_{WIDTH}	$A_{Adelman}$
	4280.79	8	−10.839	−11.13
Eu II	4129.73	21	−11.905	−11.82
	3907.10	8	−12.169	−12.12
	3971.96	10	−11.751	−12.1
Gd II	4251.73	11	−10.63	−10.55
	3957.67	11	−10.569	−10.51
	4215.02	5	−10.772	−10.71
	4217.19	9	−10.358	−10.28
	4582.38	5	−9.79	−9.72
	4053.28	16	−10.299	−10.2
	4197.68	9	−10.293	−10.21

Appendix F

Tables for Chapter 4

F.1 List of Fe I / Fe II lines used in the Fe abundance analysis

Table F.1: The complete Fe I / Fe II line list used in the Fe abundance analysis. For each line, $\log(gf)$ represents the oscillator strength; E_i, E_f the initial and final energy levels of the transition in eV; J_i, J_f the J degeneracy of initial and final levels; gl represents the Landé factor, and γ_r, γ_s and γ_w represent the radiative–, Stark–, and Van der Waals broadening, respectively (Heiter et al. 2008)

Ion	Wl[A]	log(gf)	E_i[eV]	J_i	E_f[eV]	J_f	gl	γ_r	γ_s	γ_w
Fe I	4613.203	−1.67	3.292	0	5.978	1	0.01	7.88	−5.16	−7.158
	4619.288	−1.12	3.602	3	6.286	2	1.7	8.18	−5.86	−7.26
	4643.463	−1.147	3.654	2	6.323	2	1.84	8.36	−5.07	−7.245
	4678.846	−0.833	3.602	3	6.251	4	1.3	8.15	−5.02	−7.279
	4691.412	−1.523	2.99	4	5.632	4	1.05	7.31	−6.22	−7.682
	4707.275	−1.08	3.241	3	5.874	4	1.08	7.88	−5.27	−7.203

APPENDIX F

Table F.1

Ion	Wl[A]	log(gf)	E_i[eV]	J_i	E_f[eV]	J_f	gl	γ_r	γ_s	γ_w
	4736.773	−0.752	3.211	4	5.828	5	1.26	7.89	−5.35	−7.218
	4789.651	−0.958	3.546	2	6.134	3	0.98	7.46	−6.21	−7.8
	4871.318	−0.363	2.865	3	5.410	2	1.02	8.18	−5.41	−7.259
	4872.138	−0.567	2.882	1	5.426	1	2.28	8.18	−5.41	−7.255
	4878.211	−0.888	2.885	0	5.426	1	3.01	8.18	−5.41	−7.255
	4903.31	−0.926	2.882	1	5.410	2	2.24	8.18	−5.41	−7.259
	4924.77	−2.241	2.279	2	4.795	2	1.33	8.2	−5.89	−7.578
	4946.388	−1.17	3.368	4	5.874	4	1.34	7.9	−5.27	−7.204
	4966.089	−0.871	3.332	5	5.828	5	1.41	7.91	−5.35	−7.218
	4969.918	−0.71	4.217	1	6.711	1	1.52	8.47	−4.72	−7.158
	4973.102	−0.95	3.96	1	6.452	1	0.66	8.18	−5.46	−7.262
	4988.95	−0.89	4.154	3	6.639	3	1.42	8.47	−4.58	−7.204
	4991.268	−0.67	4.191	2	6.674	3	0.72	8.46	−4.69	−7.181
	4994.13	−3.08	0.915	4	3.396	3	1.5	7.24	−6.15	−7.744
	5389.479	−0.41	4.415	3	6.715	3	1.01	8.32	−4.63	−7.159
	5393.168	−0.715	3.241	3	5.539	4	1.5	8.04	−5.41	−7.235
	5400.502	−0.16	4.371	4	6.666	4	1.16	8.31	−5.41	−7.187
	5415.199	0.642	4.386	5	6.675	6	1.17	8.3	−4.66	−7.182
	5463.276	0.11	4.434	4	6.703	4	1.1	8.28	−4.69	−7.166
	5466.396	−0.63	4.371	4	6.639	3	0.73	8.31	−4.58	−7.204
	5473.9	−0.76	4.154	3	6.419	3	1.49	8.47	−5.34	−7.266
	5497.516	−2.849	1.011	1	3.266	2	2.26	7.15	−6.22	−7.751
	5501.465	−3.047	0.958	3	3.211	4	1.88	7.18	−6.22	−7.757
	5506.779	−2.797	0.99	2	3.241	3	2.01	7.16	−6.22	−7.753
	5569.618	−0.486	3.417	2	5.642	1	0.75	8.06	−5.38	−7.204

APPENDIX F

Table F.1

Ion	Wl[A]	log(gf)	E_i[eV]	J_i	E_f[eV]	J_f	gl	γ_r	γ_s	γ_w
	5572.842	−0.275	3.396	3	5.62	2	1.02	8.06	−5.42	−7.211
	5576.089	−1	3.43	1	5.653	0	−0.01	8.06	−5.39	−7.201
	5586.756	−0.12	3.368	4	5.587	3	1.13	8.06	−5.38	−7.221
	5615.644	0.05	3.332	5	5.539	4	1.19	8.06	−5.41	−7.234
	5658.816	−0.793	3.396	3	5.587	3	1.38	8.05	−5.38	−7.221
	5762.992	−0.45	4.209	2	6.359	3	1.2	8.19	−5.29	−7.273
	5816.373	−0.601	4.548	4	6.679	5	0.81	8.33	−4.33	−7.51
	5934.655	−1.17	3.928	2	6.017	3	1.05	7.78	−5.29	−7.153
	6003.012	−1.12	3.881	4	5.946	4	1.27	7.75	−5.38	−7.181
	6020.169	−0.27	4.607	3	6.666	4	1.44	8.33	−5.41	−7.189
	6024.058	−0.12	4.548	4	6.606	5	1.17	8.32	−5.06	−7.225
	6065.482	−1.53	2.608	2	4.652	2	0.68	8.07	−6.29	−7.584
	6136.615	−1.4	2.453	4	4.473	3	0.84	7.96	−6.08	−7.609
	6137.692	−1.403	2.588	3	4.607	3	1.08	8.08	−6.29	−7.589
	6170.507	−0.44	4.795	2	6.804	2	1.31	8.3	−5.02	−7.119
	6213.43	−2.482	2.223	1	4.217	1	2.01	8.31	−6.16	−7.691
	6219.281	−2.433	2.198	2	4.191	2	1.66	8.29	−6.16	−7.694
	6230.723	−1.281	2.559	4	4.548	4	1.24	8.07	−6.09	−7.597
	6246.319	−0.733	3.602	3	5.587	3	1.58	8.07	−5.38	−7.221
	6252.555	−1.687	2.404	6	4.386	5	0.95	8.02	−6.07	−7.621
	6256.361	−2.408	2.453	4	4.434	4	0.96	7.99	−6.08	−7.615
	6265.134	−2.55	2.176	3	4.154	3	1.58	8.3	−6.16	−7.7
	6335.331	−2.177	2.198	2	4.154	3	1.16	8.3	−6.16	−7.698
	6336.824	−0.856	3.686	1	5.642	1	2.02	8.08	−5.38	−7.207
	6393.601	−1.432	2.433	5	4.371	4	0.91	8.05	−6.06	−7.622

APPENDIX F

Table F.1

Ion	Wl[A]	log(gf)	E_i[eV]	J_i	E_f[eV]	J_f	gl	γ_r	γ_s	γ_w
	6400.001	−0.29	3.602	3	5.539	4	1.27	8.07	−5.41	−7.232
	6411.649	−0.595	3.654	2	5.587	3	1.18	8.07	−5.38	−7.221
	6419.95	−0.24	4.733	3	6.664	3	1.29	8.41	−4.24	−7.193
	6421.351	−2.027	2.279	2	4.209	2	1.5	6.81	−6.13	−7.62
	6430.846	−2.006	2.176	3	4.103	4	1.24	8.29	−6.16	−7.704
	6546.239	−1.536	2.758	3	4.652	2	0.82	8.07	−6.28	−7.626
	6592.914	−1.473	2.727	4	4.607	3	1.03	8.08	−6.28	−7.633
	6593.87	−2.422	2.433	5	4.312	5	1.13	8.01	−6.08	−7.629
	6677.987	−1.418	2.692	5	4.548	4	1.1	8.07	−6.09	−7.643
Fe II	4075.954	−4.792	2.544	2.5	5.585	1.5	1.27	8.56	−6.6	−7.796
	4273.326	−3.303	2.704	1.5	5.605	0.5	2.16	8.56	−6.53	−7.873
	4296.572	−2.933	2.704	1.5	5.589	2.5	0.58	8.47	−6.53	−7.881
	4303.176	−2.511	2.704	1.5	5.585	1.5	1.43	8.56	−6.53	−7.875
	4384.319	−3.684	2.657	5.5	5.484	4.5	0.67	8.47	−6.53	−7.886
	4385.387	−2.582	2.778	0.5	5.605	0.5	1.33	8.56	−6.53	−7.875
	4416.83	−2.602	2.778	0.5	5.585	1.5	0.77	8.56	−6.53	−7.875
	4472.929	−3.531	2.844	2.5	5.615	1.5	1.45	8.47	−6.53	−7.88
	4489.183	−2.971	2.828	3.5	5.589	2.5	1.39	8.47	−6.53	−7.88
	4491.405	−2.756	2.856	1.5	5.615	1.5	0.42	8.47	−6.53	−7.88
	4508.288	−2.349	2.856	1.5	5.605	0.5	0.5	8.56	−6.53	−7.873
	4515.339	−2.54	2.844	2.5	5.589	2.5	1.04	8.47	−6.53	−7.88
	4541.524	−2.973	2.856	1.5	5.585	1.5	0.77	8.56	−6.53	−7.875
	4555.893	−2.421	2.828	3.5	5.549	3.5	1.25	8.47	−6.53	−7.883
	4576.34	−2.976	2.844	2.5	5.553	2.5	1.18	8.56	−6.53	−7.875
	4582.835	−3.224	2.844	2.5	5.549	3.5	1.63	8.47	−6.53	−7.883

Table F.1

Ion	Wl[A]	log(gf)	E_i[eV]	J_i	E_f[eV]	J_f	gl	γ_r	γ_s	γ_w
	4620.521	−3.315	2.828	3.5	5.511	3.5	1.31	8.56	−6.53	−7.879
	4656.981	−3.643	2.891	2.5	5.553	2.5	1.67	8.56	−6.5	−7.871
	4666.758	−3.368	2.828	3.5	5.484	4.5	1.51	8.47	−6.53	−7.886
	4993.358	−3.684	2.807	4.5	5.289	3.5	0.62	8.51	−6.53	−7.894
	5197.577	−2.348	3.23	2.5	5.615	1.5	0.67	8.47	−6.53	−7.88
	5234.625	−2.279	3.221	3.5	5.589	2.5	0.87	8.47	−6.53	−7.88
	5284.109	−3.195	2.891	2.5	5.237	3.5	0.65	8.56	−6.5	−7.887
	5325.553	−3.324	3.221	3.5	5.549	3.5	1.13	8.47	−6.53	−7.883
	6084.111	−3.881	3.199	4.5	5.237	3.5	0.71	8.56	−6.53	−7.892
	6147.741	−2.827	3.889	1.5	5.905	0.5	0.83	8.51	−6.52	−7.87
	6149.258	−2.841	3.889	0.5	5.905	0.5	1.35	8.51	−6.52	−7.87
	6247.557	−2.435	3.892	2.5	5.876	1.5	1.03	8.51	−6.52	−7.87
	6416.919	−2.877	3.892	2.5	5.823	2.5	1.46	8.51	−6.52	−7.873
	6432.68	−3.687	2.891	2.5	4.818	2.5	1.82	8.49	−6.5	−7.899
	6456.383	−2.185	3.903	3.5	5.823	2.5	1.18	8.51	−6.52	−7.873

F.2 List of stars for which Fe abundances have been calculated in this work

APPENDIX F

Table F.2: The list of stars for which Fe I / Fe II abundances have been calculated in this work, where columns $A_{Fe\,\mathrm{I}}$, $A_{Fe\,\mathrm{II}}$ show the derived abundances; $SE_{Fe\,\mathrm{I}}$, $SE_{Fe\,\mathrm{II}}$, the standard error, and $n_{Fe\,\mathrm{I}}$, $n_{Fe\,\mathrm{II}}$, the number of Fe I / Fe II lines contributing to the analysis. For comparison, the Fe solar abundance is −4.52 (Anders & Grevesse 1989)

Star	T_{eff} (K)	$A_{Fe\,\mathrm{I}}$	$SE_{Fe\,\mathrm{I}}$	$n_{Fe\,\mathrm{I}}$	$A_{Fe\,\mathrm{II}}$	$SE_{Fe\,\mathrm{II}}$	$n_{Fe\,\mathrm{II}}$
HD2883	6269	−5.12	0.04	65	−4.29	0.16	29
HD5823	7176	−4.22	0.08	60	−3.79	0.15	28
HD8783	8250	−3.78	0.08	62	−3.78	0.16	30
HD21799	7108	−4.14	0.10	60	−3.59	0.16	28
HD22032	6964	−4.05	0.11	62	−3.27	0.16	30
HD23207	8064	−3.52	0.10	63	−3.25	0.15	30
HD23715	7625	−3.75	0.06	63	−3.19	0.14	31
HD26726	8008	−3.06	0.14	58	−2.63	0.17	27
HD29578	7554	−4.12	0.07	63	−3.81	0.15	30
HD30849	5889	−4.94	0.09	63	−3.46	0.14	30
HD31973	8203	−3.84	0.09	60	−3.71	0.18	30
HD33629	7321	−3.53	0.08	62	−3.26	0.22	29
HD34205	8143	−3.84	0.08	63	−3.84	0.17	30
HD40765	6914	−3.62	0.08	57	−3.06	0.27	25
HD41385	7826	−3.83	0.12	59	−3.28	0.19	30
HD42075	7365	−3.55	0.11	60	−2.97	0.18	31
HD42605	8191	−3.75	0.08	61	−3.30	0.20	29
HD43901	7982	−3.83	0.08	63	−3.81	0.17	30
HD44226	7816	−3.35	0.09	62	−3.06	0.21	29

APPENDIX F

Table F.2

Star	$T_{\rm eff}$ (K)	$A_{Fe\,\rm I}$	$SE_{Fe\,\rm I}$	$n_{Fe\,\rm I}$	$A_{Fe\,\rm II}$	$SE_{Fe\,\rm II}$	$n_{Fe\,\rm II}$
HD46665	9062	−3.45	0.08	61	−3.01	0.17	31
HD50620	8321	−3.79	0.09	61	−3.49	0.20	30
HD50627	7755	−3.91	0.05	65	−3.46	0.11	31
HD51203	7583	−3.65	0.12	58	−3.06	0.21	28
HD52599	7790	−4.01	0.09	63	−3.95	0.20	28
HD52696	8132	−4.06	0.07	61	−4.45	0.16	28
HD52847	7874	−2.93	0.12	63	−2.49	0.16	30
HD55540	9107	−2.09	0.24	53	−2.05	0.17	29
HD55719	9054	−3.20	0.10	60	−3.35	0.14	30
HD57040	7484	−3.45	0.15	58	−2.52	0.20	29
HD59437	8851	−3.24	0.12	60	−2.83	0.15	31
HD61731	7867	−3.92	0.08	59	−3.08	0.12	29
HD62244	8593	−3.24	0.11	62	−3.28	0.18	28
HD62905	9251	−3.42	0.11	55	−3.36	0.18	31
HD68480	9878	−2.81	0.16	88	−2.88	0.18	62
HD69013	7390	−3.58	0.13	64	−2.91	0.23	31
HD69862	8158	−3.73	0.09	63	−3.86	0.13	30
HD72316	9477	−2.52	0.13	63	−2.37	0.14	31
HD74629	8354	−3.99	0.06	59	−4.02	0.12	29
HD76276	7774	−4.48	0.07	59	−3.80	0.17	27
HD76460	7574	−3.97	0.06	65	−3.68	0.16	31
HD76877	8006	−4.03	0.09	63	−3.97	0.15	31
HD77438	7875	−3.93	0.06	65	−3.01	0.10	31
HD79539	8253	−3.62	0.09	64	−3.62	0.15	31
HD81588	7863	−3.77	0.12	62	−3.30	0.22	31

APPENDIX F

Table F.2

Star	$T_{\rm eff}$ (K)	$A_{Fe\,\rm I}$	$SE_{Fe\,\rm I}$	$n_{Fe\,\rm I}$	$A_{Fe\,\rm II}$	$SE_{Fe\,\rm II}$	$n_{Fe\,\rm II}$
HD82417	8160	−4.01	0.07	61	−3.28	0.08	30
HD82989	6744	−3.95	0.05	65	−4.11	0.20	28
HD85284	8814	−3.57	0.12	64	−3.80	0.12	31
HD88241	7458	−4.17	0.07	65	−4.24	0.13	30
HD88385	9671	−2.89	0.09	56	−2.58	0.14	31
HD88701	9557	−2.40	0.15	62	−2.52	0.15	31
HD91087	8224	−3.81	0.09	63	−3.53	0.13	30
HD92499	7604	−3.31	0.13	58	−2.71	0.15	30
HD94455	8105	−3.02	0.13	63	−3.08	0.20	31
HD95158	7627	−3.79	0.07	63	−3.45	0.10	29
HD96237	7674	−3.35	0.13	60	−3.10	0.18	30
HD97394	8006	−3.00	0.14	64	−2.75	0.20	31
HD102333	8122	−3.96	0.08	63	−3.90	0.12	31
HD106215	8707	−2.67	0.14	56	−2.62	0.18	30
HD110072	7196	−4.23	0.12	63	−3.58	0.16	30
HD110274	7921	−3.58	0.13	63	−3.18	0.16	31
HD115220	8004	−3.02	0.06	65	−3.26	0.23	27
HD115440	7041	−5.08	0.16	42	−3.81	0.13	31
HD116423	7372	−4.81	0.10	55	−4.04	0.15	31
HD117290	8046	−3.50	0.11	62	−3.30	0.15	30
HD117691	7243	−3.99	0.09	65	−3.08	0.12	30
HD121661	8976	−3.20	0.11	61	−2.74	0.14	31
HD121788	7348	−4.54	0.08	58	−4.06	0.19	28
HD121840	8052	−3.62	0.06	63	−2.74	0.11	31
HD122525	8279	−3.57	0.10	63	−3.67	0.11	30

APPENDIX F

Table F.2

Star	$T_{\rm eff}$ (K)	$A_{Fe\,\rm I}$	$SE_{Fe\,\rm I}$	$n_{Fe\,\rm I}$	$A_{Fe\,\rm II}$	$SE_{Fe\,\rm II}$	$n_{Fe\,\rm II}$
HD122659	9218	−1.13	0.08	65	−3.39	0.30	29
HD126297	7687	−4.46	0.07	65	−4.62	0.15	31
HD131141	7844	−3.40	0.06	65	−2.76	0.16	31
HD132205	7653	−3.72	0.11	61	−3.15	0.19	31
HD135396	6998	−4.43	0.05	65	−4.20	0.13	31
HD135815	7987	−3.93	0.08	62	−3.88	0.20	31
HD138426	8433	−4.29	0.06	61	−4.29	0.11	31
HD138927	7514	−4.42	0.06	62	−4.05	0.10	30
HD140748	8144	−3.75	0.08	63	−3.60	0.12	31
HD143487	6812	−3.96	0.15	61	−2.83	0.21	31
HD146631	7629	−3.71	0.07	63	−3.34	0.08	29
HD148593	7714	−3.83	0.10	63	−3.25	0.19	30
HD150862	6203	−4.89	0.07	58	−4.34	0.28	27
HD151860	6901	−4.57	0.08	65	−4.25	0.13	30
HD153183	7813	−3.88	0.11	61	−3.90	0.20	31
HD158205	8468	−3.55	0.10	60	−3.56	0.15	28
HD158293	8185	−2.91	0.13	60	−3.00	0.16	29
HD161423	7688	−3.76	0.13	61	−3.11	0.16	30
HD161704	6303	−4.48	0.04	65	−4.11	0.13	30
HD162316	7607	−3.65	0.11	62	−2.99	0.18	31
HD163833	9199	−2.61	0.14	59	−2.98	0.17	31
HD166223	10591	−2.32	0.10	61	−2.79	0.11	31
HD169380	9328	−2.04	0.16	54	−1.83	0.15	31
HD172626	8074	−3.47	0.10	63	−3.50	0.14	30
HD172703	9419	−2.80	0.13	61	−3.23	0.15	31

APPENDIX F

Table F.2

Star	$T_{\rm eff}$ (K)	$A_{Fe\,\rm I}$	$SE_{Fe\,\rm I}$	$n_{Fe\,\rm I}$	$A_{Fe\,\rm II}$	$SE_{Fe\,\rm II}$	$n_{Fe\,\rm II}$
HD177268	8202	−3.69	0.10	62	−3.07	0.13	31
HD177765	7756	−3.26	0.09	65	−2.98	0.14	30
HD179902	6771	−4.37	0.10	62	−3.51	0.17	31
HD180303	8677	−3.67	0.11	56	−3.45	0.15	31
HD184120	7824	−3.54	0.11	57	−2.78	0.15	31
HD184343	11333	−1.19	0.10	63	−2.89	0.22	31
HD185129	8067	−3.49	0.11	61	−3.10	0.16	31
HD185204	7586	−3.68	0.10	63	−3.09	0.16	31
HD186038	6003	−4.89	0.05	65	−3.21	0.09	31
HD189963	8001	−3.32	0.11	62	−3.04	0.17	31
HD191695	7311	−4.62	0.07	64	−4.35	0.18	31
HD196470	7546	−3.76	0.11	60	−3.16	0.18	29
HD209605	7720	−3.71	0.10	62	−3.42	0.17	30
HD219391	7911	−3.82	0.05	63	−3.28	0.11	31
HD221127	6262	−5.10	0.04	65	−4.37	0.16	31
HD222925	5836	−5.74	0.03	65	−4.76	0.13	31

Appendix G

Tables for Chapter 5

G.1 List of Nd II / Nd III and Pr II / Pr III lines used in the REE Abundance Analysis

Table G.1: The complete Nd II / Nd III / Pr II / Pr III line list used in the Pr / Nd abundance analysis in this work. For each line, $\log(gf)$ represents the oscillator strength; E_i , E_f the initial and final energy levels of the transition in eV; J_i , J_f the J degeneracy (combined spin−orbit coupling) of initial and final levels; gl represents the Landé factor, and γ_r, γ_s and γ_w represent the radiative–, Stark–, and Van der Waals broadening, respectively (Heiter et al. 2008)

Ion	Wl[A]	log(gf)	E_i[eV]]	J_i	E_f[eV]	J_f	gl	γ_r	γ_s	γ_w
Nd II	4061.080	0.550	0.471	7.5	3.524	8.5	1.07	0.000	−5.327	0.000
	4706.543	−0.710	0.000	3.5	2.634	2.5	0.61	0.000	0.000	0.000
	4811.342	−1.015	0.064	4.5	2.640	3.5	0.77	0.000	0.000	0.000
	5033.507	−0.470	1.136	9.5	3.599	8.5	1.09	0.000	0.000	0.000
	5063.722	−0.620	0.976	8.5	3.423	7.5	1.15	0.000	0.000	0.000

APPENDIX G

Table G.1

Ion	Wl[A]	log(gf)	E_i[eV]]	J_i	E_f[eV]	J_f	gl	γ_r	γ_s	γ_w
	5077.154	−1.047	0.823	7.5	3.264	6.5	0.73	0.000	0.000	0.000
	5165.129	−0.740	0.680	6.5	3.080	5.5	0.51	0.000	0.000	0.000
	5311.453	−0.420	0.986	6.5	3.319	5.5	1.00	0.000	−5.704	0.000
	5319.815	−0.140	0.550	5.5	2.880	4.5	0.26	0.000	−5.819	0.000
	5399.099	−1.419	0.933	3.5	3.229	2.5	−0.10	0.000	0.000	0.000
	5533.820	−1.230	0.559	6.5	2.799	6.5	1.05	0.000	0.000	0.000
	6514.959	−1.883	0.182	5.5	2.085	4.5	1.17	0.000	0.000	0.000
	6636.182	−0.940	2.059	8.5	3.927	8.5	1.17	0.000	−5.535	0.000
	6637.187	−0.840	1.452	4.5	3.319	5.5	0.95	0.000	−5.682	0.000
	6637.960	−0.320	1.773	8.5	3.641	7.5	0.83	0.000	0.000	0.000
	6650.517	−0.110	1.953	9.5	3.816	8.5	0.95	0.000	0.000	0.000
	6680.137	−0.720	1.686	6.5	3.541	6.5	1.03	0.000	−5.627	0.000
Nd III	4796.500	−1.650	0.141	5.0	2.725	6.0	1.54	0.000	0.000	0.000
	5286.753	−1.900	0.631	8.0	2.976	7.0	1.50	0.000	0.000	0.000
	5294.113	−0.690	0.000	4.0	2.341	4.0	0.62	0.000	0.000	0.000
	5633.554	−2.220	0.141	5.0	2.341	4.0	1.43	0.000	0.000	0.000
	5677.179	−1.450	0.631	8.0	2.815	7.0	1.60	0.000	0.000	0.000
	5845.020	−1.180	0.631	8.0	2.752	9.0	1.10	0.000	0.000	0.000
	5987.683	−1.260	0.461	7.0	2.531	8.0	1.06	0.000	0.000	0.000
	6145.068	−1.330	0.296	6.0	2.313	7.0	1.00	0.000	0.000	0.000
	6327.265	−1.410	0.141	5.0	2.100	6.0	0.94	0.000	0.000	0.000
	6550.231	−1.490	0.000	4.0	1.892	5.0	0.85	0.000	0.000	0.000
	6690.830	−2.460	0.461	7.0	2.313	7.0	1.12	0.000	0.000	0.000
Pr II	4368.334	−0.393	0.000	4.0	2.837	5.0	1.79	0.000	0.000	0.000
	4405.825	−0.392	0.550	8.0	3.363	8.0	1.20	0.000	0.000	0.000

Table G.1

Ion	Wl[A]	log(gf)	E_i[eV]]	J_i	E_f[eV]	J_f	gl	γ_r	γ_s	γ_w
	4408.819	−0.278	0.000	4.0	2.811	5.0	1.31	0.000	0.000	0.000
	4449.825	−0.436	0.204	6.0	2.990	6.0	1.02	0.000	0.000	0.000
	4477.261	−0.995	0.204	6.0	2.973	6.0	1.11	0.000	0.000	0.000
	4510.153	−0.298	0.422	6.0	3.170	7.0	1.17	0.000	0.000	0.000
	4535.923	−0.852	0.000	4.0	2.733	5.0	1.79	0.000	0.000	0.000
	4628.741	−0.900	0.055	5.0	2.733	5.0	0.94	0.000	0.000	0.000
	4664.653	−0.850	0.422	6.0	3.079	6.0	1.02	0.000	0.000	0.000
	4672.087	−0.781	0.216	5.0	2.869	6.0	1.56	0.000	0.000	0.000
Pr III	6071.085	−2.360	0.359	6.5	2.400	6.5	1.11	0.000	0.000	0.000
	6090.010	−0.820	0.359	6.5	2.394	5.5	1.05	0.000	0.000	0.000
	6160.233	−0.980	0.173	5.5	2.185	4.5	0.89	0.000	0.000	0.000
	6161.194	−1.140	1.549	5.5	3.561	4.5	1.31	0.000	0.000	0.000
	6706.703	−1.640	0.552	7.5	2.400	6.5	1.48	0.000	0.000	0.000

G.2 List of stars for which ND / Pr abundances have been calculated in this work

APPENDIX G

Table G.2: The list of stars for which Nd II / Nd III and Pr II / Pr III abundances have been calculated in this work, where columns A_{ion} show the derived abundances for each ion species, and n_{ion} the number of lines contributing to the analysis.

Star	$T_{\rm eff}$ (K)	$A_{Nd\,II}$	$n_{Nd\,II}$	$A_{Nd\,III}$	$n_{Nd\,III}$	$A_{Pr\,II}$	$n_{Pr\,II}$	$A_{Pr\,III}$	$n_{Pr\,III}$
HD2883	6269	−9.63	11	−8.80	2	−8.89	10	−6.60	1
HD5823	7176	−9.01	9	−7.01	11	−8.31	8	−8.02	3
HD8783	8250	−7.59	7	−7.96	7	−7.70	9	−7.39	3
HD21799	7108	−8.52	13	−6.14	11	−7.57	9	−7.06	5
HD22032	6964	−8.51	15	−5.86	11	−6.91	8	−6.71	5
HD23207	8064	−7.48	9	−7.02	10	−6.97	10	−7.57	5
HD23715	7625	−8.98	6	−8.62	5	−7.40	7	−7.80	1
HD26726	8008	−6.87	8	−6.81	9	−6.35	7	−6.81	3
HD29578	7554	−8.45	7	−7.53	11	−8.12	10	−8.10	4
HD30849	5889	−8.45	9	−5.80	9	−8.00	8	−6.70	5
HD31973	8203	−8.14	5	−7.87	9	−6.46	5	−7.75	3
HD33629	7321	−8.23	12	−7.11	11	−8.14	8	−7.69	5
HD34205	8143	−7.76	9	−7.90	8	−8.02	10	−8.14	4
HD40765	6914	−8.17	11	−8.27	8	−8.02	9	−7.46	3
HD41385	7826	−8.18	14	−6.46	11	−6.69	9	−6.51	5
HD42075	7365	−8.01	14	−5.87	11	−6.99	8	−6.44	4
HD42605	8191	−7.81	8	−6.80	10	−6.47	6	−7.49	5
HD43901	7982	−8.27	11	−8.22	8	−7.91	9	−7.87	3
HD44226	7816	−7.93	12	−6.71	11	−7.67	9	−7.27	5
HD46665	9062	−7.28	16	−6.84	11	−7.42	9	−7.34	5
HD50620	8321	−7.91	8	−7.52	10	−7.37	9	−7.93	5

APPENDIX G

Table G.2

Star	$T_{\rm eff}$ (K)	$A_{Nd\,\rm II}$	$n_{Nd\,\rm II}$	$A_{Nd\,\rm III}$	$n_{Nd\,\rm III}$	$A_{Pr\,\rm II}$	$n_{Pr\,\rm II}$	$A_{Pr\,\rm III}$	$n_{Pr\,\rm III}$
HD50627	7755	−9.01	13	−8.37	6	−8.82	9	−9.28	2
HD51203	7583	−7.73	14	−5.94	11	−7.26	9	−7.02	5
HD52599	7790	−8.82	9	−8.36	7	−8.47	8	−7.79	3
HD52696	8132	−8.37	10	−8.45	9	−8.28	10	−8.01	2
HD52847	7874	−7.03	12	−6.16	10	−6.43	10	−6.91	4
HD55540	9107	−5.49	8	−5.84	9	−4.85	7	−6.14	4
HD55719	9054	−7.97	5	−7.72	5	−6.91	9	−7.54	2
HD57040	7484	−7.17	16	−5.52	11	−6.39	8	−6.63	4
HD59437	8851	−7.88	7	−7.43	9	−6.56	8	−7.74	4
HD61731	7867	−8.18	13	−6.60	11	−7.81	6	−7.37	5
HD62244	8593	−7.22	11	−7.57	9	−7.22	8	−7.62	3
HD62905	9251	−6.97	15	−7.34	10	−6.46	10	−7.50	5
HD68480	9878	−6.15	12	−6.35	11	−5.76	7	−6.80	5
HD69013	7390	−7.74	16	−5.90	11	−6.51	9	−7.06	5
HD69862	8158	−7.95	9	−8.31	6	−7.61	9	−7.27	1
HD72316	9477	−6.64	10	−7.09	10	−6.78	7	−6.83	5
HD74629	8354	−8.33	7	−7.95	9	−7.11	9	−8.32	4
HD76276	7774	−8.93	7	−7.62	11	−8.17	7	−8.66	3
HD76460	7574	−8.95	9	−8.10	8	−7.50	9	−8.46	3
HD76877	8006	−8.63	10	−7.97	10	−7.85	9	−8.37	5
HD77438	7875	−9.13	12	−8.64	5	−9.13	7	−9.28	2
HD79539	8253	−8.12	12	−8.11	8	−7.77	10	−8.05	4
HD81588	7863	−7.61	15	−6.55	11	−7.75	10	−7.46	5
HD82417	8160	−8.70	4	−8.68	4	−7.53	8	−99.00	0
HD82989	6744	−9.35	11	−8.26	8	−7.99	8	−8.06	2

APPENDIX G

Table G.2

Star	$T_{\rm eff}$ (K)	$A_{Nd\,\rm II}$	$n_{Nd\,\rm II}$	$A_{Nd\,\rm III}$	$n_{Nd\,\rm III}$	$A_{Pr\,\rm II}$	$n_{Pr\,\rm II}$	$A_{Pr\,\rm III}$	$n_{Pr\,\rm III}$
HD85284	8814	−7.88	13	−8.07	9	−7.63	10	−7.74	5
HD88241	7458	−9.10	12	−8.04	11	−8.39	10	−8.79	4
HD88385	9671	−7.07	12	−7.04	10	−5.96	8	−6.85	5
HD88701	9557	−5.63	9	−6.70	9	−6.61	7	−6.52	5
HD91087	8224	−8.10	15	−7.41	11	−7.44	9	−7.66	5
HD92499	7604	−7.77	14	−5.38	11	−6.95	8	−6.51	5
HD94455	8105	−7.77	10	−7.05	9	−6.14	10	−7.39	3
HD95158	7627	−9.08	4	−8.21	2	−7.70	7	−7.37	1
HD96237	7674	−7.18	17	−5.60	11	−6.10	7	−5.84	3
HD97394	8006	−6.91	15	−6.45	11	−6.51	10	−6.86	5
HD102333	8122	−8.34	10	−8.18	10	−8.27	9	−8.60	4
HD106215	8707	−6.70	9	−7.28	8	−5.88	7	−6.98	5
HD110072	7196	−8.69	14	−6.65	11	−8.41	9	−6.96	5
HD110274	7921	−7.86	12	−7.10	11	−7.53	9	−7.74	5
HD115220	8004	−8.54	13	−8.66	10	−7.08	6	−7.26	2
HD115440	7041	−8.81	8	−7.13	11	−9.51	8	−7.34	5
HD116423	7372	−8.34	14	−7.49	11	−8.59	8	−7.51	5
HD117290	8046	−8.27	8	−7.74	9	−7.02	9	−8.05	3
HD117691	7243	−9.23	10	−8.68	6	−8.12	9	−7.54	1
HD121661	8976	−7.22	15	−7.34	10	−7.19	9	−7.15	5
HD121788	7348	−9.04	7	−8.93	4	−8.75	6	−7.98	1
HD121840	8052	−8.65	11	−8.59	7	−7.40	9	−8.28	4
HD122525	8279	−7.95	10	−8.36	8	−7.97	9	−7.60	4
HD122659	9218	−6.92	14	−7.61	8	−5.77	8	−7.17	3
HD126297	7687	−9.20	5	−9.04	2	−9.09	9	−7.98	1

APPENDIX G

Table G.2

Star	$T_{\rm eff}$ (K)	$A_{Nd\,\rm II}$	$n_{Nd\,\rm II}$	$A_{Nd\,\rm III}$	$n_{Nd\,\rm III}$	$A_{Pr\,\rm II}$	$n_{Pr\,\rm II}$	$A_{Pr\,\rm III}$	$n_{Pr\,\rm III}$
HD131141	7844	−8.71	12	−8.17	6	−7.03	9	−8.53	2
HD132205	7653	−7.97	12	−6.46	11	−7.09	9	−7.36	5
HD135396	6998	−9.60	7	−9.22	3	−8.55	8	−9.05	2
HD135815	7987	−8.09	5	−8.57	5	−8.28	9	−8.15	2
HD138426	8433	−8.14	12	−8.19	10	−8.22	8	−8.42	4
HD138927	7514	−9.19	9	−9.37	5	−7.63	8	−9.28	2
HD140748	8144	−8.11	10	−8.00	10	−8.04	9	−8.41	4
HD143487	6812	−7.81	16	−5.91	11	−7.07	9	−6.25	5
HD146631	7629	−8.71	8	−8.68	3	−7.89	8	−8.20	1
HD148593	7714	−7.73	14	−6.38	11	−6.72	10	−6.89	5
HD150862	6203	−9.25	7	−8.43	5	−8.63	8	−7.12	1
HD151860	6901	−8.80	15	−7.22	11	−8.53	10	−8.09	4
HD153183	7813	−8.89	4	−8.31	9	−8.05	8	−7.96	3
HD158205	8468	−8.02	6	−8.07	6	−7.22	7	−7.81	3
HD158293	8185	−7.63	6	−7.66	8	−6.19	9	−7.18	4
HD161423	7688	−7.90	17	−6.28	11	−6.75	9	−7.38	5
HD161704	6303	−9.44	11	−8.67	4	−8.34	9	−8.15	2
HD162316	7607	−7.82	16	−6.14	11	−7.07	10	−6.87	5
HD163833	9199	−6.73	10	−6.38	10	−6.51	9	−6.66	5
HD166223	10591	−5.72	10	−6.99	10	−6.26	7	−6.65	5
HD169380	9328	−6.61	5	−5.94	10	−5.20	7	−5.92	3
HD172626	8074	−7.32	10	−7.63	8	−7.38	10	−7.86	5
HD172703	9419	−6.89	13	−7.46	10	−6.67	9	−7.03	5
HD177268	8202	−7.76	10	−7.70	10	−7.79	9	−7.66	4
HD177765	7756	−8.31	12	−7.22	10	−6.98	10	−7.13	4

Table G.2

Star	$T_{\rm eff}$ (K)	$A_{Nd\,II}$	$n_{Nd\,II}$	$A_{Nd\,III}$	$n_{Nd\,III}$	$A_{Pr\,II}$	$n_{Pr\,II}$	$A_{Pr\,III}$	$n_{Pr\,III}$
HD179902	6771	−8.79	15	−6.51	11	−7.60	8	−6.78	5
HD180303	8677	−7.71	8	−7.70	9	−7.71	6	−7.48	4
HD184120	7824	−8.05	12	−7.34	9	−7.52	8	−7.14	5
HD184343	11333	−5.35	6	−7.60	4	−3.50	9	−6.61	2
HD185129	8067	−8.29	8	−7.64	9	−8.06	9	−7.70	5
HD185204	7586	−8.31	15	−6.72	11	−6.84	8	−7.54	5
HD186038	6003	−9.42	14	−7.85	8	−9.14	9	−7.18	3
HD189963	8001	−7.54	8	−7.48	8	−7.35	9	−7.74	4
HD191695	7311	−8.78	15	−6.92	11	−8.70	10	−7.72	4
HD196470	7546	−7.90	11	−5.91	10	−6.64	8	−6.93	5
HD209605	7720	−7.84	6	−7.69	8	−7.15	7	−7.50	2
HD219391	7911	−8.75	6	−8.77	3	−7.56	7	−99.00	1
HD221127	6262	−9.71	12	−8.21	3	−9.34	9	−8.43	2
HD222925	5836	−10.19	10	−9.18	2	−9.98	7	−7.89	1